Ecole Doctorale Sciences de la Matière, du Rayonnement et de l'Environnement
Spécialité Géosciences, Ecologie, Paléontologie, Océanographie

Ecole Doctorale Sciences Pour l'Ingénieur
Spécialité Mécanique, Génie Civil, Energétique, Matériaux

Université de Lille

Laboratoire d'Océanologie et de Géosciences, UMR LOG 8187
Laboratoire de mécanique de Lille, FRE 3723

Dynamique des copépodes dans les écoulements turbulents

Thèse de doctorat présentée par **Hamidreza Ardeshiri**

Soutenue publiquement le 12 Octobre 2016 devant le jury composé de:

Directeur de thèse	François SCHMITT	DR CNRS
Co-directeur de thèse	Enrico CALZAVARINI	MdC Université de Lille
Rapporteurs	Ivana VINKOVIC	PR Université Claude Bernard Lyon 1
	Eric CLIMENT	PR Université Toulouse III – Paul Sabatier
Examinateurs	Sami SOUISSI	PR Université de Lille
	Federico TOSCHI	PR Eindhoven University of Technology
	Emmanuel LERICHE	PR Université de Lille
	Sergio CHIBBARO	MdC Université Pierre et Marie Curie

Doctoral School SMRE – Material, Radiation And Environment Science
Geosciences, Ecology, Paleontology, Oceanography

Doctoral School SPI – Sciences For Engineer
Mechanics, Civil Engineering, Energy, Materials

University of Lille

Laboratory of Oceanology and Geoscience, UMR LOG 8187
Mechanic Laboratory of Lille, FRE 3723

Dynamics of Copepods in Turbulent Flows

PhD dissertation presented by **Hamidreza Ardeshiri**

Publicly defended in October 12th, 2016 in the presence of the thesis jury members:

Director	François SCHMITT	DR CNRS
Co-director	Enrico CALZAVARINI	MdC University of Lille
Reviewers	Ivana VINKOVIC	PR University of Claude Bernard Lyon 1
	Eric CLIMENT	PR University of Toulouse III – Paul Sabatier
Examiners	Sami SOUISSI	PR University of Lille
	Federico TOSCHI	PR Eindhoven University of Technology
	Emmanuel LERICHE	PR University of Lille
	Sergio CHIBBARO	MdC University Pierre and Marie Curie

Declaration of Authorship

I, Hamidreza Ardeshiri, declare that this thesis titled, "Dynamics of Copepods in Turbulent Flows" and the work presented in it are my own. I confirm that:

- This work was done wholly or mainly while in candidature for a research degree at this University.
- Where any part of this thesis has previously been submitted for a degree or any other qualification at this University or any other institution, this has been clearly stated.
- Where I have consulted the published work of others, this is always clearly attributed.
- Where I have quoted from the work of others, the source is always given. With the exception of such quotations, this thesis is entirely my own work.
- I have acknowledged all main sources of help.
- Where the thesis is based on work done by myself jointly with others, I have made clear exactly what was done by others and what I have contributed myself.

Signed:

Date:

Abstract

The most common family of multi-celled organisms in the zooplankton is a rather diversified group of crustaceans known with the name of copepods. Among them the most numerous ones have a characteristic elongated body shape. Copepods have a major role in the marine ecosystem because they are the secondary producers in the ecological food-chain linking phytoplankton cells (the primary producers) to fish larvae and even to large mammals such as whales. Copepods are carried by marine currents in the same way suspension of nearly neutrally buoyant particles are transported by the flow. However, differently from material particles, copepods have the capability to swim and so to add small-scale deviations to the - so called - passive trajectory. In this sense phytoplancton (such as algae) can be thought as a suspension of small passive particles, while zooplankton and in particular copepods may be viewed as kind of (slightly larger and non spherical) active particles.

Copepods swimming behavior usually exhibits quick powerful jumps. Such an aptness is used to escape from high shear regions, which may be caused either by flow perturbations, produced by a large predator (*i.e.,* fish larvae), or by the inherent highly turbulent dynamics of the ocean. The research presented this thesis is organized into three steps. First, recorded velocity tracks of copepods displaying escape response jumps in still water are here analyzed and used to define and tune a Lagrangian copepod (LC) model. Second, the model is further employed to simulate the behavior of thousands of copepods in a fully developed hydrodynamic turbulent flow obtained by direct numerical simulation of the Navier-Stokes equations. Third, numerical data analysis are performed to quantify copepods' dynamics in turbulence and make a comparison with available experimental observations of copepods in turbulence.

Through this combined experimental and numerical study, we investigate the small-scale distribution of copepods in a turbulent environment and its dependency on the jump intensity, jump orientation, jump latency time and geometrical aspect ratio of the copepods. At last, possible ecological implications of the observed clustering on encounter rates and mating success are provided.

Keywords: Lagrangian turbulence, Direct numerical simulation, Spectral method, Fractal dimension, Copepod's behavior

Acknowledgements

I am deeply grateful to all the people who have helped me in various ways throughout these three years as a PhD student.

First I would like to express all my gratitude to *François Schmitt* and *Enrico Calzavarini* for supervising me and their kind supports in all the moments. I would like to thank them for being patient and for all the scientific stimulating discussions and motivating suggestions.

I am grateful to *Federico Toschi* for enlightening discussions, comments and advices in various occasions. His deep insight has been invaluable to me and my work.

I would like to thank *Sami Souissi* who helped me a lot to better understand the ecological problems and to increase the quality of my studies. I also acknowledge *Ibtissem Benkeddad* for providing the experimental data.

There are many researchers with whom I have had interesting and useful discussions on a wide variety of scientific topics. I would especially like to thank *Stefano Berti*.

I acknowledge my friends for being excellent company in the Lille 1 University and Eindhoven University of Technology and my special thanks go to my family for their strong supports.

To all of you: *Thank you!*

Hamidreza Ardeshiri

Contents

List of Figures

List of Tables

List of Abbreviations

DNS	**D**irect **N**umerical **S**imulation
LC	**L**agrangian **C**opepod
PTV	**P**article **T**racking **V**elocimetry
TPL	**T**hin **P**hytoplankton **L**ayer
HIT	**H**omogeneous **I**sotropic **T**urbulence
TKE	**T**urbulent **K**inetic **E**nergy
MKE	**M**ean **K**inetic **E**nergy
RMS	**R**oot **M**ean **S**quare
PIV	**P**article **I**mage **V**elocimetry
LES	**L**arge **E**ddy **S**imulation
RANS	**R**eynolds **A**veraged **N**avier **S**tokes
FDM	**F**inite **D**ifference **M**ethod
FVM	**F**inite **V**olume **M**ethod
FEM	**F**inite **E**lement **M**ethod
MWR	**M**ethod of **W**eighted **R**esiduals
PDE	**P**artial **D**ifferential **E**quation
FFT	**F**ast **F**ourier **T**ransform
DFT	**D**iscrete **F**ourier **T**ransform
ODE	**O**rdinary **D**ifferential **E**quation
LOG	**L**aboratory of **O**ceanology and **G**eoscience
PDF	**P**robability **D**ensity **F**unction
TGV	**T**aylor **G**reen **V**ortex
MSD	**M**ean **S**quared **D**isplacement

List of Symbols

Re	Reynolds number	
Re_λ	Taylor Reynolds number	
ν	Kinematic viscosity	$\mathrm{m^2\,s^{-1}}$
v	Particle's (copepods') velocity	$\mathrm{m\,s^{-1}}$
u	Fluid velocity	$\mathrm{m\,s^{-1}}$
ρ_f	Fluid density	$\mathrm{m^3\,kg^{-1}}$
ρ_p	Particle's density	$\mathrm{m^3\,kg^{-1}}$
p	Pressure	$\mathrm{kg\,m^{-1}\,s^{-2}}$
μ	Dynamic viscosity	$\mathrm{m^5\,s^{-1}\,kg^{-1}}$
λ	Mean free path	m
L_{phys}	Physical length scale	m
Kn	Knudson number	
u′	fluctuation velocity	$\mathrm{m\,s^{-1}}$
K	Turbulent kinetic energy	$\mathrm{m^2\,s^{-2}}$
ϵ	Turbulent kinetic energy dissipation rate	$\mathrm{m^2\,s^{-3}}$
η	Kolmogorov length scale	m
u_η	Kolmogorov velocity scale	$\mathrm{m\,s^{-1}}$
τ_η	Kolmogorov time scale	s
u_{rms}	Root mean square velocity	$\mathrm{m\,s^{-1}}$
E	Total turbulent energy	$\mathrm{m^3\,s^{-2}}$
$\mathcal{V}_p$	Particle's volume	$\mathrm{m^3}$
a	Particle's radius	m
F_b	Body force	$\mathrm{kg\,m\,s^{-2}}$
F_s	Surface force	$\mathrm{kg\,m\,s^{-2}}$
$F_{gravity}$	Gravity force	$\mathrm{kg\,m\,s^{-2}}$
g	Gravitational acceleration	$\mathrm{m\,s^{-2}}$
F_{drag}	Drag force	$\mathrm{kg\,m\,s^{-2}}$
C_D	Drag coefficient	
$F_{addedmass}$	Added mass force	$\mathrm{kg\,m\,s^{-2}}$

C_M	Added mass coefficient	
$\boldsymbol{\sigma}$	Stress tensor	$\mathrm{kg\,m^{-1}\,s^{-2}}$
F_{lift}	Lift force	$\mathrm{kg\,m\,s^{-2}}$
C_L	Lift coefficient	
ω	Flow vorticity	$\mathrm{s^{-1}}$
β	Density ratio	
τ_p	Particle's stokes time	s
v_s	Particle's (copepods') slipping velocity	$\mathrm{m\,s^{-1}}$
ϕ_n	Trial functions	$\mathrm{m\,s^{-1}}$
$\hat{\mathscr{F}}_k$	Fourier operator	
$\mathcal{S}$	Fluid deformation rate symmetric tensor	$\mathrm{s^{-1}}$
$\boldsymbol{\Omega}$	Fluid rotation rate antisymmetric tensor	$\mathrm{s^{-1}}$
α	Particle's aspect ratio	
$\boldsymbol{p}$	Particle's jump direction	
$\boldsymbol{I}$	Identity tensor	
$\boldsymbol{B}$	Gyrotactic response time	s
D_R	Rotional diffusivity coefficient	$\mathrm{s^{-1}}$
$\boldsymbol{\xi}$	Uniformly random vector is space	
$\dot{\gamma}$	Shear rate	$\mathrm{s^{-1}}$
$\dot{\gamma}_T$	Shear rate threshold	$\mathrm{s^{-1}}$
ψ	Streamfunction	$\mathrm{m^2\,s^{-1}}$
$C(r)$	Correlation function	m
D_2	Correlation dimension	

To my lovely angels
Elham & Taranom

Chapter 1

Introduction

Particulate flow modelling is a fundamental research in different branches of science and has attracted enormous interests in last decades. It is of great importance in astronomy where formation of the planets are due to the collision of small dust grains, also in atmospheric science where aggregation and collision of small drops lead to rain. Another line of research in simulation of particles motion suspended in fluid flows, is in marine biology. Thousands of diversified species can be found in ocean where their feeding and mating patterns and also the mutual effects of species and oceanic flows need precise understanding of the dynamics of these planktonic organisms.

The present study aims to better understand this latter subject by focusing on special plankton species called copepod. The goal is to quantify copepods' dynamics in oceanic turbulent flows through a combined experimental and numerical study. Turbulence is an important factor in the interaction between suspended particles and the surrounding flows. Thus a fundamental understanding of the two-phase flows and the physical processes governing particle-turbulence interactions is needed which shed new light on problems of biological/physical coupling.

Apart form the previous studies on the effect of turbulence on particle transport (Squires and Eaton, 1991; Wang and Maxey, 1993; Squires and Yamazaki, 1995), many studies have been performed to characterize copepods' behavior in the aquatic environment (Strickler, 1975; Alcaraz and Strickler, 1988; Yen and Fields, 1992; Fields and Yen, 1997), however only few recent experimental studies (Waggett and Buskey, 2007; Yen, Rasberry, and Webster, 2008; Moison et al., 2009; Michalec, Souissi, and

Holzner, 2015; Michalec et al., 2015) considered copepods in turbulence with density of copepods lower than the one that can be encountered in the field.
In this study, we will introduce a Lagrangian Copepod (LC) model based on experimental observations to mimic copepods' behavior in turbulent flows. In chapter 2 an introduction on copepods is given in order to understand their geometrical shape, size, living environment, their locomotion and also their interaction with the surrounding fluid from the point of view of a physicist. Mechanism of the copepods' jump, the component of the fluid flow which copepods react to and the recent controversial studies on copepods' dynamics are addressed in this chapter.
Chapter 3 will focus on hydrodynamic turbulence where governing equations of the fluid flows are introduced in the Eulerian framework. Homogeneous isotropic turbulence and basic theory of turbulence are briefly discussed. Moreover the equations of motion of the particles are described in detail from a Lagrangian point of view and direct numerical simulation (DNS) of the Navier-Stokes equations using Fourier Pseudo-spectral method is addressed in this chapter along with all the details of the numerical methods used to perform this study.
Copepods' trajectories from experiment, the experimental set-up and experimental data analysis are addressed in chapter 4 where key parameters are quantified in copepods jumping behavior. The findings from this chapter are used to define and develop a Lagrangian model for copepods' dynamics in turbulent flows.
The interaction of turbulence with copepods and its possible impacts on these microorganisms (growth rate, encounter rate and thin plankton layer formation) are briefly discussed in chapter 5. Previous studies on Lagrangian modeling of particles in fluid flows with focus on active swimmers/phytoplankton are given here, then based on our previous findings the Lagrangian copepod (LC) model is developed and discussed in full detail. The LC model is then tuned to be implemented in turbulence. As a case study, the implementation of the LC model in Taylor-Green Vortex (TGV) flow is presented at the end of chapter 5.
Copepods' behavior is then simulated in turbulence using the LC model and the results of the simulations are presented in chapter 6. Single point

statistics show qualitative agreements with the available experimental observations of Michalec, Souissi, and Holzner (2015). More importantly, small scale patchiness of copepods in turbulent flows as the main feature of the LC model is addressed in this chapter. The effect of particle orientational dynamics and jump latency time on the clustering are presented. The encounter rate of copepods in the presence of turbulence is discussed in chapter 7 where the influence of the clustering on the copepods' contact rate is assessed. A preliminary study of an Eulerian modeling of copepods' dynamics is described as a perspective and the main difficulties are addressed in this chapter.

Chapter 2

Copepods from the standpoint of a physicist

A brief introduction on Plankton with focus on copepods will be given. Copepods' characteristics are described here and the main feature of copepods in their interaction with fluid flow, especially turbulence are recognized. The necessary parameters and unknowns which may play a role in numerical modeling of their behaviour, are assessed.

2.1 Plankton's life

Understanding the plankton's life is essential to discover the entire ecosystem. Plankton are a large number of organisms wandering in the currents. They cover a wide range of size from microscopic viruses to krill and jellyfish. Plankton is a word which refers to microorganisms having limited swimming abilities and have drifting with the currents and flows of environment. Their living pattern is quite different among species; some of these microorganisms spend their entire life as plankton while others only spend their larval stages as plankton. Phytoplankton and microbial plankton generally play an important role in the global carbon cycle. This cycle captures the Sun's energy and the atmosphere's CO_2 at the surface of the ocean and transfers the recycled materials throughout the food web by larger and larger zooplankton (from micro scale to meso scale and macro scale) and also stores it at the bottom of seas. There are basically

Larval stage
The active immature form of an insect

two categories of plankton: zooplankton and phytoplankton. The differences between them can be summarized as follows (Barnes and Hughes, 1999):

- Phytoplankton are plants, while zooplankton are animals.
- Phytoplankton is found on the surface of the water, where there is a lot of sunlight. Zooplankton frequents often but not always, the darker and cooler places in the waters.
- Any visible changes in the amount or type of phytoplankton in the water indicates a change in ocean health.
- Phytoplankton release oxygen through the process of photosynthesis.

It is interesting to know that Photosynthetic plankton organisms account for almost half of global primary production and 90% of primary production in marine ecosystems. Survival of larger zooplankton, fishes, and marine mammals depends on these plankton. For instance, larval fish production depends on matching/mismatching in time with larval food production (*i.e.* plankton) which itself depends on natural factors (current variation such as water temperature and nutrient availability). The production can also be affected by man-made factors (*e.g.*, river dams). Plankton species composition is directly linked to the changes in climate, which can change the feeding pattern of lager plankton such as larval fish and ultimately the entire food web and ecosystem (Ray and McCormick-Ray, 2004).

Primary production The synthesis of new organic material from inorganic molecules such as H_2O and CO_2

Understanding the plankton's life at different depths in the ocean allows scientists to get a global view and better understanding of the marine ecosystem from small to global scales.

2.2 What are Copepods?

Around two thousand years ago, scientists observed copepods, but the word Copepod (Greek word for paddle-footed or oar-footed) was introduced in 1830 by a french zoologist named Henri Milne Edwards

(Damkaer, 2002). Copepods are aquatic, meaning that they can not survive without water. This is the first law of their survival. They are also referred as "insects of the sea". Hopefully they are not annoying as much as real insects but they still can be harmful to human by eating fishes infected by copepods. In this chapter the copepods will be studied mostly in the physical point of view. Their habitats, size range, feeding pattern, anatomy and their interaction with fluid flow will be addressed here. Large number of literature is available on copepods (more than 57,000 publications (Morales, 2016)), however the following relevant information which gives us a good vision to better quantify copepods' dynamics in physical point of view, is extracted from well-known resources, such as *A Mechanistic Approch to Plankon Ecology* a book of Kiørboe (2008), *The copepodologist's cabinet, The biographical and bibliographical history* a book of Damkaer (2002), review of Jiang and Osborn (2004) on copepods' hydrodynamics and many journal articles such as Strickler (1975), Alcaraz and Strickler (1988), Yen and Fields (1992), Fields and Yen (1997), Lenz and Hartline (1999), Kiørboe, Saiz, and Visser (1999), Kiørboe and Visser (1999), Lenz, Hower, and Hartline (2004), Duren and Videler (2003), Buskey, Lenz, and Hartline (2002), Buskey and Hartline (2003), Woodson et al. (2005), and Woodson et al. (2007). More resources and information can be found on *World Association of Copepodologists* (Morales, 2016) and website of *The world of copepod* (Walter and Boxshall, 2016).

2.2.1 Copepod's habitat

Copepods are the most diversified and the largest group of crustaceans that can be found in aquatic environment. They are a group of small zooplankton who live almost everywhere there is a fresh water. They can be found in ocean, sea, lake, rivers, or even in swamps, puddles and also under the leaf fallen on wet forest. Plants growing near the seashores are another habitat for copepods species. Some of copepods species are active in open water while others can live in wet sands or muds. Many of them swim near the surface of the ocean, however copepods can also be found in deep waters around 10,000 meters, or even deeper in undersea

caves. Some species live in extremely salty lakes on earth while some can be found on the slopes of mountains at an elevation of 5,000 meters. Figure 2.1 shows ocean copepod diversity based on temperature, salinity and Chlorophyll a of water (Rombouts et al., 2009).

Chlorophyll a
A form of Chlorophyll which is essential for most photosynthetic organisms

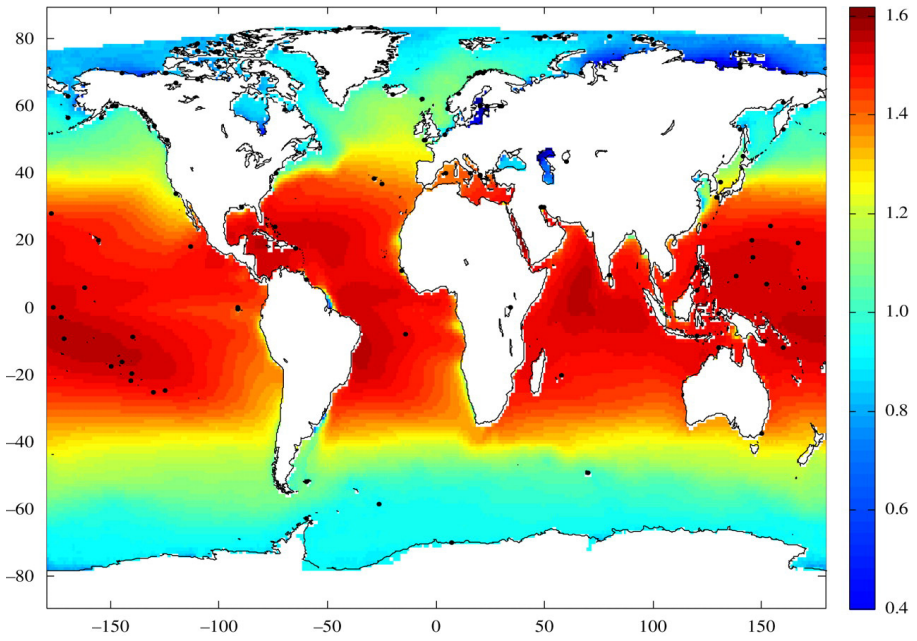

FIGURE 2.1: World ocean copepod diversity. Vertical scale bar represents log of taxonomic richness where taxonomy means defining groups of biological organisms on the basis of shared characteristics (Rombouts et al., 2009).

2.2.2 Copepod's size, population density

These zooplankton (copepods) are visible by unequipped eyes. Their size ranges from 0.2 mm to 10 mm but the typical length of copepods is 1-2 mm. There are different biological classifications of copepods which may not be interesting in physical point of view, however copepods are found in over 250 families, 2,600 genera and the current number of accepted species is $\sim$ 14,638 (Walter and Boxshall, 2016). A very detailed and precise introduction on copepod's classification and their evolution can be found in Huys and Boxshall (1991). Because of their very small size, copepods have no heart and blood vessels (there might be a group with heart but no blood vessels). They absorb oxygen directly into their body and for survival like other species in the world, copepods need to

Size range
0.2 mm to 10 mm

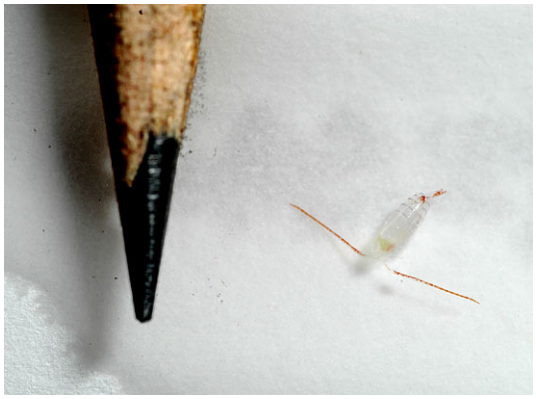

FIGURE 2.2: Calanus glacialis, is kind of copepod with a size of a pencil's tip. Some adults species may be very short (0.2 mm) or very large (10 mm). Photo by Chris Linder, WHOI.

Rotifer
Small ($50 - 1000\,\mu m$) zooplankton that exists in freshwater and marine environments

be fed. This is in fact the second law of survival. Green algae, bacteria, rotifers, tiny insect larvae and other tiny plankton species can be a source of food for the dominant forms of the marine plankton. Copepods may attack larval fishes and even kill a fish when they come in large number. On average 1000 copepods can be found in 1 litre of water. The way copepods capture their food at low Reynolds number was studied in detail by Koehl and Strickler (1981). Copepods can be eaten by other copepods. Fish, leopard frog, aquatic insects and other plankton eaters are other predators of these multicellular animals. Copepods' mass density is assumed to be equal to the one of the fluid ($1\,mg\,mm^{-3}$) meaning that they are considered to be neutrally buoyant (Kiørboe, Jiang, and Colin, 2010). The relationship of copepods in nature (their preys, predators and their shelter) is listed in table 2.1.

Population density
1000 species per 1 litre

2.2.3 Anatomy of copepods

Copepods may differ in shape but generally they possess shrimp-like cylindrical body with four or five pairs of swimming legs, tail and the antennae which are considered as the main parts of their body to swim in fluid flow. Figure 2.3 illustrates different forms of copepods and their diversity. Detailed anatomy of a copepod is illustrated in figure 2.4. Male and female of a the same copepod's family might also have some differences in their anatomy but what is important in the physical point of view

PREY/FOOD	PREDATOR	SHELTER
Green Algae	Creek Chub	Greater Bladderwort
Amoeba	Eastern Mosquitofish	Long-leaf Pondweed
Euglena	Eastern Lamp Mussel	Common Duckweed
Paramecium	Rotifer/American Eel	Lizard's Tail
Water Flea	Ebony Jewelwing	Common Cattail
Asian Tiger Mosquito	Green Darner	Common Reed
Copepod	Golden Shiner	Pickerelweed
Eastern Mosquitofish	Greater Bladderwort	Tussock Sedge
Creek Chub	Largemouth Bass	Buttonbush
Rotifer	Three-lined Salamander	Arrow Arum
Predatory Nematode	Southern Leopard Frog	Yellow Pond Lily
Brainworm Nematode	American Toad	
Flatworm	Eastern Newt	
Green Hydra	Spring Peeper/Copepod	
	Northern Hog Sucker	
	Flatworm/Green Hydra	
	Fragile Forktail	

TABLE 2.1: Relationship of copepods in nature; their prey/food, predators and their shelter. Copepods can be predators of other copepods species (Brandl, 2005).

is the general behaviour of these animals. For a detailed description of copepod's shape diversity and their anatomy comparison one can refer to Boxshall (1985), Hausch, Shurin, and Matthews (2013), and Boxshall (2004).

2.2.4 Copepod's locomotion

Copepods use an array of mechanoreceptive hairs, called setae, on all of their appendages to detect a disturbance in the surrounding environment. Their antennae possess most concentrated sensitive setae which can act as a sensory organ to sense the changes in fluid flow. The disturbance can be produced by the presence of predators (Trager, Achituv, and Genin, 1994), foods (Yen and Strickler, 1996), mates (Duren, Stamhuis, and Videler, 1998), by high turbulent regions in the flow (Fields and Yen, 1997) or by the changes in water quality due to dissolved chemical substances (Moore, Fields, and Yen, 1999) or even by changes in light energy distribution (Fields et al., 2012).

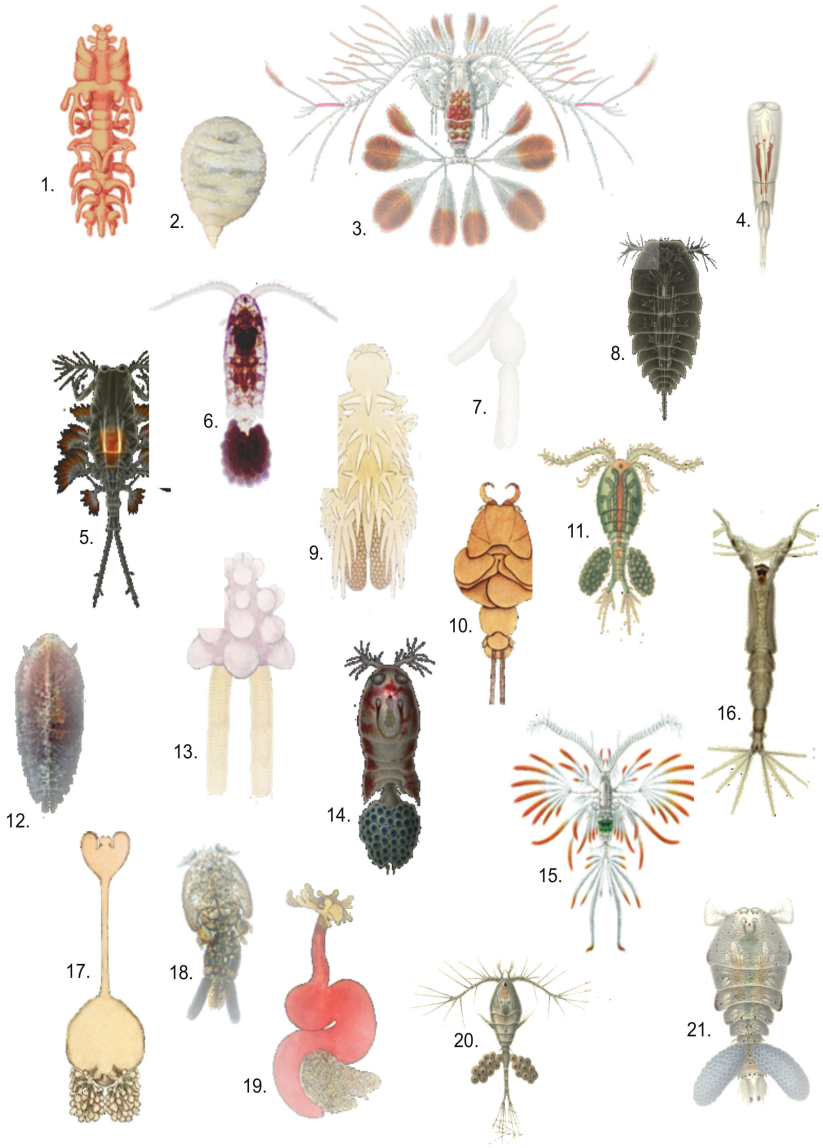

FIGURE 2.3: Diversity of copepod's shape. 1. *Philichthys xiphiae* 2. *Sarcotaces sp*. 3. *Calocalanus pavo* 4. *Farranula rostrata* 5. *Copilia vitrea* 6. *Paracalanus parvus* 7. *Clavella adunca* 8. *Copilia quadrata* 9. *Chondracanthus zei* 10. *Phyllothyreus cornutus* 11. *Acanthocyclops vernalis* 12. *Sapphirina ovatolanceolata* 13. *Chondracanthus ornatus* 14. *Corycaeus obtusus* 15. *Euaugaptilus filigerus* 16. *Monstrilla longispinosa* 17. *Sphyrion lumpi* 18. *Caligus elongatus* 19. *Lernaeocera branchialis* 20. *Oithona nana* 21. *Sapphirina auronitens* (Bron et al., 2011).

The most important feature of copepods is their ability to exhibit a rapid escape in the flow which is often dubbed as a jump. The escape may be elicited by different stimulus, such as photoic (PH), hydrodynamic (HY)

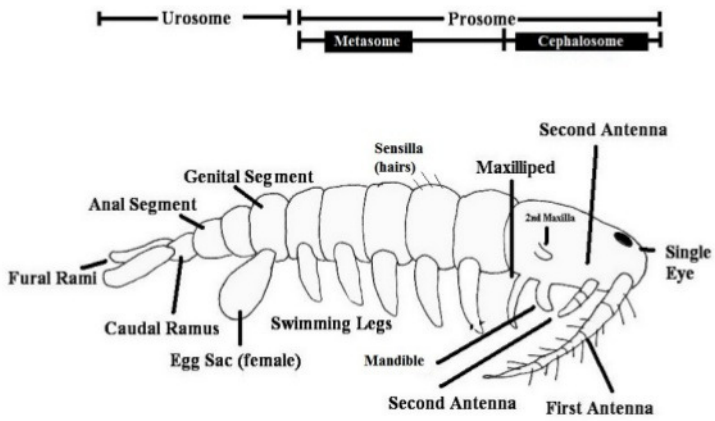

FIGURE 2.4: Anatomy of a parasitic copepod. Normally the body consists of two main parts: the anterior (Prosome) and posterior (Urosome). Each part contains several segments.

stimuli, etc. Due to this quick powerful jump, the hydrodynamics of jumping copepods differ significantly from the one of steady swimming (foraging) copepods (Jiang and Kiørboe, 2011).
Strickler (1975), Alcaraz and Strickler (1988), and Duren and Videler (2003) addressed how copepods use their swimming legs and antennae to perform jumps. They discovered that a jump starts with power stroke followed by return stroke where power stroke consists of the beating of the first antennae and pairs of swimming legs and in the return stroke, the legs move back to their initial position. Reaction time and force production in power stroke were studied in Lenz and Hartline (1999) and Lenz, Hower, and Hartline (2004) while Borazjani et al. (2010) numerically investigated the role of the antennae in force production during jumps. These authors showed that reversible motion of copepod's antennae either in rigid form or in deformable shape has large contribution to force production while jumping. Figure 2.5 shows typical trend of force production during a jump. This quantity is accompanied by several time parameters like latency, rise, preparation, etc which can be found in detail in this figure. Up to now nothing has been reported on the deformation of copepod's shape while performing a jump.

Living in a fluid environment characterised by body-scale Reynolds number up to 1000, copepods are subject to the physics of the flow field both in viscous and inertial regime (Yen, 2000). Body-scale Reynolds

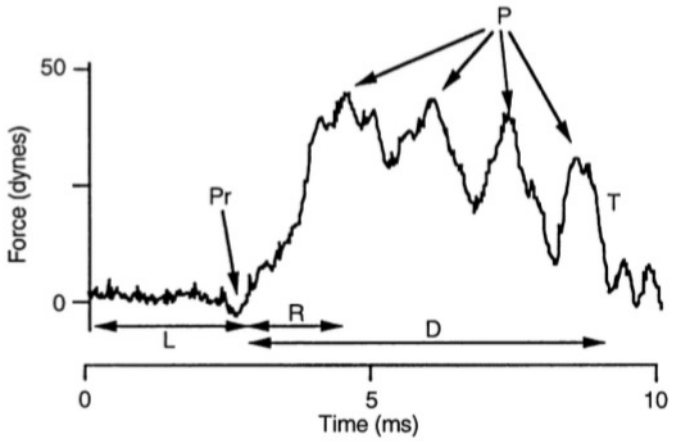

FIGURE 2.5: Force production of *Undinula vulgaris giesbrechti* in response to sinusoidal stimulus as function of time. Jump production is associated with several parameters: *L* latency to forward propulsion; *R* rise; *D* kick duration; *Pr* preparation; *P* force peaks; *T* termination (Lenz and Hartline, 1999).

number (also called particle Reynolds number) in still water is defined as:

$$Re = \frac{vl}{\nu} \tag{2.1}$$

Reynolds number
A dimensionless quantity that is used to help predict similar flow patterns in different fluid flow situations

where v and l are animal's velocity and length respectively and ν is kinematic viscosity of the carrier fluid.

Escape response of copepods which is followed by their interaction with fluid flows is essential for survival of these microorganisms. Their response to different stimulus and also the threshold value to trigger the jumps were assessed in several studies (Yen and Fields, 1992; Duren and Videler, 2003; Buskey, Lenz, and Hartline, 2002; Buskey and Hartline, 2003; Fields and Yen, 1997; Woodson et al., 2005; Woodson et al., 2007). Buskey, Lenz, and Hartline (2002) and Buskey and Hartline (2003) recorded copepod's swimming speed in the presence of light and hydrodynamic stimulus. An example of copepod's response to disturbance can be found in figure 2.6. Buskey, Lenz, and Hartline (2002) and Buskey and Hartline (2003) observed that the nature of the disturbance is important and that copepods respond differently to different stimulus. As illustrated in figure 2.6, copepod's velocity can reach high values like $\sim$ 500 mms^{-1}. This is huge compared to their foraging velocity (also

called cruise) which is of the order of $\mathcal{O}(1)\ mm/s$. This big swimming velocity swings indicates that copepods can sense large range of fluid forces. As mentioned before, copepods are affected either by viscosity (low body-scale Reynolds number, considering $\nu = 10^{-6}\ m^2/s$, $l = \mathcal{O}(1)mm$ and $v = \mathcal{O}(1)\ mm/s$, then $Re \sim 1$) or by inertia ($Re > 100$), thus the body-scale Reynolds number of jumping copepods can be very large ($Re \sim 1000$) compared to foraging copepods.

Copepods produce large acceleration during their jump. *Acartia tonsa*'s acceleration in response to hydrodynamic signal is shown in figure 2.7. Positive acceleration may associate to the power stroke when copepods start their jumps while the return stroke (moving the swimming legs back to initial position) leads to negative acceleration. He also reported that male and female have lots of discrepancy in their escape response, such as response latency time, jump speed, number of thrusts, jumps duration, etc. One can extract lots of information about copepods from table 2.2 which has listed these differences. Response latency time for the light disturbance is much more than the hydrodynamic one, also males make quick powerful jumps with more thrusts whilst females have less velocity and acceleration but spend more time and go through more distance to escape from the disturbance.

Parameter	Male		Female	
	PH	HY	PH	HY
Response latency (ms)	62.2	3.6	68.2	3.5
Initial turn (deg)	74.1	82.1	41.3	45.9
Jump speed ($mm\,s^{-1}$)	293	213	256	188
Maximum speed ($mm\,s^{-1}$)	294	432	446	372
Max. acceleration ($mm\,s^{-2}$)	128	163	93	112
Number of Thrusts	4.9	3.1	7.5	3.3
Minimum speed between thrusts ($mm\,s^{-1}$)	147	166	130	133
Thrust duration (ms)	8.1	6.1	8.8	6.6
Jump duration (ms)	44.5	19.3	74.6	24.1
Distance jumped (mm)	8.6	4.2	12.5	4.6

TABLE 2.2: Comparison of mean escape response parameters for adult males and adult females of *Acartia tonsa* stimulated with photoic (PH) or hydrodynamic (HY) stimulus. Data are from table 2 of Buskey and Hartline (2003).

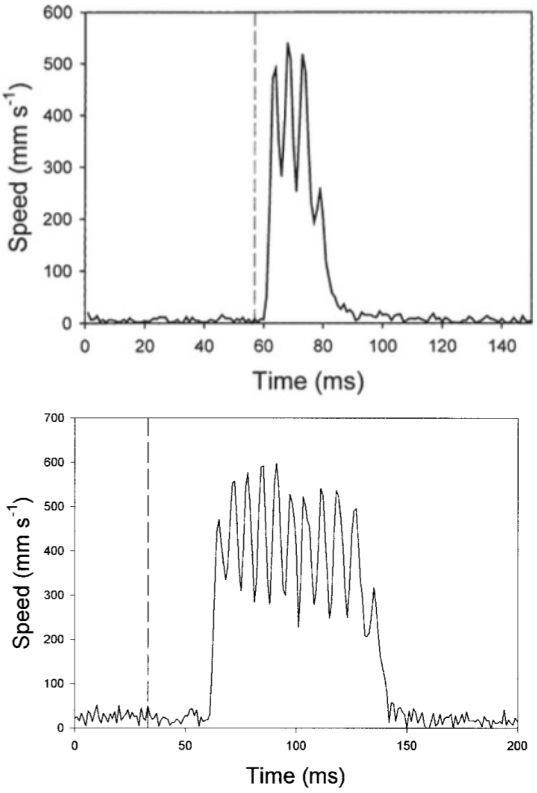

FIGURE 2.6: Example of *Acartia tonsa*'s escape response to photoic and hydrodynamic disturbances. Top: response of adult male to hydrodynamic signal (Buskey, Lenz, and Hartline, 2002). The stimulus occurred 3 ms before the initiation of the escape response (dashed line). Bottom: response of adult female to light stimulus (Buskey and Hartline, 2003). The copepod was adapted to a light intensity of 100 μmol photons $m^{-2}s^{-1}$ and subjected to a 100% decrease in light intensity. Dashed line represents the beginning of light intensity decrease.

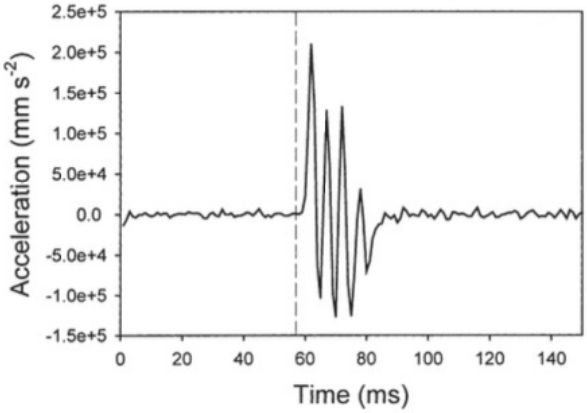

FIGURE 2.7: Acceleration of *Acartia tonsa* in response to hydrodynamic disturbances. Dashed line represents the beginning of the stimulation (Buskey and Hartline, 2003).

Copepods escape from danger by exhibiting rapid jumps through the locomotion of their swimming legs. Effectiveness of this jump is associated to many parameters, *i.e.,* how far from a disturbance or how fast a copepod is and in which direction this organism escapes. Several studies showed that copepods have different jumping behavior confronting different stimulus (Buskey, Lenz, and Hartline, 2002; Buskey and Hartline, 2003). The jump direction of males and females also differs. Figure 2.8 represents different jump direction of copepods male and female (*Acartia tonsa*) in response to hydromechanical disturbance. Buskey, Lenz, and Hartline (2002) revealed that escape often begins with rapid reorientation from the source of the disturbance with maximum turning rate of $\sim 30^\circ\, ms^{-1}$ and the overall jump direction distribution is upward or lateral.

2.2.5 Interaction with the flow

Basic question remains open here; what copepods sense facing the fluid flow disturbance in order to execute this rapid jump escape and which characteristics of the flow stimulate them to jump. The detected signals by copepods are from velocity gradient, but one has to quantify all the

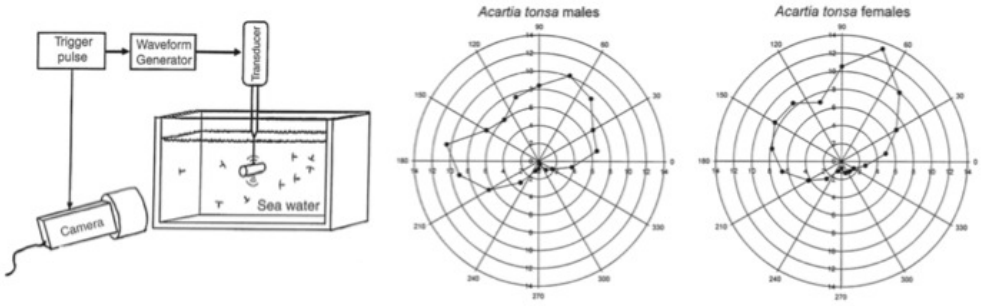

FIGURE 2.8: Experimental set up of Buskey, Lenz, and Hartline (2002). A trigger pulse stimulates a piezoelectric transducer to produce hydrodynamical disturbance. The same pulse drives a camera. Jump direction of male (middle) and female (left) *Acartia tonsa* is recorded.

quantities which are comprised of spatial gradient of the velocity components in the fluid flow. These quantities can be shear rate, vorticity, acceleration, etc. Many scientists tried to identify the component of the flow which elicits escape response of copepods (Singarajah, 1969; Singarajah, 1975; Landry, 1978; Landry and Gilbert, 1988; Fields and Yen, 1997; Fields and Yen, 1996; Haury, Kenyon, and Brooks, 1980). Among them comprehensive studies of Kiørboe, Saiz, and Visser (1999), Kiørboe and Visser (1999), Woodson et al. (2005), and Woodson et al. (2007) are of great importance. In 1999, Kiørboe, Saiz, and Visser (1999) and Kiørboe and Visser (1999) performed series of experiments, investigating the effect of non uniform flow motion on copepods. In order to find the component of the flow which copepods react the most to, the copepods were put into a time dependent siphon flow, in an oscillating chamber, in a couette device, and finally in a rotating cylinder.

A suction device submerged in fluid, produces velocity gradient which is a pure longitudinal deformation. It will accelerate the fluid flow but there would be no vorticity and no shear deformation. By noting the distance at which copepods (*Acartia tonsa*) react to the siphon flow, Kiørboe estimated the response threshold for longitudinal deformation rate and acceleration. Copepods were put in an oscillating chamber where they experience only acceleration. In couette device which consists of two cylinders, one inside the other, velocity gradient perpendicular to the direction of the flow exists and by rotating one or both of the cylinders, copepods will face

combination of pure shear deformation, vorticity and acceleration. Eventually to make copepods face pure vorticity, these animals were put in a rotating cylinder. Fluid inside the cylinder can rotate as a solid body after a short time, which generates only the vorticity inside the cylinder. The conclusion of this study was that copepod's species (*Acartia tonsa*) react to the flow deformation rate. The threshold value of the deformation rate to trigger a response is size dependent and is about $\sim 0.4\,s^{-1}$ for a copepod with $1\,mm$ in length in siphon flow. The threshold increases for smaller copepods. Sensitivity to strain rate (velocity gradient) was reported to be $\sim 0.025\,s^{-1}$ by Woodson et al. (2005) and Woodson et al. (2007) by putting copepods species (*Acartia tonsa* and *Temora longicornis*) in a plane jet flume apparatus which mimics ocean characteristics.

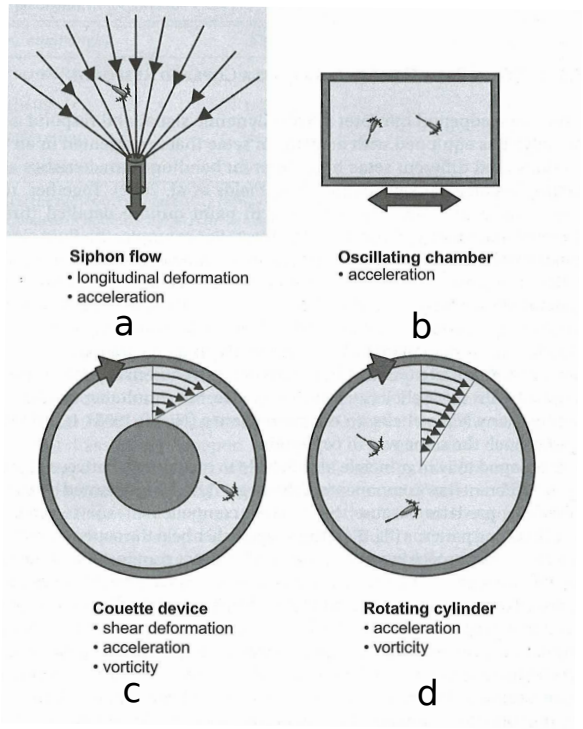

FIGURE 2.9: Hydrodynamic devices used by Kiørboe to examine copepod's (*Acartia tonsa*) response to different components of a fluid disturbance. a) Siphon flow with pure longitudinal deformation and acceleration, b) Oscillating chamber with acceleration, c) Couette device with shear deformation, acceleration and vorticity, d) Rotating cylinder with acceleration and vorticity (Kiørboe, 2008).

Kiørboe also reported (Kiørboe, 2008) that there are two threshold values of the deformation rate: the upper one, around $10\,s^{-1}$, corresponds to

either the presence of a predators or to a region where turbulence intensity is high, and the lower one, $1\,s^{-1}$, corresponds to regions in the flow where turbulence intensity is lower or food abundance is not enough for copepods. These tiny crustaceans find themselves at ease in regions in between these two thresholds.

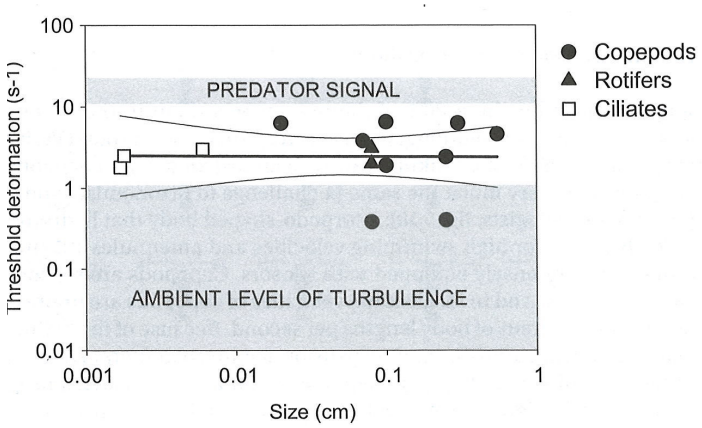

FIGURE 2.10: Two threshold values of the deformation rate to elicit escape response of organisms as a function of their size (Kiørboe, 2008).

Although it was believed that copepods react to deformation rate for long time, recently Webster, Young, and Yen (2015) examined the behavioral response of *Acartia tonsa* and *Temora longicornis* in turbulent vortex. They put copepods in Burger vortex apparatus (Fig. 2.11) which mimics flow characteristics of isotropic turbulence with simple vortex model. What he observed is interesting since *Acartia tonsa* reacts to vorticity but *Temora longicornis* does not show any reaction to turbulent level variation. This result may indicate that different species react differently to fluid flow and the component of the flow which can stimulate the response, is not the same for different species. However the fact that *Acartia tonsa* reacts to vorticity is in contradiction to previous results of Kiørboe, Saiz, and Visser (1999) and Kiørboe and Visser (1999) and also Woodson et al. (2005) and Woodson et al. (2007).

In the last two decades many studies have been conducted to quantify the dynamics of copepods. Most of them focused on their behaviour in still water (Lee et al., 2011; Souissi et al., 2010; Schmitt and Seuront, 2008), while less studies have studied the copepods dynamics in their natural

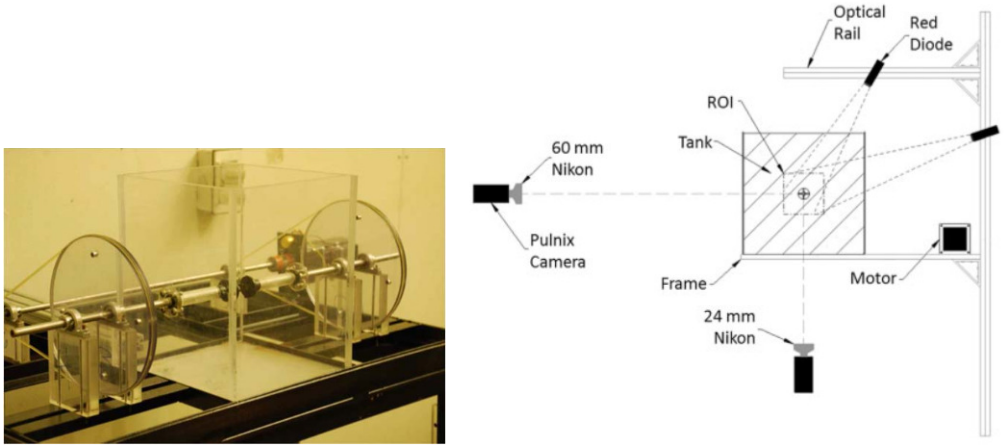

FIGURE 2.11: Experimental set up and schematic of the camera and lighting arrangement (from side perspective), as well as the region of interest (ROI) surrounding the Burgers' vortex (Webster, Young, and Yen, 2015).

living environment because of the difficulties of such experimental investigations. Few works have been devoted to the dynamics of copepods in turbulent flows (Moison et al., 2009; Waggett and Buskey, 2007; Yen, Rasberry, and Webster, 2008; Michalec, Souissi, and Holzner, 2015; Michalec et al., 2015). However, the densities of copepods used in these studies are often lower than the maximum densities that can be encountered in the field.

The experiment of Moison et al. (2009) cannot reproduce in laboratory real turbulence conditions which is observed in-situ; however in order to approach realistic situations where the intensity of turbulence can be variable in time at a given location, their experiment has focused on the consequences of alternation of hydro dynamically stable but very different environments. The conclusion is that copepods' behavior are affected greatly by turbulence. Waggett and Buskey (2007) performed similar study to Kiørboe, Saiz, and Visser (1999) by putting copepods species (*Paracalanus parvus* and *Temora turbinata*) in turbulent siphon flow and reported deformation rates of $6.16\,s^{-1}$ and $3.93\,s^{-1}$ for *P. parvus* and *T. turbinata* respectively. Copepod species vary in their response threshold value but several values reported for a single species (*Acartia tonsa*) is believed by Waggett and Buskey (2007) to be due to the culture of copepods, since wild copepods and cultured copepods respond to different level of deformation rate. Yen, Rasberry, and Webster (2008) quantified copepods

kinematics in laboratory turbulence. This study shows that copepods can control their motion in low turbulent flows whilst at higher turbulence intensity, their movement is dominated by fluid flow motion. 3D particle tracking velocimetry (PTV) method was used by Michalec, Souissi, and Holzner (2015) in homogeneous isotropic turbulence to reconstruct the trajectories of *Eurytemora affinis*. Their findings are in accordance with the one of Yen, Rasberry, and Webster (2008), that copepods adjust their behaviour and swimming effort according to the background flow. The experimental set-up of their study is shown in figure 2.12.

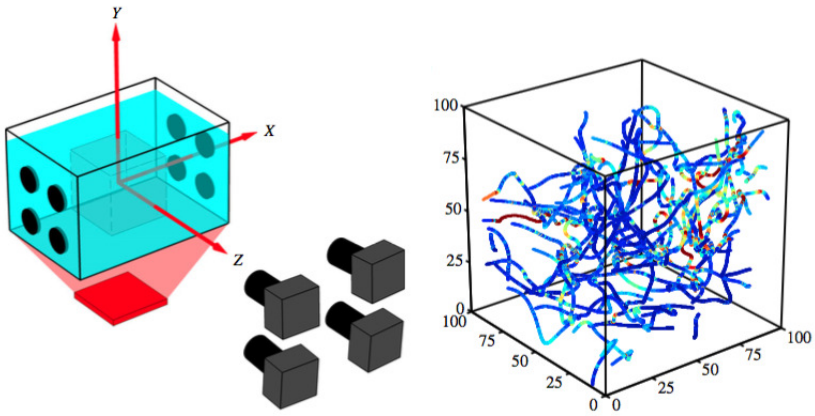

FIGURE 2.12: Sketch of the experimental set-up by Michalec, Souissi, and Holzner (2015). Four cameras are located around 50 cm away from the centre of the coordinate system and are angled on an experimental volume (shown as a dashed line cube) located in the middle of the aquarium. Turbulence is generated via eight counter-rotating discs located on the side of the aquarium and illumination is provided by an infrared diode array mounted beneath the aquarium. Trajectories of male species is shown in the right side (Michalec, Souissi, and Holzner, 2015).

2.2.6 Copepod's role in nature

Copepods can be free-living organisms or even be either direct or intermediate host for parasites. Infected copepods may be dangerous for human life. Human can receive these parasites by eating infected fishes, or even by drinking water containing infected copepods. It has been shown that copepods can be a carrier of cholera (Damkaer, 2002).
However copepods are not always dangerous. They can be beneficial to

human life. They are important to global ecology and to the carbon cycle (Frangoulis, Christou, and Hecq, 2005; Satapoomin, 1999; Jonasdottir et al., 2015). Although copepods are not at the top of the food web, they have a major role in the marine ecosystem because they are the secondary producers in the ecological food web, linking phytoplankton cells (the primary producers) to fish larvae and even to large mammals such as whales. To picture the food web, phytoplankton are the primary carbon producers on earth. Then in the second level, zooplankton feed on phytoplankton while they will be eaten by larger organisms like fishes. Copepods also consume the mosquito larvae, acting as control mechanism for malaria (Walter and Boxshall, 2016). They are of great importance in fishery industry. A central issue in breeding fish species, is the external food supply. Most fishes prefer copepods to other zooplankton species (*i.e.* rotifers) and they grow bigger in shorter time on a diet of copepods (Theilacker and Kimball, 1984; Souissi, Souissi, and Hansen, 2014).

Moreover the aggregation of phytoplankton and zooplankton which is known mostly as Thin Phytoplankton Layer (TPL), has drawn the attention in last four decades (Dekshenieks et al., 2001; Benoit-Bird, Cowles, and Wingard, 2009; Durham and Stocker, 2012). Planktonic microorganisms form a layer with a vertical thickness up to few centimeters and a length of kilometers. This layer can change ocean light distribution, which itself affects the feeding pattern and habitat of other species in the ocean. This extraordinary concentration of different species in aquatic environment can also change the primary production and mating rate of copepods.

Thin Layer
Aggregation of planktonic microorganisms in the ocean

Chapter 3

Hydrodynamic Turbulence

Governing equations of fluid flows (Eulerian approach), also the equation of motion for particles (Lagrangian approach) are described in this chapter. The numerical method employed to simulate the oceanic homogenous isotropic turbulence is presented.

3.1 Eulerian point of view

As discussed in chapter 2, it is clear that the biggest habitat of this microorganisms are oceans where the flow field is rarely laminar but often is turbulent. To describe the motion of fluids, there are two mathematical representations of fluid flow. The first is the Eulerian approach, using a fixed referential, where the fluid motion is studied in a specific location through which the fluid passes over the time. Eulerian approach can be used to have clearer idea of the fluid flow at one particular moment. One can visualize the entire domain by means of streamlines, *i.e.*, representing tangent to the local velocity vector. The velocity field in Eulerian coordinate system can be expressed as $\mathbf{u}(\mathbf{x}(t), t)$, to be a function of space and time. Other properties of fluid flow such as density, pressure, temperature, mass, etc can also be represented as a function of fixed position and time as the one of the velocity.
The Lagrangian approach is another representation of fluid flows where individual particles are followed over time and space: the referential is moving with the fluid parcel. This is to be discussed later in more detail.

3.1.1 Governing equations of fluid flow

Oceanic mixed layers and intense oceanic currents are good examples of turbulence. Almost all of the fluid flows in nature are turbulent and they are characterised by dimensionless quantity which is termed Reynolds number (Re). This number is defined as the ratio of inertial to viscous forces,

$$Re = \frac{\mathrm{u}L}{\nu} \tag{3.1}$$

with fluid velocity amplitude u, characteristic length L and kinematic viscosity ν, which indicates how turbulent a flow is (Batchelor, 1967). When inertial forces are dominant, chaotic eddies and instabilities are produced and the flow becomes turbulent.

Continuum approach is used to describe the equations of motion where the fluid is characterized by large number of individual molecules. Knudsen number which is a ratio of molecular mean free path λ and physical length scale L_{phys},

Knudsen number The ratio of the molecular mean free path length to a representative physical length scale

$$Kn = \lambda / L_{phys} \tag{3.2}$$

shows to what extent the continuum mechanic formulation of fluid dynamics can be used.

The equations describing the motion of viscous fluids are the Navier-Stokes equations, which can be obtained by applying the Newton's second law of motion for fluids and in incompressible condition can be written as:

$$\rho(\partial_t \mathbf{u} + \mathbf{u} \cdot \nabla \mathbf{u}) = -\nabla p + \mu \Delta \mathbf{u} + \boldsymbol{f} \tag{3.3}$$

where $\mathbf{u}(\mathbf{x}(t), t)$ is the fluid velocity field, $p(\mathbf{x}(t), t)$ is the pressure, $\mu = \rho\nu$ is the dynamic viscosity and ρ is the fluid density that is assumed to be constant due to incompressibility. The $\boldsymbol{f}$ is the external forces which are applied to the fluid (Batchelor, 1967). What causes turbulence is the non-linear term in this equation ($\mathbf{u} \cdot \nabla \mathbf{u}$), when it becomes large enough compared to the viscous term ($\mu \Delta \mathbf{u}$). Continuity equation:

$$\nabla \cdot \mathbf{u} = 0 \tag{3.4}$$

which implies the conservation of mass is always solved together with Navier-Stokes equations, representing the conservation of momentum.
Because of the complexity of Navier-Stokes equations, finding an analytical solution of these equations has been an interesting challenge to mathematicians over the past decades, however under certain limitations, *i.e.*, flow between two parallel plates, analytical solution of the equations can be obtained. In more complex situations and geometries, the Navier-Stokes equations have to be solved numerically.

3.1.2 Homogeneous and isotropic turbulence

Homogeneous Isotropic Turbulence
An idealized state where the turbulent flow has two properties, statistically isotropic and statistically homogeneous

High intermittency and irregular characteristics of turbulence make it complicated so that it is not possible to solve the Navier-Stokes equations analytically and after a century of concerted efforts, there is no unique theory of turbulence. Homogeneous Isotropic Turbulence (HIT) is the most idealized form of turbulence and the classic one which can be found in nature at sufficiently small scales, however experiences show that behavior of natural turbulence is not far from the idealized form.
First we clarify the terms *homogeneous* and *isotropic*, then we explain why this kind of turbulence is interesting for researchers.
It is often convenient to express the velocity in turbulence as:

$$\mathbf{u}(\mathbf{x},t) = \langle \mathbf{u}(\mathbf{x},t) \rangle + \mathbf{u}'(\mathbf{x},t) \tag{3.5}$$

This is called Reynolds decomposition (Tennekes and Lumley, 1972) where $\langle \mathbf{u}(\mathbf{x},t) \rangle$ implies mean value of velocity (mean velocity):

$$\langle \mathbf{u}(\mathbf{x},t) \rangle = \frac{1}{T} \int_t^{t+T} \mathbf{u}(\mathbf{x},t) dt \tag{3.6}$$

Turbulent kinetic energy
The kinetic energy per unit mass associated with eddies in turbulent flow

and $\mathbf{u}'(\mathbf{x},t)$ represents fluctuating components of the flow velocity where $\langle \mathbf{u}'(\mathbf{x},t) \rangle = 0$. Turbulent kinetic energy (TKE) which is a measure of the intensity of turbulence is written as:

$$K = \frac{1}{2} \left(\langle u'^2 \rangle + \langle v'^2 \rangle + \langle w'^2 \rangle \right) \tag{3.7}$$

which can be produced by internal or external forces in fluid flows (Tennekes and Lumley, 1972). Similarly mean kinetic energy (MKE) can be defined by considering the mean velocity values instead of the fluctuating velocities.
A turbulent flow is statistically *homogeneous* if:

- Spatial gradient of any averaged quantity is zero.

In other words, a flow is said to be homogeneous if the statistics of the flow is independent of space. We call this translational invariance.
The term statistically *isotropic* is given to a flow when:

- Mean flow does not exist. Non-zero mean flow with orientation may cause anisotropy in turbulence.
- Buoyancy and rotation are negligible, since these forces act as a barrier against vertical motions which lead to anisotropy in turbulent flows.

It is equivalent to say that homogeneous isotropic turbulence is a flow in which statistics of the flow are temporally stationary or decaying from an initial condition, uniform in space without a preferential direction and also without any effects of boundaries. Note that homogeneous turbulence is statistically invariant under translation, for example,

$$\langle u'^2(\mathrm{x})\rangle = \langle u'^2(\mathrm{x}+r)\rangle \quad \forall \mathrm{r} \in \mathbb{R}^3 \tag{3.8}$$

while isotropic turbulence is statistically invariant under rotation and reflection of the coordinate system, for instance,

$$\langle u'^2(\mathrm{x})\rangle = \langle v'^2(\mathrm{x})\rangle = \langle w'^2(\mathrm{x})\rangle \tag{3.9}$$

satisfies the statistical invariance under counter-clock wise rotation of 90°.
In order to keep the flow isotropic under arbitrary rotations, the derivatives of these quantities in corresponding normal directions need to be equal as well.

$$\frac{\partial\langle u'^2\rangle}{\partial x} = \frac{\partial\langle v'^2\rangle}{\partial y} = \frac{\partial\langle w'^2\rangle}{\partial z} \tag{3.10}$$

One should bear in mind that isotropy requires homogeneity, but the opposite is not valid.
Homogeneity in space allows using periodic boundary conditions which provides a condition to study the turbulence in a fraction of space, nevertheless, to obtain real turbulence, the scale of the domain must be large enough compared to the motion of interest ($L_{BOX} \gg l$ where l is the integral scale or size of the large eddies). In addition, mathematical description and the solution of the equations of motion of the fluid flows becomes simpler by taking into account the homogeneous approximation. It is indeed simplified by considering isotropic approximation which together with homogeneity allow some analysis of turbulence dynamics.
Fig. 3.1 represents the velocity magnitude for statistically homogeneous isotropic turbulence performed by direct numerical simulation (DNS).

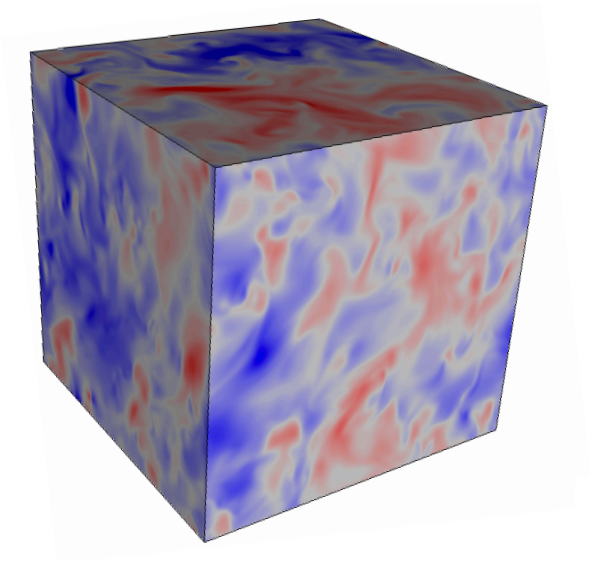

FIGURE 3.1: DNS of statistically homogeneous isotropic turbulence. Contours show the velocity magnitude at $Re_\lambda \sim 125$. The solution domain is a cube of length $L = 2\pi$ with $N^3 = 512^3$ grid points.

3.1.3 Energy cascade and Kolmogorov theory

More than 500 years ago Leonardo da Vinci, recognized turbulence. He used a term *turbolenze* for this behavior of the fluid flow and observed that

turbulence is composed by many eddies of different size. The concept of energy cascade was first introduced by Lewis F. Richardson (Richardson, 1922) in 1922 with his famous verse:

> Big whirls have little whirls
> that feed on their velocity,
> And little whirls have lesser whirls
> and so on to viscosity

and was developed by Kolmogorov in 1941 (Kolmogorov, 1991a; Kolmogorov, 1991b).

FIGURE 3.2: Leonardo da Vinci's drawing of turbulence (Zollner, 2004).

The idea is that large scale eddies contain energy which is injected by an external force. These eddies are unstable and eventually will break up into smaller eddies and this process will be repeated for the smaller eddies. So the energy will be transferred from large scale eddies to smaller ones until it reaches to very small length scale where viscosity is able to dissipate the kinetic energy into internal energy. The whole process is known as *turbulent cascade* which is represented in the cartoon in figure 3.3.

In order to have steady state turbulence, energy must be added at large scales, otherwise the total kinetic energy will gradually decay through the cascade process.

Are there any universal aspects of turbulence? This is a question which remained unanswered until 1941, when Kolmogorov made 3 hypothesis on Richardson's findings. He supposed that for very high Re number, the

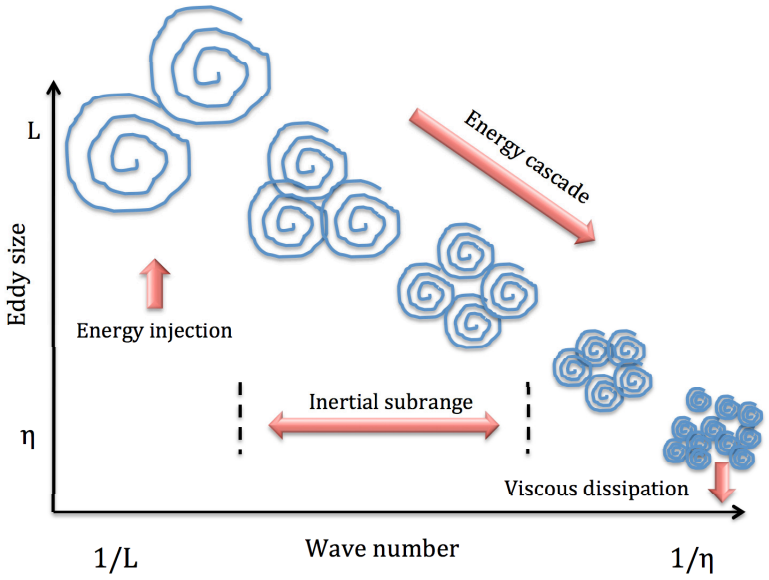

FIGURE 3.3: Richardson's turbulent cascade. Energy-containing eddies break up into smaller eddies and energy is transferred until it is dissipated by viscosity.

turbulent motions of eddies much smaller than energy-containing or forcing scales, are statistically isotropic, in other words are independent of the motions of large eddies. In reality the motions of large scale eddies (L), can be inhomogeneous and anisotropic but in the cascade the information is lost so that the motion of very small scale can be locally homogeneous and isotropic.

The second hypothesis of Kolmogorov was that at very high Re number the statistics of these small scale turbulent motions are independent from large scales and characterized by the kinematic viscosity (ν) and the average rate of dissipation of turbulence kinetic energy per unit mass (ϵ). By means of dimensionless analysis, Kolmogorov scales were introduced as follows:

Energy dissipation, ϵ The average rate of dissipation of turbulence kinetic energy per unit mass

$$\eta = \left(\frac{\nu^3}{\epsilon}\right)^{1/4} \tag{3.11}$$

$$u_\eta = (\nu\epsilon)^{1/4} \tag{3.12}$$

$$\tau_\eta = \left(\frac{\nu}{\epsilon}\right)^{1/2} \tag{3.13}$$

where η is Kolmogorov length scale, u_η is Kolmogorov velocity scale and τ_η is Kolmogorov time scale.
Therefore, turbulence exists over a wide range of vortex size from L to η (Inertial range). Energy injection takes place at large scales while energy dissipation occurs at dissipative scale (Kolmogorov scale). When Re number is high, the two scales can differ by several order of magnitude. What happens at scales between these two ($\eta \ll l \ll L$) where l is larger than dissipative scale and still smaller than large scales? From Kolmogorov's second hypothesis, viscosity cannot play a role in dissipating energy since at this point, the scale of an eddy is much larger than η and in fact energy is just transferred to smaller scales.
Third hypothesis of Kolmogorov was that the statistics of a scale in range $\eta \ll l \ll L$, are determined by the rate of energy dissipation (ϵ) and the scale (l) itself. This intermediate region is called *inertial range*, since the inertial forces are still dominant here compared to the viscous forces.
The rate at which energy (per unit mass) is passed down the energy cascade from the largest eddies is:

$$\Pi \sim \frac{u^2}{L/u} = \frac{u^3}{L} \tag{3.14}$$

In case of statistically steady conditions, this must match exactly the rate of dissipation of energy at the smallest scales, otherwise there would be an accumulation of energy at some intermediate scales (Paladin and Vulpiani, 1987; Davidson, 2004). The rate of dissipation of energy at the smallest scales is:

$$\epsilon \sim \nu \mathcal{S} : \mathcal{S} \tag{3.15}$$

where $\mathcal{S}$ is the rate of strain associated with the smallest eddies (to be discussed later), $\mathcal{S} \sim u_\eta/\eta$. This yields:

$$\epsilon \sim \nu(\frac{u_\eta^2}{\eta^2}) \tag{3.16}$$

Since the dissipation of turbulent energy ϵ, must match the rate at which energy enters the cascade, Π, we have:

$$\frac{u^3}{L} \sim \nu(\frac{u_\eta^2}{\eta^2}) \tag{3.17}$$

We also know that Re based on u_η and η is of order unity, therefore combining these expressions we find:

$$\eta \sim LRe^{-3/4} \tag{3.18}$$

Taylor Reynolds number
A turbulence Reynolds number calculated based on the Taylor microscale

Taylor-scale Reynolds number Re_λ is another dimensionless parameter and analogous to eq. 3.1, it is written as $Re_\lambda = u_{rms}\lambda/\nu$ (Taylor, 1938). Here u_{rms} indicates root mean square velocity fluctuation and is equal to $u_{rms} = \sqrt{\langle u'^2\rangle + \langle v'^2\rangle + \langle w'^2\rangle}$ and

$$\lambda = \frac{\langle u_i^2\rangle^{1/2}}{\langle(\partial u_i/\partial x_i)^2\rangle^{1/2}} \tag{3.19}$$

here u_i^2 can be substituted by u^2,v^2 or either w^2, according to eq. 3.9. It is more common to use Re_λ instead of Re in turbulence research to compare the strength of turbulent flows. Moreover Re_λ makes use of a scale which is independent of the size of the domain.

Oboukov (1941) took advantage of Taylor's introduction of Fourier transforms and power spectra in turbulence and expressed length scales as wave numbers by choosing $k = 2\pi/l$, so that energy is transferred to large wave numbers where it is dissipated. Thus the time scale characteristic of interaction at large wave numbers must be very much smaller than the time scale of the energy-containing eddies.

Velocity correlation tensor for the turbulent velocity is defined in the following manner:

$$R_{ij}(r) = \left\langle \mathrm{u}_i'(\mathrm{x})\mathrm{u}_j'(\mathrm{x}+r)\right\rangle \tag{3.20}$$

Since the turbulent velocity field is homogeneous and isotropic (by assumption), the correlation tensor is a function only of the distance r between the two points and not on their location x within the velocity field. Because turbulence exists with a range of eddy sizes, it is frequently convenient to take the Fourier transform of the velocity field in order to

consider the Fourier components of different wavenumber. The Fourier transform of the velocity correlation tensor is the energy spectrum tensor:

$$\Phi_{ij}(k) = \frac{1}{(2\pi)^3} \int \mathrm{u}'(r) e^{-ikr} d^3 r \tag{3.21}$$

The spectrum $\Phi_{ij}(k)$ tells how much kinetic energy is contained in eddies with wavenumber k (Davidson, 2004). In a homogeneous isotropic turbulent flow, it is possible, and also useful, to define an energy spectrum function $E(k)$ such that:

$$E(k) = 2\pi k^2 \sum_i \Phi_{ii}(k) \tag{3.22}$$

The total turbulent kinetic energy per unit mass is then:

$$\frac{1}{2}\langle u_i u_i \rangle = \int_0^\infty E(k) dk \tag{3.23}$$

where $< . >$ indicates an ensemble average and the rate of energy dissipation can be written as:

$$\epsilon = 2\nu \int_0^\infty k^2 E(k) dk \tag{3.24}$$

Since the dimension of $E(k)$ is $L^3 T^{-2}$, one can write a relation between energy spectrum, rate of dissipation and wave number using dimensionless analysis:

$$E(k) = C\epsilon^{2/3} k^{-5/3} \tag{3.25}$$

where C is a constant (Davidson, 2004). This equation is known as Kolomogorov-Obukhov's 5/3 law, indicating the energy spectrum at single wave number in the inertial range, which is also shown in figure 3.4.

3.2 Lagrangian point of view

Keeping track of individual particles in fluid flow and determining their properties as they move in time, is another way of looking to the fluid which is called Lagrangian approach. Fluid flow properties, for instance

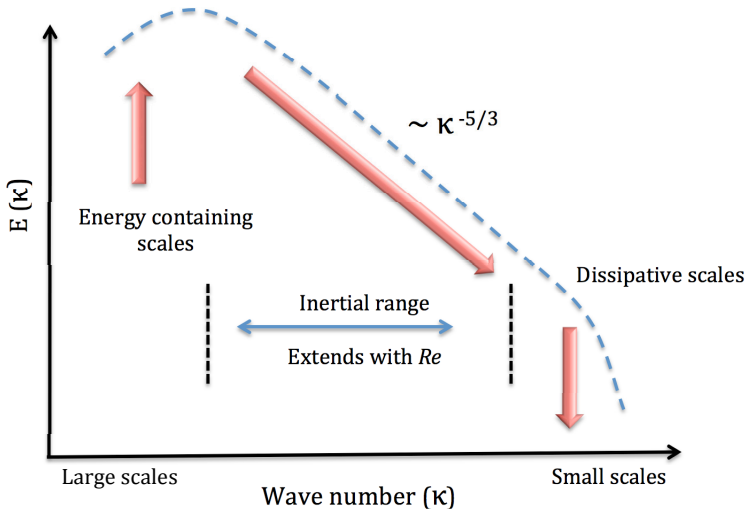

FIGURE 3.4: Turbulent energy spectrum and Kolmogorov-Obukhov's 5/3 law.

velocity can be written as $\mathbf{u}(\mathbf{x}_0, t)$ where $\mathbf{x}_0$ refers to the initial position of a particle, or even simply by $\mathbf{u}(t)$, suggesting that one can obtain the velocity of a particle at some time t, after the particle was released. The trajectories of a followed particle is called pathline, on which the coordinate system is installed and advances in time unlike the Eulerian approach where the coordinate system is fixed.

For steady flows where the velocity is just a function of space ($\mathrm{u}(\mathrm{x}, t) = \mathrm{u}(\mathrm{x})$), Eulerian and Lagrangian approaches are the same and it does not matter if one follows a particle or watch the flow from a fixed position in space through the time. Pathlines and streamlines are the same in this special case.

It is possible to rewrite the equations which is written in Lagrangian framework, in Eulerian frame of reference as well. Let us consider a property like velocity which is $\mathbf{u}(\mathbf{x}, t)$ or more precisely $\mathbf{u}(\mathrm{x}(t), \mathrm{y}(t), \mathrm{z}(t), t)$, since position of a particle changes in time. Rate of change of a quantity for a point in Lagrangian frame of reference is shown as D/Dt and it is called material derivative or substantial derivative which can be written

Material derivative
The time derivative for a moving fluid particle

as (Batchelor, 1967):

$$\begin{aligned} \frac{D\mathbf{u}}{Dt} &= \frac{\partial \mathbf{u}}{\partial t} + \frac{\partial \mathbf{u}}{\partial x}\frac{\partial \mathrm{x}}{\partial t} + \frac{\partial \mathbf{u}}{\partial y}\frac{\partial \mathrm{y}}{\partial t} + \frac{\partial \mathbf{u}}{\partial z}\frac{\partial \mathrm{z}}{\partial t} \\ \frac{D\mathbf{u}}{Dt} &= \frac{\partial \mathbf{u}}{\partial t} + \mathbf{u}\cdot\nabla\mathbf{u} \end{aligned} \tag{3.26}$$

This equations relates Eulerian and Lagrangian approaches indicating that Lagrangian rate of change is equal to Eulerian rate of change plus convective rate of change of a quantity.
Lagrangian approach is of great importance in studies where transport and dispersion of particles are point of interests, such as oceanography, atmospheric science and dispersion of air pollutants, etc. It is also practical in experimental studies of fluid flows where properties of the flow can be obtained by using tracer particles.

3.2.1 Tracers

Fluid tracers are Lagrangian particles which allow the flow to be followed in a Lagrangian way. Tracking the evolution of the flow with time and recording the history of an individual particle can be obtained by using these particles which are also called passive tracers, *e.g.*, polystyrene with diameter of $\phi = 10\mu m$ which is used in Particle Image Velocimetry (PIV) methods.

Particle Image Velocimetry
A non-intrusive laser optical measurement technique for research and diagnostics into flow, turbulence, microfluidics, spray atomization and combustion processes

Such particles in general are carried by the flow without having any effect on the flow field, while the motion of inertial particles, to be discussed, is affected by several forces and the flow field is subjected to changes due to the interaction with inertial particles.
Therefore, tracers can be considered as same as the fluid elements with the same density as that of the fluid ($\rho_p = \rho_f$). These particles are ideally point-like with the same velocity of the underlying fluid:

$$\frac{d\mathbf{x}}{dt} = \mathbf{v}(t) = \mathbf{u}(\mathbf{x}(t), t) \tag{3.27}$$

where $\mathbf{x}$ and $\mathbf{v}$ are position and velocity of tracers, respectively and $\mathbf{u}$ is the fluid velocity.

These non-inertial particles are of great importance in some experimental techniques of fluid flows, so-called velocimetry techniques such as Particle Image Velocimetry (PIV) which is based on Eulerian approach and Particle Tracking Velocimetry (PTV) which relies on Lagrangian method. In these methods, very small particles, which follow the flow dynamics, are used to quantify the velocity and direction of the flow. Stokes number which is a ratio of the particle relaxation time to the time for fluid velocity change, can be used to define a criterion to characterize a fluid tracer. Small Stokes numbers indicate that particle's motion is tightly coupled with fluid velocity whilst large Stokes number means that the response time of a particle is longer than the time fluid needs to act on it, so the particle is not affected by the fluid.

3.2.2 Inertial particles

Particles whose density differs from the fluid density ($\rho_p \neq \rho_f$, here ρ_f is the density of water), either less (*e.g.*, bubbles) or more (*e.g.*, sand grains), will have additional component in their advection. Their velocity is different from the one of the fluid and their size, shape, friction (Stokes drag) and interfacial properties are responsible for reveal hydrodynamic forces that should be taken into account to quantify their dynamics.
The equation of the motion of particles is given by Newton's second law:

$$\rho_p \mathcal{V}_p \frac{d\mathbf{v}}{dt} = \sum F_b + F_s \tag{3.28}$$

where $\mathcal{V}_p$ stands for the volume ($4/3\pi a^3$) of a particle with radius a, F_b and F_s are body and surface forces respectively.

- Gravity force:
  Gravitational force is a kind of body force which can be applied to a particle and is given by:

$$F_{gravity} = \rho_p \mathcal{V}_p \mathbf{g} \tag{3.29}$$

- Drag force:
  The difference between the velocity of a particle and of the underlying fluid causes the Drag force. The first theoretical approach to this force was introduced by (Stokes, 1851). It is written as follows:

$$F_{drag} = -C_D \frac{\pi a^2}{2} \rho_p (\mathbf{v} - \mathbf{u}) |\mathbf{v} - \mathbf{u}| \tag{3.30}$$

  where C_D depends on particle's Re number. This coefficient is chosen to have the form:

$$C_D = \frac{24}{Re_p} (1 + 0.15\, Re^{0.687}) \tag{3.31}$$

  which is a good approximation whenever $Re_p < 1000$ (Schiller and Neumann, 1933; Clift, Grace, and Weber, 1978).

- Added mass:
  When a particle move through the fluid, certain amount of fluid must move around the particle. In case, acceleration or deceleration is imposed on the flow, additional fluid force will act on the surface in contact with fluid. The added mass or virtual mass force accounts for this displacement of the fluid around the particle and is expressed by:

$$F_{added\ mass} = \rho_f \mathcal{V}_p C_M \left(\frac{D\mathbf{u}}{Dt} - \frac{d\mathbf{v}}{dt} \right) \tag{3.32}$$

  Taylor (1928) and Batchelor (1967) showed that added mass coefficient for a sphere is $C_M = 1/2$ and is independent of Re number of the particle. Here $D\mathbf{u}/Dt$ represents the material derivative of the fluid velocity at the position of particles, in other words along the path of fluid element and $d\mathbf{v}/dt$ is time derivative of particles' Lagrangian velocity.
  Acceleration of fluid element ($\rho_f \mathcal{V}_p \frac{D\mathbf{u}}{Dt}$) which represents the force acted on particles by the undisturbed flow, and *Archimedes* buoyant force ($-\rho_f \mathcal{V}_p \mathbf{g}$), should be taken into account as extra forces exerted

on the particles. These forces are mathematically obtained by applying the force of fluid flows on particles as:

$$\int_{S_p} \boldsymbol{\sigma} \cdot n dS = \int_{\mathcal{V}_p} \nabla \boldsymbol{\sigma} d\mathcal{V} = \int_{\mathcal{V}_p} \rho_f \left(\frac{D\mathbf{u}}{Dt} - \mathbf{g} \right) = \rho_f \mathcal{V}_p \left(\frac{D\mathbf{u}}{Dt} - \mathbf{g} \right) \tag{3.33}$$

where $\boldsymbol{\sigma}$ is the stress tensor which can be written as :

$$\sigma_{ij} = -\rho_f p \delta_{ij} + \mu_f (\partial_i u_j + \partial_j u_i) \tag{3.34}$$

- Lift force:
  Another component of the force exerted by fluid flow on particles is termed lift force that is perpendicular to the relative particle to fluid velocity due to the presence of vorticity. This force has the form:

$$F_{lift} = -C_L \rho_f \mathcal{V}_p (\mathbf{v} - \mathbf{u}) \times \omega \tag{3.35}$$

  in which ω is the flow vorticity and is equal to the curl of velocity ($\omega = \nabla \times \mathbf{u}$). C_L is the lift coefficient which can vary according to Re number (Auton, 1987).

- History force:
  This force is drag that is caused by unsteady motion of particle in a viscous medium. Time lag exists for surrounding fluid to adapt to the new condition created by particles' motion through the flow. This force for small spherical particles is expressed as:

$$F_{history} = -6\pi a^2 \mu_f \int_0^t \frac{d(\mathbf{v} - \mathbf{u})}{d\tau} \frac{d\tau}{\pi \nu (t - \tau)^{1/2}} \tag{3.36}$$

There are other kinds of forces like Brownian force which is applied to very small particles where their motion is affected by the discrete nature of molecular motion of the fluid and Thermophoresis due to the non-uniformity of the temperature profile of the carrier fluid, which are neglected here.

Adding the contribution of these forces, the equation of motion of particles can be written as follow:

$$\begin{aligned}\rho_p \mathcal{V}_p \frac{d\mathbf{v}}{dt} &= (\rho_p - \rho_f)\mathcal{V}_p \mathbf{g} + \rho_f \mathcal{V}_p C_M (\frac{D\mathbf{u}}{Dt} - \frac{d\mathbf{v}}{dt}) \\ &- C_D \frac{\pi a^2}{2} \rho_p (\mathbf{v} - \mathbf{u})|\mathbf{v} - \mathbf{u}| + \rho_f \mathcal{V}_p \frac{D\mathbf{u}}{Dt} \\ &- C_L \rho_f \mathcal{V}_p (\mathbf{v} - \mathbf{u}) \times \omega - 6\pi a^2 \mu_f \int_0^t \frac{d(\mathbf{v} - \mathbf{u})}{d\tau} \frac{d\tau}{\pi\nu(t-\tau)^{1/2}}\end{aligned} \tag{3.37}$$

which can be simplified for heavy particles ($\rho_p/\rho_f \gg 1$) to drag and gravity forces while for light particles ($\rho_p/\rho_f \sim 0$), inertial forces are also important. The above equation was developed firstly by Maxey and Riley (1983), Gatignol (1983), and Auton, Hunt, and M.Prud'Homme (1988) and is complicated to be solved. A commonly used version of this equation for passively advected finite size particles is:

$$\frac{d\mathbf{v}}{dt} = \beta \frac{D}{Dt}[\mathbf{u}(\mathbf{x}(t), t)] - \frac{1}{\tau_p}[\mathbf{v}(t) - \mathbf{u}(t)] \tag{3.38}$$

where $\beta = 3\rho_f/(2\rho_p + \rho_f)$ is the density ratio and $\tau_p = a^2/(3\beta\nu)$ is the stokes time of the particle. Note that this equation is valid for small Re_p. Dynamics of inertial particles have been studied extensively in the past either numerically (Salazar et al., 2008; Squires and Eaton, 1991; Balkovsky, Falkovich, and Fouxon, 2001; Mazzitelli, Lohse, and Toschi, 2003b; Mazzitelli, Lohse, and Toschi, 2003a; Bec et al., 2006; Cencini et al., 2006; Calzavarini et al., 2008a; Calzavarini et al., 2008b) or experimentally (Eaton and Fessler, 1994; Salazar et al., 2008; Saw et al., 2008; Yang and Shy, 2005; Voth et al., 2001) and the most important phenomenon observed in these studies which is the direct result of the simplified equation 3.38, is preferential concentration of inertial particles. This means that particles with different density than the fluid density, tend not to remain uniformly distributed even in homogeneously isotropic turbulent flows. It has been shown that light particles ($\beta = 3$) are trapped by vortices in the flow (Toschi and Bodenschatz, 2009) while heavy particles ($\beta = 0$) accumulate in low vorticity regions (Squires and Eaton, 1991; Wang and Maxey, 1993). Another quantity which plays a key role in the strength

of preferential concentration of particles is Stokes number ($St = \tau_p/\tau_\eta$), where τ_η is Kolmogorov time scale. As defined previously, it is a good control parameter to describes particles' motion in the flow. A particle with a low Stokes number follows fluid streamlines (perfect advection), while a particle with a large Stokes number is dominated by its inertia and continues along its initial trajectory. Acceleration statistics of the inertial particles and their dependancy on Stokes number have been studies previously in Bec et al. (2006), Ayyalasomayajula et al. (2006), Ayyalasomayajula, Warhaft, and Collins (2008), Volk et al. (2008), Qureshi et al. (2008), and Zamansky, Vinkovic, and Gorokhovski (2011).

Stokes number
A dimensionless number characterising the relaxation time of a particle with respect to typical fluctuation velocity in a flow

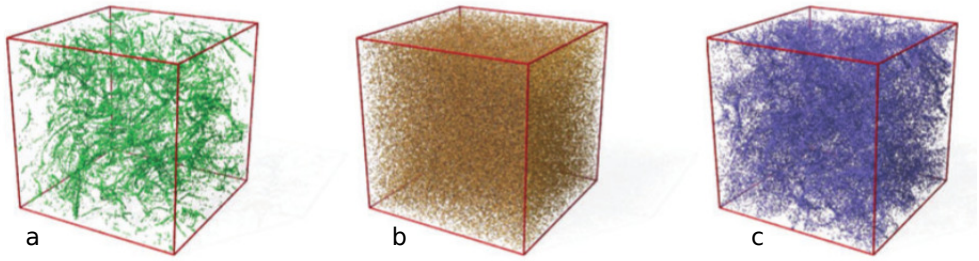

FIGURE 3.5: Snapshots of particle distributions in a turbulent flow field at $St = 0.6$ for (a) $\beta = 3$ (bubbles), (b) $\beta = 1$ (tracers) and (c) $\beta = 0$ (heavy particles) from (Calzavarini et al., 2008a).

3.2.3 Active particles

As mentioned previously, microorganisms can drift in fluid flows. These features allow them to swim with different velocity rather than the fluid velocity, hence they are called active particles. Apart from all the forces exerted on passive particles, physicist have proposed a simple model for microorganism's motility (Kessler, 1985; Pedley and Kessler, 1992) in which their trajectories can be obtained by integrating the following equation:

$$\frac{d\mathbf{x}}{dt} = \mathbf{u}[\mathbf{x}(t), t)] + \mathbf{v}_s\mathbf{p} \tag{3.39}$$

where $\mathbf{p}$ is the orientation vector. This equation indicates that active particles can swim with fluid velocity plus a slipping velocity ($\mathbf{v}_s$) in a direction

of **p**. This model is dubbed as *Chlamydomonas* model (Kessler, 1985; Pedley and Kessler, 1992).
In general, particles can orient inside the flow due to the velocity gradient, strain and deformation rate in particular. One can also consider the effect of gravity in the evolution of **p**. This is to be discussed in more detail in chapter 5.

3.3 Simulation of hydrodynamic turbulence

3.3.1 DNS: principles

Growth of computational power in the last decades, has attracted enormous attentions into numerical simulation of turbulent flows. The general classifications of numerical methods that are used to perform simulation of turbulence are direct numerical simulation (DNS), large-eddy simulation (LES) and Reynolds-averaged Navier-Stokes (RANS).
DNS is the most accurate approach to solve the governing equations of the fluid flows. All the spatial and temporal scales of the flow are resolved from integral scale (L) to dissipative scales (η), without any scale modeling, so that complex behavior of turbulence can be reproduced in very detail. Of course the computational cost increases as Reynolds number increases in DNS, because the inertial range depends on Re number and its wideness means that DNS should resolve larger range of scales of the flow. This implies that one needs very fine resolution when Re number becomes high, therefore the method is limited to not very high turbulent flows. The largest Reynolds number which was achieved by DNS is around 5200 with 4096^3 grid points conducted in 2015 by (Lee and Moser, 2015).
On the opposite, Large Eddy Simulation (LES) is a very useful approach for high-Reynolds number flows. In this technique, the scales larger than mesh size are resolved and the effects of non-resolved small scales are taken in to account using many models. Another way to perform numerical simulation of turbulence is to average all the stochastic turbulent

fluctuations and solve only the averaged equations, which gives approximate time-averaged solutions to the Navier-Stokes equations. However this formulation is not closed. One needs a closure, *e.g.*, $k-\epsilon$ or $k-\omega$ methods in which extra equations are needed. Figure 3.6 represents the differences between the methods in terms of computational cost, degree of freedom and model influence. However due to the nonlinear character of Navier-Stokes equations, the modeled term either in LES or in averaged model, is not properly modeled. These models have thus strong limitations (Pope, 2000; Schmitt, 2007).

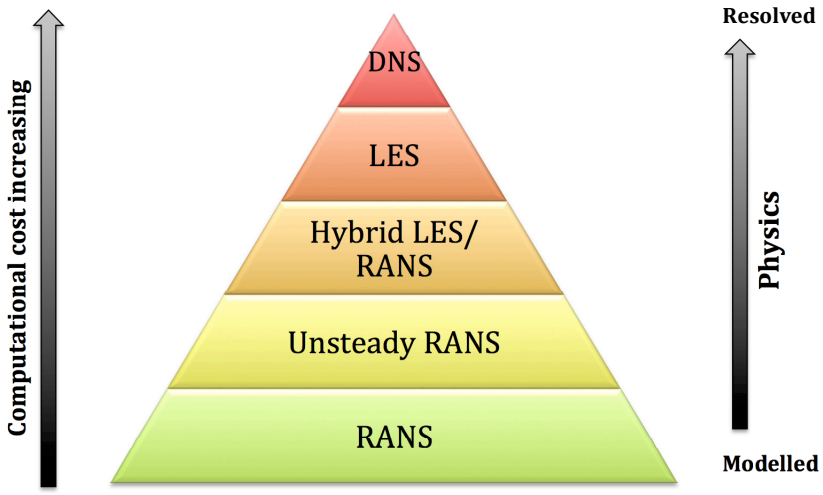

FIGURE 3.6: Schematic view of comparison of direct numerical simulation, large-eddy simulation and Reynolds-averaged Navier-Stokes simulation adapted from Sagaut, Deck, and Terracol (2006).

The simplest realization to study the intrinsic nature of turbulence by means of DNS, is a periodic box where isotropic homogeneous turbulent can be achieved under periodic boundary conditions. Such a flow is in accordance with Kolmogorov's hypothesis that at small scales, statistics are locally isotropic and homogeneous while it may not be the case for large scales in box turbulence. We have already seen from eq. 3.18 that the Kolmogorov microscale is $\eta \sim LRe^{-3/4}$, where L is the size of large eddies. It is easy to estimate the number of points at which velocity must be calculated to resolve every eddy in turbulence (Paladin and Vulpiani,

1987; Davidson, 2004). When Re is large, η is small, however the maximum allowed size of grid spacing in DNS is:

$$\Delta x \sim \eta \sim LRe^{-3/4} \tag{3.40}$$

The number of data points required at any instant for a three-dimensional simulation is then:

$$N \sim \left(\frac{L_{BOX}}{\Delta x}\right)^3 \sim \left(\frac{L_{BOX}}{L}\right)^3 Re^{9/4} \tag{3.41}$$

Here L_{BOX} is the size of the computational domain. The factor $Re^{9/4}$ is referred to as the number of degrees of freedom of the turbulence (Landau and Lifshitz, 1959). It is now evident that:

$$N \geq Re^{9/4} \tag{3.42}$$

Moreover time resolution also depends on the Reynolds number. In order to solve the Navier-Stokes equations, they need to be integrated in time. The maximum permissible time step in a simulation, is of the order of $\Delta t \sim \Delta x/u_\eta \sim \eta/u_\eta$ since, in order to maintain numerical stability and accuracy, we cannot let a fluid particle move by more than one grid spacing in each time step. If T is the total duration of the simulation then the minimum number of time steps needed to complete the simulation is:

$$N_t \sim \frac{T}{\Delta t} \sim \frac{T}{\eta/u_\eta} \sim \frac{T}{l/u_\eta} Re^{3/4} \tag{3.43}$$

As can be seen the computational cost of direct numerical simulation is very high even for low Reynolds number flows. However, DNS is the best tool to obtain very accurate information out of the turbulent flows which are extremely difficult to be done experimentally. This is the reason, DNS is often called *numerical experiment* and can be used as a benchmark for development of other numerical approaches such as LES.
This is also the reason why we perform our simulations by means of DNS. Copepod's size is of the order of dissipative scales in ocean. If we are interested in copepods' dynamics in turbulent flows, we need to be able to

capture the Kolmogorov scale and study their interactions with microorganisms. In addition, experimental study of copepods in turbulent situation at laboratory which mimics oceanic turbulence is almost impossible at the moment. DNS can provide this experiment, numerically.

3.3.2 Numerical methods

Direct numerical simulation is used to solve the Navier-Stokes equations in box turbulence. There are several numerical methods such as finite difference methods (FDM), finite volume methods (FVM), finite element method (FEM) and also spectral methods to perform DNS. In the following, a brief introduction on spectral methods and differences between the available techniques is given to see why this method has been of great importance to engineers in the last decades and why we choose this method. The basic principle of spectral methods and detailed numerical techniques used here to simulate the box turbulence will be addressed in this section.

Spectral Methods vs Physical space methods

Finite difference method is the oldest numerical technique which is based on the application of Taylor expansion to approximate the derivative of a function by local argument ($u' \sim u(x+h) - u(x-h)/2h$ where h is grid spacing) (Lomax, Pulliam, and Zingg, 1999). The strategy in FDM is to use a square network of lines dubbed as mesh which can be applied to a wide range of geometries and approximate the solution according to the available gird points. Accuracy depends on the order of approximation, which in turns depends on the number of grid points. To obtain higher accuracy, higher order approximation is needed and accordingly more points should be used to calculate derivatives (Lomax, Pulliam, and Zingg, 1999).
Finite volume methods have become popular in CFD as a result, primarily, of two advantages. First they ensure that the discretization is conservative, *i.e.*, mass, momentum and energy are conserved in a discrete sense.

While this property can usually be obtained using a finite difference formulation, it is obtained naturally from a finite volume formulation. Second finite volume methods do not require a coordinate transformation in order to be applied on irregular meshes. As a result they can be applied on unstructured meshes consisting of arbitrary polyhedra in three dimensions or arbitrary polygons in two dimensions. This increased flexibility can be used to a great advantage in generating grids about arbitrary geometries(Lomax, Pulliam, and Zingg, 1999). The basic concept in the Finite element methods is the subdivision of the computational domain into disjoint (non-overlapping) components of simple geometry called finite elements or elements for short. The response of each element is expressed in terms of a finite number of degrees of freedom characterized as the value of an unknown function, or functions, at a set of nodal points. The response of the mathematical model is then considered to be approximated by that of the discrete model obtained by connecting or assembling the collection of all elements (Reddy, 2005). Compared to FEM, in spectral methods only one global function is used to be valid over the entire computational domain. Key factors to choose among these techniques, are the complexity of the domain and the needed level of accuracy, where spectral methods have the great advantage of being most accurate and cost effective methods for simple geometries compared to physical space techniques.

In general all these methods are considered as a development of method of weighted residuals (MWR). The method of weighted residuals employs trial functions[1] as basis functions for a truncated series expansion of the solution, and test functions[2]. The use of test functions is to minimize the residual which is formed by the substitution of the approximate solution into the partial differential equations (PDE), to be sure that the approximate solution satisfies the differential equations (Canuto et al., 2007; Boyd, 2001). The choice of trial and test functions, distinguishes the spectral methods from physical space techniques mentioned here. This is to be discussed in the following.

[1] It is also called approximating functions or expansion functions.
[2] It is also known as weight functions.

Basic principle of spectral methods

The idea behind the spectral methods is to approximate the solution of partial differential equation as a sum of smooth basis functions (Canuto et al., 2007; Boyd, 2001).

$$u(\mathbf{x}) = \sum_{n=0}^{N} \tilde{u}_n \phi_n(\mathbf{x}) \tag{3.44}$$

where the $\phi_n(\mathbf{x})$ are polynomials or trigonometric functions and $\tilde{u}_n$ are unknown coefficients. The goal in spectral method as a method of weighted residuals (MWR) is to minimize the residual by using test functions. The choice of the test functions distinguishes between the three most commonly used spectral schemes, namely Galerkien, Collocation and Tau methods (Fornberg, 1996). Another classification is based on the choice of trial functions. In general trial functions should satisfy three requirements (Canuto et al., 2007):

1. Convergence: the approximation $\sum_{n=0}^{N} \tilde{u}_n \phi_n(\mathbf{x})$ should converge rapidly to $u(\mathbf{x})$.
2. Derivation: given the coefficients $\tilde{u}_n$, one can easily determine $\tilde{u}'_n$ such that
$$\frac{d}{d\mathbf{x}}\left(\sum_{n=0}^{N} \tilde{u}_n \phi_n(\mathbf{x})\right) = \sum_{n=0}^{N} \tilde{u}'_n \phi_n(\mathbf{x}) \tag{3.45}$$
3. Transformation: reconstruction of the solution ($u(\mathbf{x})$) at nodes from the expansion coefficient ($\tilde{u}_n$) should be easy.

Therefore, for periodic problems, trigonometric expansions (Fourier series) which fulfil the requirements can be chosen while the first two conditions are satisfied obviously and the third condition is possible through the invention of the Fast Fourier Transform (FFT) algorithm, which was developed by Cooley and Tukey (1965). In fact spectral methods became popular and more practical when innovate algorithm of FFT replaced discrete Fourier Transform (DFT). The difference is that computational complexity of FFT is of the order of $\mathcal{O}(N\,log(N))$ while it is of $\mathcal{O}(N^2)$ for DFT. For non-periodic problems trigonometric expansions fail to satisfy the

conditions, hence orthogonal polynomials such as Legendre and Chebyshev are taken as basis functions. Here, we focus on periodic box turbulence and implement Fourier pseudo-spectral method. For more information on several types of spectral methods one can refer to Fornberg (1996), Canuto et al. (2007), Hussaini and Zang (1987), and Boyd (2001).

Fourier Pseudo-spectral method for the Navier-Stokes equations

Here we try to write the formulation of Navier-Stokes equations in a periodic box. Velocity field is expanded by means of Fourier series as basis functions and can be expressed as:

$$\mathbf{u}(\mathbf{x},t) = \sum_{\mathbf{k}} e^{i\mathbf{k}\cdot\mathbf{x}}\ \hat{\mathbf{u}}(\mathbf{k},t) \tag{3.46}$$

with periodic boundary condition of $\mathbf{u}(\mathbf{x}+L,t) = \mathbf{u}(\mathbf{x},t)$ for all $\mathbf{x}$. As mentioned at the beginning of this chapter, this imposed boundary condition can affect the real turbulence situation. In order to attenuate the effect of this artificial boundary condition L should be large compared to the integral length scale. Wave vectors are defined as:

$$\mathbf{k}_j = \frac{2\pi}{L}(j_1, j_2, j_3) \qquad j_\alpha = -N/2, \dots N/2 \tag{3.47}$$

N is the number of grid points and Fourier modes are read as $e^{i\mathbf{k}\cdot\mathbf{x}} = e^{i\mathrm{k}_{j_1}x_1}e^{i\mathrm{k}_{j_2}x_2}e^{i\mathrm{k}_{j_3}x_3}$. Since the Fourier modes $e^{i\mathbf{k}\cdot\mathbf{x}}$ are non-random and fixed in time, Fourier coefficients should be time dependent. Applying Fourier operator $\hat{\mathscr{F}}_k\{\}$ to the Navier-Stokes equation :

$$\frac{\partial u_j}{\partial t} + u_j\frac{\partial u_l}{\partial x_l} = -\frac{1}{\rho}\frac{\partial p}{\partial x_j} + \nu\frac{\partial^2 u_j}{\partial x_j \partial x_j} + f \tag{3.48}$$

leads to set of ordinary differential equations (ODE) for the coefficients:

$$\frac{d\hat{u}_j}{dt} + \hat{\mathscr{F}}_k\{u_j\frac{\partial u_l}{\partial x_l}\} = -ik_j\hat{p} + \nu k^2\hat{u}_j + \hat{f} \tag{3.49}$$

One of the important issue here, is the way the pressure term should be treated. Normally Poisson equation is used to obtain the pressure field,

however one can introduce a projector operator which ensures the compressibility of the velocity field (u) without computing the pressure *i.e.*, without solving the Poisson equation. This is in fact the big advantage of the spectral methods (Pope, 2000).
These equations can be solved by taking the inverse Fourier transform. The non-linear advection term in the spectral space gives the convolution, which increases the complexity of the transfer operation. To overcome this problem, derivative of velocity field is evaluated in Fourier space, then the result is transferred to the real space to perform the multiplication and eventually the product is taken to Fourier space. This evaluation of the spectral convolution in physical space is usually called *Pseudo-spectral* evaluation of the nonlinear terms. Aliasing error is a problem which is linked to the computation of the non-linear advection term and can be handled by filtering the top one-third of the wavenumbers (Orszag, 1971). There are several methods in order to control the aliasing error which are out of the scope of this thesis. More information can be found in Phillips (1959), Cooley and Tukey (1965), Jr and Orszag (1971), Choi, Dongarra, and Walker (1995), and Bowman and Roberts (2011).
Navier-Stokes and continuity equations are given by:

$$\partial_t \mathbf{u} + \mathbf{u} \cdot \nabla \mathbf{u} = -\nabla p/\rho + \nu \Delta \mathbf{u} + \boldsymbol{f} \tag{3.50}$$

and

$$\nabla \cdot \mathbf{u} = 0 \tag{3.51}$$

Note that the $\boldsymbol{f}$ is the forcing which is applied on large scales to sustain the statistically stationary turbulence. It should be solenoidal which means that it has to satisfy the incompressibility $\nabla \cdot \boldsymbol{f} = 0$. In DNS there are two kinds of forcing. One has the following form in Fourier space:

$$\boldsymbol{f}(\mathbf{k}, t) = \frac{\epsilon \mathbf{u}(\mathbf{k}, t)}{\sum_{\mathrm{k_{low}}} |\mathbf{u}(\mathbf{k}, t)|^2} \tag{3.52}$$

where ϵ is the energy input rate and $\mathrm{k_{low}}$ refers to low wave numbers or their equivalent of large scales. This can be obtained by multiplying the Navier-Stokes equations by the velocity field and make the average which yields to a constant energy injection rate (Lamorgese, Caughey, and Pope,

2005). Another type of the forcing is to multiply the velocity in Fourier space $\mathbf{u}(k)$ at each time step, by a constant which ensures the energy contain at large scales to be constant, where the decay is consistent with the $k^{-5/3}$ law (Chen et al., 1993). The latter is used in this study.
Moreover, In this study, we considered a vector-potential form of the Navier-Stokes equation by taking:

$$\mathbf{u}(\mathbf{x},t) = \nabla \times \mathbf{b}(\mathbf{x},t) \tag{3.53}$$

substituting this in eq. 3.51 gives:

$$\nabla \cdot \mathbf{u} = \nabla \cdot (\nabla \times \mathbf{b}) \tag{3.54}$$

where the divergence of a curl of a vector ($\nabla \cdot (\nabla \times \mathbf{b}) = 0$) is always zero, therefore the incompressibility is always satisfied and there is no need for pressure term in the Navier-Stokes equation. Eq. 3.50 in the vector potential form is:

$$\frac{\partial(\nabla \times \mathbf{b})}{\partial t} + \mathbf{u} \cdot \nabla \mathbf{u} = \nu \Delta (\nabla \times \mathbf{b}) + \boldsymbol{f} \tag{3.55}$$

Taking into account that $\Delta(\nabla \times \mathbf{b}) = \nabla \times (\Delta \mathbf{b})$, eq. 3.55 can be rewritten as:

$$\nabla \times \frac{\partial \mathbf{b}}{\partial t} + \mathbf{u} \cdot \nabla \mathbf{u} = \nu \Delta (\nabla \times \mathbf{b}) + \boldsymbol{f} \tag{3.56}$$

we then take the curl ($\nabla\times$) of the full equation and use $\nabla \times (\nabla \times \mathbf{b}) = \nabla(\nabla \cdot \mathbf{b}) - \Delta \mathbf{b}$,

$$\nabla \left(\nabla \cdot \frac{\partial \mathbf{b}}{\partial t} \right) - \Delta \frac{\partial \mathbf{b}}{\partial t} + \nabla \times (\mathbf{u} \cdot \nabla \mathbf{u}) = \nu \nabla \left(\nabla \cdot \Delta \mathbf{b} \right) - \nu \Delta \Delta \mathbf{b} + \nabla \times \boldsymbol{f} \tag{3.57}$$

It is known that from vector calculus identities, $(\nabla \cdot \Delta \mathbf{b}) = \Delta(\nabla \cdot \mathbf{b})$, so the eq. 3.57 is:

$$\nabla \left(\frac{\partial}{\partial t} (\nabla \cdot \mathbf{b}) \right) - \Delta \frac{\partial \mathbf{b}}{\partial t} + \nabla \times (\mathbf{u} \cdot \nabla \mathbf{u}) = \nu \nabla \left(\Delta (\nabla \cdot \mathbf{b}) \right) - \nu \Delta \Delta \mathbf{b} + \nabla \times \boldsymbol{f} \tag{3.58}$$

now we choose $\nabla \cdot \mathbf{b} = 0$. Notice that this condition does not affect $\mathbf{u}$, therefore eq. 3.58 becomes:

$$-\Delta \frac{\partial \mathbf{b}}{\partial t} + \nabla \times (\mathbf{u} \cdot \nabla \mathbf{u}) = -\nu \Delta \Delta \mathbf{b} + \nabla \times \boldsymbol{f} \tag{3.59}$$

by taking the inverse laplacian operator Δ^{-1} and multiplying the eq. 3.59 by -1, the final form of the Navier-Stokes equation with the condition of $\nabla \cdot \mathbf{b} = 0$ is:

$$\frac{\partial \mathbf{b}}{\partial t} - \Delta^{-1} \left[\nabla \times (\mathbf{u} \cdot \nabla \mathbf{u})\right] = \nu \Delta \mathbf{b} - \Delta^{-1} \left(\nabla \times \boldsymbol{f}\right) \tag{3.60}$$

Similar to the eq. 3.49, pseudo-spectral method can be applied to eq. 3.60 where the pressure term is removed from the equations by taking the vector-potential form of the velocity field. The vector $\mathbf{b}(\mathbf{x}, t)$ is expanded in a discrete Fourier series in each direction on an equispaced grid and its equations are advanced in time by the second-order Adams-Bashforth scheme.

3.3.3 Summary

A Direct Numerical Simulation (DNS) approach was used to solve the incompressible Navier-Stokes equations (eq. 3.50 and 3.51) in homogeneous and isotropic conditions by means of the pseudo-spectral method, based on vector potential formulation:

$$\frac{\partial \mathbf{b}}{\partial t} - \Delta^{-1} \left[\nabla \times (\mathbf{u} \cdot \nabla \mathbf{u})\right] = \nu \Delta \mathbf{b} - \Delta^{-1} \left(\nabla \times \boldsymbol{f}\right) \tag{3.61}$$

The solution domain is a cube of length $L = 2\pi$ with $N^3 = 128^3$ grid points, subject to periodic boundary conditions. Aliasing error is controlled by omitting the wavenumber larger than $k = 2/3 \times (2\pi N/L)$.
In isotropic turbulence, the dissipation rate is equal to:

$$\epsilon = 2\nu \mathcal{S} : \mathcal{S} = 15\nu \left\langle \left(\frac{\partial u_i}{\partial x_i}\right)^2 \right\rangle \tag{3.62}$$

Here $\mathcal{S}$ represents the symmetric part of the gradient of the velocity field. Eq. 3.19 can relate λ to ϵ by:

$$\epsilon = 15\nu\frac{u^2}{\lambda^2} \tag{3.63}$$

therefore, substituting into the definition of Re_λ, Taylor Reynolds number of the flow is $Re_\lambda = \sqrt{15}u_{rms}^2/(\nu\epsilon)^{1/2}$ (Tennekes and Lumley, 1972), which in our simulations is ≈ 80. The accuracy of the solution in time is guaranteed by the small Courant number $C = u_{rms}\Delta t/\Delta x \approx 1/30$, with $\Delta x = L/N$ the mesh size. $k_{max}\eta > 1.4$, in which $k_{max} = N/3$ and η is the Kolmogorov length scale, assures that small scales structures are well resolved.

Chapter 4

Analysis of copepods' trajectories from experiments

*Aquaculture of two copepod species **Acartia tonsa** and **Eurytemora affinis**, are described in this section. By means of high speed camera, their trajectories are recorded and statistical data analysis are performed in order to quantify their dynamics in still water.*

4.1 Copepod species

Females and males of the species *Eurytemora affinis* and *Acartia tonsa* were filmed by Ibtissem Benkeddad in May 2015 during Master 1 internship in Wimereux. An aquarium was used with a high speed camera, in order to extract trajectories, velocities and accelerations. We have used Mrs. Benkeddad's measurements in this thesis, thus the experimental conditions are here described. For more information, one refers to her Master 1 report (Benkeddad, 2015).

Copepods originated from the Seine river estuary (France) are maintained in the laboratory of Oceanology and Geoscience (LOG) under optimal conditions for several generations. They are fed using red algae species *Rhodomonas baltica*, which is rich in lipid and can stimulate copepod's growth rate. Red algae species are also cultivated in the same laboratory and feeding process occurs twice in a week in order to keep copepods active. *Rhodomonas baltica* is kept in special containers (Figure 4.1), having oxygen continuously, under light (photoperiod $12h/12h$) and with a

Rhodomonas
A genus of algae

Photoperiod
$12h/12h$

temperature of $18 - 19°C$.

Temprature
$18 - 19°C$

FIGURE 4.1: Culture of *Rhodomonas baltica* in container conserved in incubator at temperature of $18 - 19°C$ with oxygenation and photoperiod $12h/12h$ (Benkeddad, 2015).

Copepod species are also kept in special containers in similar conditions except for its salinity (Figure 4.2 and 4.3). The separation of species is applied even to copepod's gender meaning that females and males of copepods are conserved separately in several containers. The salinity of water for species *Eurytemora affinis* and *Acartia tonsa* is 15 *psu* and 30 *psu* respectively. One should keep in mind that *Rhodomonas baltica* needs the same surveillance as copepods. They should be fed with vitamins and minerals twice in a week. After reaching the optimal growth level, preparation will be done, which means that water of each container is filtered and poured into special device for centrifuge. When centrifuge process in done (1 minute), it will be diluted with water.

Salinity
The dissolved salt content of a body of water

PSU
Practical salinity unit, $1\,psu = 1\,g/kg$

4.2 Experimental set up

To start the experiment, large individuals of male and female of *Eurytemora affinis*, or even egg-bearing (ovigerous) females are taken randomly to have adult species in the aquarium. The experimental set up which is made specifically for this project, is a shallow-depth aquarium, $63 \times 53 \times 6\,mm^3$ in length, height and depth respectively as shown in

Aquarium size
$63 \times 53 \times 6\,mm^3$ in length, height and depth

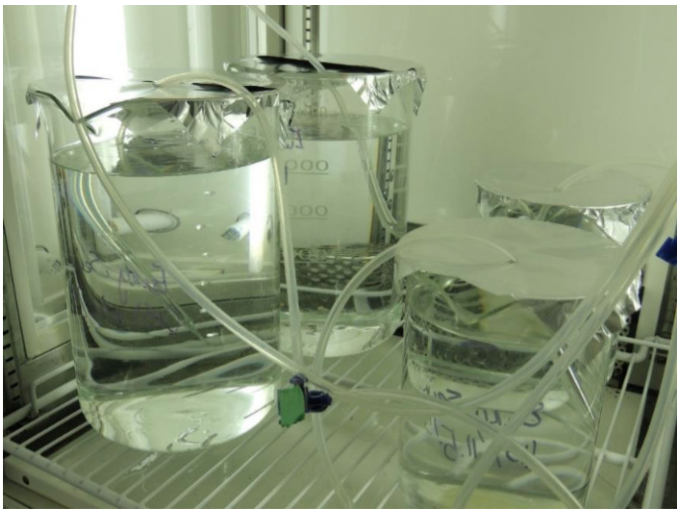

FIGURE 4.2: Culture of copepod species *E. affinis* in container conserved in incubator at temperature of $18 - 19°C$ with oxygenation and photoperiod $12h/12h$. Salinity of water is 15 *psu* (Benkeddad, 2015).

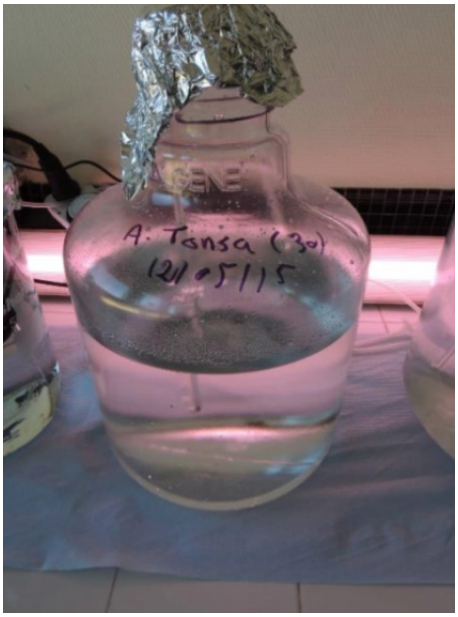

FIGURE 4.3: Culture of copepod species *A. tonsa* in container at ambient temperature with same photoperiod as for *E. affinis* species. Salinity of water is 30 *psu* (Benkeddad, 2015).

figure 4.4. The background is dark so that copepods will be visible. The water is kept still and at temperature of $(18 \pm 1)\,^{\circ}\mathrm{C}$ and salinity of 15 *psu* for *E. affinis*. Each individual is introduced one at a time in the aquarium and their dynamics are filmed. The same procedure is performed for *A. Tonsa* with different salinity. A total of 28 individuals are analysed here (14 males and 14 females).

FIGURE 4.4: Experimental set up made of Acrylic with total volume of 8 ml and dimension of $63 \times 53 \times 6\,mm^3$ in length, height and depth respectively (Benkeddad, 2015).

In order to stimulate copepods, two light sources on the lateral side ($53 \times 6\,mm^2$) of the aquarium are used (Figure 4.5). The species tend to attract lights (positive phototaxis), so a copepod in the aquarium tends to jump preferentially along the horizontal direction by switching on just one of the light sources. The light is switched on and off manually in a non-monotonic way where the switching time of the lights is much more larger than the jump frequency of the copepod species. The copepod's dynamics in a vertical plane are recorded by a high speed camera (1000 frames/second) as shown in figure 4.5 and 4.6 and the single trajectory is extracted by means of a particle tracking velocimetry software (TEMA Motion by Image Systems). The resolution of camera is $512 \times 384\,pixel$ ($45.3 \times 34\,mm$) and with limitation on capacity, recording up to 25 seconds is possible. Here trajectories of $14 - 22\,s$ for *E. affinis* and $10 - 22\,s$ for *A. Tonsa* are recorded. Figure 4.7 shows copepods in the aquarium captured by the high speed camera.

Phototaxis
A kind of taxis, or locomotory movement, that occurs when a whole organism moves towards or away from stimulus of light

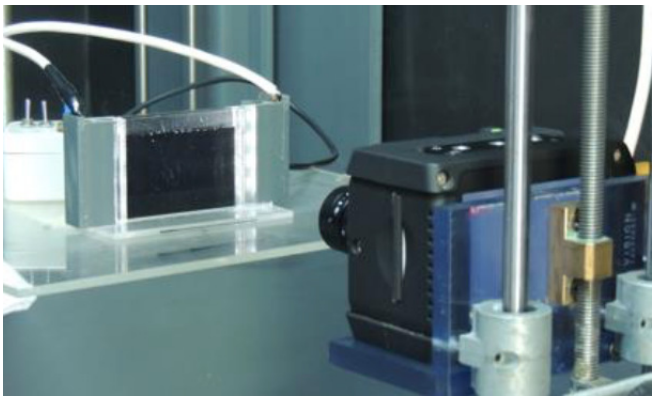

FIGURE 4.5: Light sources are located at the lateral side of the aquarium with high speed camera in front to capture copepods statistics (Benkeddad, 2015).

FIGURE 4.6: Phantom high speed camera is capable of capturing 1000 frames per seconds. The resolution of the camera is 512×384 *pixel* and it is connected to a software called Phantom Camera Control application (PCC) (Benkeddad, 2015).

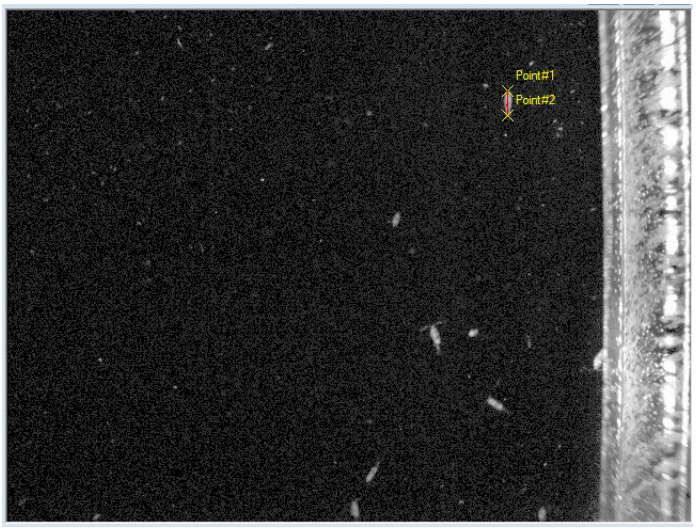

FIGURE 4.7: Copepod species in the experimental set-up captured by the high speed camera.

Copepod species are conserved in micro-tubes, after recording was done to identify their gender and calculate their size using a microscope (Figure 4.8, 4.8 and 4.10). During recording each species shows a specific behavior, *e.g.,* ovigerous females are very active when stimulated and individuals of the species *A. tonsa* prefer to swim at the walls, which creates problem for recordings. Thus the number of replicates per individual will depend on these behaviors: Ten replicates per individual for *E. affinis* against five replicates per individual for *A. tonsa*, because many times the individuals of the latter were not found during the experiment, which leads to the reduced duration of video footage unlike *E. affinis*.

With the help of particle tracking velocimetry software (TEMA), copepod's individuals are followed image by image. This software can extract hundreds of trajectories, velocity and acceleration of copepods in real time. The only point is to convert the pixel into millimetre which can be obtained from the resolution of the camera ($512 \times 384\, pixel$ ($45.3 \times 34\, mm$)) and is $1\, pixel = 0.0885\, mm$. The output of this software can be used as the base of our data analysis in next section.

FIGURE 4.8: Labelled micro-tubes containing copepod species for identification (Benkeddad, 2015).

FIGURE 4.9: Olympus microscope connected to a software to calculate the size and identify the gender of copepod species (Benkeddad, 2015).

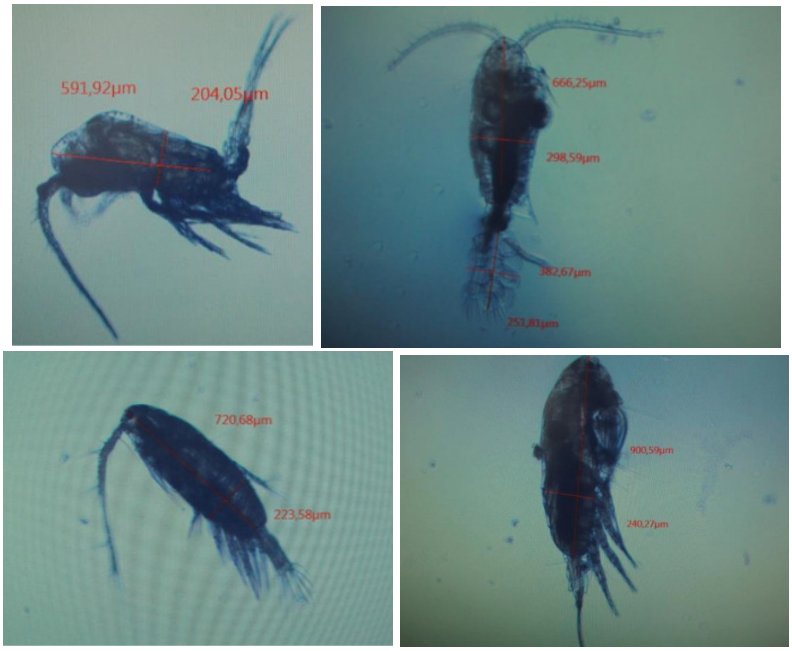

FIGURE 4.10: Length measurement of male *E. affinis* (top left), ovigerous female *E. affinis* (top right), male *A. tonsa* (bottom left) and female *A. tonsa* (bottom right) (Benkeddad, 2015).

4.3 Experimental Data Analysis

All of the experiments described in sections 4.1 and 4.2, were performed by I. Benkeddad. The authors contribution here is in the analysis of the measurements.

Recorded velocity track of copepods' trajectories will be analysed here. A typical copepod velocity signal as a function of time is shown in figure 4.11. We see extremely abrupt spikes (jumps) alternating to calm, nearly immobile phases. These jumps are the response of copepods to the changes in light distribution. To see what is exactly happening during a jump, one can zoom in on the signal. Figure 4.12 represents how larger the jump amplitude velocity of a copepod is compared to the calm phase and how this velocity changes during escape response of copepods. High speed camera captures this behaviour (the growing and the decaying of velocity) precisely which was impossible in previous studies on copepods. Scientists were able to observe only the spikes and not the decaying behaviour of copepods in their past analysis.

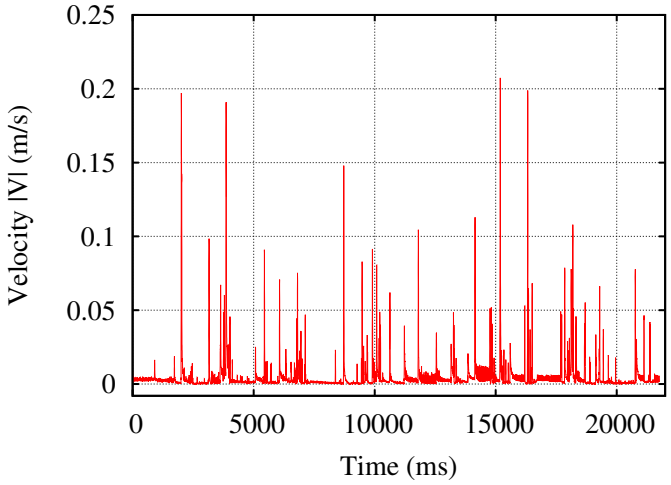

FIGURE 4.11: The copepod (*E. affinis*) velocity relative to temporal sequence with multiple jumps occurred in response to stimulus.

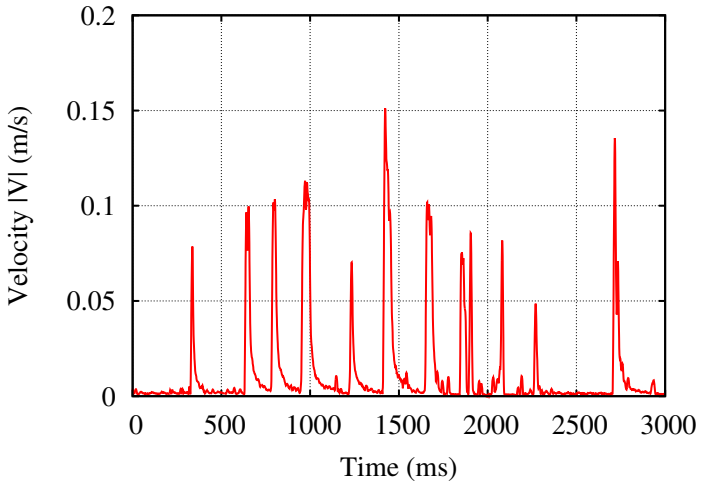

FIGURE 4.12: Response behaviour of copepod in response to light stimulus. Change of velocity amplitude of a copepod while jumping is shown here.

In order to see if the velocity signal of the jump events share some common features, we zoom in on the signal and superpose several jumps by a shift taking as reference their peak position. In figure 4.13 we can appreciate that almost all of the jumps, after a steep rise, display a similar decay. We associate such a decay to a purely hydrodynamical effect. It can be interpreted as a drag-induced decay of an instantaneous acceleration.

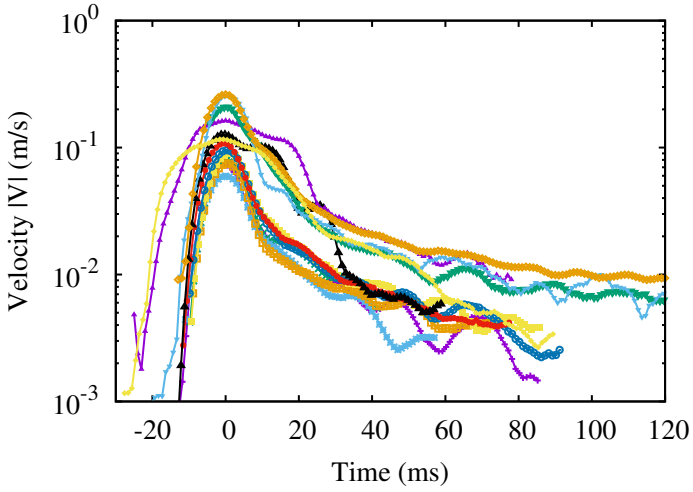

FIGURE 4.13: A sample of jump intensity superposition for copepod species *E. affinis*. Several jumps superposed by a shift, taking as reference time that are associated with their peak position. Almost all of the jumps decay exponentially.

Note that spikes are identified based on a threshold on the time-averaged velocity of the copepods over all copepod's trajectory. We then average the dataset of jumps in order to obtain an averaged shape of jump. This is shown in figure 4.14, from which we can deduce the average jump velocity amplitude $u_J = 0.0836\,m/s$ and the mean decaying time $\tau_J = 8.073\,ms$. We also see that for long time the velocity reaches a very low plateau at $5.3 \times 10^{-3}\,m/s \sim 1/20\,u_J$, which we are tempted to associate to a weak random wandering behaviour of the copepod.

E. Affinis
Jump velocity amplitude:
$u_J = 0.0836\,m/s$,
Jump decaying time:
$\tau_J = 8.073\,ms$

The same behavioral response occurs for species *A. tonsa* as shown in figure 4.15. *A. tonsa* has slightly higher jump amplitude ($u_J = 0.0838\,m/s$) and less decaying time ($\tau_J = 7.351\,ms$) compared to *E. affinis*. Level of plateau and wandering behavior here ($2.92 \times 10^{-3}\,m/s \sim 1/30\,u_J$) is even much lower than the case for copepod species *E. affinis*.

A. tonsa
Jump velocity amplitude:
$u_J = 0.0838\,m/s$,
Jump decaying time:
$\tau_J = 7.351\,ms$

Probability distribution function (PDF) of jump intensity (Fig. 4.16)

shows that most of copepod's jumps occur with amplitude of $\sim 0.07\,m/s$ while the probability of jumps with higher amplitude is low. Lots of events have very low amplitude which implies that these events can be associated to the wandering behavior of copepods and can be neglected by the threshold on the time-averaged velocity of the copepods, since their amplitude is very small compared to the maximum amplitude of jumps.

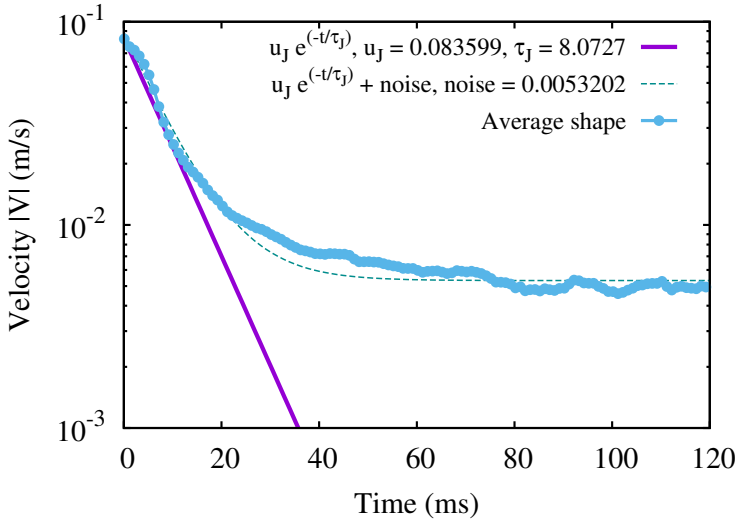

FIGURE 4.14: Average shape of jump velocity for copepod species *E. affinis*. Blue line: mean value. Purple line: Fitted exponential function $u_J e^{-t/\tau_J}$ where u_J is the jump intensity and τ_J is the decaying time of the jump. Green line: Same fit with the addition of a noise velocity offset.

The probability density function of time difference of successive jumps can be obtained by considering the absolute difference among the peak velocity amplitudes of two successive jumps. Let us say $Dv = v_{peak}(i+1) - v_{peak}(i)$, then Dt is the difference of time of these two events. This PDF suggests that the distribution of jumps in time in the experimental dataset does not follow an exponential distribution suggesting the existence of a memory effect. Poisson process is a name which is given to renewal process where the events are independent. In probability, the unique property of such a distribution of non negative numbers, is their memorylessness. For instance let us consider X the waiting time to the next event in a Poisson process, then memorylessness is a property of the

Poisson process
A type of random mathematical object that consists of points randomly located on a mathematical space

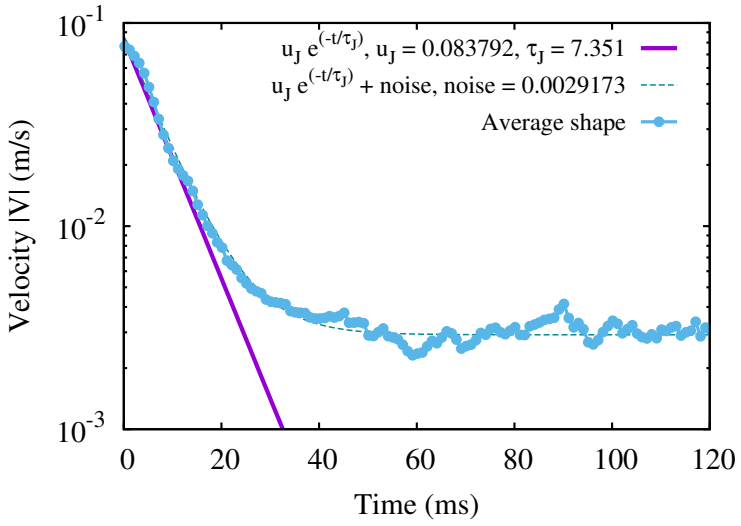

FIGURE 4.15: Average shape of jump velocity for copepod species *A. tonsa*. Blue line: mean value. Purple line: Fitted exponential function $u_J e^{-t/\tau_J}$ where u_J is the jump intensity and τ_J is the decaying time of the jump. Green line: Same fit with the addition of a noise velocity offset.

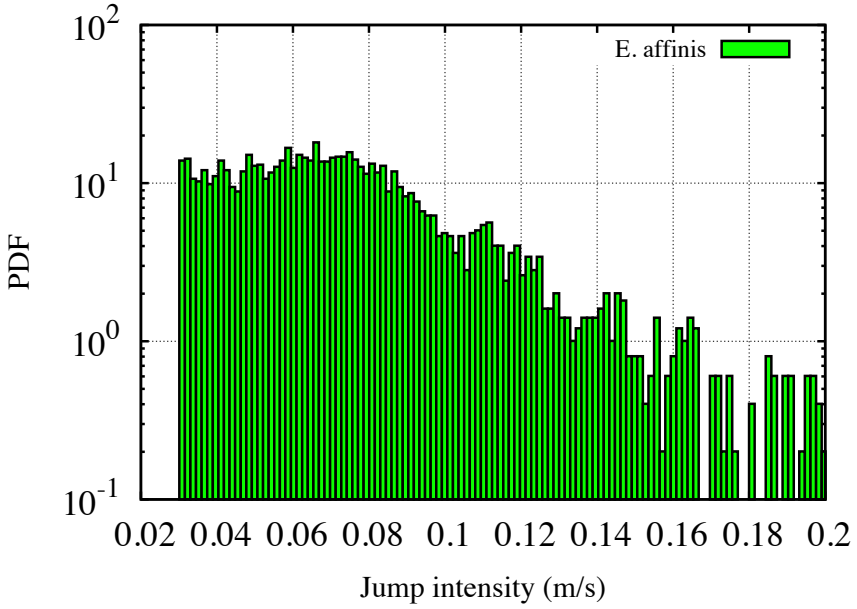

FIGURE 4.16: Probability density function of jump intensities of copepod species *E. affinis*.

following form:

$$Pr(X > m + n \,|\, X > m) = Pr(X > n) \tag{4.1}$$

this suggests that, given that the arrival has not occurred by time m, the distribution of the remaining waiting time (given by n in eq. 4.1) is the same as the original waiting time distribution (right hand side of eq. 4.1). In very simpler words, an event can occur independently from previous events. Figure 4.17 represents the PDF of time between successive jumps in logarithmic scale, showing no exponential behavior, which means that copepod's jump occurrence depends on previous events. It is also evident that the time between most of the jumps is very small indicating that the jumps occur very quickly in time. This quantity is $\sim 1\,ms$ for *E. affinis* and $\sim 7\,ms$ for *A. tonsa* as can be seen in figure 4.17.

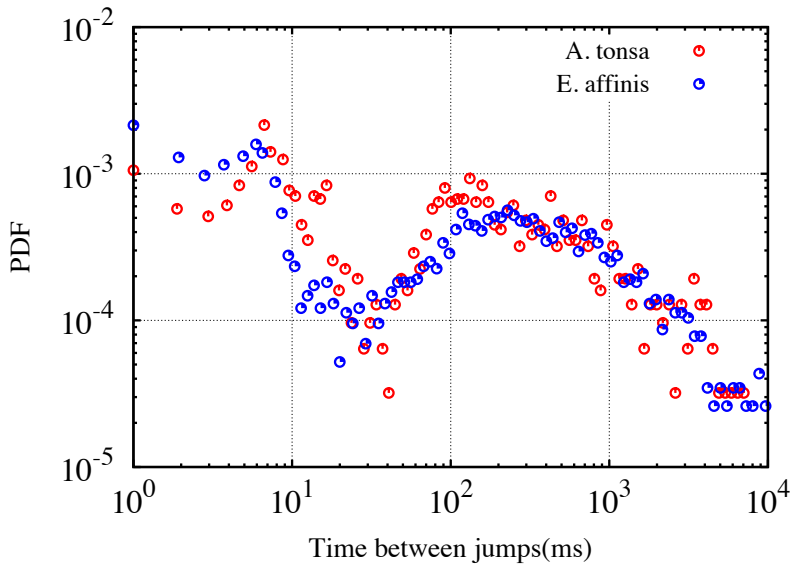

FIGURE 4.17: Probability density function of time between successive jumps of copepod species *E. affinis* and *A. tonsa*.

4.4 Summary

Our analysis revealed that copepods species react abruptly to the stimulus, however, their velocity decreases with lower rate in time, the interesting behavior which was captured by the aid of the high speed camera. It was also observed that copepods' jump velocity share common features; they decay exponentially with almost the same pattern. Considering a copepod with initial velocity $\mathrm{v}(0) = V$ which has obtained due to an acceleration at no-flow condition $\mathrm{u} = 0$, then eq. 3.38 becomes:

$$\frac{d\mathbf{v}}{dt} = -\frac{1}{\tau_p}\mathbf{v}(t) \tag{4.2}$$

The solution of this equation clearly indicates the stokes drag decreases copepod's velocity $\mathrm{v}(t) = Ve^{-t/\tau_p}$. These results have been published in Ardeshiri et al. (2016) which is also given in Appendix A.
Furthermore, the PDF of time difference of successive jumps, suggested the existence of a memory effect for both copepod species *E. affinis* and *A. tonsa*, however, it is not easy to obtain a functional behavior from this PDF. One may need more data and different type of stimulus in order to make a robust conclusion for copepods' behavior in still water.
These analysis are considered as the basis of the Lagrangian model which will be discussed later, despite the fact that the recorded data belong to copepods' behavior in still water. We believe that turbulence can affects the jump intensity but the decaying time associate to a purely hydrodynamical effect (Stokes drag of copepods). The effect of these parameters on copepods' behavior in turbulent flows will be discussed in the next chapters.

Chapter 5

Development of a Lagrangian model for copepods' dynamics

The effect of turbulence on copepods' behavior is discussed in this chapter, as a motivation to quantify their dynamics. Previous studies on active particles are reviewed and eventually our Lagrangian Copepod model in turbulent flows is introduced based on copepods' characteristics which were discussed previously.

5.1 Copepods in Turbulence

Turbulence is now widely recognized to have major impact on plankton's life *i.e.*, in micro-scales where predator-prey encounter rate, planktonic growth, mating rate and feeding pattern are affected to a great extent, whereas eddies in turbulence can shape large-scale distribution of the plankton. Here the goal is to provide more explanation on the effect of turbulence on copepods and vice versa.

Effect of Turbulence on copepods' growth Copepods like other planktonic species, rely on nutrient uptake to survive and grow. This process reduces the concentration boundary layer, a layer which is generated by decreasing the amount of nutrient and flow at the surface of the planktonic species (Kiørboe, 2008; Nishihara and Ackerman, 2009). Studies shows that turbulence can enhance nutrient uptake and increase copepods' (plankton) growth (Karp-Boss, Boss, and Jumars, 1996; Kiørboe, Ploug, and Thygesen, 2001) by reducing the thickness of the nutrient concentration boundary layer (Arin et al., 2002; Peters et al., 2006). In general,

Concentration boundary layer A layer which is generated when nutrient uptake reduces the nutrient concentration at the cell surface

plankton species feel the turbulence differently based on their size relative to the Kolmogorov length scale η. Karp-Boss, Boss, and Jumars (1996) found that a size of 60 μm is required for significantly increased nutrient uptake in turbulence, although this threshold is sensitive to turbulence intensity. Copepods' size range fits in this condition, so that turbulence has great impact on their growth rate. Not only the size, but many other parameters such as shape, physiology and environmental nutrient conditions can influence the nutrient uptake, hence the growth of copepods. Given that the interaction between turbulence and copepods' growth depend strongly on all this factors, it is a natural conclusion that environmental conditions can affect local community composition and size structure of species (Margalef, 1997).

Copepods' encounter rate In addition to affecting the community composition, copepods' growth and nutrient uptake, turbulence changes the sedimentation rates (Ruiz, as, and Peters, 2004; Ross, 2006) and affects the grazing pattern of copepods by enhancing the encounter rate (Rothschild and Osborn, 1988). Gerritsen and Strikler (1977) introduced the encounter rate for the first time in a laminar flow and many other authors (Rothschild and Osborn, 1988; Evans, 1989; Dower, Miller, and Leggett, 1997; Visser and MacKenzie, 1998; Seuront, Schmitt, and Lagadeuc, 2001) improved this theory and included the contribution of turbulence. Although turbulence increases the contact rates, on the other hand it can negatively affect ingestion (MacKenzie et al., 1994; Dolan et al., 2003) by decreasing the time of contact. High level of turbulence can directly affect copepods' ability to sense and capture their prey by interfering with hydromechanical signals copepods receive to locate prey. Finally, whereas increased encounter rates can enhance foraging rate for copepods, these copepods can experience increased contact rate with their predators, thus higher risk of mortality may balance the increased foraging rate (Visser, Mariani, and Pigolotti, 2009). Since laboratory experiments may interfere with organism behaviour, either predator or prey, it is difficult to characterize the real behavior and interaction of copepods. Although the effects of turbulence on encounter rates are studied mostly for the predator-prey interaction, this can be applied to any process that depends on the contact between particles *i.e.*, aggregate formation, copepods' mating, etc. Figure

5.1, illustrates the interaction of turbulence with plankton.

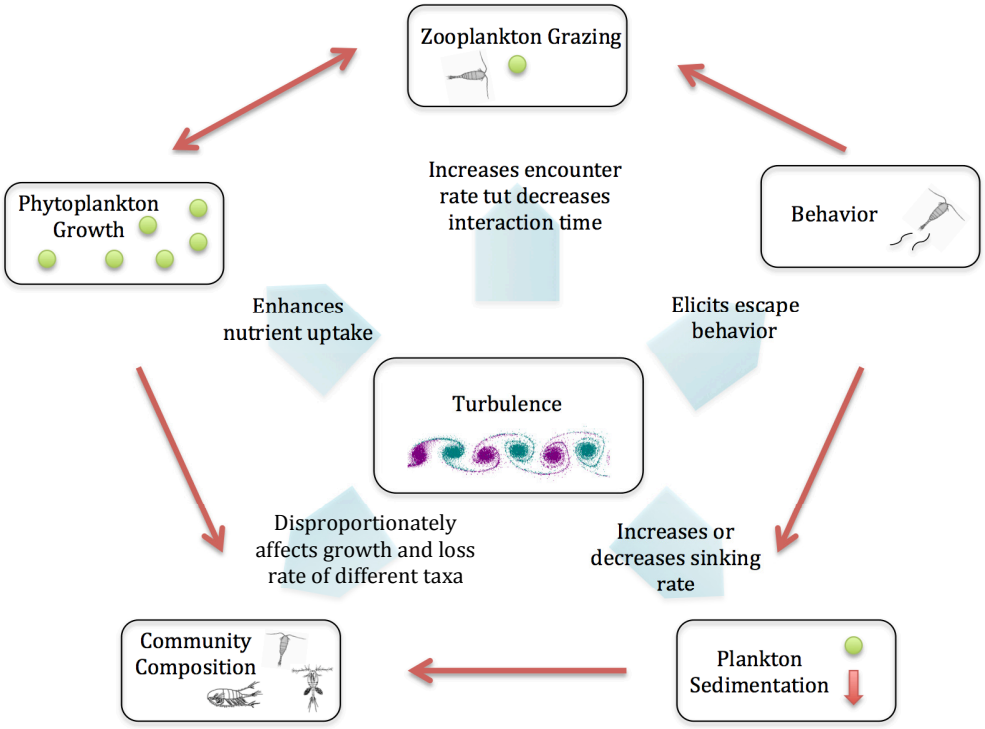

FIGURE 5.1: Schematic diagram illustrating potential impacts of turbulence on small-scale plankton processes and interactions between the small-scale plankton processes. Figure is adapted from (Jennifer et al., 2012).

Thin Plankton Layers The distribution of Plankton in the ocean is highly heterogeneous over length-scales ranging from thousands of kilometers down to few centimeters. Plankton can be patchy in their vertical distribution in the water column on meter scales normally less than $5\,m$ thick (Dekshenieks et al., 2001; Benoit-Bird, Cowles, and Wingard, 2009; Durham and Stocker, 2012). Small scale patchiness likely arises from interactions of plankton with small-scale chemical or hydrodynamics gradients (Durham, Climent, and Stocker, 2011; Seymour, Marcos, and Stocker, 2009; Gallager, Yamazaki, and Davis, 2004; Waters, Mitchell, and Seymour, 2003) whilst at large scales, growth rates favored by mesoscale processes such as nutrient upwelling and front formation (Gallager, Yamazaki, and Davis, 2008) lead to heterogeneity. This pervasive heterogeneity can affect the mean abundance of both phytoplankton and their

predators through their nonlinear interaction. Thin plankton layer is a particular form of this patchiness and occurs when large numbers of photosynthetic microorganisms are found within a small depth interval. This layers have a thickness of several centimeters to few meters, so they present strong vertical concentration gradients and are extending in several kilometers in the horizontal direction (Dekshenieks et al., 2001). Experimental observation of such a layer which is widespread is shown in Fig. 5.2. Multiple layers comprising distinct phytoplankton species can occupy different depths in the same water column. The depth is correlated with strong gradients in fluid density (stratification) and vertical shear (Rines et al., 2010).

Thin plankton layer
A layer with several kilometers in length and up to few meters in width

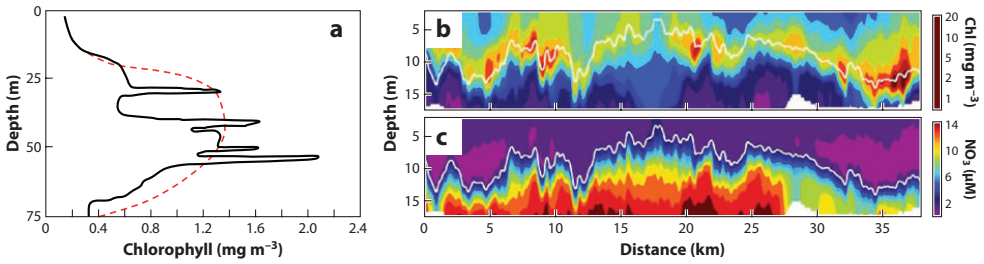

FIGURE 5.2: Thin phytoplankton layers observed in 1967 off La Jolla, California. The black line shows the continuous vertical chlorophyll concentration profile measured using a submersible pump and a ship-based fluorometer. The red dashed line shows the profile obtained using values from discrete depths, mimicking what would be obtained from bottle casts. This study revealed that the vertical distribution of phytoplankton often contains fine-scale spatial variability that eluded quantification by traditional sampling techniques. (b) Thin layers of chlorophyll (Chl), likely dominated by the flagellate Akashiwo sanguinea, observed at night in Monterey Bay using an autonomous underwater vehicle. (c) Concurrent measurements revealing that the upper portion of the water column was depleted of nitrate. Layers formed at night, as a result of downward vertical migration to the nutricline. Phytoplankton cells aggregated at the 3 μM nitrate isocline (white line in panels b and c). Panel a from Strickland (1968), b and c from Durham and Stocker (2012).

There are several mechanisms which describe the formation and persistence of thin layers, *i.e.*,

- **straining** which transforms initial horizontal phytoplankton heterogeneity into a thin layer, by progressively tilting a phytoplankton patch.
- **convergent swimming** in which species' motility are guided toward desirable conditions like nutrient concentration or daylight intensity, etc.
- **buoyancy** which applies on organisms whose density differs from that of the carrier fluid, results accumulation of plankton at their depth of neutral buoyancy.
- **gyrotactic trapping** which is to be discussed mathematically, is the interaction of the vertical migration of motile plankton species with shear rate, which results in tumbling of the microorganisms and trapping them in depth in a form of thin layer.
- **in situ growth** results formation of thin layer where growth rate is enhanced, for instance in region with highly nutrient concentration and suitable light intensities.
- **intrusion** which transports waters comprising high plankton concentration into adjacent waters containing lower concentrations, leads to layer formation.

These mechanisms are illustrated in Fig. 5.3. Notice that the most abundant form of plankton is copepod, so one can estimate the effect of thin layer formation on copepods' encounter rate, mating and feeding pattern. Planktonic species can have mutual influence on turbulence such as changing the viscosity at small scales or modify the background fluid by adding rearward momentum to the fluid. Jennifer et al. (2012) and Jenkinson and Sun (2010) provide more description on this topic.

5.2 Previous works

The study of swimming microorganisms and their interaction with fluid flows has attracted enormous attention in the last decade. A line of research has focused on characterizing individual swimming strategies by

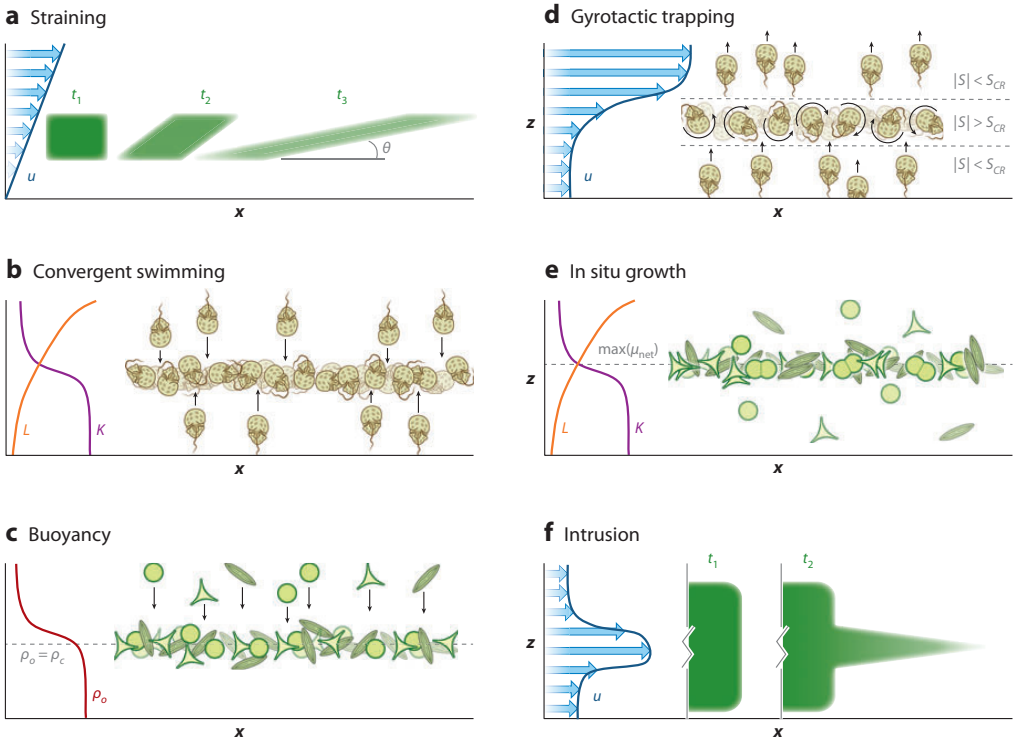

FIGURE 5.3: Diverse mechanism which drive thin layer formation a) straining, b) convergent swimming, c) buoyancy, d) gyrotactic trapping, e) in situ growth and f) intrusion from (Durham and Stocker, 2012).

means of experiments (Berg and Turner, 1979; Leonardo et al., 2010; Visser and Kiørboe, 2006) as well as by theoretical and numerical modelling (Lauga, 2016; Teran, Fauci, and Shelley, 2010). A second direction of study devoted to the consequences of swimming on population dynamics, *e.g.*, by focusing on encounter rates and other collective behaviours (Hernandez-Ortiz, Stoltz, and Graham, 2005; Baskaran and Marchetti, 2009; Lambert et al., 2013; Lushi, Wioland, and Goldstein, 2014; Drescher et al., 2011). A third direction focused on the mutual interactions of microorganisms with the fluid flow environment, in particular bio-induced flow fluctuations, sometimes dubbed as bacterial turbulence (Hohenegger and Shelley, 2010; Dunkel et al., 2013; Kaiser et al., 2014), or vice-versa, on active matter clustering induced by non homogeneous flows or fluid turbulence (Croze et al., 2013; Durham et al., 2013; Pedley and Kessler, 1992; Warnaas and Hondzo, 2006; Guasto, Rusconi, and Stocker, 2012; Bergstedt, Hondzo, and J. B, 2004; Stocker, 2012; Gustavsson et al., 2016; Lillo et al., 2014).

Here we limit ourself to the previous studies which have been performed on Lagrangian modeling of particles in fluid flows with focus on active swimmers/phytoplankton. A commonly used model for locomotion of swimming microorganisms, was first proposed by Pedley and Kessler (1992) where active particles can swim with slipping velocity in a preferred direction in addition to the contribution of carrier fluid velocity.

$$\frac{d\mathbf{x}}{dt} = \mathbf{u}[\mathbf{x}(t), t)] + \mathbf{v}_s\mathbf{p} \tag{5.1}$$

and spatiotemporal evolution of $\mathbf{p}$ can be obtained from:

$$\frac{d\mathbf{p}}{dt} = \frac{1}{2}\mathbf{\Omega}\times\mathbf{p} + \frac{\alpha^2-1}{\alpha^2+1}\mathbf{p}\cdot\mathcal{S}\cdot[\mathbf{I}-\mathbf{pp}] + \frac{1}{2\mathbf{B}}[\mathbf{k}-(\mathbf{k}\cdot\mathbf{p})\mathbf{p}] + \sqrt{D_R}\mathbf{\Sigma}(p)\boldsymbol{\xi} \tag{5.2}$$

in which $\mathbf{\Omega}$ is the fluid rotation rate antisymmetric tensor, defined as $\Omega_{ij} = 1/2(\partial_i u_j - \partial_j u_i)$, $\alpha \equiv l/d$ is the aspect ratio of the swimmers given by the ratio of length (l) to their diameter (d), $\mathcal{S}$ is the fluid deformation rate symmetric tensor, defined as $S_{ij} = 1/2(\partial_i u_j + \partial_j u_i)$, $\mathbf{I}$ the identity tensor, $\mathbf{B}$ the characteristic time that active particles take to reorient toward vertical direction, $\mathbf{k}$ is the preferential swimming direction, D_R is rotational diffusivity coefficient, $\mathbf{\Sigma}(p)$ is expressed by $\mathbf{\Sigma}(p) = \mathbf{I} - \mathbf{pp}/|\mathbf{p}|^2$,

and ξ is uniformly random vector in space.
The first term in the right hand side of eq. 5.2 accounts for tilting of particles by vorticity while the second term takes into account the effect of particles' shape. Rate of strain ($\mathcal{S}$) comes into play when particle is either oblate ($\alpha < 1$) or prolate ($\alpha > 1$) (Fig. 5.4). In fact spheroids are subjected

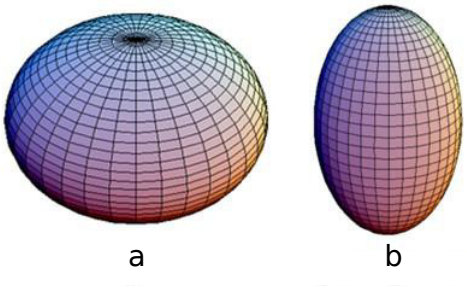

FIGURE 5.4: a) Oblate ($\alpha < 1$) and b) prolate ($\alpha > 1$) spheroids.

to the rate of strain tensor and undergo periodic rotation in so-called Jeffery's orbits. Full derivation of the second term and Jeffery's orbits are detailed in Jeffery (1922). Its phenomenology in turbulent flows has been investigated more recently in Parsa et al. (2012) where they only considered the first two terms of the right hand side of eq. 5.2.
The third term in the equation is pronounced when particle's center of symmetry is not the same as its center of mass. In this case, swimming direction can be guided in a preferential direction which results from the competition of gravitational force and viscous torque and is called *Gyrotaxis*. Kessler (1985) studied this phenomenon to explain hydrodynamics of motile alga cells and later on Pedley and Kessler (1992) and Jeffery (1922) proposed widely known form of swimming direction evolution. Eventually the last term is responsible for the stochastic rotational diffusivity of particles.

Gyrotaxis
Any directed locomotion resulting from a combination of gravitational and viscous torques in a flow

Similar models have been successfully employed for the description of the behaviour of phytoplankton, such as chlamydomonas (Torney and Neufeld, 2007; Durham, Climent, and Stocker, 2011; Ardekani and Gore, 2012) in laminar flows. Taylor-Green Vortex (TGV) flow (Solomon and Gollub, 1988) were used in their studies where Torney and Neufeld (2007) and Ardekani and Gore (2012) studied orientation of spheroidal particles by neglecting gyrotaxis and rotational diffusivity and showed that

the spatial distribution of microorganisms depends on motility, vorticity strength and rheological properties of the background fluid. Durham, Climent, and Stocker (2011) instead considered the gyrotactic phytoplankton and ignored the stochastic rotational diffusion. They showed that coupling between flow and motility in some conditions leads to aggregation of swimmers, where relative swimming speed of particles and gyrotactic orientation parameter (**B**) are important parameters. This suggests that vortical flows (TGV) can be used to separate species with different motility characteristics.
More recently, Durham et al. (2013), Croze et al. (2013), Lillo et al. (2014), and Zhan et al. (2014) applied this model in turbulent flows, among them Croze et al. (2013) considered all the contributions in eq. 5.2 to study the dispersion of swimming algae, while others neglected the last term. Their findings shows that turbulence can generate clustering of particles which is given by the gyrotactic effect and is a non-isotropic effect induced by the presence of the the external gravity field.
Copepods and zooplankton in general, display higher complexity compared *e.g.*, to algae species because of their higher motility. In the following we describe our Lagrangian model.

5.3 Model equation for copepods dynamics

In this section we introduce a simple model system of copepod's dynamics. This representation is based on the idea that the copepod's trajectories in a fluid can be mimicked by properly defined active particles.
The model relies both on biological and hydrodynamical assumptions.

- We assume that copepods respond always in the same way to external flow disturbances.
- Their jump reaction is embedded in their neural system.
- The stimulus triggering the jump is highly stylised, we only take into account a mechanical signal with a single-threshold, to be specified

later on, and ignore any other activity induced by light, food, or chemistry (*e.g.,* pheromones).

- Copepods have no memory of their previous jumps.

On the mechanical side:

- We assume that copepods are small enough that their centre of mass can be considered a perfect fluid tracer in a flow, except for the time when a jump event takes place. In hydrodynamic terms this means that copepods are assumed to be rigid, homogeneous, neutrally buoyant particles with a size which is of the order of the dissipative scale of the flow.
- Gravity force has no role in producing acceleration or torque. Only the drag force effect is taken into account during the jumps.
- Copepods are coupled to the fluid in a one-way fashion, they react and are carried by the fluid but they do not modify the surrounding flow.
- Copepods-copepods interactions are also neglected.

Adding all together the above hypothesis the LC equation of motion is as follows:

$$\dot{\mathbf{x}}(t) = \mathbf{u}(\mathbf{x}(t), t) + \boldsymbol{J}(t, t_i, t_e, \dot{\gamma}, \mathbf{p}) \tag{5.3}$$

where $\mathbf{u}(\mathbf{x}(t), t)$ is the velocity of the carrying fluid at time t and position $\mathbf{x}(t)$ and $\boldsymbol{J}$ is an added velocity term that describes the active behaviour (jump) of the copepod. $\boldsymbol{J}(t, t_i, t_e, \dot{\gamma}, \mathbf{p})$ is a function of time t, it depends also on an initial and a final time t_i and t_e, on flow shear rate value $\dot{\gamma}$ and on orientation vector $\mathbf{p}$. If copepods are taken to be spherical in shape, their orientation dynamics is given by:

$$\dot{\mathbf{p}}(t) = \boldsymbol{\Omega} \cdot \mathbf{p}(t) \tag{5.4}$$

with

$$\mathbf{\Omega} = \frac{1}{2}(\nabla \mathbf{u} - (\nabla \mathbf{u})^T) = \begin{bmatrix} 0 & \frac{1}{2}(\frac{\partial u}{\partial y} - \frac{\partial v}{\partial x}) & \frac{1}{2}(\frac{\partial u}{\partial z} - \frac{\partial w}{\partial x}) \\ \frac{1}{2}(\frac{\partial v}{\partial x} - \frac{\partial u}{\partial y}) & 0 & \frac{1}{2}(\frac{\partial v}{\partial z} - \frac{\partial w}{\partial y}) \\ \frac{1}{2}(\frac{\partial w}{\partial x} - \frac{\partial u}{\partial z}) & \frac{1}{2}(\frac{\partial w}{\partial y} - \frac{\partial v}{\partial z}) & 0 \end{bmatrix} \tag{5.5}$$

While in general the following form of eq. 5.2, which is valid for axisymmetric ellipsoidal particles, is chosen:

$$\dot{\mathbf{p}}(t) = \left(\mathbf{\Omega} + \frac{\alpha^2-1}{\alpha^2+1}\left(\mathcal{S} - \mathbf{p}^{\boldsymbol{T}}(t) \cdot \mathcal{S} \cdot \mathbf{p}(t)\right)\right) \cdot \mathbf{p}(t) \tag{5.6}$$

Aspect ratio of copepod is typically around 3 for *Eurytemora affinis* species available in Laboratory of Oceanology and Geoscience (LOG).
Notice that here we designate by $\mathcal{S}$ the fluid deformation rate symmetric tensor:

$$\mathcal{S} = \frac{1}{2}(\nabla \mathbf{u} + (\nabla \mathbf{u})^T) = \begin{bmatrix} \frac{\partial u}{\partial x} & \frac{1}{2}(\frac{\partial u}{\partial y} + \frac{\partial v}{\partial x}) & \frac{1}{2}(\frac{\partial u}{\partial z} + \frac{\partial w}{\partial x}) \\ \frac{1}{2}(\frac{\partial v}{\partial x} + \frac{\partial u}{\partial y}) & \frac{\partial v}{\partial y} & \frac{1}{2}(\frac{\partial v}{\partial z} + \frac{\partial w}{\partial y}) \\ \frac{1}{2}(\frac{\partial w}{\partial x} + \frac{\partial u}{\partial z}) & \frac{1}{2}(\frac{\partial w}{\partial y} + \frac{\partial v}{\partial z}) & \frac{\partial w}{\partial z} \end{bmatrix} \tag{5.7}$$

and the shear rate is then defined as $\dot{\gamma} = \sqrt{2\,\mathcal{S} : \mathcal{S}}$ where $\sqrt{\mathcal{S} : \mathcal{S}}$ means norm of the fluid deformation rate symmetric tensor which is given by *Frobenius* norm or the *Hilbert-Schmidt* norm $||\mathcal{S}|| = \sqrt{trace(\mathcal{S}^T\mathcal{S})}$. We note that the fact that the jump term is assumed to depend on $\dot{\gamma}$ represents a generalization to the 3D geometry of Kiørboe's empirical findings (Kiørboe, 2008).
For the jump term we propose the following functional form:

$$\boldsymbol{J}(t, t_i, t_e, \dot{\gamma}, \mathbf{p}) = H[\dot{\gamma}(t_i) - \dot{\gamma}_T]\, H[t_e - t] u_J\, e^{\frac{t_i - t}{\tau_J}}\, \mathbf{p}(t_i) \tag{5.8}$$

where $H[x]$ denotes the Heaviside step function, $\dot{\gamma}_T$ is a threshold value of the shear rate, u_J and τ_J are two characteristic parameters characterising the jump shape, its velocity amplitude (u_J) and duration τ_J respectively. The first H step function models the fact that a jump can begin only when the shear rate is above the given threshold value, while the second step function accounts for the fact that the jump time span is finite. Figure 5.5 illustrates better the kinematics of copepods' jump when the shear rate is

above the threshold value. The jumps are sharp at initial time and decay

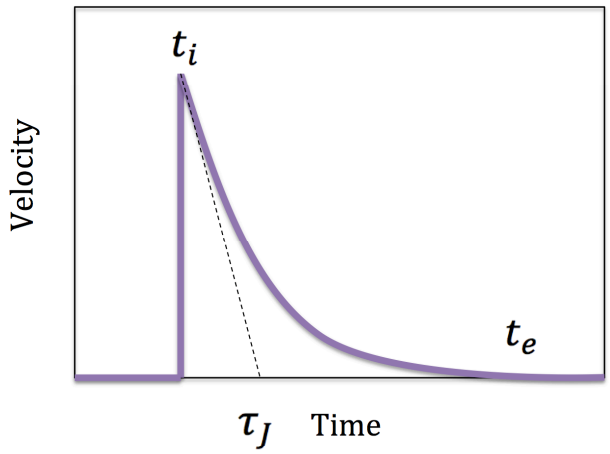

FIGURE 5.5: Kinematics of a jump of a copepod in regions where $\dot{\gamma} > \dot{\gamma}_T$. It is a function of t_i, t_e, u_J and τ_J.

exponentially with latency time of τ_J as we obtained this from experimental jump data analysis. The initial and final time of a jump are defined as:

$$t_i = t \quad \text{if} \quad (\dot{\gamma}(t) > \dot{\gamma}_T) \cap (t > t_e) \tag{5.9}$$

$$t_e = t_i + c\,\tau_J = t_i + \log(10^2)\,\tau_J \tag{5.10}$$

In other words we assume that a jump can not begin if a previous jump has not finished ($t > t_e$) and that a jump terminates when its amplitude has decreased to a negligible level, here taken as one percent of the initial amplitude, *i.e.*, $|\boldsymbol{J}(t_e)| = 10^{-2}|\boldsymbol{J}(t_i)|$.
As mentioned, according to our LC model, drag is the only force acting on jumping behavior of copepods. Taking into account the simplified equation of motion of particles in the flow (eq. 3.38) and ignoring the added mass effect:

$$\ddot{\boldsymbol{x}} = \frac{1}{\tau_p}(\mathbf{u} - \dot{\boldsymbol{x}}) \tag{5.11}$$

thus, formal solution of this equation with initial condition of $\dot{\boldsymbol{x}}(0) = \mathbf{u}(0) + \mathbf{u}_J$, and $\mathbf{u}(0) = 0$, can be written as:

$$\dot{\boldsymbol{x}}(\tau) \cong \mathbf{u}(0) + \mathbf{u}_J e^{-\tau/\tau_p} \tag{5.12}$$

where $\tau_p = \frac{a^2}{3\beta\nu}$ is the Stokes response time of a copepod. Based on this finding, we can associate τ_J, the copepods' jump decay time that we extracted from the experiments to be the effective response time of the copepods. We note that by assuming a nominal copepod radius of $0.5\,mm$ with $\rho_p \simeq \rho_f$, one can estimate the Stokes particle response time which is $\tau_p = 83.3\,ms$, but the effective particle response time may be smaller due to the non-linear effect induced by a high Reynolds number of the copepod (Re_p) which can be of the order of $\mathcal{O}(10^2)$. If we assume that a copepod can swim with a velocity of $v \simeq 2 \cdot 10^{-1} ms^{-1}$, then $Re_p \simeq 200$. By using the Shiller-Neumann relation (Schiller and Neumann, 1933) for the response time, $\tau_{p,min} = \frac{a^2}{3\beta\nu}\left(\frac{1}{1+C_{Re_p}}\right)$ where $C_{Re_p} = 0.15\,Re_p^{0.687}$, one obtains $\tau_{p,min} = 12.3ms$ which is closer to our estimation from the experiments ($\tau_J \simeq 8ms$).

5.3.1 Model tuning for turbulent flows

We now take into account the presence of the oceanic flow environment surrounding the copepods. The properties of oceanic turbulence relevant for our work have been studied, among others by MacKenzie and Leggett (1993) and Jiménez (1997). In these surveys it was observed that the mean value of the turbulent kinetic energy dissipation rate, $\epsilon = 2\nu\mathcal{S} : \mathcal{S}$, varies from about $10^{-8}\,m^2s^{-3}$ in open ocean to $10^{-4}\,m^2s^{-3}$ in coastal zones (although it is also sensitive to the wind speed conditions and on the depth). The value of ϵ along with the kinematic viscosity of sea water, ν, allow to estimate the Kolmogorov scales of ocean turbulence: The dissipative length $\eta = (\nu^3/\epsilon)^{1/4}$, time $\tau_\eta = (\nu\epsilon)^{1/2}$ and velocity $u_\eta = (\nu\epsilon)^{1/4}$. The order of magnitude estimate as from Ref. Jiménez (1997) for these quantities are reported in table 5.1. According to the same authors the typical Taylor-scale Reynolds number Re_λ in the ocean can reach values up to $\mathcal{O}(10^2)$.

Given that the typical size of copepods is of the order of millimetres, it is clear that the relevant flow scales for their dynamics are close to the Kolmogorov scale or below in turbulence (Yen, 2000). Figure 5.6 shows

the smallest and largest scale present in the ocean in terms of ϵ and a parameter N which is the buoyancy or *Brunt-Väisälä* frequency. The smallest scale (Kolmogorov scale) is shown by L_K in this figure.

Brunt-Väisälä frequency
The angular frequency at which a vertically displaced parcel will oscillate within a statically stable environment

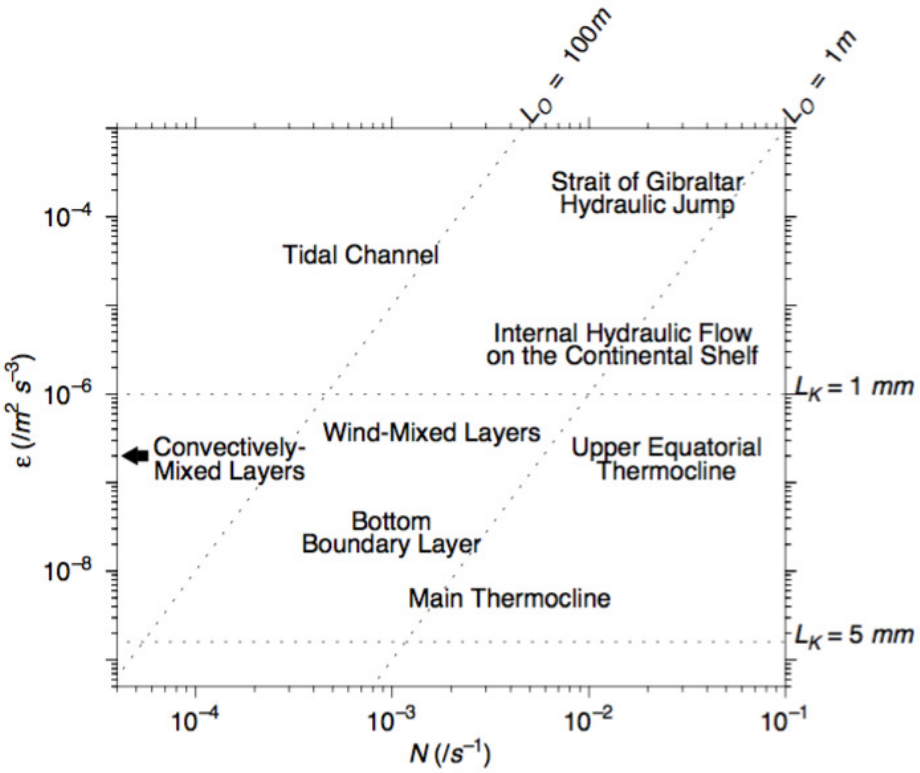

FIGURE 5.6: Regimes of ocean turbulence located with respect to stratification and energy dissipation. Dotted lines indicate Ozmidov[1] and Kolmogorov length scales (Smyth and Moum, 2001).

When the LC model is recast in a dimensionless form in terms of these scales we get three dimensionless groups of parameters: τ_J/τ_η, u_J/u_η and $\tau_\eta\dot{\gamma}_T$. These parameters, together with the flow Re_λ fully specify the working conditions (or tuning) of the copepods-in-turbulence model.

Three control parameters
τ_J/τ_η, u_J/u_η and $\tau_\eta\dot{\gamma}_T$

In this study we take as reference for the energy dissipation rate the value $\epsilon = 10^{-6}\, m^2 s^{-3}$, and by taking into account the dimensional values estimated for the copepods jump intensity u_J and jump decaying time τ_J , the ratios $u_J/u_\eta = 83.599$ and $\tau_J/\tau_\eta = 0.0080727$ can be deduced from the

[1] A length scale for the description of turbulent flows under stable stratification, defined as the square root of the ratio between the dissipation rate of turbulent kinetic energy and the third power of the Brunt-Väisälä frequency.

similarity analysis for copepod species *E. affinis*. These dimensionless values for copepod species *A. tonsa* is $u_J/u_\eta = 83.792$ and $\tau_J/\tau_\eta = 0.007351$. This tells us that in ordinary turbulence conditions the copepods possess an almost instantaneous reaction, since their response time is about one hundredth of the smallest scale of turbulence. On the opposite the velocity reached during a jump is of a magnitude that is comparable if not higher to the one of turbulent velocity fluctuations. Finally, we note that we do not have any experimental guess for the magnitude of $\dot{\gamma}_T$, therefore the value $\tau_\eta \dot{\gamma}_T$ is a free parameter of our model.

Parameter	Unit	Range		This study
ν	$m^2 s^{-1}$	$\sim 10^{-6}$		10^{-6}
ϵ	$m^2 s^{-3}$	10^{-8}	10^{-4}	10^{-6}
η	m	3×10^{-3}	3×10^{-4}	10^{-3}
τ_η	s	10	0.1	1
u_η	ms^{-1}	3×10^{-4}	3×10^{-3}	10^{-3}
Re_λ	–	$\mathcal{O}(10^2)$		80

TABLE 5.1: Reference properties of the ocean turbulent flow as from Jiménez (1997). ϵ is the mean turbulent energy dissipation rate, η, τ_η and u_η are the turbulence space, time and velocity dissipative scales. Re_λ is the Taylor-scale based Reynolds number. Their approximate range of variability is given together with the reference values chosen for the similarity analysis in the present study.

5.4 Case study: Taylor - Green Vortex flow

The Taylor-Green vortex (TGV) is a canonical problem in fluid dynamics developed to study vortex dynamics, turbulent transition, turbulent decay and the energy dissipation process. The TGV problem contains several key physical processes in turbulence in a simple construct and therefore is an excellent case for the evaluation of turbulent flow simulation methodologies.

Here two-dimensional TGV (also known as cellular flow or Solomon and Gollub flow (Solomon and Gollub, 1988)) is taken in order to study the behavior of passive/active particles under the Lagrangian Copepod (LC)

model in a simple vortex flow. The incompressible cellular flow is composed of a periodic array of two-dimensional eddies in square cells of size L and can be specified by the following streamfunction:

$$\psi(\mathrm{x},\mathrm{y},t) = \frac{A}{k}\, sin\left(k\left(\mathrm{x} - b\, sin\left(\omega t\right)\right)\right)\, sin\left(k\left(\mathrm{y} - b\, sin\left(\omega t + \phi\right)\right)\right) \quad (5.13)$$

where the choice of A, k, b, ω and ϕ can be different. Here we choose $A = U_0$ where U_0 is the fluid velocity at the cell boundaries, $L = 2\pi$, $k = \pi/L$, $b = L/4$, $\omega = 1/\tau$ where $\tau = L/U_0$ and $\phi = \pi/2$. The components of the fluid velocity vector $\mathbf{u}$ are:

$$\mathrm{u_x} = \frac{\partial \psi}{\partial \mathrm{y}} = A\, sin\left(k\left(\mathrm{x} - b\, sin\left(\omega t\right)\right)\right)\, cos\left(k\left(\mathrm{y} - b\, sin\left(\omega t + \phi\right)\right)\right) \quad (5.14)$$

$$\mathrm{u_y} = -\frac{\partial \psi}{\partial \mathrm{x}} = -A\, cos\left(k\left(\mathrm{x} - b\, sin\left(\omega t\right)\right)\right)\, sin\left(k\left(\mathrm{y} - b\, sin\left(\omega t + \phi\right)\right)\right) \quad (5.15)$$

in the steady state, the eq. 5.14 and 5.15 are simplified to:

$$\mathrm{u_x} = U_0\, sin\left(\frac{\pi \mathrm{x}}{L}\right)\, cos\left(\frac{\pi \mathrm{y}}{L}\right) \quad (5.16)$$

$$\mathrm{u_y} = -U_0\, cos\left(\frac{\pi \mathrm{x}}{L}\right)\, sin\left(\frac{\pi \mathrm{y}}{L}\right) \quad (5.17)$$

Fig. 5.7 illustrates the velocity profile and streamlines of the cellular flow in 2D. This configuration can be repeated with opposite direction alternately along axis, so that the general shape of TGV flows can be reached (Fig. 5.8). Here we focus only on the interval $[0, L]$ as shown in Fig. 5.7 to study the dynamics of particles and copepods in a simple vortex flow, which may give us a good vision of their behavior in real turbulent flows consisting of more complicated eddies.

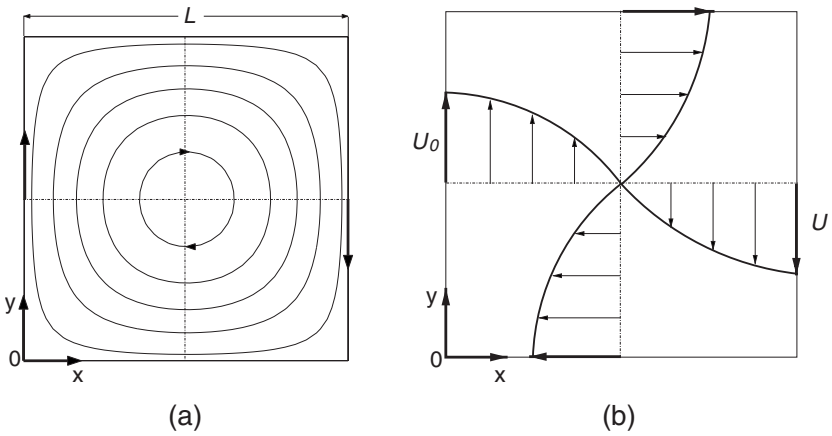

FIGURE 5.7: a) Streamlines and b) velocity profiles for the periodic cellular flow field. The arrows show direction of the flow (Marchioli, Fantoni, and Soldati, 2007).

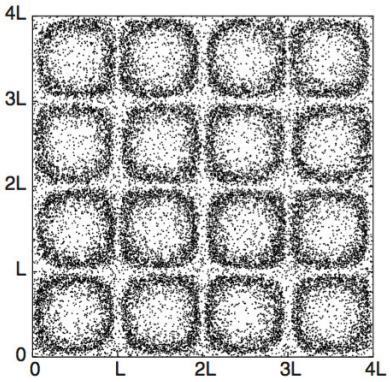

FIGURE 5.8: General configuration of 2D TGV flows (Marchioli, Fantoni, and Soldati, 2007). It consists of several eddies placed homogeneously in a plane. The rotation direction of vortices changes alternately.

This flow can illustrate clearly the differences between the tracers' motion and the displacement of heavy/light particles in the flow, for this special case in a vortex flow. As mentioned in chapter 3, the simplified equation of motion of particles is written as:

$$\frac{d\mathbf{v}}{dt} = \beta \frac{D}{Dt}[\mathbf{u}(\mathbf{x}(t), t)] - \frac{1}{\tau_p}[\mathbf{v}(t) - \mathbf{u}(t)] \tag{5.18}$$

with $\beta = 3\rho_f/(2\rho_p + \rho_f)$, the density ratio and $\tau_p = a^2/(3\beta\nu)$, the stokes time of the particle. Tracers follow the streamlines of the flow since they do not experience any forces from the carrier fluid, however as discussed

before, light particles are trapped by the vortex while heavy particles tend to accumulate in low vorticity regions. Fig. 5.9 illustrates this behavior of light and heavy particles in the 2D - TGV flow. Visualization of tracers,

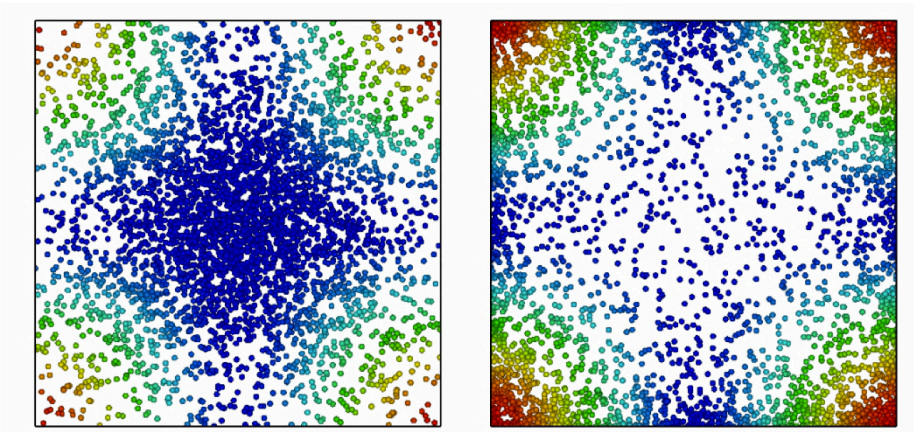

(a) (b)

FIGURE 5.9: Snapshots of the flow taken after 2 eddy turnover time from initially homogeneously distributed condition showing that a) light particles ($St = 0.03, \beta = 1.5$) accumulate in the high vorticity region while b) heavy particles ($St = 0.4, \beta = 0.09$) are taken away from the vortex's core. Colors correspond to the amplitude of the shear rate.

heavy and light particles in the steady cellular flow can be found in:

- Tracers: https://www.dropbox.com/s/4vbjyhfr5i2tk2y/Tracers.mpg?dl=0
- Light particles: https://www.dropbox.com/s/ieglyx9mudm7fta/Light-particles-0.5.mpg?dl=0
- Heavy particles: https://www.dropbox.com/s/726lsutcbu8844l/Heavy-particles-15.mpg?dl=0

The colors in Fig. 5.9 correspond to the amplitude of the shear rate which can be estimated through the following relations. Based on the definition, the energy dissipation rate ϵ can be obtained by:

$$\epsilon = \frac{\nu}{2} \sum_{ij} \left(\partial_i u_j + \partial_j u_i\right)^2 \tag{5.19}$$

which is linked to the rate-of-strain tensor $\epsilon = 2\nu < \mathcal{S}_{ij}\mathcal{S}_{ij} >$ and of course to the shear rate by $\dot{\gamma} = \sqrt{2\,\mathcal{S} : \mathcal{S}}$. The distribution of this quantity can be found in Fig. 5.10 where it indicates that the central region of the domain has the lowest shear rate, however this quantity is maximum in the corners. Implementing the LC model in this flow and taking

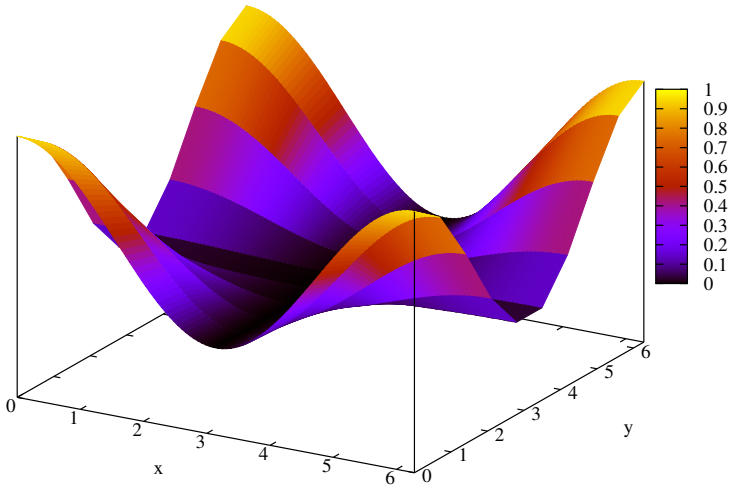

FIGURE 5.10: Distribution of the shear rate in TGV flow. High shear rate intensities are found in the corners and regions with low shear rate intensities are in the center.

into account the existence of only one threshold value of the shear rate (the upper threshold as described in Kiørboe (2008)), copepods have to escape from regions with high shear rate intensities. This is shown in Fig. 5.11 where copepods avoid the corners by jumping into calm regions and in fact they accumulate at the interface of high and low shear rate regions. The threshold value of the shear rate in this flow is set to 0.33 and copepods jump in random direction in a plane. The visualization has been done with and without the flow to better see the performance of LC model and investigate the influence of the flow on copepods. This can be found in:

- Copepods in TGV domain without flow: https://www.dropbox.com/s/nog726bldn2rsvi/Copepod-in-TGV-no-Flow.mpg?dl=0
- Copepods in steady TGV flow: https://www.dropbox.com/s/v9yqurbqggbcsiv/Copepod-in-TGV-steady.mpg?dl=0

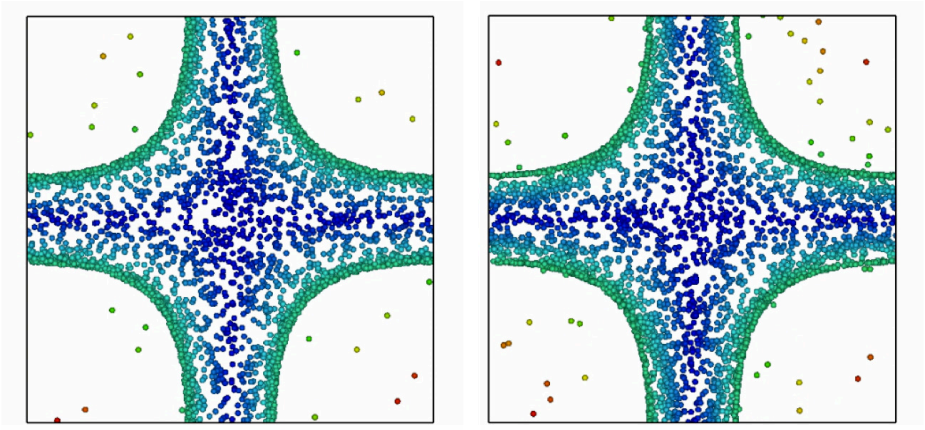

FIGURE 5.11: Snapshots of the flow taken after 2 eddy turnover time from initially homogeneously distributed condition showing the distribution of copepods in TGV a) without flow and b) in the presence of the flow. The shear rate threshold value is set to 0.33 in the domain (Fig. 5.10 represents the distribution of shear rate value).

It is evident that copepods jump into the calm regions, however some individuals can be found in regions with shear rate higher than the given threshold as can be seen from Fig. 5.11 (a). This is due to a very small random walk of copepods that has been imposed which takes some copepods in the forbidden regions and makes them to react. Panel (b) of Fig. 5.11, represents the distribution of copepods in the presence of the carrier flow. It is expected to have more individuals in the forbidden regions in this case. The copepods are dispersed in TGV flow in almost one dimensional manner quantified by a correlation dimension (to be discussed in next chapter) $D_2 \approx 1.4$ in no-flow and $D_2 \approx 1.2$ in the presence of the flow.

Time dependent TGV flow is more complicated and needs more effort to understand the particles' behavior in its chaotic flow. The behaviour of particles and copepods can be found in:

- Tracers in time-dependent TGV: https://www.dropbox.com/s/uirrpbt5b4fg1mv/Tracers-in-time-dependent-TGV.mpg?dl=0
- Copepods in time-dependent TGV: https://www.dropbox.com/s/7pkgdixq9em8gds/Copepod-in-time-dependent-TGV.mpg?dl=0

Compared to TGV flows, turbulence is much more complicated where we have a hierarchy of time and spatial scales. This is to be discussed in detail in the next chapter.

Chapter 6

Analysis of spatial distribution of Lagrangian copepods

In this section the results of the implemented LC model in the homogeneous isotropic turbulent flow will be addressed. First the single point statistics of the copepods are assessed. Later we will quantify the non-homogenous distribution of copepods by using a technique which is introduced in a separate section. Moreover the influence of the geometrical aspect ratio, the direction of the jump and the jump time latency on particles' spatial distribution are recognized.

As mentioned in previous chapter, the LC model is characterised by three control parameters: the jump intensity u_J, the decaying time of the jump τ_J and the shear rate threshold value $\dot{\gamma}_T$, which are conveniently presented in dimensionless form in terms of turbulence dissipative scale units. Since the LC model is just one-way coupled to the fluid, in the numerics we can perform simultaneous simulations of several families of copepods in the same turbulent flow, where each family is characterized by the triplet $\left[u_J/u_\eta, \tau_J/\tau_\eta, \dot{\gamma}_T\tau_\eta\right]$.
In agreement with the experimental observation we always keep fixed the decaying time of the jump to the value $\tau_J/\tau_\eta = 10^{-2}$, while the other parameters are varied independently in the ranges $u_J/u_\eta \in [1, 400]$ and $\tau_\eta\dot{\gamma}_T \in [0, 4]$. Note that if $\dot{\gamma}_T = 0$, according to the model, all the particles will jump in a synchronous way. In order to avoid such an unphysical feature, the time t_e for each particle is initialized by a random variable with homogeneous distribution in the interval $[0, \log(10^2)\,\tau_J]$.
We perform a series of simulations with multiple families, with about

2.56×10^5 particles per family[1]. The simulation was started and particles were let displace for about 2 eddy turnover times, after that during the following ∼2 eddy turnover times about 10 instantaneous distributions of LC particles were saved for analysis. Copepods are modeled as solid sphere particles and orientation vector affected by fluid rotation rate (eq. 5.4), unless otherwise noted. For comparison a set of passive fluid tracers are also included in all our simulations.

6.1 Single Point Statistics

Distribution of the shear rate $\dot{\gamma}_T$, as one of the main control parameters, gives us a better view on the copepods activity in turbulence. Figure 6.1 which represents this quantity, indicates that Probability Density Function (PDF) of the shear rate varies in a narrow range. Since our LC model in linked to the spatial distribution of the shear rate, we expect copepods to be more sensitive in this range and be less active in regions with higher shear rate intensity

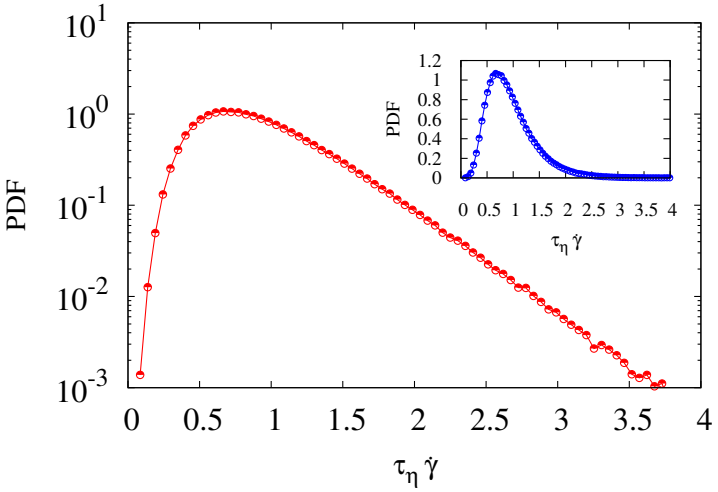

FIGURE 6.1: Probability distribution function of the shear rate in turbulence at $Re \sim 80$.

In order to see how the LC dynamics in turbulence differ from that of a fluid tracer, we first address the velocity single point statistics. The PDF of

[1] In physical dimension this corresponds to a number density of $\mathcal{O}(1)$ LC particles per cm^3, a density comparable to the one found for real copepods estuarine water.

the absolute value of single component velocity for the copepods, *i.e.*, $|\dot{x}_i|$, is shown in figure 6.2. Tracers, the particles which move along the streamlines, agree with a Gaussian distribution, while for copepods a slower decaying tail is found. Gaussian distribution is a statistical distribution, here with probability density function of:

$$P(x) = \frac{2}{\sigma\sqrt{2\pi}} e^{-(x-\mu)^2/2\sigma^2} \tag{6.1}$$

where σ is the measured root mean square velocity of the Eulerian field and μ is mean velocity equal to zero.

This deviation becomes more pronounced at increasing the jump intensity for a given threshold value of the shear rate, as shown in figure 6.2(a). It also appears that low jump intensities $u_J < 10\,u_\eta$ are not strong enough to make effective changes on the copepods PDF. On the other hand, increasing the threshold value of the shear rate leads to fewer jumps, therefore in this case copepods behave almost like tracers. Their deviation in velocity distribution from the Gaussian, indeed increases by decreasing the shear rate threshold value as can be seen in figure 6.2(b).
The general trend of the observed deviation from Gaussianity can be predicted by means of the following probabilistic model. We suppose that the instantaneous single cartesian component velocity of LC particles can be approximated by the sum of three statistical independent random variables. The first variable accounts for the turbulent velocity field contribution, therefore it is a Gaussian with zero mean and same standard deviation as the one measured in the DNS. The second and the third variable mimic respectively the jump direction and its intensity: we assume that the orientation is random uniform in the solid angle and that the jumps happen uniformly in time. One can obtain the resulting PDF for the LC particle velocity from the convolution of the three elementary PDFs associated to the three described random variables. The resulting density distribution function when compared to the LC measurements at low threshold value $\tau_\eta \dot{\gamma}_T = 0.21$ (*i.e.*, when copepods jump very frequently), shows an overall qualitative agreement with a slight deviation in the tails (see Fig. 6.2(b)).
Such a discrepancy comes from the fact that in reality the jump directions

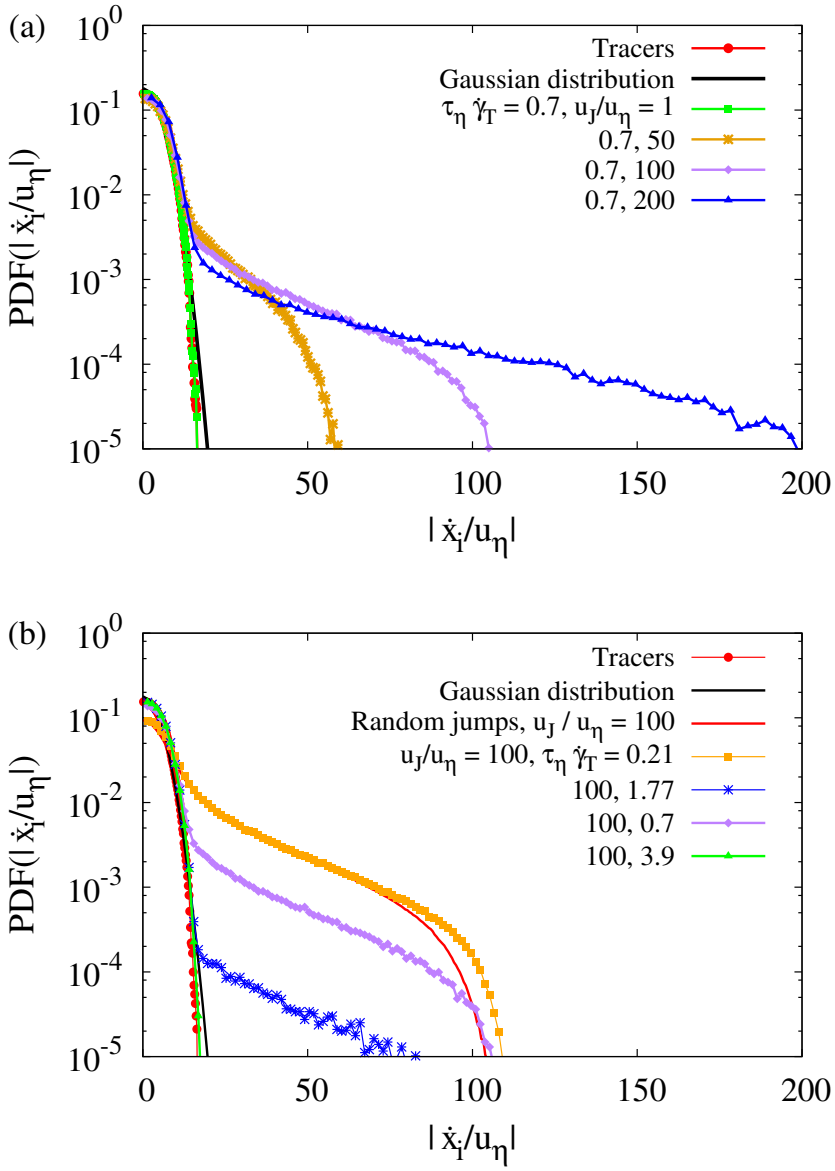

FIGURE 6.2: Probability density function of absolute value of single component velocity $|\dot{x}_i/u_\eta|$ for the copepods. (a) at constant threshold value $\tau_\eta\dot{\gamma}_T = 0.7$ and different jump intensities. Gaussian distribution is a statistic distribution here with the measured root mean square velocity of the Eulerian field as the standard deviation. (b) at constant jump intensity $u_J/u_\eta = 100$ for different shear rate threshold values. Random jumps correspond to the expected velocity distribution when randomly oriented jumps occur uniformly in time on top of the turbulent velocity field.

develop some correlations with the underlying flow, via Eq. 5.4, while the probabilistic model neglects it. One can make use of the approximate

probabilistic model to estimate the average fraction of particle performing jumps as a function of the shear-rate threshold value. This is done by introducing an adjustable parameter accounting for the probability that a given particle is actually jumping, and by fitting the model to the PDF curves. This is shown in equation below:

$$\dot{\mathbf{x}}(t) = \mathbf{U} + \alpha\, \mathbf{p}\, \mathrm{u}_J\, e^{-t/\tau_J} \tag{6.2}$$

where $\mathbf{U}$ is the Gaussian random variable with zero mean and standard deviation equal to the one in turbulent flow, α is the jumping fraction and $\mathbf{p}$ is random jump vector. Jump intensity is shown with u_J while τ_J is a flat random between zero and the final time of the jump ($[0, t_e]$). Figure 6.3 shows the fitted predictions obtained with such a procedure (which confirms the validity of the probabilistic model), while the inset of the same figure displays the inferred jump percentage as a function of the shear rate threshold value. We observe an exponential decrease as $\dot{\gamma}_T$ is raised. For the value $\tau_\eta \dot{\gamma}_T = 0.5$, the jumping particle fraction is around 50%.

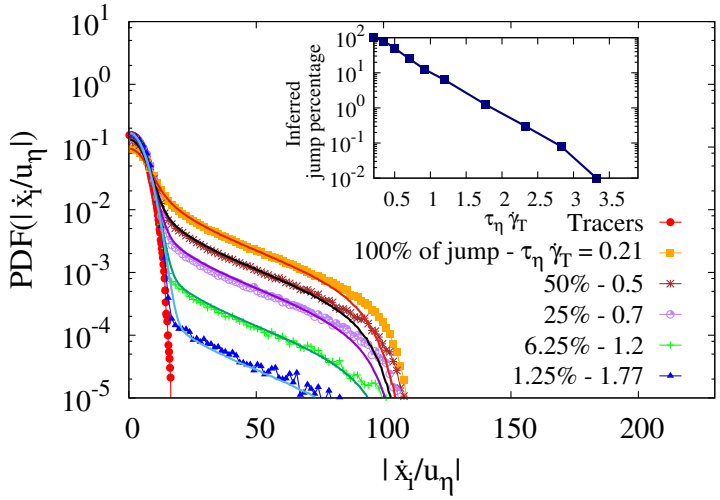

FIGURE 6.3: Probability density function of absolute value of single component velocity $|\dot{x}_i/u_\eta|$ for the copepods at constant jump intensity $u_J/u_\eta = 100$ for different shear rate threshold values. Fitted PDF curves correspond to the percentage of jump of copepods. (Inset) Deduced percentage of jump as a function of the shear rate threshold value $\tau_\eta \dot{\gamma}_T$.

We finally observe that the shape of the PDF displayed by the LC model, is also in qualitative agreement with a recently published experimental study (Michalec, Souissi, and Holzner, 2015), despite the fact that the experiment has been performed in low Reynolds number conditions (up to $Re_\lambda \simeq 30$).

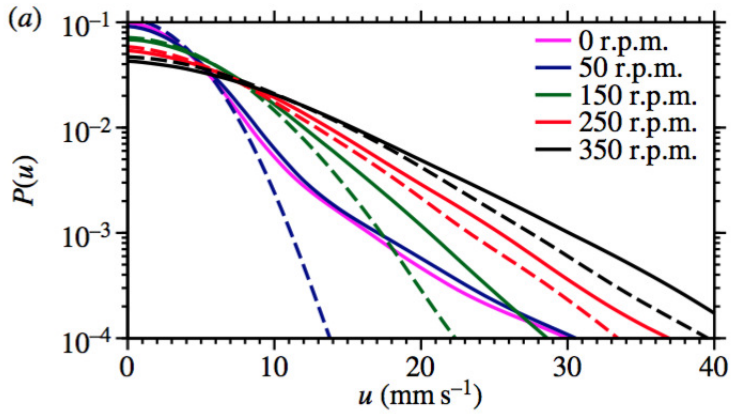

FIGURE 6.4: Probability density function of the magnitude of the velocity for the copepods species *E. affinis* at different turbulent intensities from Michalec, Souissi, and Holzner (2015).

What has not been reported yet in experimental studies is a quantification of the three-dimensional spatial distribution of copepods in turbulence. We do this in the next sections by means of a fractal dimension characterization.

6.2 Introduction to the correlation dimension

Chaos detection can be estimated by the calculation of the fractal dimension. The most intuitive concept to characterize a geometrical shape is its dimension where a single point has no dimension, curve has one dimension, plane and space have 2 and 3 dimensions respectively. This can be justified by the fact that each point of a curve can be set in continuous correspondence with a unique real number x. Analogously, this idea can be established between a point of surface and couple of real numbers (x, y),

indeed for a point in space and real numbers (x, y, z). Therefore a geometrical object has a dimension d, when its points are in correspondence with elements $(x_1, x_2, \ldots, x_d)$ within a set of $\mathbb{R}^d$. This non-negative integer lower than or equal to the dimension of the space in which the object is embedded, is said to be *topological dimension*.
This integer dimension d, however might be insufficient to characterize the dimensionality of a set of points, or never ended patterns which are called *fractal* (Cencini, Cencini, and Vulpiani, 2009).
Figure 6.5 shows the fractal von Koch, which is produced by dividing a unitary segment into 3 equal parts, then removing the central part and replacing it by two segments of equal length $1/3$.

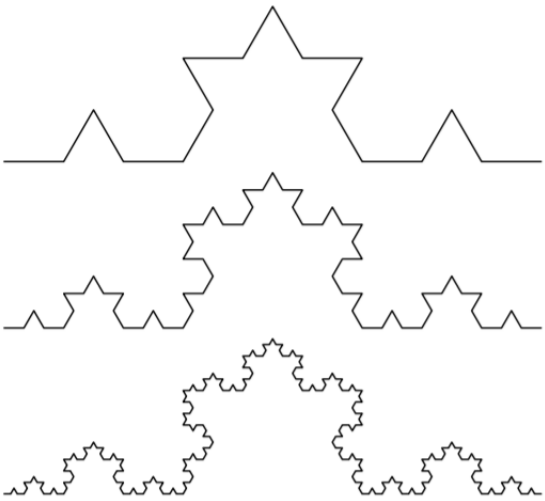

FIGURE 6.5: Iterative procedure to construct the fractal von Koch curve from Zhu, Zhou, and Jia (2003).

This procedure is repeated for each edge and after some steps the outcome is a weird shape, as can be seen in Fig. 6.5. The number of segments at each step is equal to $N(k+1) = 4\,N(k)$ with $N(0) = 1$, and the length of each segment is equal to $l(k) = (1/3)^k$. So the total length of the curve at $n - th$ generation is:

$$L(n) = \left(\frac{4}{3}\right)^n \tag{6.3}$$

since at each step, it comprises $N(n) = 4^n$ segments of lenght $l(n) = (1/3)^n$. By eliminating n between $N(n)$ and $l(n)$, one obtains:

$$N(l) = l^{-D_2} \tag{6.4}$$

in which exponent D_2 is the fractal dimension and is written as:

$$D_2 = -\lim_{l \to 0} \frac{LnN(l)}{Lnl} \tag{6.5}$$

For fractal von Koch, this quantity is equal to $D_2 = Ln4/Ln3 = 1.2618$. So the fractal dimension of this curve is not equal to its dimension ($D_2 \neq d$). In general a name fractal is given to any objects characterized by $D_2 \neq d$. Each part of a fractal reproduces the same complex pattern of the whole object. This property is titled *self-similarity*, which can be found in nature as well, like the beautiful pattern in the sunflowers, snowflakes or even fractal like nature of some coastlines (Fig. 6.6).

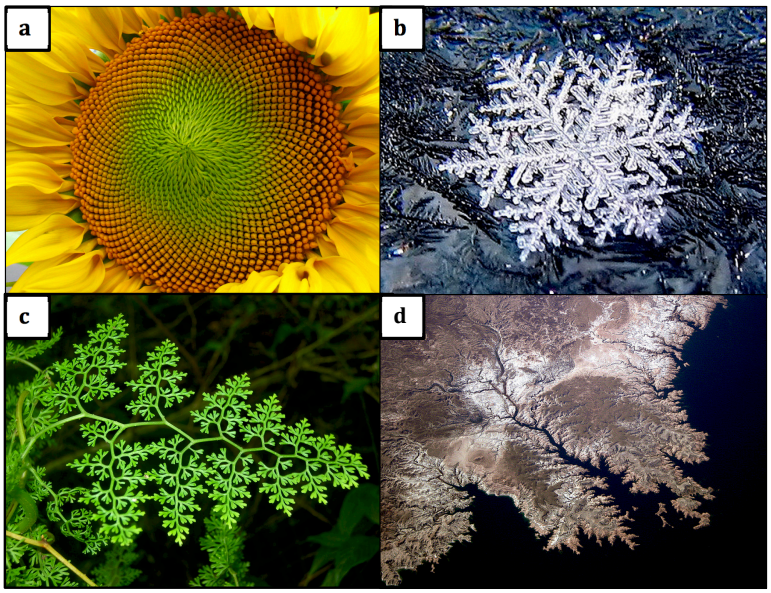

FIGURE 6.6: Examples of self-similarity in nature a) sunflowers, b) snowflake, c) leaf and d) coastline.

Fully developed turbulence is another generous source of natural fractals. For instance, the energy dissipated is known to concentrate on small scale fractal structures. Bernard et al. (2006) quantified the fractals in turbulent

flows with a dimension of $D_2 = 4/3$. Fig. 6.7 shows the isolines of zero-vorticity in two-dimensional turbulence in the inverse cascade regime. Colors identify different vorticity clusters, *i.e.,* regions with equal sign of the vorticity. Bernard et al. (2006) showed that the boundaries of these clusters have self-similarity behavior and are in fact the fractals.

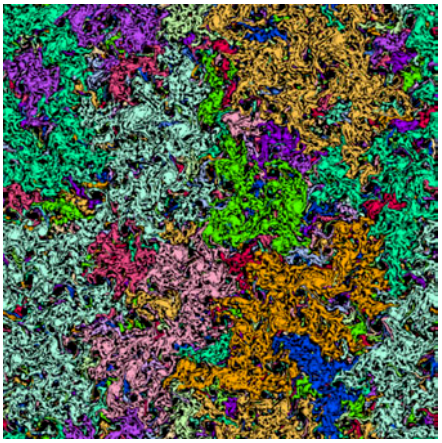

FIGURE 6.7: Colors identify different vorticity clusters and their boundaries are fractal with $D_2 = 4/3$ (Bernard et al., 2006).

There are several types of fractals where their reconstruction are quite different with respect to the Koch curve and typically have more complex self-similar properties. There are also several ways to quantify the fractal dimension of different patterns. Some of these algorithms are box-counting algorithm, Grassberger-Procaccia algorithm, stretch and fold mechanism and multifractal analysis. Here we focus only on the Grassberger-Procaccia algorithm.

The Grassberger-Procaccia (GP) algorithm (Grassberger and Procaccia, 1983), is used to estimate the correlation (fractal) dimension of a set of points. Given a d-dimensional dynamical system, the main idea of this algorithm is to compute $C(r)$ the correlation sum:

$$C(r) = \frac{2}{N(N-1)} \sum_{i<j} H(r - |x_i - x_j|) \tag{6.6}$$

where N denotes the number of points $x_1, x_2, \ldots, x_N$ in space, $|x_i - x_j|$ represents the distance between any pair of points, H is the Heaviside step function. $C(r)$ is then defined as the fraction of pairs whose distance

is smaller than r. This sum in monotonically decreasing to zero as $r \to 0$. If $C(r)$ decreases like a power law, $C(r) \sim r^{D_2}$, then the correlation dimension can be written in the following form:

$$D_2 = \lim_{r \to 0} \frac{\log C(r)}{\log r} \tag{6.7}$$

More information on the general form of the correlation dimension can be found in Cencini, Cencini, and Vulpiani (2009). In the next section, this analysis will be applied on copepods to see their behavior more carefully.

6.3 Analysis of clustering by correlation dimension

The distribution of the LC particles is illustrated by figure 6.8, where we show the instantaneous particle positions in two-dimensional slices of thickness $\sim \eta$, visualising at the same time the values of shear-rate of the carrying flow. Contrary to fluid tracers, LC particles are non-homogeneously dispersed in regions where turbulence intensity is below the given shear-rate threshold, according to the model. In the panels of figure 6.8, we also highlight the $\dot{\gamma}_T$ values by contour lines, we name respectively *comfort* and *alert* regions the locations which are below or above these fixed $\dot{\gamma}_T$ values. In Fig. 6.8(a), which corresponds to $\dot{\gamma}_T = 0.35\ \tau_\eta^{-1}$, the alert region is the dominant one. In this situation the great majority of LC particles are jumping but they manifestly fail to reach the few available comfort islands. This may be due both to the fact that islands are small and that they are short lived: one shall bear in mind the interplay between space and time in this problem. The panel (b) shows a condition where comfort and alert regions are equally probable. We notice a pronounced aggregation of particles in the alert areas surrounding the comfort regions, while the latter are efficiently evacuated. Finally, the panel (c) illustrates what happens when the alert behaviour is triggered only by few extreme shear rate filamentary regions. The LC particles manage

to avoid them quite efficiently but in the overall picture they seems to be mostly homogeneously distributed.

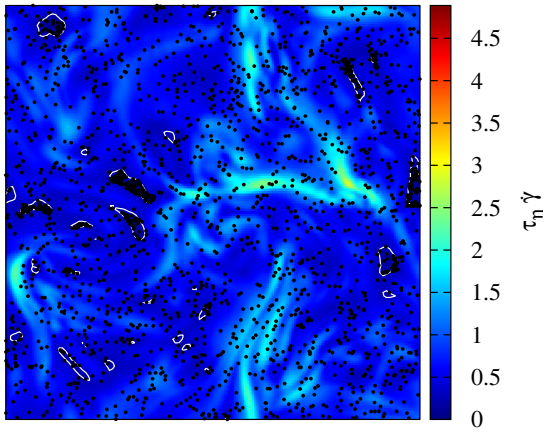

(a) $\tau_\eta \dot{\gamma}_T = 0.35$

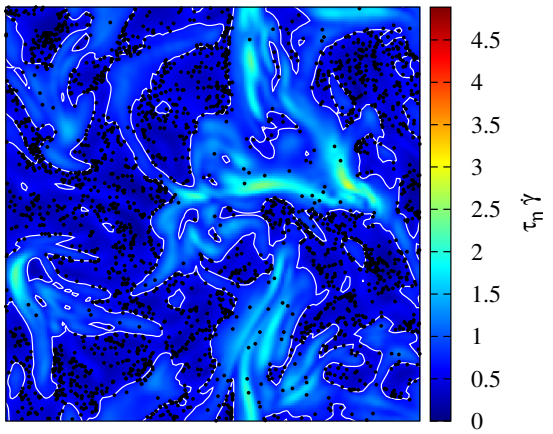

(b) $\tau_\eta \dot{\gamma}_T = 0.92$

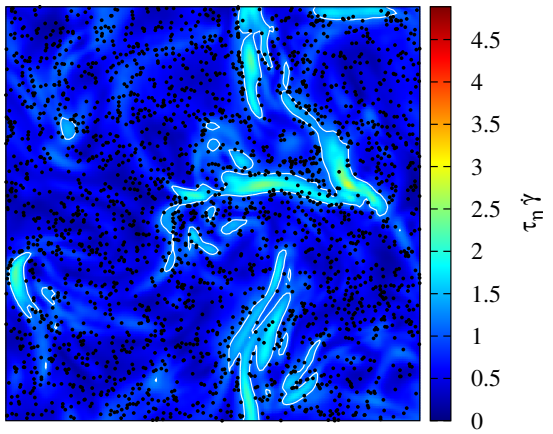

(c) $\tau_\eta \dot{\gamma}_T = 1.77$

FIGURE 6.8: Patchiness of the copepods from the simulations. Shading shows the instantaneous field of the absolute value of the shear rate of the Eulerian field, (a) distribution of the copepods with $u_J/u_\eta = 250$ and $\tau_\eta \dot{\gamma}_T = 0.35$, (b) distribution of the copepods with $u_J/u_\eta = 250$ and $\tau_\eta \dot{\gamma}_T = 0.92$, (c) distribution of the copepods with $u_J/u_\eta = 250$ and $\tau_\eta \dot{\gamma}_T = 1.77$. Contour lines are traced at the corresponding value of $\dot{\gamma}_T$ on each panel.

In order to better quantify the patchiness of the LC particles we compute their correlation dimension. According to the Grassberger-Procaccia algorithm, the D_2 is defined as the scaling exponent of the probability of finding a pair of particles with a separation distance less than r

$$P_2(|X_2 - X_1| < r) \propto r^{D_2} \tag{6.8}$$

as $r \to 0$. Figure 6.9 shows the D_2 value in the two dimensional parameter space composed by the intensity of the jump and the shear rate threshold value. The clustering ($D_2 < 3$) is discernible when the prescribed shear rate threshold value is less than 2.8 τ_η^{-1}, and it is maximal, $D_2 \simeq 2.3$, at around 0.5 τ_η^{-1}. On the other hand we observe a saturation of clustering as u_J is increased. In order to better appreciate these two features, *i.e.*, the minimum with respect to $\tau_\eta \dot{\gamma}_T$ and a saturation as a function of u_J/u_η, two two-dimensional cuts of the $D_2(\dot{\gamma}_T, u_J)$ surface are shown in Fig. 6.10.

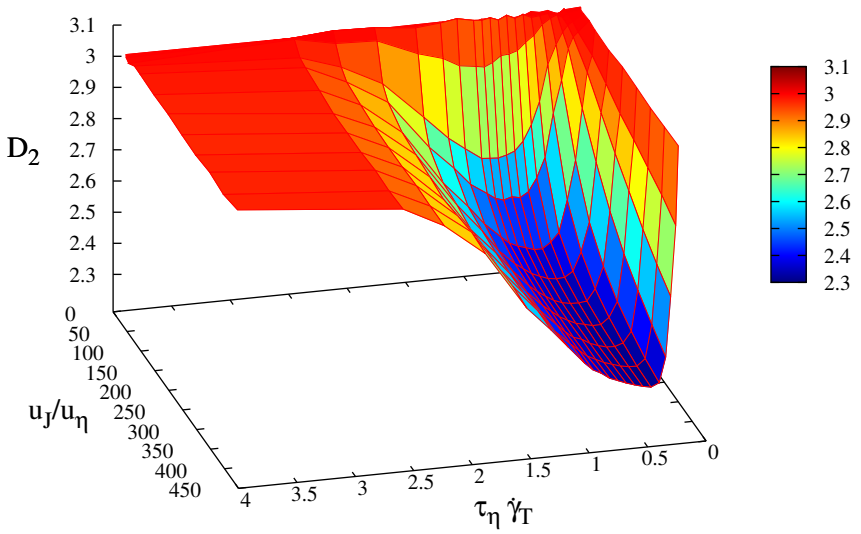

FIGURE 6.9: Correlation dimension D_2 of copepods as a function of jump intensity u_J/u_η and threshold value $\tau_\eta \dot{\gamma}_T$.

One may wonder why there is an optimum and what is its physical meaning. Copepods are prone to jump in order to escape from regions of alert ($\dot{\gamma} > \dot{\gamma}_T$), to reach regions where $\dot{\gamma} < \dot{\gamma}_T$, therefore the chance for a jump to be successful (assuming it to be randomly oriented) depends on the size of the comfort region, in other words to the volume, $\mathcal{V}_{\dot{\gamma}<\dot{\gamma}_T}$ (see Fig. 6.11).

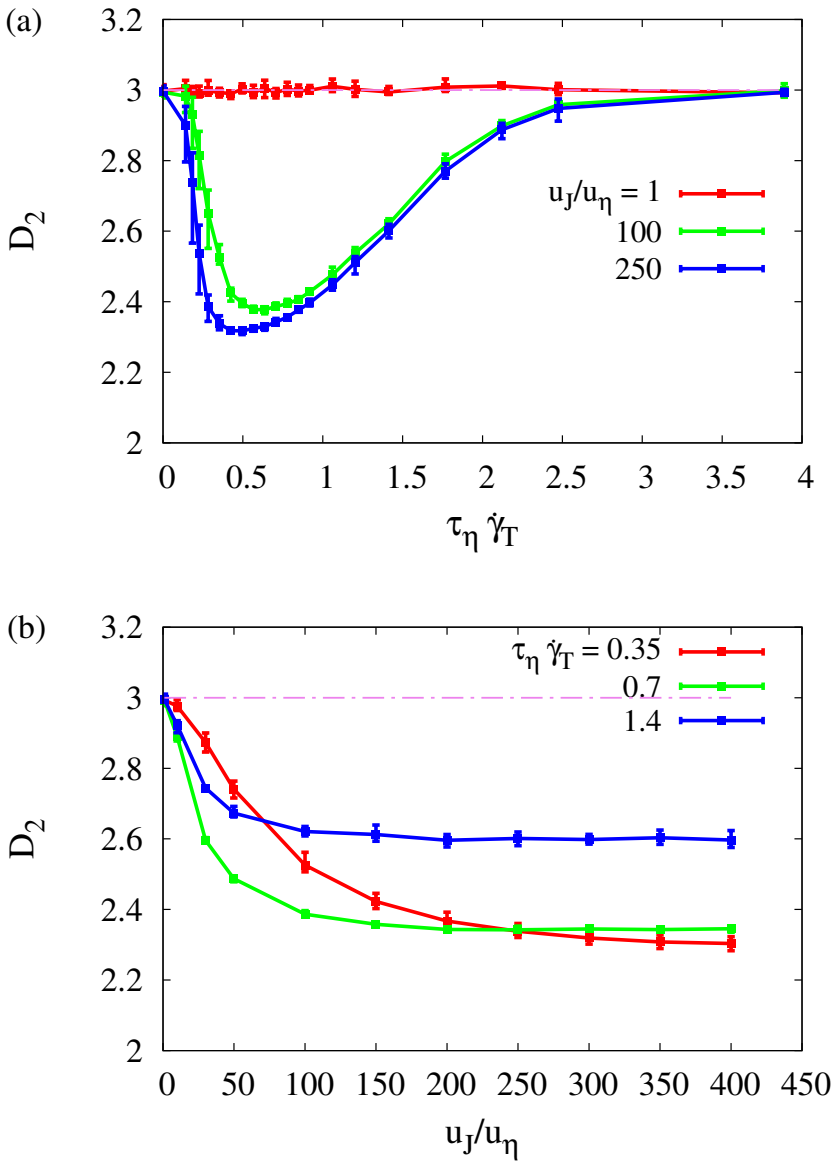

FIGURE 6.10: Lateral view of correlation dimension of the copepods as a function of the jump intensity u_J/u_η and threshold value $\tau_\eta \dot{\gamma}_T$. Error bars indicate the range of variability of the measurements from 10 independent particle snapshots.

On the other hand, clustering would be maximum if we have numerous successful jumps and obviously the number of jumps depends on $\mathcal{V}_{\dot{\gamma}>\dot{\gamma}_T}$. This implies that copepods clustering is expected to be proportional to $\mathcal{V}_{\dot{\gamma}<\dot{\gamma}_T} \cdot \mathcal{V}_{\dot{\gamma}>\dot{\gamma}_T}$. Now, substituting the volume of comfortable regions with $\mathcal{V}_{tot} - \mathcal{V}_{\dot{\gamma}>\dot{\gamma}_T}$ leads to $\mathcal{V}_{\dot{\gamma}>\dot{\gamma}_T} \cdot (\mathcal{V}_{tot} - \mathcal{V}_{\dot{\gamma}>\dot{\gamma}_T})$. One direct consequence is that the clustering would be maximum when $\mathcal{V}_{\dot{\gamma}>\dot{\gamma}_T} = \mathcal{V}_{tot}/2$.

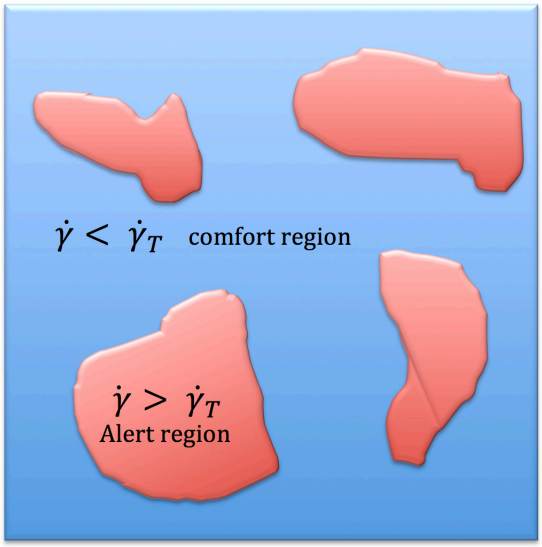

FIGURE 6.11: Illustration of comfort and alert regions in the computational domain according to the shear rate threshold value.

This can explain the existence of the optimum of D_2 as a function of $\tau_\eta \dot{\gamma}_T$ as shown in figure 6.10(a) as well as its trend as a function of $\dot{\gamma}_T$. Note however that this argument is based on the simplifying assumption that there is no correlation between the orientation of a LC particle at jump and its position respect to the comfort area and also it neglects the spatial structure of the shear rate field.

How can we determine the value of $\dot{\gamma}$ for which the condition of $\mathcal{V}_{\dot{\gamma}>\dot{\gamma}_T} = \mathcal{V}_{tot}/2$ occurs? One possibility is to perform an Eulerian measurement of the $\dot{\gamma}(x,t)$ field over space and time. Another option is to look at the fraction of time spent by tracers in alert regions, $T_{\dot{\gamma}>\dot{\gamma}_T}/T_{tot}$ (with T_{tot} the total time of the measurement). Since tracers explore evenly all the region of the flow this is equivalent to measure the volume ratio $\mathcal{V}_{\dot{\gamma}>\dot{\gamma}_T}/\mathcal{V}_{tot}$. In particular in order to increase the statistical sampling we look at the global

mean value $\langle T_{\dot{\gamma}>\dot{\gamma}_T}\rangle / T_{tot}$ where the average is over the total number of particles (N_{tot}):

$$\langle T_{\dot{\gamma}>\dot{\gamma}_T}\rangle = \frac{1}{N_{tot}} \sum_{i=1}^{N_{tot}} \int_0^{T_{tot}} H(\dot{\gamma}_i(t) - \dot{\gamma}_T)\, dt. \tag{6.9}$$

The plot in figure 6.12 shows the trend of $\langle T_{\dot{\gamma}>\dot{\gamma}_T}\rangle / T_{tot}$ as function of $\dot{\gamma}_T$ both for tracers and LC particles. It confirms that copepods reside less in alert regions compared to tracers. Moreover the difference among the two time fractions can be used as an alternative clustering indicator. It has in fact a similar trend as the $D_2(\dot{\gamma}_T)$ function and shows a peak for the same value of $\dot{\gamma}_T$ (inset of Fig. 6.12). The prediction that clustering varies as $\mathcal{V}_{\dot{\gamma}>\dot{\gamma}_T} \cdot (\mathcal{V}_{tot} - \mathcal{V}_{\dot{\gamma}>\dot{\gamma}_T})$ is in qualitative agreement with the observed trend, it is in quite good agreement in the large $\dot{\gamma}_T$ regime, however it fails to capture the correct value at which the maximum appears, giving $\tau_\eta \dot{\gamma}_T = 0.85$ instead of 0.5. Finally, we note that the case of maximal clustering at $D_2 \simeq 2.3$ corresponds to a condition where the LC particles concentrate in nearly two-dimensional sheets which envelop the *alert* regions (as can be also inferred from the visualisation in Fig. 6.8(b)).

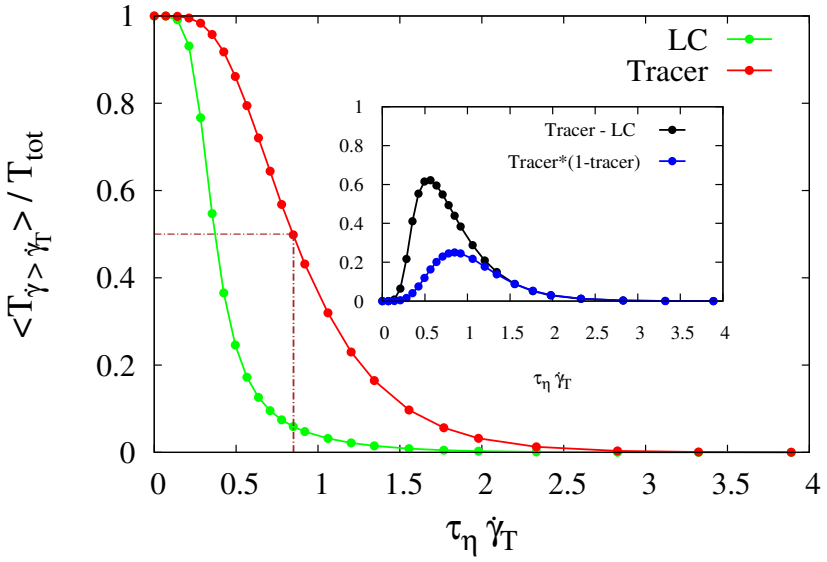

FIGURE 6.12: Time fraction spent in alert regions by tracer and copepods as a function of the threshold value. Inset: difference of time fraction between tracers and LC particles, and prediction based on $\mathcal{V}_{\dot{\gamma}>\dot{\gamma}_T}/\mathcal{V}_{tot}$ measurement.

We can offer a qualitative physical explanation for the observed D_2 saturation for high values of u_J at fixed $\dot{\gamma}_T$, (figure 6.10(b)). The argument is as follow: one may expect that there is clustering if the time to escape from an alert region is less than the lifetime of such a region: $\tau_{escape} < \tau_{\dot{\gamma}_T}$. The former time can be estimated as $\tau_{escape} = l_{\dot{\gamma}_T}/u_J$, where $l_{\dot{\gamma}_T}$ is the typical size of the alert region characterised by a shear-rate $\dot{\gamma} > \dot{\gamma}_T$. This implies that LC particles form clusters and the D_2 measure is lead to saturate to a constant value if $u_J > l_{\dot{\gamma}_T}/\tau_{\dot{\gamma}_T}$. This latter ratio can be thought as a threshold dependent escape velocity $u_{\dot{\gamma}_T} = l_{\dot{\gamma}_T}/\tau_{\dot{\gamma}_T}$. From the correlation dimension measurement this escape velocity is estimated to be of the order of $100\,u_\eta$, *i.e.,* of the order of the large scale velocity, with a weak decreasing trend at increasing $\dot{\gamma}_T$.

We finally observe that when the flow field associated to the Lagrangian particles, $\boldsymbol{v} = \dot{\boldsymbol{x}}$, displays a weak compressibility, it can be shown (Falkovich, Gawedzki, and Vergassola, 2001; Durham et al., 2013) that D_2 depends on the flow divergence by the relation $D_2 = 3 - c\langle \nabla \cdot v \rangle^2$ with c a proportionality constant and angular brackets denoting time and space average. If this argument is applied to the LC model we observe that the divergence can be different form zero only at the interface between comfort and alert regions. This is because in comfort regions ($\nabla \cdot \boldsymbol{v} = \nabla \cdot \boldsymbol{u} = 0$) and in alert regions ($\nabla \cdot \boldsymbol{v} = \nabla \cdot \boldsymbol{u} + \nabla \cdot \boldsymbol{J} = 0$, as we can safely assume the jump term to be spatially constant). At the interface however, the change from the fluid velocity intensity u to $u + u_J$ has a spatial transition scale roughly proportional to $u_J \cdot \log(10^2)\tau_J$ which leads to a non-null divergence. This explains the LC accumulation that we observe in correspondence of the alert/comfort interfaces, which effectively acts as sink or source term of the LC velocity field (see in particular the central panel of Fig. 6.8). By following this line of reasoning, one can guess that the minimum value of D_2 will correspond to the case where the surface of alert/comfort interface is maximum (and not of volumes, as stated above). This has clearly a dependence on the threshold $\dot{\gamma}_T$ and much less, if any, on u_J. Despite the qualitative agreement of this observation with our numerical results, we have not been able yet to confirm it quantitively in the weakly compressible limit of the LC model.

6.4 Particle Orientational Dynamics

What is the importance of particle orientation for the non homogenous distribution of particles? The effect of the geometrical aspect ratio of the particles, together with the direction of their jump on the fractal dimension are addressed here.
The fluid deformation rate symmetric tensor S_{ij} comes into play by modelling copepods as elongated particles with aspect ratio equal to 3 (*e.g.*, the relevant aspect ratio for *Eurytemora affinis* copepod) as can be seen in the equation below:

$$\dot{\mathbf{p}}(t) = \left(\mathbf{\Omega} + \frac{\alpha^2-1}{\alpha^2+1}\left(\mathcal{S} - \mathbf{p}^T(t)\cdot\mathcal{S}\cdot\mathbf{p}(t)\right)\right)\cdot\mathbf{p}(t) \tag{6.10}$$

Its effect on the jump direction selection leads to enhanced clustering of the particles for jump intensity $u_J/u_\eta = 250$. Copepods can also jump in random direction in the solid angle independently from the rotation rate and deformation rate of the Eulerian field. Less clustering in this case is logical since the jumping direction has no relation with the fluid flow. These behaviors can be found in more details in figure 6.13, where we address the influence of jump direction on the PDF of the copepods velocity.

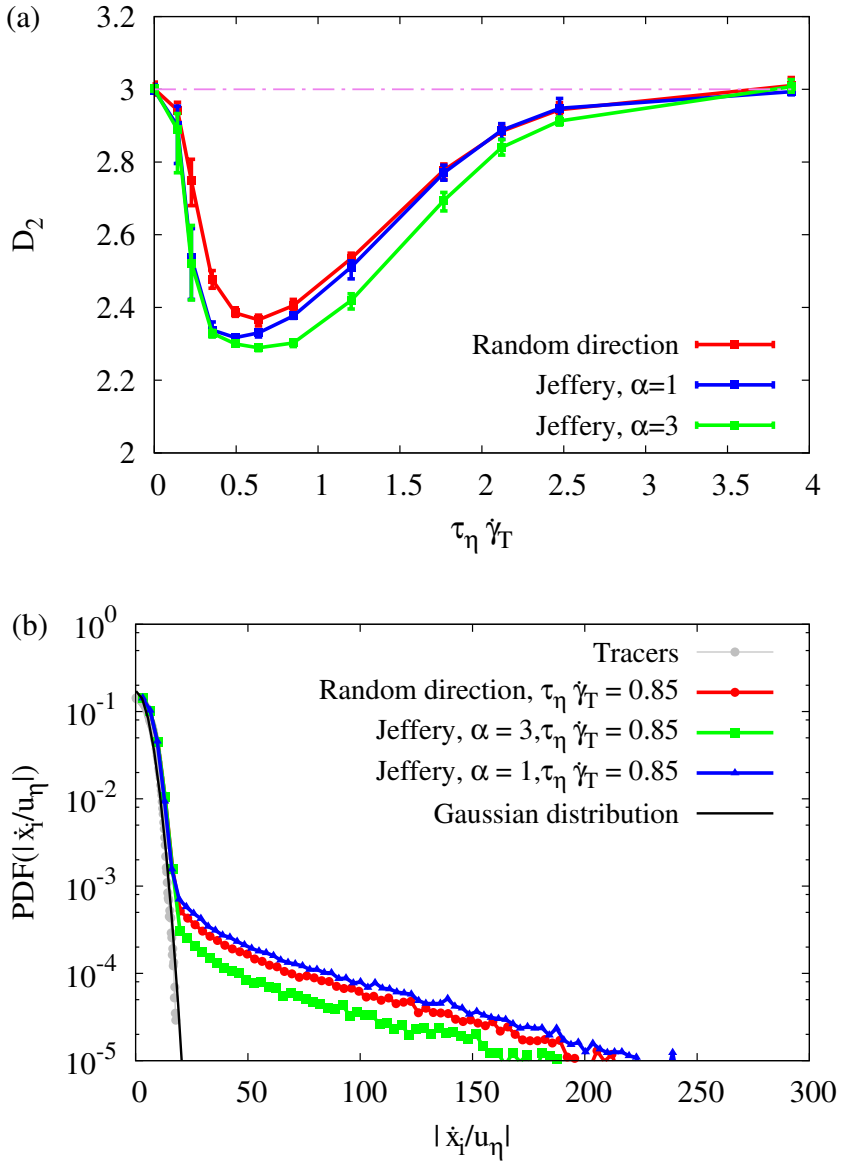

FIGURE 6.13: (a) Effect of the aspect ratio and direction of the jump on the fractal dimension, (red) Copepod as solid sphere particles, their direction of the jump is random in the solid angle; (blue) Copepod as solid sphere particles with an orientation and (green) as elongated particles. Both jump in a direction following the Jeffery's equation. (b) PDF of the absolute value of the single component velocity for (red) random direction case, and (green) Jeffery's case with aspect ratio of 3. All cases are computed at $u_J/u_\eta = 250$.

6.5 Effect of the jump time latency

Up to now, copepods were considered to be able to jump whenever they are in alert regions and their previous jump has finished. Since copepods have certain amount of energy and during each jump, they lose lots of energy (the mechanical energy produced during their escape is reported to be very high ($8 \times 10^{-5} J/s$) according to Lenz and Hartline (1999)), then it is more realistic to include this feature of copepods in the LC model.
The experimental data analysis revealed that a copepod has memory on its previous jumps, thus the future jump depends on the history and cannot always occur right after the previous jump.
Unfortunately based on available data and our analysis, no general rule can be established to consider this feature in the LC model of copepods, instead one can play with latency time of the jump. This is shown in Fig. 6.14 where $\tau_{wait_{default}}$ represents the default value of the latency time. According to the LC model, the final time a jump has the following form:

$$t_e = t_i + \log(10^2)\, \tau_J \tag{6.11}$$

so the default value of the waiting time or the latency time of the jump is equal to

$$\tau_{wait} = t_e - t_i = \log(10^2)\, \tau_J \tag{6.12}$$

dividing by τ_η gives the dimensionless waiting time to be equal to 0.046. Increasing this quantity means that copepods are less reactive, therefore they jump less compared to the default case. By varying this parameter, the jump memory of copepods and their limited amount of energy can be embedded in the LC model.

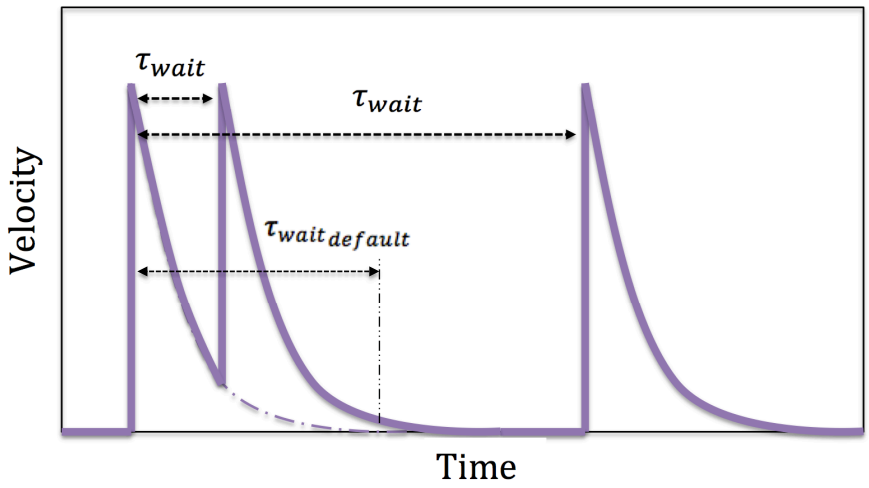

FIGURE 6.14: Kinematics of the jump of a copepod by variation of the jump time latency τ_{wait}.

The effect of the jump latency time on the correlation dimension can be seen in Fig. 6.15. The jump intensity is fixed ($u_J/u_\eta = 250$) and τ_{wait}/τ_η varies in $[0.02, 10]$.

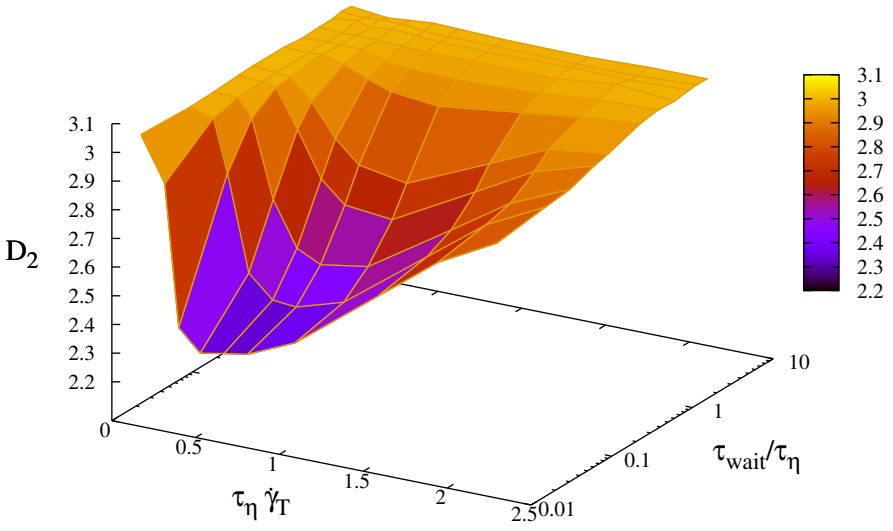

FIGURE 6.15: Effect of the jump latency time on copepods' clustering.

For $\dot{\gamma}\tau_\eta = 0.5$, Fig. 6.16 shows a $2D$ plot in which the default case is shown in blue and vertical lines correspond to $\tau_J/\tau_\eta = 0.01$, $\tau_{wait}/\tau_\eta = 1$ and the large eddy turn-over time ($T = L/U$) divided by Kolmogorov time scale (τ_η). This figure indicates that the LC model leads to clustering when $\tau_{wait} < \tau_\eta$, otherwise the patchiness will disappear.

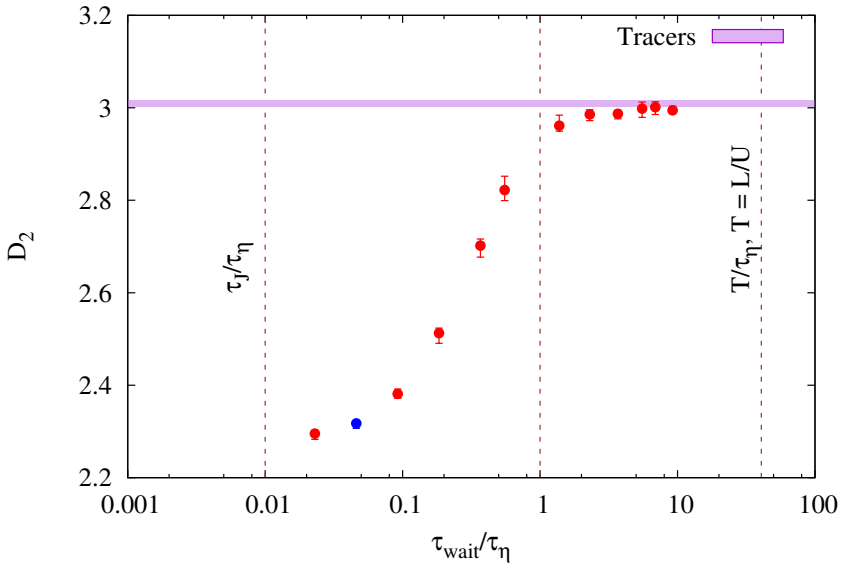

FIGURE 6.16: Effect of the jump latency time on copepods' clustering. The point in blue corresponds to the default case and asymptotic value is shown for tracers.

Chapter 7

Encounter rates study and future perspectives

In this chapter the encounter rate of copepods from the Lagrangian model will be assessed and its effect on copepods' mating will be discussed. As a perspective an Eulerian approach for the simulation of copepods' motion will be introduced.

7.1 Encounter rate of copepods from the LC model

An essential aspect in marine biology is the encounters between individual organisms which is vital for males and females in order to mate or for predators to locate their prey to capture and consume them (Hein and McKinley, 2013; Menden-Deuer, 2006; Kiørboe, 2008). Finding a suitable habitat (colonization) for organisms is also encounter-dependent (Wosniack et al., 2014). Organism speed, size, motility and abundance can affect the biological encounter rates, the rates at which individuals meet other organisms of the same or different species. It is thus fundamentally important to understand the phenomenon that affect the encounter rates and the biological processes in oceanic flows.

The encounter rate of plankton species has been studied by many authors in the past (Gerritsen and Strikler, 1977; Rothschild and Osborn, 1988; Evans, 1989; MacKenzie et al., 1994; Visser and MacKenzie, 1998; Kiørboe and Saiz, 1995). Gerritsen and Strikler (1977) were the pioneers

who introduced the theory of contact rate in laminar flow. However living habitats of the plankton species are rarely laminar. It is now widely known that turbulence has a strong influence on dispersal, feeding and reproduction of plankton. Not only the small-scale but also other scales within the turbulence spectrum are important contributors to encounter process (Visser and MacKenzie, 1998). Some authors regarded the small-scale turbulent processes as homogenizing factors, so that the encounter-rate model, assumed the distribution of plankton to be random in space and time (Kiørboe and Saiz, 1995; Sundby and Fossum, 1990; Davis et al., 1991; MacKenzie and Leggett, 1991; Caparroy and Carlotti, 1996), whilst turbulence increases inhomogeneity at small scales (Frisch, 1995; Toschi and Bodenschatz, 2009; Schmitt and Huang, 2016).

The encounter rate in oceanic turbulence is governed by two biologically- and physically-driven processes (Kiørboe and Saiz, 1995; Seuront, Schmitt, and Lagadeuc, 2001; Dzierzbicka-Glowacka, 2006). First, it is likely due to the behavior of organisms (biologically-driven process) and secondly it is affected by the turbulent motion of the carrier fluid (physically-driven process). However notice that turbulence has a great impact on microorganisms and can induce some behavioral responses in swimmers (Jennifer et al., 2012; Durham and Stocker, 2012). Hence, it is more reasonable not to sum up the contribution of these processes linearly as it is the case for Seuront, Schmitt, and Lagadeuc (2001), Kiørboe and Saiz (1995), and Dzierzbicka-Glowacka (2006). The encounter rate formulation developed by Sundaram and Collins (1977), Wang, Wexler, and Zhou (1998), Reade and Collins (2000), and Collins and Keswani (2004) can be used in turbulence in case of preferential concentration of species. Despite many studies which have been performed on the effect of the preferential concentration on the coagulation of colloidal particles (Wang, Wexler, and Zhou, 2000; Lian, Charalampous, and Hardalupas, 2013; Falkovich, Fouxon, and Stepanov, 2002; Brunk, Koch, and Lion, 1998), only few studies (Squires and Yamazaki, 1995; Schmitt and Seuront, 2008) are available in the context of copepods ecology whilst the study of Squires and Yamazaki (1995) was published before including the precise effect of the preferential concentration in the theory of contact rate. Rather than swimming behavior, other mechanisms can also play a role in

encounter rate for copepods, *i.e.*, chemoreception and mechanoreception (Buskey, 1984; Weissburg, Doall, and Yen, 1998), prey movement detection (Visser, 2001; Jiang, Osborn, and Meneveau, 2002) and feeding currents (Marrasé et al., 1990), which are outside the scope of the present study.

The encounter rate, *i.e.*, the number of encounters per unit time under the condition of statistically homogeneous and isotropic movement can be written in the following form:

$$E(r) = n\pi r^2 \, g(r) \, \langle \delta v_{rad}(r) \rangle \tag{7.1}$$

where n is the organisms number density, r is the encounter or perceptive radius of organisms and $\langle \delta v_{rad}(r) \rangle$ is the mean radial velocity between two particles separated by a distance r (Sundaram and Collins, 1977; Wang, Wexler, and Zhou, 1998; Collins and Keswani, 2004; Reade and Collins, 2000). In the latter expression $\langle . \rangle$ indicates ensemble average and $\delta v_{rad}(r)$ is the amplitude of the relative radial velocity:

$$\delta v_{rad}(r) = |(\boldsymbol{v}(\boldsymbol{x} + \boldsymbol{r}) - \boldsymbol{v}(\boldsymbol{x})) \cdot \hat{\boldsymbol{r}}| \tag{7.2}$$

A detailed explanation on the appropriate choice of the mean radial velocity to be used in expression 7.1, can be found in Saffman and Turner, 1956; Wang, Wexler, and Zhou, 1998. $g(r)$ represents the radial distribution function, which describes the variation of the particles' density from a reference particle. This is linked to the fractal dimension (Grassberger and Procaccia, 1983) for very small values of r. It has thus the following form:

$$g(r) = \frac{1}{4\pi r^2} \frac{1}{N\rho} \sum_{i=1}^{N} \sum_{k \neq i}^{N} \delta \left(r - |r_k - r_i| \right) \tag{7.3}$$

r in this equation represents the given distance from a particle, N is the total number of particles, $\rho = N/V$ is an average number density of N particles in a volume V and $|r_k - r_i|$ is the distance between pair of particles.

The pair correlation function of LC model is shown in figure 7.1 where

the slope of $g(r)$ at small r is linked to the correlation dimension of copepods' distribution in turbulence, as can be found in the inset of this figure. This slope increases by increasing the shear rate threshold value up to $\tau_\eta \dot{\gamma}_T = 0.5$, then further growth of the shear rate threshold value, decreases the steepness of $g(r)$. The inset of the Fig. 7.1 confirms these descriptions. The mean radial velocity between two copepods is shown in

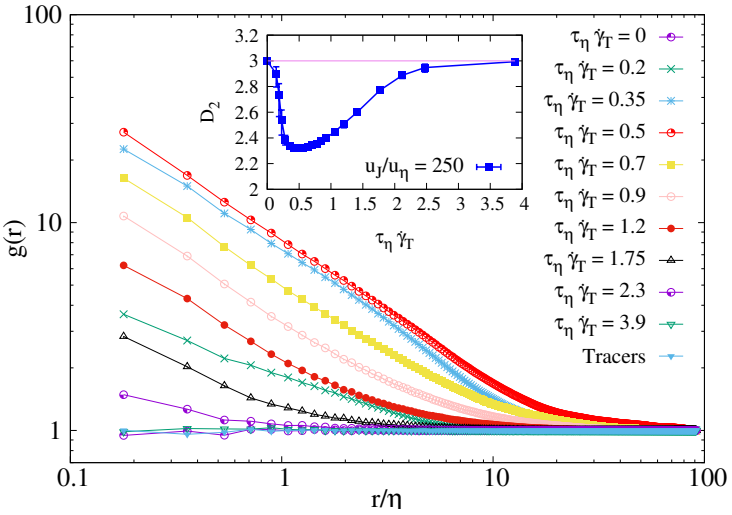

FIGURE 7.1: Pair-radial-distribution function $g(r)$ for different Lagrangian copepod families with different threshold values of the deformation-rate $\tau_\eta \dot{\gamma}_T$. Inset represents the correlation dimension of copepod distribution with different jump intensity.

Fig. 7.2. Our findings for tracers are in good agreement with the Eulerian longitudinal velocity structure function of the fluid, given by the empirical approximation of Borgas and Yeung (2004):

$$\bar{S}_{II} = \frac{2Re_\lambda}{15^{1/2}} \left[1 - exp\left(-\frac{r}{(15C)^{3/4}} \right) \right]^{4/3} \left(\frac{15^3 r^4}{15^3 r^4 + (2Re_\lambda / C)^6} \right)^{1/6} \tag{7.4}$$

with $C = 2$ and $\langle \delta v_{rad}(r) \rangle = (2\bar{S}_{II}/\pi)^{1/2}$. The Eulerian structure function grows linearly as r^{ζ_d} with $\zeta_d = 1$ for dissipative scales (small r) and at inertial-range it is proportional to r^{ζ_i} with $\zeta_i = 1/3$. Copepods with the shear rate threshold value of $\tau_\eta \dot{\gamma}_T = 3.9$ have less frequent jump behavior, so that they behave almost like a tracers and they are advected by the flow. For this reason they go very close to the prediction given by expression 7.4. In a case where all the copepods are in alert regions ($\tau_\eta \dot{\gamma}_T = 0$),

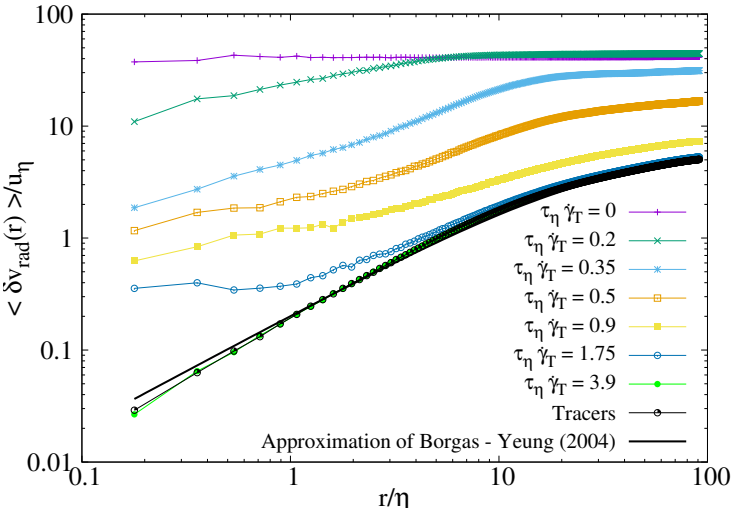

FIGURE 7.2: Radial velocity $\langle \delta v_{rad}(r) \rangle$ between two particles separated by a distance r.

one can expect the Brownian like motion of copepods according to the LC model. The diffusivity of the copepods would be dimensionally proportional to a relation of the type $u_J^2 \tau_J$. For this case, the copepod's relative velocity tends to be constant and its amplitude would be proportional to the jump intensity (u_J). For other cases (different shear rate threshold values $\tau_\eta \dot{\gamma}$), such an estimation is not applicable since the exponential term does not exist for copepods in safe regions. Therefore for copepods, estimation of such a relation (Borgas and Yeung (2004)) is not straightforward. It might be due to the fact that copepods at distance r may have different behavior. This is shown in Fig. 7.3 where two copepods at an immediate vicinity may have very large velocity difference. Establishing the Eulerian structure function, thus is linked to the local threshold value of the shear rate. Scaling exponents ζ_d, ζ_i for copepod families through power law fits are shown in Fig. 7.4. The change of the power law scaling exponent in inertial-range is smooth, but in dissipative scale it shows non monotonic behavior. Having the pair correlation function $g(r)$ and mean radial velocity $\delta v_{rad}(r)$ one can estimate the encounter rate kernel $E(r)$. In reality there is no contact between tracers, since they are passive particles advected by the flow where the fluid streamlines does not cross each other. However to have an effective contact rate, it is not necessary for copepods to have physical contacts. Copepods thus can grab their prey or an incoming mate before the contact happens (Schmitt and Seuront,

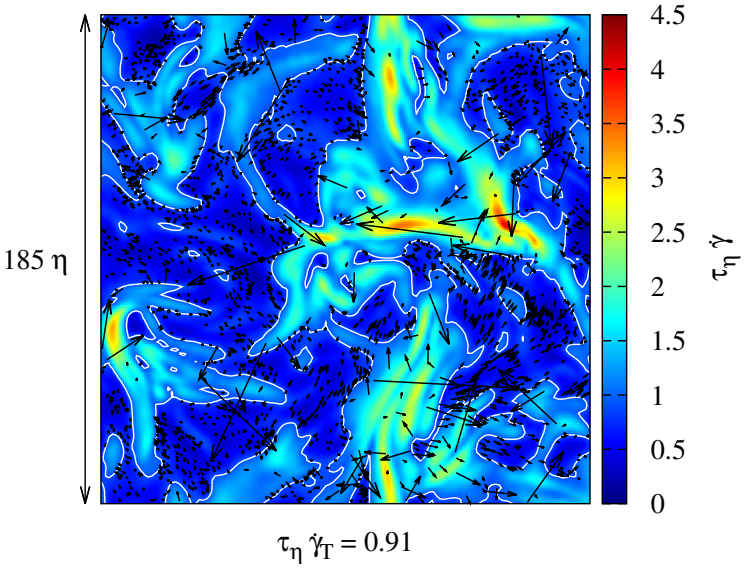

FIGURE 7.3: Spatial distribution of copepods in turbulent flow along with their velocity vectors. Shading represents the instantaneous field of the absolute value of the shear rate of the Eulerian field. Contour lines are traced at threshold value of $\tau_\eta \dot{\gamma}_T = 0.91$.

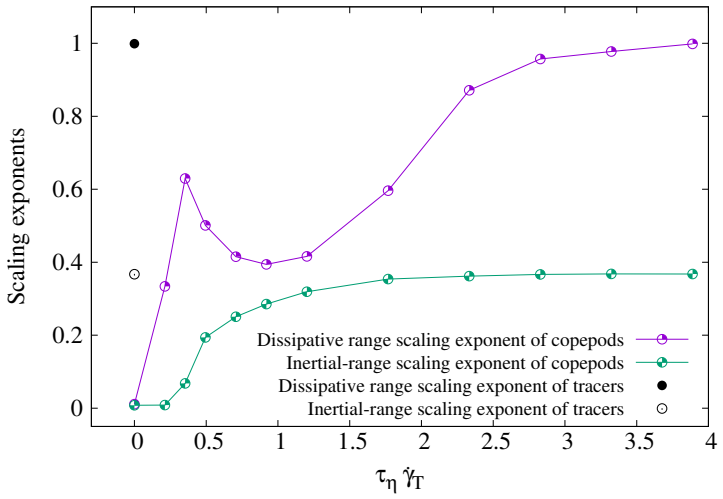

FIGURE 7.4: Scaling exponents of $\langle \delta v_{rad}(r) \rangle$ vs. r from power law fits in the dissipative r^{ζ_d} and inertial-range limit r^{ζ_i}.

2008). This is why r in eq. 7.1 represents the radius of perception of particles rather than their their characteristic radius of geometry.
Fig. 7.5 represents the encounter kernel as a function of r for different copepod families. Here the encounter rate of copepods are introduced as a reference case for other copepod families. Notice that copepod-copepod interaction has been neglected from the beginning as an assumption to introduce LC model. It is evident that by increasing the shear rate threshold value ($\tau_\eta \dot{\gamma}_T$), the encounter rate of copepods decreases monotonically, although the growth of the shear rate $\tau_\eta \dot{\gamma}_T$ had non-uniform impact on the pair correlation dimension (see Fig. 7.1).
The vertical line shows the radius of perception for Lagrangian copepod particles, here 5 times greater than the Kolmogorov length scale of the carrier fluid. The ratio of the radius of perception to the copepods' body size is reported to be in the range of $1-3$ (Lenz and Yen, 1993; Bagoien and Kiørboe, 2005; Doall et al., 1998). In terms of η unit, this means that the radius of perception of copepods is of the order of $\mathcal{O}(1)$. In order to see how effective the shear rate threshold value is on the encounter rate of Lagrangian copepods at different perception radius, one can estimate the ratio between the encounter rates experienced by copepod families and tracers. This is shown in Fig. 7.6 where it is realistic to have larger encounter rate at small distances, nevertheless this figure suggests that at optimum clustering corresponding to the shear rate threshold value of $\tau_\eta \dot{\gamma}_T = 0.5$, the encounter rate can be of the order of $\mathcal{O}(10)$ with respect to the tracers at $r = 5\eta$. The LC model shows no contact rate enhancement at shear rate values larger than 2.75.

The LC model shows an enhanced contact rate with respect to the case where copepods are considered as passive particles. This enhancement comes from two terms in the contact rate expression; one is the variation of the $g(r)$ which accounts for the preferential concentration and the other one is the variation of the $\langle \delta v_{rad}(r) \rangle$, which comes from the fact that copepods are swimming. Both contributions are important in the encounter rate enhancement in zooplankton which is a key parameter for sexual reproduction and feeding of plankton species.
Here we have shown that the small scale clustering of copepods which

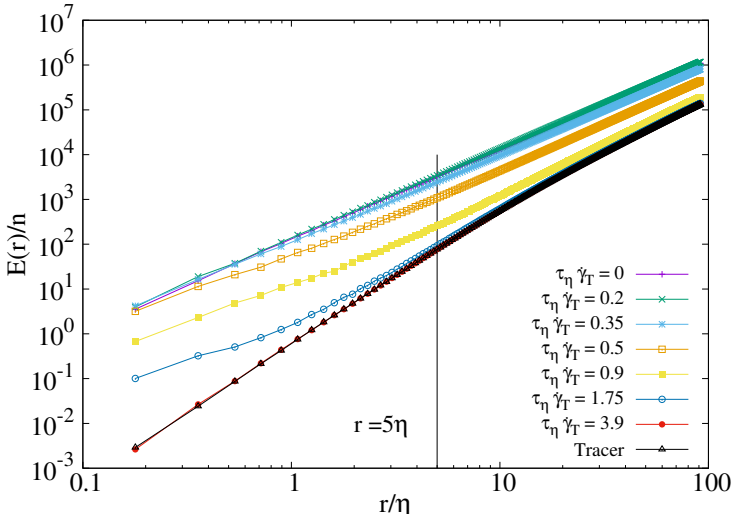

FIGURE 7.5: Encounter rate per unit particle density for different Lagrangian copepod families with different values of deformation-rate thresholds $\dot{\gamma}_T$.

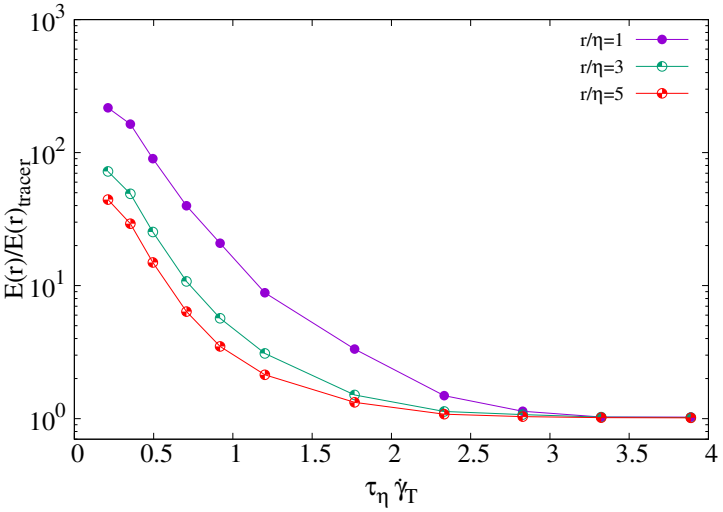

FIGURE 7.6: Ratio between encounter rates experienced by Lagrangian copepod particles and the one experienced by fluid tracer particles with the same perception radius.

is linked to behavioral model in turbulence, can increase largely the encounter rate. Our studies show that, this increase depends on copepods' perception radius and can be of the order of $\mathcal{O}(10^2)$ at dissipative scales. The enhancement of the contact rate is relevant for mating behavior of copepods but it is less relevant for the nutrient uptake. As a perspective it would be interesting to see the consequence of our LC model for the nutrient uptake by using the Lagrangian model of copepods in one side and larger particles drifting in the flow which represent modeling predators. A manuscript describing the performed analysis can be found in appendix B.

7.2 Eulerian modelling of copepods' dynamics in turbulent flows

Up to now, we have quantified the clustering of copepods for limited number of individuals at small scales by means of a Lagrangian copepod model, but it is also useful to have a model which describes copepods' behavior in large scales, for instance in thin plankton layers where the congregations of zooplankton in the water column and the dynamics of microorganisms are of interest and more generally in oceanography domain. Therefore we have to think to an equivalent Eulerian model for the Lagrangian copepod (LC) model in turbulence which describes the evolution of the concentration of copepods in a given region. The basic equation that can be used is the advection-diffusion equation for the concentration of copepods:

$$\frac{\partial C}{\partial t} + \mathrm{u} \cdot \nabla C = K \Delta C \tag{7.5}$$

where C represents the concentration of microorganisms here copepods, u is the fluid velocity and K is the diffusion coefficient. The term in the right hand side represents the diffusion term which needs to be adapted here in our case according to copepods' dynamics. In order to simplify the simulations, let us assume that copepods can either exhibit an abrupt

jump in certain conditions or have a small velocity additional to the velocity of the fluid. In both cases, the additional velocity and jumps are randomly oriented, therefore the two behaviors can be described with the diffusion coefficient, but this coefficient (K) is not a constant. One possibility is to write the diffusion term as $\nabla\left(K \cdot \nabla C\right)$. Another way to express this term is to use $\Delta(KC)$, where K in both forms depends on space (Kampen, 2007). Furthermore, since copepods react to the shear rate, the diffusion coefficient (K) depends not directly on space but through its dependancy on the shear rate ($\dot{\gamma}$).

The two plausible ways of expressing the diffusion term are different. Which one among $\nabla\left(K \cdot \nabla C\right)$ and $\Delta(KC)$ should be used? The choice is based on physical interpretation. Our interpretation here is to find an equivalent Eulerian model for the Lagrangian copepod model, according to which, homogenous distribution of copepods ended up into non-homogenous spatial distribution. We observed that the second choice leads to the clustering of particles. Let us expand the term $\Delta(KC)$:

$$\Delta(KC) = \nabla \cdot \nabla(KC) = \nabla \cdot (C\nabla K + K\nabla C) \tag{7.6}$$

then,

$$\Delta(KC) = C\Delta K + 2\nabla K\nabla C + K\Delta C \tag{7.7}$$

This indicates that starting from a uniform distribution, $C\Delta K$ is the only term which is responsible for the clustering.

In order to obtain the value of the diffusivity in alert regions, the standard link between the Brownian motion and diffusivity is taken, meaning that if copepods are put all in the alert region, they will jump continuously in different directions. Computing the mean squared displacement (MSD), which measures the deviation over time between the position of a particle and its reference position, is directly linked to the diffusivity by:

$$\left\langle (x(t) - x_0)^2 \right\rangle = 2d\,K\,t \tag{7.8}$$

where x_0 refers to the reference (initial) position, d is the dimension of the domain (here $d = 2$), K is the corresponding diffusion coefficient of copepods in alert regions and t is the time. The diffusion coefficient of

copepods in alert regions (K_a) for jump intensity of $u_J/u_\eta = 250$, is then equal to $K_a = 130$ by MSD analysis. There is a diffusion for copepods in safe regions (K_s) that we added for numerical reasons. This coefficient for copepods is $K_s = 0.01$ which corresponds to the fact that in the Eulerian framework copepods can have small Brownian motions on the top of the velocity of the fluid. At the interface of the alert and the safe regions, there are copepods which can jump from the alert regions into the safe regions. Therefore the transition of the diffusivity can not be sharp and should be treated carefully at the interface. As a first attempt we choose an hyperbolic step function of the following form:

$$K = K_s + (K_a - K_s)\left(0.5 + 0.5 \times tanh\left(\frac{\dot{\gamma} - \dot{\gamma}_T}{\delta\dot{\gamma}}\right)\right) \tag{7.9}$$

which indicates that the transition should be smooth as shown in Fig. 7.7. The parameter $\delta\dot{\gamma}$ corresponds to the width of a region where this transition should occur. Two dimensional Taylor-Green vortex flow is used

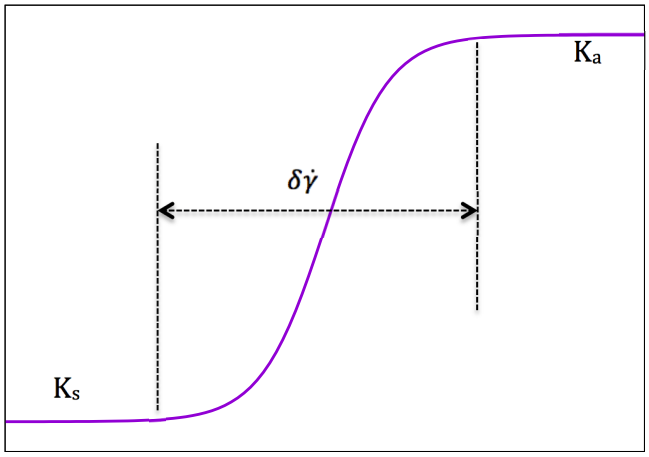

FIGURE 7.7: Transition of diffusivity from safe (K_s) to alert (K_a) region.

to compare the Eulerian model with the Lagrangian copepod model in a periodic boundary condition. Here the following form of the advection-diffusion equation is solved via pseudo-spectral method, with diffusivity which varies according to the eq. 7.9 with $K_a = 130$ and $K_s = 0.01$. The

parameter $\delta\dot{\gamma}$ needs to be tuned. Here it has a value equal to 0.05. C represents the concentration of copepods which is chosen to be uniform in the entire computational domain and u is the fluid velocity in TGV flows which follows the form of eq. 5.16 and eq. 5.17.

$$\frac{\partial C}{\partial t} + \mathbf{u} \cdot \nabla C = \Delta\left(KC\right) \tag{7.10}$$

Figure 7.8 shows this comparison for the corresponding values of the diffusivity however one can observe that visually the choice of $K_a = 1$ fits better into the LC model. This implies that the parameter $\delta\dot{\gamma}$ should be

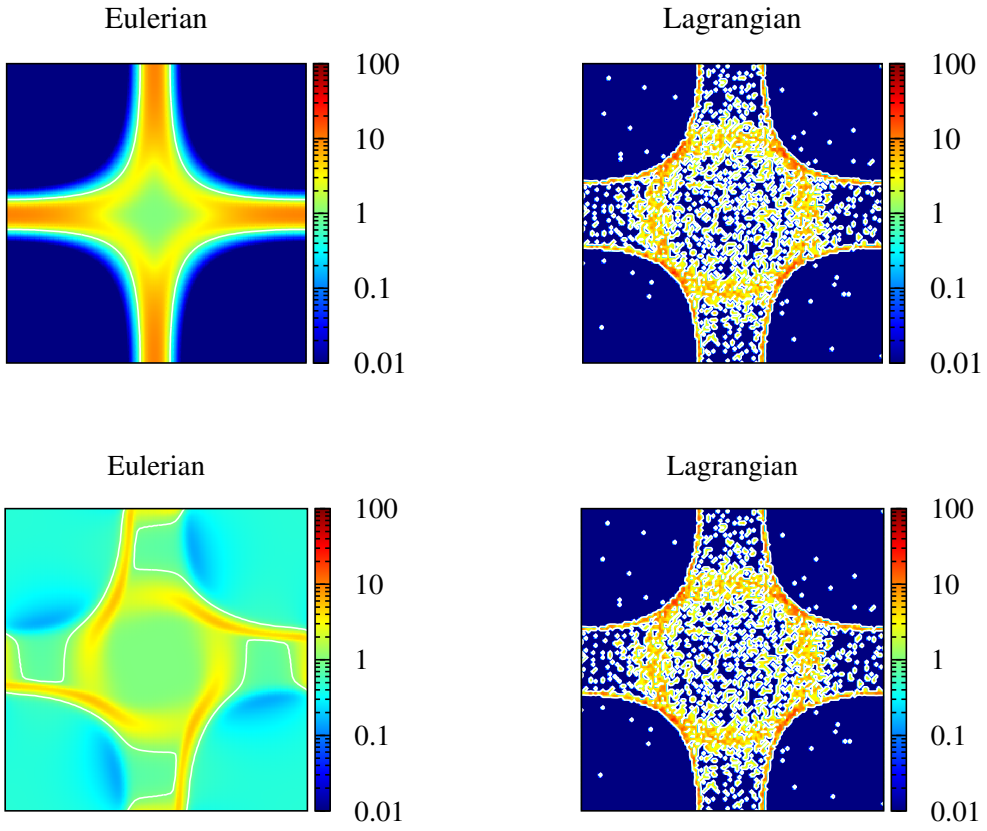

FIGURE 7.8: Snapshot of the comparison of the normalized particle density concentration ($\rho(x)/\rho_h$ where $\rho(x)$ represents the particle's density concentration of a cell and ρ_h is the same quantity corresponding to the homogenous distribution at initial time. Contour lines are traced at value of $\rho(x)/\rho_h = 1$) of the Eulerian and Lagrangian approaches in TGV flow with $K_s = 0.01$ and top) $K_a = 130$ and bottom) $K_a = 1$. The transition width is $\delta\dot{\gamma} = 0.05$ for both cases.

treated carefully, since in our simulation is not tuned correctly.

7.2.1 Difficulties

The main issue in this model is the way to treat the parameter $\delta\dot{\gamma}$. The problem arises from the fact that the transition of the diffusivity at the interface cannot be sharp, because high speed copepods go to the low speed regions until their jumps finish. Therefore we need to translate this behavior to $\delta\dot{\gamma}$. One idea is to estimate from a linear approximation (Taylor expansion of the shear rate) which gives:

$$\dot{\gamma} = \dot{\gamma}_T + \frac{\partial\dot{\gamma}}{\partial x}|_{x_T}(x - x_T) \tag{7.11}$$

generalizing this to two-dimensions suggests that $\delta\dot{\gamma} = ||\nabla\dot{\gamma}|| \cdot \Delta x$ with $\Delta x \sim u_J\tau_J$. The expression 7.9 can be rewritten as:

$$K = K_s + (K_a - K_s)\left(0.5 + 0.5 \times tanh\left(\frac{\dot{\gamma} - \dot{\gamma}_T}{||\nabla\dot{\gamma}|| \cdot \Delta x}\right)\right) \tag{7.12}$$

One needs to evaluate the norm of the gradient of the shear rate at the interface. In this flow the shear rate $\dot{\gamma}$ has an analytical expression as a function of position. Although it seems to be reasonable in the TGV flow, however it is more complicated in turbulent flows.
What we observe from eq. 7.10 and eq. 7.7, if we take into account that diffusivity is a function of $\dot{\gamma}$ and the shear rate depends on space, then (in one dimension):

$$\frac{\partial}{\partial x}\frac{\partial}{\partial x}K = \frac{\partial}{\partial x}\left[\frac{\partial K}{\partial\dot{\gamma}} \cdot \frac{\partial\dot{\gamma}}{\partial x}\right] \tag{7.13}$$

and:

$$\frac{\partial}{\partial x}\left[\frac{\partial K}{\partial\dot{\gamma}}\right] \cdot \frac{\partial\dot{\gamma}}{\partial x} + \frac{\partial K}{\partial\dot{\gamma}}\frac{\partial^2\dot{\gamma}}{\partial x^2} \tag{7.14}$$

finally:

$$\frac{\partial^2 K}{\partial x^2} = \left(\frac{\partial\dot{\gamma}}{\partial x}\right)^2 \frac{\partial^2 K}{\partial\dot{\gamma}^2} + \frac{\partial K}{\partial\dot{\gamma}}\frac{\partial^2\dot{\gamma}}{\partial x^2} \tag{7.15}$$

generalizing the eq. 7.15 to three-dimension and replacing into eq. 7.7:

$$\Delta(KC) = \left(\Delta\dot{\gamma}\frac{dK}{d\dot{\gamma}} + (\nabla\dot{\gamma})^2\frac{d^2K}{d\dot{\gamma}^2}\right)C + 2\nabla\dot{\gamma}\frac{dK}{d\dot{\gamma}}\nabla C + K\Delta C \tag{7.16}$$

finally the laplacian term turns into:

$$\Delta(KC) = K\Delta C + \frac{dK}{d\dot{\gamma}}\left(C\Delta\dot{\gamma} + 2\nabla\dot{\gamma}\nabla C\right) + \frac{d^2K}{d\dot{\gamma}^2}\left(\left(\nabla\dot{\gamma}\right)^2 C\right) \tag{7.17}$$

Eq. 7.17 shows the complexity of the problem. In a case when C is chosen to be uniform, the terms contributing to the creation of the clustering are $\frac{dK}{d\dot{\gamma}}\left(C\Delta\dot{\gamma}\right)$ and $\frac{d^2K}{d\dot{\gamma}^2}\left(\left(\nabla\dot{\gamma}\right)^2 C\right)$. This shows that it is linked not only to the first derivative but also to the second derivative of diffusivity, therefore the system of tuning is very delicate and our choice of eq. 7.9 may not be the best.

This is a preliminarily discussion on this topic and can be used to develop an equivalent Eulerian model of Lagrangian copepod model in turbulent flows.

Chapter 8

Conclusions

In this thesis we have considered a Lagrangian model for active particles. The model is trimmed in a way to reproduce some dynamical features experimentally observed in the motion of copepods in still water. Its main characteristics is the possibility to locally acquire an extra-velocity (jump) in response to a variation of the fluid flow conditions surrounding the particle. The direction of the jump is ruled by the hydrodynamics of small neutrally-buoyant particles. The Lagrangian model has been coupled to a turbulent developed flow described by the incompressible Navier-Stokes equations.

We have shown that jump escape reaction from spatio-temporal events characterised by high shear-rate leads to non homogeneous spatial distributions of active particles. This clustering mechanisms however is effective only when the reaction threshold is close to values of the order of τ_η^{-1} in a very narrow range. The fact that the range is narrow is ultimately linked to the intermittent distribution of the turbulence dissipation rate (Frisch, 1995). We have shown that clustering approaches its maximum when the threshold rate value $\dot{\gamma}_T$ roughly divide the shear-rate $(\dot{\gamma})$ spatial field in equal volume regions. Since this mechanisms mainly depends on the average value of small-turbulence scales rather than on their fluctuations we expect it to have a weak dependence on the Reynolds number of the turbulent flow. A second implication of the model is that for any given shear-rate reaction value $\dot{\gamma}_T$ there is a maximal intensity jump velocity beyond which clustering can not be further increased. Finally, the analysis of the correlation dimension suggests the formation of local quasi-bidimensional clusters enclosing the non-permitted flow regions.

From a physicist viewpoint we remark that the clustering mechanism at work in turbulence for the LC model is different form the one shown in other model systems of particulate active matter. For instance the clustering observed for motile algal cells in turbulence is given by the gyrotactic effect, which is a non-isotropic effect induced by the presence of the the external gravity field (Lillo et al., 2014). On the opposite, the LC model discussed here is isotropic but it is non-homogeneous in space (it depends on the local value of the shear-rate). We have tested the fact that clustering also appears when LC particles are made sensitive to other flow quantities such as enstrophy or fluid acceleration. The minimal fractal dimension we observed is always above the value of 2, confirming the fact that particles in this case aggregate in order to cover the surface of the forbidden regions. Based on these observations we do not expect that such clustering processes could lead to filamentary like clusters, $D_2 \simeq 1$, as the ones observed for microbubbles in turbulent flows. Another notable result is the negligible impact of the particle orientational dynamics on the clustering. This is likely to be linked to the limited duration of jumps (note that here $\tau_J \ll \tau_\eta$), but might become important for longer jumps, particularly in the modelling of larger motile plankton. Moreover we observed that only a prompt reaction leads to clusters. The negligible impact of orientation for the case examined here, suggests the possibility to formulate accurate Eulerian mean-field particle models based on the introduction of a space-dependent effective diffusivity (κ) whose amplitude may be linked directly to jump shape parameters, via a dimensional relation of the type $\kappa \propto u_J^2 \tau_J$. We showed that this diffusivity depends not directly on space but through its dependancy to the shear rate $(\dot{\gamma})$. However there are some difficulties in tuning the parameters for complex flows.

From a more biological perspective, although behavioural mechanisms leading to clustering had been already suggested in the past, such as the formation of patches through swimming against the flow (Genin et al., 2005), the possibility of cluster formation by escape jumps in a no-mean flow situation was never reported before. As discussed in Schmitt and Seuront (2008), clustering of copepods has an ecological importance: an effect may be to strongly increase the contact rate with mates and hence improve the reproduction. Indeed several models have been proposed

to express copepod contact rates in turbulence (Rothschild and Osborn, 1988; Evans, 1989; Visser and MacKenzie, 1998), reviewed in Lewis and Pedley (2000). In case of clustering, the contact rate is strongly increased (Wang, Wexler, and Zhou, 1998; Reade and Collins, 2000; Collins and Keswani, 2004; Schmitt and Seuront, 2008). The clustering which would result from a behaviour of predator avoidance (a reaction to turbulent shears similar to predator's signals) would have as side-effect a positive consequence with a strong enhancement of the mating contact rate. Our analysis showed that the encounter rate can be increased by a factor of the order of $\mathcal{O}(10^3)$ at dissipative scales. Of course such copepod concentration could also attract predators. Due to different trade-offs, each copepod species may have an optimal jump behaviour in response to turbulence. For example the copepod *Eurytemora affinis* used in our experimental section is an estuarine species adapted to maintain the bulk of its population in a salinity gradient in highly turbulent conditions (Devreker et al., 2008; Schmitt et al., 2011). By using high frequency sampling data of all life stages of *E. affinis*, Schmitt et al. (2011) confirmed that the late developmental stages (mainly adults) exhibited active vertical migration during the flood. Consequently the population was not homogeneously distributed in the water column, as dense patches are observed during short time window and near the bottom (Devreker et al., 2008).

8.1 Perspectives

Our model can be improved in the future to test such situations with tidally induced turbulence in shallow estuaries where copepods can use their jump abilities to simply avoid to be flushed out their optimal habitat. This could lead to the identification of some optimal clustering strategy that may be in relation with the dome-shapes proposed earlier, on purely speculative intuitions (Cury and Roy, 1989; MacKenzie, 2000). The presented LC model can also be improved by refining the jumping protocol in order to take into account the fact that the temporal sequence of jumps in copepods occurs in fast sequences (bursts) interposed to inactive moments. Another possible direction of research concerns the investigation

of the impact of a spatial radius of perception for copepods to react to turbulent shear. This may produce a smoothing or a delay in the perceived turbulent signal.
Furthermore an Eulerian mean-field particle model can be developed and tuned to be applicable for turbulent situations. Such a model describes the evolution of the concentration of copepods in a given region and can be used for studies in oceanography domain.

Appendix A

Lagrangian model of copepod dynamics: Clustering by escape jumps in turbulence - PHYSICAL REVIEW E 93, 043117 (2016)

PHYSICAL REVIEW E **93**, 043117 (2016)

Lagrangian model of copepod dynamics: Clustering by escape jumps in turbulence

H. Ardeshiri,[1,2,*] I. Benkeddad,[2] F. G. Schmitt,[2] S. Souissi,[2] F. Toschi,[3,4] and E. Calzavarini[1]
[1]*Université de Lille, CNRS, FRE 3723, LML, Laboratoire de Mécanique de Lille, F 59000 Lille, France*
[2]*Université de Lille, CNRS, Université de Littoral Cote d'Opale, UMR 8187, LOG, Laboratoire d'Océanologie et de Géoscience, F 62930 Wimereux, France*
[3]*Department of Applied Physics and Department of Mathematics and Computer Science, Eindhoven University of Technology, 5600 MB, Eindhoven, The Netherlands*
[4]*Istituto per le Applicazioni del Calcolo CNR, Via dei Taurini 19, 00185 Rome, Italy*
(Received 8 January 2016; published 18 April 2016)

Planktonic copepods are small crustaceans that have the ability to swim by quick powerful jumps. Such an aptness is used to escape from high shear regions, which may be caused either by flow perturbations, produced by a large predator (i.e., fish larvae), or by the inherent highly turbulent dynamics of the ocean. Through a combined experimental and numerical study, we investigate the impact of jumping behavior on the small-scale patchiness of copepods in a turbulent environment. Recorded velocity tracks of copepods displaying escape response jumps in still water are here used to define and tune a Lagrangian copepod (LC) model. The model is further employed to simulate the behavior of thousands of copepods in a fully developed hydrodynamic turbulent flow obtained by direct numerical simulation of the Navier-Stokes equations. First, we show that the LC velocity statistics is in qualitative agreement with available experimental observations of copepods in turbulence. Second, we quantify the clustering of LC, via the fractal dimension D_2. We show that D_2 can be as low as $\sim$2.3 and that it critically depends on the shear-rate sensitivity of the proposed LC model, in particular it exhibits a minimum in a narrow range of shear-rate values. We further investigate the effect of jump intensity, jump orientation, and geometrical aspect ratio of the copepods on the small-scale spatial distribution. At last, possible ecological implications of the observed clustering on encounter rates and mating success are discussed.

DOI: 10.1103/PhysRevE.93.043117

I. INTRODUCTION

The study of swimming microorganisms and their interaction with fluid flows has attracted enormous attention in the past decade. A line of research has focused on characterizing individual swimming strategies by means of experiments [1–3] as well as by theoretical and numerical modeling [4,5]. A second direction of study devoted to the consequences of swimming on population dynamics, e.g., by focusing on encounter rates and other collective behaviors [6–10]. A third direction focused on the mutual interactions of microorganisms with the fluid-flow environment, in particular bioinduced flow fluctuations, sometimes dubbed as bacterial turbulence [11–13], or, vice-versa, on active matter clustering induced by nonhomogeneous flows or fluid turbulence [14–22]. The present study will focus on this latter aspect, in particular on copepod's dynamics in turbulent flow.

Copepods are the most diversified crustaceans in the aquatic environment whose length ranges from 0.1 mm to a few millimeters. They are important to global ecology and to the carbon cycle [23] (see also Refs. [24] and [25]). Although copepods are not at the top of the food web, they have a major role in the marine ecosystem because they are the secondary producers in the ecological food web linking phytoplankton cells (the primary producers) to fish larvae and even to large mammals such as whales. Copepods also consume the mosquito larvae, acting as control mechanism for malaria [26]. They are of great importance in fishery industry. A central issue in breeding fish species is the external food supply. Most fishes prefer copepods to other zooplankton species (i.e., rotifers) and they grow bigger in shorter time when eating copepods [27,28].

Living in a fluid environment characterized by body-scale Reynolds number up to 1000, they are subjected to the physics of the flow field both in viscous and inertial regime [29]. Copepods typically have a short, cylindrical body with antennas, few pairs of swimming legs, and tales. Using their antennas, copepods can sense the disturbance, which is caused either by the presence of predators or by high turbulent regions in the flow. Kiørboe *et al.* [30,31] performed series of experiments, investigating the effect of nonuniform flow motion on copepods. In order to find the component of the flow that copepods react the most to, the copepods were put into a time-dependent siphon flow (which ideally generates a pure longitudinal deformation rate), in an oscillating chamber where copepods experience only acceleration, in a couette device producing shear deformation, and finally in a rotating cylinder where acceleration and vorticity are both present. The conclusion of this study was that these small crustaceans react to the flow deformation rate. Kiørboe also reported [32] that there are two threshold values of the deformation rate: the upper one, around $10\,s^{-1}$, which corresponds to either the presence of predators or to a region where turbulence intensity is high, and the lower one, $1\,s^{-1}$, which corresponds to regions in the flow where turbulence intensity is lower or food abundance is not enough for copepods. These tiny crustaceans find themselves at ease in regions in between these two thresholds. To avoid uncomfortable regions, copepods exhibit a rapid escape in the flow that is often dubbed a *jump*. Buskey *et al.* [33,34] showed that copepod's velocity can reach the rate of 500 body length per second (0.5 m/s) while jumping. The mechanical energy produced during their

*hamidreza.ardeshiri@polytech-lille.fr

escape is reported to be very high (8×10^{-5} J/s) [35], which makes copepods, relative to their size, among the fastest and the strongest animals in the world.

Buskey [33,34] also reported that males and females respond differently to hydrodynamic stimulus in terms of response latency, jump speed, number of thrusts, distance jumped, and many other parameters. According to their investigations, copepods jump in an unpredictable direction, but rarely in the backward direction of their motion. Other studies have considered the mating behavior of copepods [36] and the effect of salinity on copepod's dynamics and copepod's encounter rate [37,38]. Copepods are also sensitive to light stimuli, being attracted by natural light sources [39].

In the past two decades many studies have been conducted to quantify the dynamics of copepods. Most of them focused on their behavior in still water [36–38], while less studies have studied the dynamics in their natural living environment because of the difficulties of such experimental investigations. Few works have been devoted to the dynamics of copepods in turbulent flows [40–44]. However, the densities of copepods used in these studies are often lower than the maximum densities that can be encountered in the field.

The numerical simulation can provide a tool that integrates our current knowledge on copepod dynamics and uses a high number of individuals. The objective of the present study is to simulate copepods numerically in turbulence to characterize their dynamics induced by a behavior model. To achieve this goal, our strategy is twofold: on one hand, new experimental measurements and observations available in the literature [45–51], along with the aforementioned copepods properties, should be considered in detail in order to introduce a realistic and physical model. On the other hand, fundamental knowledge on simulation of particles in turbulent flows, available in numerical and experimental studies on particles in turbulence [52–56], is needed to couple the physics and biology in the numerical model.

The paper is organized as follows: Sec. II describes the experimental framework used to stimulate copepods. We then analyze copepods' trajectories to introduce a model equation describing copepods' behavior. Furthermore, similarity analysis is performed to tune the LC model and its numerical implementation is explained at the end of this section. Section III details the single-point statistics, fractal dimension, and orientation dynamics of copepods. The paper ends with conclusion and outlook on future works.

II. METHODS

A. Experimental jump data analysis

We begin by presenting an analysis of a new experimental trajectory data set of the estuarine copepod, *Eurytemora affinis*, recorded at LOG Laboratory between May and June 2015. Copepods that originated from the Seine river estuary (France) are maintained in the laboratory under optimal conditions for several generations. The experimental setup is a shallow-depth aquarium, $63 \times 53 \times 6\,\mathrm{mm}^3$ in length, height, and depth, respectively, with two light sources on the lateral side ($53 \times 6\,\mathrm{mm}^2$). The water is kept still and at a temperature of $(18 \pm 1)^\circ$C and salinity of 15 psu. Copepods

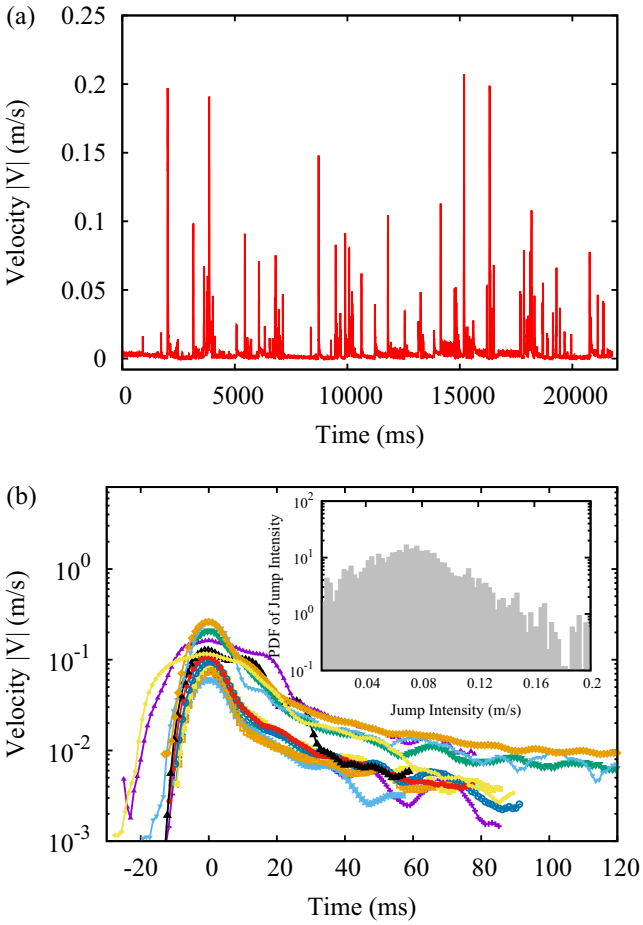

FIG. 1. (a) The copepod velocity relative to temporal sequence with multiple jumps occurring in response to stimulus. (b) Several jumps superposed by a shift, taking as reference time that are associated with their peak position. Almost all of the jumps decay exponentially. (Inset) The probability density function (PDF) of the jump intensity.

were introduced one at a time into the aquarium and their dynamics were filmed. A total of 14 individuals were analyzed (7 males and 7 females). A copepod in the aquarium is lead to jump preferentially along the horizontal direction by switching on just one of the light sources. The copepod dynamics in a vertical plane is recorded by a high-speed camera (1000 frames/s) and the single trajectory is extracted by means of particle-tracking velocimetry software (TEMA Motion by Image Systems). In such a way hundreds of trajectories are recorded, each with an average time length of 19 s. A typical copepod velocity signal as a function of time is shown in Fig. 1(a). We see extremely abrupt spikes (jumps) alternating to calm, nearly immobile, phases.

In order to see if the velocity signal of the jump events share some common features, we zoom in on the signal and superpose several jumps by a shift taking as reference their peak position. In Fig. 1(b) we can appreciate that almost all of the jumps, after a steep rise, display a similar decay. We associate such a decay to a purely hydrodynamical effect. It can be interpreted as a drag-induced decay of an instantaneous acceleration. The inset panel in Fig. 1 shows that

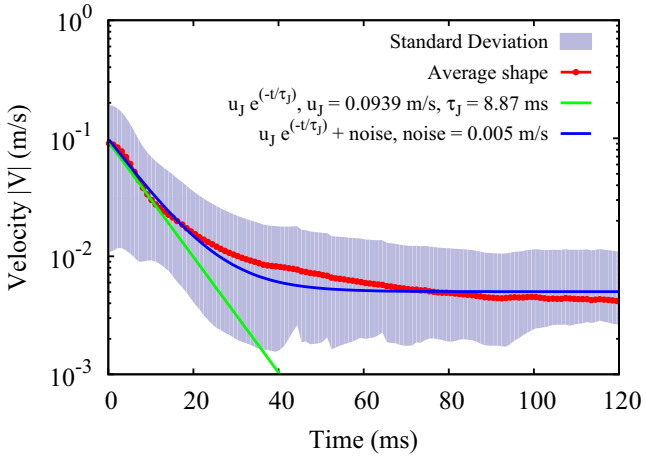

FIG. 2. Average shape of copepod velocity (over about 730 jumps): mean value (red line) and standard deviation (shaded area). Note that an error along the horizontal direction due to the uncertainty in the identification of jump peaks may be present but has been omitted here. Green line: Fitted exponential function $u_J e^{-t/\tau_J}$ where u_J is the jump intensity and τ_J is the decaying time of the jump. Blue line: Same fit with the addition of a noise velocity offset.

the probability density function (PDF) of the jump intensity has a maximum value around $\sim$0.07 m/s. Note that spikes are identified based on a threshold on the time-averaged velocity of the copepods in each copepod's trajectory.

We then average the data set of jumps in order to obtain an averaged shape of jump. This is shown in Fig. 2, from which we can deduce the average jump velocity amplitude $u_J = 0.0939$ m/s and the mean decaying time $\tau_J = 8.87$ ms. We also see that for a long time the velocity reaches a very low plateau at 5×10^{-3} m/s $\sim 1/20\, u_J$, which we are tempted to associate to a weak random wandering behavior of the copepod.

The distribution of jumps in time in the experimental data set seems to deviate from an exponential distribution, suggesting the existence of a memory effect. This may, however, be dependent on the type of stimulus (the light source), which is continuous in time, very different from the one due to the presence of a variable-flow shear rate. This aspect will, therefore, not be taken into account in the model presented in the next section. We plan to investigate interjump statistics more carefully in the future, when experiments with mechanically induced stimulus may be available.

B. Model equation for copepods dynamics

In this section we introduce a simple model system of copepods' dynamics. This representation is based on the idea that the copepods' trajectories in a fluid can be mimicked by properly defined active particles. Similar models have been successfully employed for the description of the behavior of phytoplankton, such as chlamydomonas [16,57,58], both in laminar and, more recently, in turbulent flows [14,15,22]. Copepods, and zooplankton in general, display higher complexity compared, e.g., to algae species because of their higher motility. The model relies both on biological and hydrodynamical assumptions. First, we assume that copepods respond always in the same way to external flow disturbances. Their jump reaction is embedded in their neural system. Furthermore, the stimulus triggering the jump is highly stylized; we only take into account a mechanical signal with a single threshold, to be specified later on, and ignore any other activity induced by light, food, or chemistry (e.g., pheromones). On the mechanical side, we assume that copepods are small enough that their center of mass can be considered a perfect fluid tracer in a flow, except for the time when a jump event takes place. In hydrodynamic terms, this means that copepods are assumed to be rigid, homogeneous, neutrally buoyant particles with a size that is of the order of the dissipative scale of the flow. Gravity force has no role in producing acceleration or torque. Only the drag force effect is taken into account during the jumps. Finally, copepods are coupled to the fluid in a one-way fashion, they react and are carried by it, but they do not modify the surrounding flow; copepods-copepods interactions are also neglected. Adding all together the above hypothesis, the LC equation of motion is as follows:

$$\dot{\mathbf{x}}(t) = \mathbf{u}(\mathbf{x}(t),t) + \boldsymbol{J}(t,t_i,t_e,\dot{\gamma},\mathbf{p}), \tag{1}$$

where $\mathbf{u}(\mathbf{x}(t),t)$ is the velocity of the carrying fluid at time t and position $\mathbf{x}(t)$ and where $\boldsymbol{J}$ is an added velocity term that describes the active behavior (jump) of the copepod. $\boldsymbol{J}(t,t_i,t_e,\dot{\gamma},\mathbf{p})$ is a function of time t; it depends also on an initial and a final time t_i and t_e, on flow shear rate value $\dot{\gamma}$, and on orientation vector $\mathbf{p}$. If copepods are taken to be spherical in shape, their orientation dynamics is given by

$$\dot{\mathbf{p}}(t) = \boldsymbol{\Omega} \cdot \mathbf{p}(t), \tag{2}$$

where $\boldsymbol{\Omega}$ is the fluid rotation rate antisymmetric tensor, defined as $\Omega_{ij} = 1/2(\partial_i u_j - \partial_j u_i)$. A more general form of Eq. (2), valid for axisymmetric ellipsoidal particles, is as follows:

$$\dot{\mathbf{p}}(t) = \left\{ \boldsymbol{\Omega} + \frac{\alpha^2 - 1}{\alpha^2 + 1} [\mathcal{S} - \mathbf{p}^{\boldsymbol{T}}(t) \cdot \mathcal{S} \cdot \mathbf{p}(t)] \right\} \cdot \mathbf{p}(t), \tag{3}$$

where $\alpha \equiv l/d$ is the aspect ratio of the ellipsoids given by the ratio of length (l) to diameter (d), which is typically around 3 for *E. affinis*. The above equation was first proposed by Jeffery, and its full derivation is detailed in Ref. [59]. Its phenomenology in turbulent flows has been investigated more recently in Ref. [54]. Notice that here we designate by $\mathcal{S}$ the fluid deformation rate symmetric tensor as $S_{ij} = 1/2(\partial_i u_j + \partial_j u_i)$ and the shear rate is then defined as $\dot{\gamma} = \sqrt{2\,\mathcal{S} : \mathcal{S}}$. We note that the fact that the jump term is assumed to depend on $\dot{\gamma}$ represents a generalization to the 3D geometry of Kiørboe's empirical findings [32]. For the jump term we propose the following functional form:

$$\boldsymbol{J}(t,t_i,t_e,\dot{\gamma},\mathbf{p}) = H[\dot{\gamma}(t_i) - \dot{\gamma}_T]\, H[t_e - t] u_J\, e^{\frac{t_i - t}{\tau_J}}\, \mathbf{p}(t_i), \tag{4}$$

where $H[x]$ denotes the Heaviside step function, $\dot{\gamma}_T$ is a threshold value of the shear rate, u_J and τ_J are two characteristic parameters characterizing the jump shape, its velocity amplitude (u_J), and duration τ_J, respectively. The first H step function models the fact that a jump can begin only when the shear rate is above the given threshold value, while the second step function accounts for the fact that the jump time span is finite. The initial and final time of a jump

are defined as:

$$t_i = t \quad \text{if} \quad (\dot{\gamma}(t) > \dot{\gamma}_T) \cap (t > t_e), \tag{5}$$

$$t_e = t_i + c\,\tau_J = t_i + \log(10^2)\,\tau_J. \tag{6}$$

In other words, we assume that a jump cannot begin if a previous jump has not finished ($t > t_e$) and that a jump terminates when its amplitude has decreased to a negligible level, here taken as one percent of the initial amplitude, i.e., $|\boldsymbol{J}(t_e)| = 10^{-2}|\boldsymbol{J}(t_i)|$.

C. Model tuning for turbulent flows

We now take into account the presence of the oceanic flow environment surrounding the copepods. The properties of oceanic turbulence relevant for our work have been studied by, among others, MacKenzie *et al.* [60] and Jimenez [61]. In these surveys it was observed that the mean value of the turbulent kinetic energy dissipation rate, $\epsilon = 2\nu\mathcal{S} : \mathcal{S}$, varies from about $10^{-8}\,\mathrm{m^2 s^{-3}}$ in open ocean to $10^{-4}\,\mathrm{m^2 s^{-3}}$ in coastal zones (although it is also sensitive to the wind speed conditions and on the depth). The value of ϵ along with the kinematic viscosity of sea water, ν, allows us to estimate the Kolmogorov scales of ocean turbulence: The dissipative length $\eta = (\nu^3/\epsilon)^{1/4}$, time $\tau_\eta = (\nu/\epsilon)^{1/2}$, and velocity $u_\eta = (\nu\epsilon)^{1/4}$. The order of magnitude estimate as from Ref. [61] for these quantities are reported in Table I. According to the same authors the typical Taylor-scale Reynolds number Re_λ in the ocean can reach values up to $O(10^2)$.

Given that the typical size of copepods is of the order of millimeters, it is clear that the relevant flow scales for their dynamics are close to the Kolmogorov scale or below in turbulence [29]. When the LC model is recast in a dimensionless form in terms of these scales, we get three dimensionless groups of parameters: τ_J/τ_η, u_J/u_η, and $\tau_\eta\dot{\gamma}_T$. These parameters, together with the flow Re_λ, fully specify the working conditions (or tuning) of the copepods-in-turbulence model.

In this study we take as reference for the energy dissipation rate the value $\epsilon = 10^{-6}\,\mathrm{m^2 s^{-3}}$, and by taking into account the dimensional values estimated for the copepods jump intensity u_J and jump decaying time τ_J, the ratios $u_J/u_\eta = 93.9$ and $\tau_J/\tau_\eta = 0.00887$ can be deduced from the similarity analysis. This tells us that in ordinary turbulence conditions the copepods possess an almost instantaneous reaction, since their response time is about one-hundredth of the smallest scale of turbulence. On the opposite the velocity reached during a jump is of a magnitude that is comparable if not higher to the one of turbulent velocity fluctuations. Finally, we note that we do not have any experimental guess for the magnitude of $\dot{\gamma}_T$, therefore the value $\tau_\eta\dot{\gamma}_T$ is a free parameter of our model.

TABLE I. Reference properties of the ocean turbulent flow as from Ref. [61]. ϵ is the mean turbulent energy dissipation rate, and η, τ_η, and u_η are the turbulence space, time, and velocity dissipative scales, respectively. Re_λ is the Taylor-scale-based Reynolds number. Their approximate range of variability is given together with the reference values chosen for the similarity analysis in the present study.

Parameter	Unit	Range		This study
ν	$\mathrm{m^2 s^{-1}}$	$\sim 10^{-6}$		10^{-6}
ϵ	$\mathrm{m^2 s^{-3}}$	10^{-8}	10^{-4}	10^{-6}
η	m	3×10^{-3}	3×10^{-4}	10^{-3}
τ_η	s	10	0.1	1
u_η	$\mathrm{m\,s^{-1}}$	3×10^{-4}	3×10^{-3}	10^{-3}
Re_λ	—	$O(10^2)$		80

D. Numerical implementation of the LC model and of the turbulent flow simulation

The copepods-in-turbulence model system is conveniently implemented via an Eulerian-Lagrangian approach, meaning that the trajectory $\mathbf{x}(t)$ of each individual copepod is computed by means of Lagrangian tracking method applied to Eq. (1) [62,63], while the fluid flow is obtained by solving the field equations of incompressible fluid-dynamics, i.e., Navier-Stokes equations, in turbulent conditions. All the particles are advanced in time using Adams-Bashforth method with a time step equal to $\delta t = 1.4\times10^{-3}\tau_\eta$, the same time step as for the integration of the Navier-Stokes equations. Such a choice of time step shall also satisfy the constraint $\delta t \ll \tau_J$.

A direct numerical simulation (DNS) approach was used to solve the Navier-Stokes equations for homogeneous isotropic turbulence by means of a pseudospectral method:

$$\partial_t\mathbf{u} + \mathbf{u}\cdot\nabla\mathbf{u} = -\nabla p/\rho + \nu\Delta\mathbf{u} + \boldsymbol{f}, \tag{7}$$

where $\mathbf{u}(\mathbf{x}(t),t)$ is the incompressible ($\nabla\cdot\mathbf{u} = 0$) fluid velocity field, p is the pressure, ν is the kinematic viscosity, and ρ is the fluid density. The $\boldsymbol{f}$ is the forcing that is applied on large scales to sustain the statistically stationary turbulence. The solution domain is a cube of length $L = 2\pi$ with $N^3 = 128^3$ grid points, subject to periodic boundary condition. Aliasing error is controlled by omitting the wave number larger than $k = 2/3\times(2\pi N/L)$, to reach the Taylor-Reynolds number of the flow $\mathrm{Re}_\lambda = \sqrt{15}u_{\mathrm{rms}}^2/(\nu\epsilon)^{1/2} \approx 80$, where u_{rms} is the single component root mean square velocity fluctuation. $k_{\max}\eta > 1.4$, in which $k_{\max} = N/3$ and η is the Kolmogorov length scale, assures that small scales structures are well resolved.

III. RESULTS AND DISCUSSION

As mentioned above, the LC model is characterized by three control parameters: the jump intensity u_J, the decaying time of the jump τ_J, and the shear rate threshold value $\dot{\gamma}_T$, which are conveniently presented in dimensionless form in terms of turbulence dissipative scale units. Since the LC model is just one-way coupled to the fluid, in the numerics we can perform simultaneous simulations of several families of copepods in the same turbulent flow, where each family is characterized by the triplet $[u_J/u_\eta, \tau_J/\tau_\eta, \dot{\gamma}_T\tau_\eta]$.

In agreement with the experimental observation we always keep fixed the decaying time of the jump to the value $\tau_J/\tau_\eta = 10^{-2}$, while the other parameters are varied independently in the ranges $u_J/u_\eta \in [1,400]$ and $\tau_\eta\dot{\gamma}_T \in [0,4]$. Note that if $\dot{\gamma}_T = 0$, according to the model, all the particles will jump in a synchronous way. In order to avoid such an unphysical feature, the time t_e for each particle is initialized by a random variable with homogeneous distribution in the interval $[0,\log(10^2)\,\tau_J]$.

We perform a series of simulations with multiple families, with about 2.56×10^5 particles per family.[1] The simulation was started and particles were let displace for about 2 eddy turnover times, after that during the following ∼2 eddy turnover times about 10 instantaneous distributions of LC particles were saved for analysis. Copepods are modeled as solid sphere particles, and orientation vector affected by fluid rotation rate [Eq. (2)], unless otherwise noted. For comparison a set of passive fluid tracers are also included in all our simulations.

A. Single-point statistics

In order to see how the LC dynamics in turbulence differ from that of a fluid tracer, we first address the velocity single-point statistics. The PDF of the absolute value of single-component velocity for the copepods, i.e., $|\dot{x}_i|$, is shown in Fig. 3. Tracers, the particles that move along the streamlines, agree with a Gaussian distribution, while for copepods a slower decaying tail is found. This deviation becomes more pronounced at increasing the jump intensity for a given threshold value of the shear rate, as shown in Fig. 3(a). It also appears that low jump intensities $u_J < 10\,u_\eta$ are not strong enough to make effective changes on the copepods PDF. On the other hand, increasing the threshold value of the shear rate leads to fewer jumps; therefore, in this case copepods behave almost like tracers. Their deviation in velocity distribution from the Gaussian indeed increases by decreasing the shear rate threshold value as can be seen in Fig. 3(b).

The general trend of the observed deviation from Gaussianity can be predicted by means of the following probabilistic model. We suppose that the instantaneous single cartesian component velocity of LC particles can be approximated by the sum of three statistical independent random variables. The first variable accounts for the turbulent velocity field contribution; therefore, it is a Gaussian with zero mean and the same standard deviation as the one measured in the DNS. The second and third variable mimic, respectively, the jump direction and its intensity: we assume that the orientation is random uniform in the solid angle and that the jumps happen uniformly in time. One can obtain the resulting PDF for the LC particle velocity from the convolution of the three elementary PDFs associated to the three described random variables. The resulting density distribution function when compared to the LC measurements at low threshold value $\tau_\eta \dot{\gamma}_T = 0.21$ (i.e., when copepods jump very frequently), shows an overall qualitative agreement with a slight deviation in the tails [see Fig. 3(b)].

Such a discrepancy comes from the fact that in reality the jump directions develop some correlations with the underlying flow, via Eq. (2), while the probabilistic model neglects it. One can make use of the approximate probabilistic model to estimate the average fraction of particle performing jumps as a function of the shear-rate threshold value. This is done by introducing an adjustable parameter accounting for the probability that a given particle is actually jumping and by fitting the model to the PDF curves. Figure 4 shows the fitted

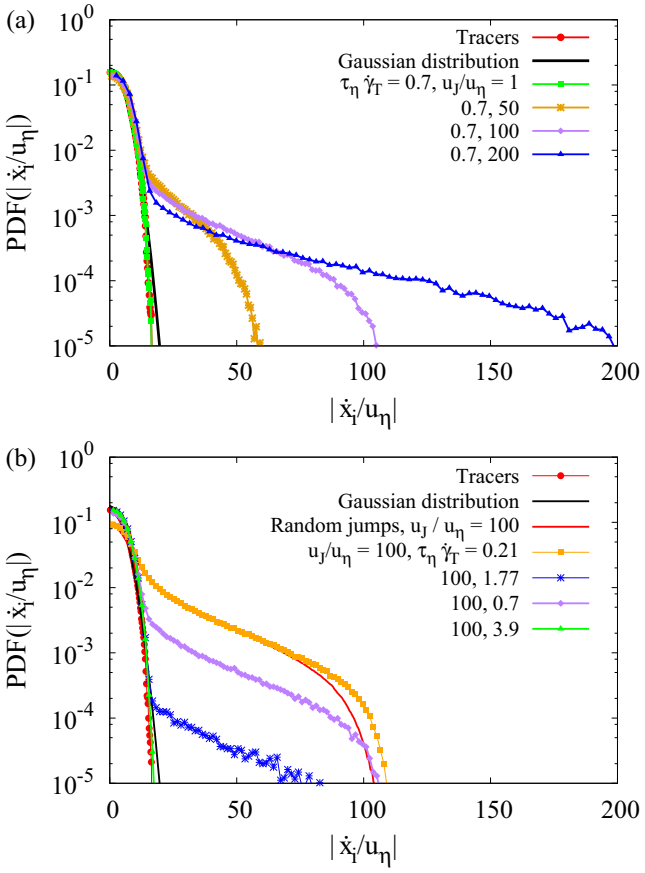

FIG. 3. Probability density function of absolute value of single component velocity $|\dot{x}_i/u_\eta|$ for the copepods (a) at constant threshold value $\tau_\eta \dot{\gamma}_T = 0.7$ and different jump intensities. Gaussian distribution is a statistic distribution here with the measured root mean square velocity of the Eulerian field as the standard deviation (b) at constant jump intensity $u_J/u_\eta = 100$ for different shear rate threshold values. Random jumps correspond to the expected velocity distribution when randomly oriented jumps occur uniformly in time on top of the turbulent velocity field.

predictions obtained with such a procedure (which confirm the validity of the probabilistic model), while the inset of the same figure displays the inferred jump percentage as a function of the shear rate threshold value. We observe an exponential decrease as $\dot{\gamma}_T$ is raised. For the value $\tau_\eta \dot{\gamma}_T = 0.5$, the jumping particle fraction is around 50%.

We finally observe that the shape of the PDF displayed by the LC model is also in qualitative agreement with a recently published experimental study [43], despite the fact that the experiment has been performed in low Reynolds number conditions (up to $\mathrm{Re}_\lambda \simeq 30$). What has not been reported yet in experimental studies is a quantification of the three-dimensional spatial distribution of copepods in turbulence. We do this in the next section by means of a fractal dimension characterization.

B. Correlation dimension analysis

The distribution of the LC particles is illustrated by Fig. 5, where we show the instantaneous particle positions in two-dimensional slices of thickness $\sim\eta$, visualizing at the same

[1] In physical dimension this corresponds to a number density of $O(1)$ LC particles per cm^3, a density comparable to the one found for real copepods estuarine water.

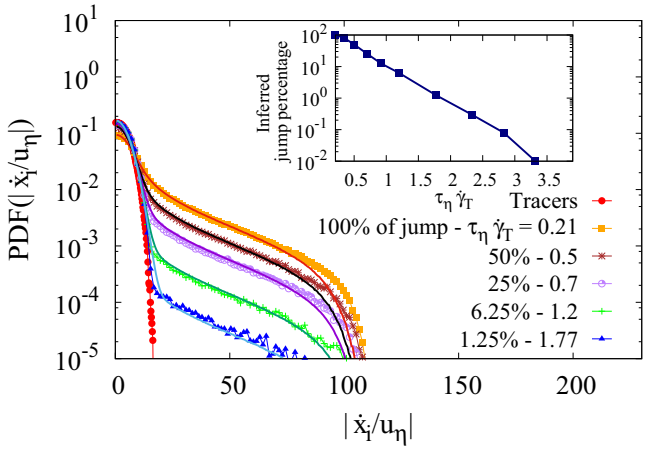

FIG. 4. Probability density function of absolute value of single-component velocity $|\dot{x}_i/u_\eta|$ for the copepods at constant jump intensity $u_J/u_\eta = 100$ for different shear rate threshold values. Fitted PDF curves correspond to the percentage of jump of copepods. (Inset) Deduced percentage of jump as a function of the shear rate threshold value $\tau_\eta \dot{\gamma}_T$.

time the values of shear-rate of the carrying flow. Contrary to fluid tracers, LC particles are nonhomogeneously dispersed in regions where turbulence intensity is below the given shear-rate threshold, according to the model. In the panels of Fig. 5, we also highlight the $\dot{\gamma}_T$ values by contour lines, we name, respectively, *comfort* and *alert* regions the locations which are below or above these fixed $\dot{\gamma}_T$ values. In Fig. 5(a), which corresponds to $\dot{\gamma}_T = 0.35\ \tau_\eta^{-1}$, the alert region is the dominant one. In this situation the great majority of LC particles are jumping but they manifestly fail to reach the few available comfort islands. This may be due both to the fact that islands are small and that they are short lived: one shall bear in mind the interplay between space and time in this problem. Figure 5(b) shows a condition where comfort and alert regions are equally probable. We notice a pronounced aggregation of particles in the alert areas surrounding the comfort regions, while the latter are efficiently evacuated. Finally, Fig. 5(c) illustrates what happens when the alert behavior is triggered only by a few extreme shear-rate filamentary regions. The LC particles manage to avoid them quite efficiently but in the overall picture they seems to be mostly homogeneously distributed. (See Supplemental Material [64] for the 2D visualization of copepods' motion in turbulent flow at $\tau_\eta \dot{\gamma}_T = 0.92$.)

In order to better quantify the patchiness of the LC particles we compute their correlation dimension (D_2), which is a measure of the dimensionality of a set of points. According to the Grassberger and Procaccia algorithm [65], the D_2 is defined as the scaling exponent of the probability of finding a pair of particles with a separation distance less than r : $P_2(|X_2 - X_1| < r) \propto r^{D_2}$ as $r \to 0$. In other words, if

$$C(r) = \frac{2}{N(N-1)} \sum_{i<j} H(r - |X_i - X_j|) \qquad (8)$$

decreases like a power law, then $D_2 = \lim_{r\to 0} \frac{\log C(r)}{\log r}$. Figure 6 shows the D_2 value in the two-dimensional parameter space

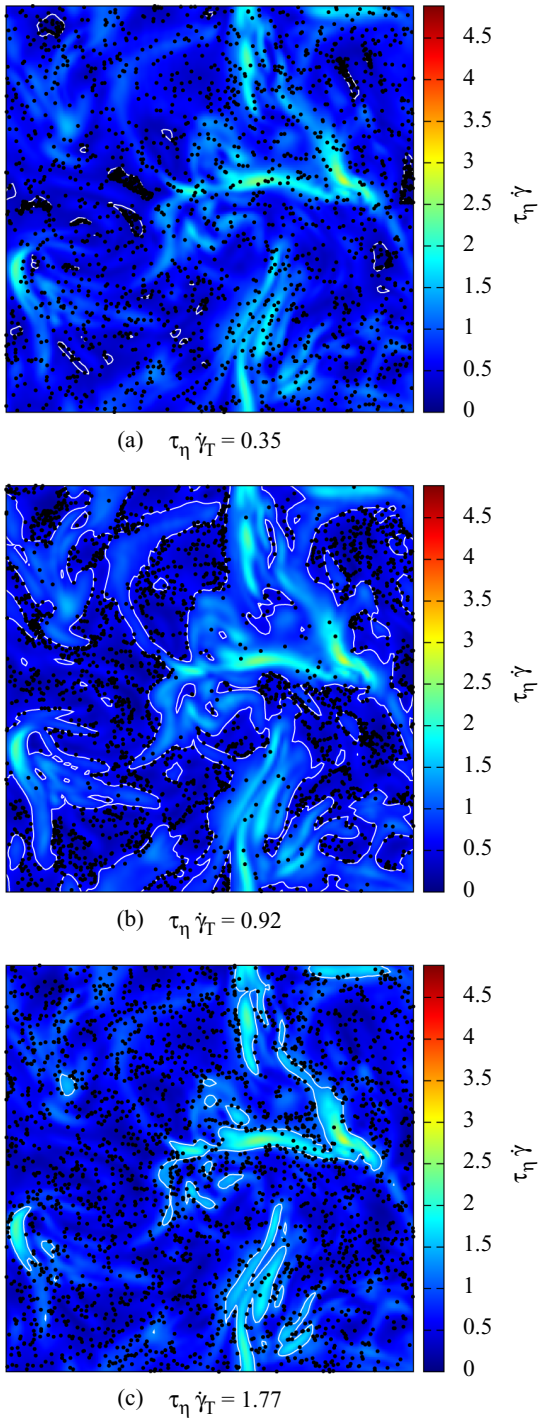

FIG. 5. Patchiness of the copepods from the simulations. Shading shows the instantaneous field of the absolute value of the shear rate of the Eulerian field (a) distribution of the copepods with $u_J/u_\eta = 250$ and $\tau_\eta \dot{\gamma}_T = 0.35$, (b) distribution of the copepods with $u_J/u_\eta = 250$ and $\tau_\eta \dot{\gamma}_T = 0.92$, and (c) distribution of the copepods with $u_J/u_\eta = 250$ and $\tau_\eta \dot{\gamma}_T = 1.77$. Contour lines are traced at the corresponding value of $\dot{\gamma}_T$ on each panel.

composed by the intensity of the jump and the shear rate threshold value. The clustering ($D_2 < 3$) is discernible when the prescribed shear rate threshold value is less than $2.8\ \tau_\eta^{-1}$,

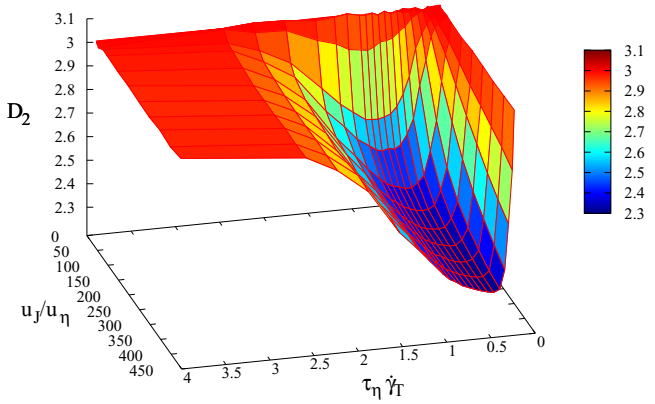

FIG. 6. Correlation dimension D_2 of copepods as a function of jump intensity u_J/u_η and threshold value $\tau_\eta \dot{\gamma}_T$.

and it is maximal, $D_2 \simeq 2.3$, at around $0.5\ \tau_\eta^{-1}$. On the other hand, we observe a saturation of clustering as u_J is increased. In order to better appreciate these two features, i.e., the minimum with respect to $\tau_\eta \dot{\gamma}_T$ and a saturation as a function of u_J/u_η, two two-dimensional cuts of the $D_2(\dot{\gamma}_T, u_J)$ surface are shown in Fig. 7.

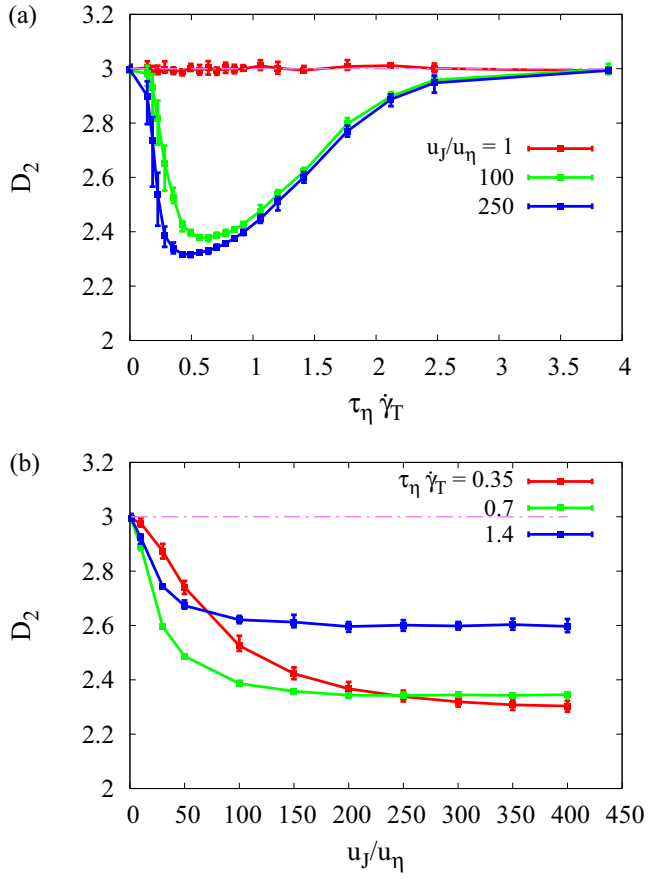

FIG. 7. Lateral view of correlation dimension of the copepods as a function of the jump intensity u_J/u_η and threshold value $\tau_\eta \dot{\gamma}_T$. Error bars indicate the range of variability of the measurements from 10 independent particle snapshots.

One may wonder why there is an optimum and what is its physical meaning. Copepods are prone to jump in order to escape from regions of alert ($\dot{\gamma} > \dot{\gamma}_T$), to reach regions where $\dot{\gamma} < \dot{\gamma}_T$; therefore, the chance for a jump to be successful (assuming it to be randomly oriented) depends on the size of the comfort region, in other words to the volume, $\mathcal{V}_{\dot{\gamma}<\dot{\gamma}_T}$. On the other hand, clustering would be maximum if we have numerous successful jumps, and obviously the number of jumps depends on $\mathcal{V}_{\dot{\gamma}>\dot{\gamma}_T}$. This implies that copepods clustering is expected to be proportional to $\mathcal{V}_{\dot{\gamma}<\dot{\gamma}_T} \cdot \mathcal{V}_{\dot{\gamma}>\dot{\gamma}_T}$. Now, substituting the volume of comfortable regions with $\mathcal{V}_{\rm tot} - \mathcal{V}_{\dot{\gamma}>\dot{\gamma}_T}$ leads to $\mathcal{V}_{\dot{\gamma}>\dot{\gamma}_T} \cdot (\mathcal{V}_{\rm tot} - \mathcal{V}_{\dot{\gamma}>\dot{\gamma}_T})$. One direct consequence is that the clustering would be maximum when $\mathcal{V}_{\dot{\gamma}>\dot{\gamma}_T} = \mathcal{V}_{\rm tot}/2$. This can explain the existence of the optimum of D_2 as a function of $\tau_\eta \dot{\gamma}_T$ as shown in Fig. 7(a) as well as its trend as a function of $\dot{\gamma}_T$. Note, however, that this argument is based on the simplifying assumption that there is no correlation between the orientation of a LC particle at jump and its position respect to the comfort area, and also it neglects the spatial structure of the shear rate field.

How can we determine the value of $\dot{\gamma}$ for which the condition of $\mathcal{V}_{\dot{\gamma}>\dot{\gamma}_T} = \mathcal{V}_{\rm tot}/2$ occurs? One possibility is to perform an Eulerian measurement of the $\dot{\gamma}(x,t)$ field over space and time. Another option is to look at the fraction of time spent by tracers in alert regions, $T_{\dot{\gamma}>\dot{\gamma}_T}/T_{\rm tot}$ (with $T_{\rm tot}$ the total time of the measurement). Since tracers explore evenly all the region of the flow this is equivalent to measure the volume ratio $\mathcal{V}_{\dot{\gamma}>\dot{\gamma}_T}/\mathcal{V}_{\rm tot}$. In particular, in order to increase the statistical sampling we look at the global mean value $\langle T_{\dot{\gamma}>\dot{\gamma}_T}\rangle/T_{\rm tot}$ where the average is over the total number of particles ($N_{\rm tot}$):

$$\langle T_{\dot{\gamma}>\dot{\gamma}_T}\rangle = \frac{1}{N_{\rm tot}} \sum_{i=1}^{N_{\rm tot}} \int_0^{T_{\rm tot}} H(\dot{\gamma}_i(t) - \dot{\gamma}_T)\, dt. \qquad (9)$$

The plot in Fig. 8 shows the trend of $\langle T_{\dot{\gamma}>\dot{\gamma}_T}\rangle/T_{\rm tot}$ as function of $\dot{\gamma}_T$ both for tracers and LC particles. It confirms that copepods reside less in alert regions compared to tracers. Moreover, the difference among the two time fractions can be used as an alternative clustering indicator. It has, in fact, a similar trend

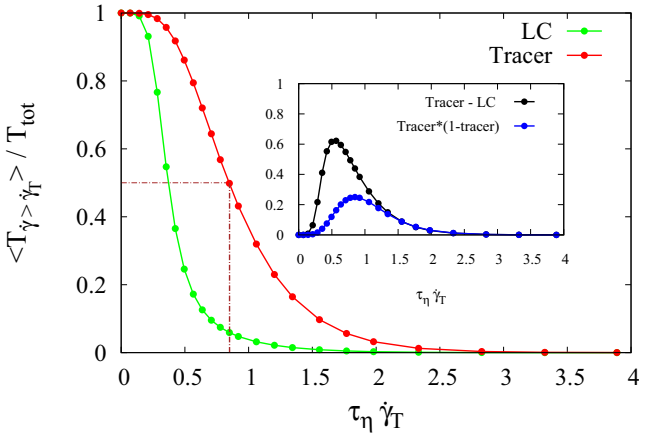

FIG. 8. Time fraction spent in alert regions by tracer and copepods as a function of the threshold value. Inset: difference of time fraction between tracers and LC particles and prediction based on $\mathcal{V}_{\dot{\gamma}>\dot{\gamma}_T}/\mathcal{V}_{\rm tot}$ measurement.

as the $D_2(\dot{\gamma}_T)$ function and shows a peak for the same value of $\dot{\gamma}_T$ (inset of Fig. 8). The prediction that clustering varies as $\mathcal{V}_{\dot{\gamma}>\dot{\gamma}_T} \cdot (\mathcal{V}_{\rm tot} - \mathcal{V}_{\dot{\gamma}>\dot{\gamma}_T})$ is in qualitative agreement with the observed trend, it is in quite good agreement in the large $\dot{\gamma}_T$ regime; however, it fails to capture the correct value at which the maximum appears, giving $\tau_\eta \dot{\gamma}_T = 0.85$ instead of 0.5. Finally, we note that the case of maximal clustering at $D_2 \simeq 2.3$ corresponds to a condition where the LC particles concentrate in nearly two-dimensional sheets, which envelop the *alert* regions [as can be also inferred from the visualisation in Fig. 5(b)].

We can offer a qualitative physical explanation for the observed D_2 saturation for high values of u_J at fixed $\dot{\gamma}_T$ [Fig. 7(b)]. The argument is as follow: one may expect that there is clustering if the time to escape from an alert region is less than the lifetime of such a region: $\tau_{\rm escape} < \tau_{\dot{\gamma}_T}$. The former time can be estimated as $\tau_{\rm escape} = l_{\dot{\gamma}_T}/u_J$, where $l_{\dot{\gamma}_T}$ is the typical size of the alert region characterized by a shear-rate $\dot{\gamma} > \dot{\gamma}_T$. This implies that LC particles form clusters and the D_2 measure is lead to saturate to a constant value if $u_J > l_{\dot{\gamma}_T}/\tau_{\dot{\gamma}_T}$. This latter ratio can be thought as a threshold-dependent escape velocity $u_{\dot{\gamma}_T} = l_{\dot{\gamma}_T}/\tau_{\dot{\gamma}_T}$. From the correlation dimension measurement this escape velocity is estimated to be of the order of $100\,u_\eta$, i.e., of the order of the large scale velocity, with a weak decreasing trend at increasing $\dot{\gamma}_T$.

We finally observe that when the flow field associated to the Lagrangian particles, $\boldsymbol{v} = \dot{\boldsymbol{x}}$, displays a weak compressibility, it can be shown [15,66] that D_2 depends on the flow divergence by the relation $D_2 = 3 - c\langle \nabla \cdot v \rangle^2$ with c a proportionality constant and angular brackets denoting time and space average. If this argument is applied to the LC model we observe that the divergence can be different form zero only at the interface between comfort and alert regions. This is because in comfort regions ($\nabla \cdot \boldsymbol{v} = \nabla \cdot \boldsymbol{u} = 0$) and in alert regions ($\nabla \cdot \boldsymbol{v} = \nabla \cdot \boldsymbol{u} + \nabla \cdot \boldsymbol{J} = 0$, as we can safely assume the jump term to be spatially constant). At the interface, however, the change from the fluid velocity intensity u to $u + u_J$ has a spatial transition scale roughly proportional to $u_J \cdot \log(10^2)\tau_J$, which leads to a non-null divergence. This explains the LC accumulation that we observe in correspondence of the alert and comfort interfaces, which effectively acts as sink or source term of the LC velocity field (see in particular the central panel of Fig. 5). By following this line of reasoning, one can guess that the minimum value of D_2 will correspond to the case where the surface of alert and comfort interface is maximum (and not of volumes, as stated above). This has clearly a dependence on the threshold $\dot{\gamma}_T$ and much less, if any, on u_J. Despite the qualitative agreement of this observation with our numerical results, we have not been able yet to confirm it quantitatively in the weakly compressible limit of the LC model.

C. Particle orientational dynamics

What is the importance of particle orientation for the nonhomogenous distribution of particles? The effect of the geometrical aspect ratio of the particles, together with the direction of their jump on the fractal dimension are addressed here. The fluid deformation rate symmetric tensor S_{ij} comes into play by modeling copepods as elongated particles with aspect ratio equal to 3 (e.g., the relevant aspect ratio for *E. affinis* copepod). Its effect on the jump direction selection leads to enhanced clustering of the particles for jump intensity $u_J/u_\eta = 250$. Copepods can also jump in random direction in the solid angle independently from the rotation rate and deformation rate of the Eulerian field. Less clustering in this case is logical since the jumping direction has no relation with the fluid flow. These behaviors can be found in more details in Fig. 9, where we address the influence of jump direction on the PDF of the copepods velocity.

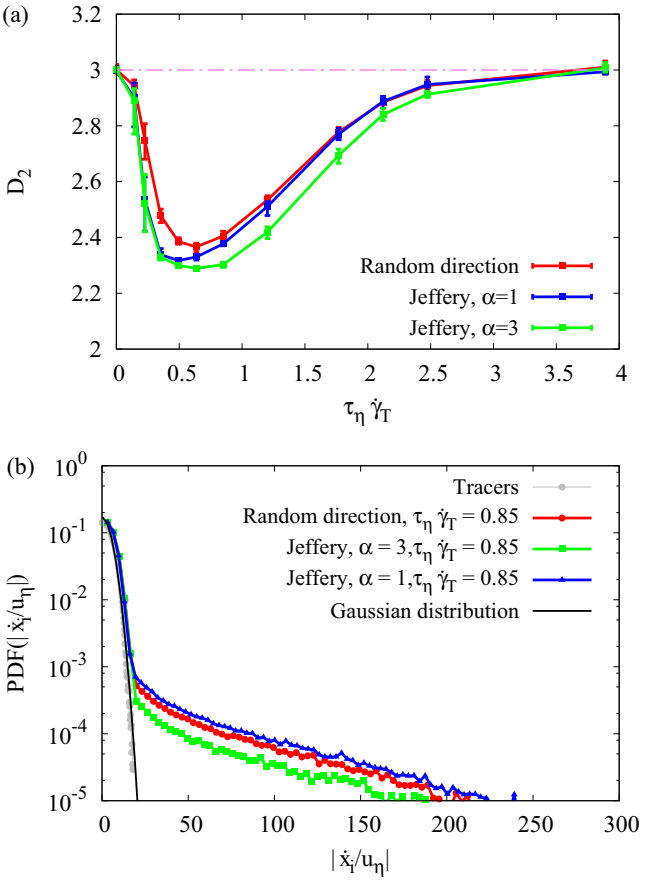

FIG. 9. (a) Effect of the aspect ratio and direction of the jump on the fractal dimension; (red) copepod as solid sphere particles, their direction of the jump is random in the solid angle; (blue) copepod as solid sphere particles with an orientation; and (green) as elongated particles. Both jump in a direction following the Jeffery's equation. (b) PDF of the absolute value of the single component velocity for (red) random direction case and (green) Jeffery's case with aspect ratio of 3. All cases are computed at $u_J/u_\eta = 250$.

IV. CONCLUSIONS AND PERSPECTIVES

In this study we have considered a Lagrangian model for active particles. The model is trimmed in a way to reproduce some dynamical features experimentally observed in the motion of copepods in still water. Its main characteristics is the possibility to locally acquire an extra-velocity (jump) in response to a variation of the fluid-flow conditions surrounding the particle. The direction of the jump is ruled by the hydrodynamics of small neutrally buoyant particles. The

Lagrangian model has been coupled to a turbulent developed flow described by the incompressible Navier-Stokes equations.

We have shown that jump escape reaction from spatiotemporal events characterized by high shear-rate leads to nonhomogeneous spatial distributions of active particles. This clustering mechanisms, however, is effective only when the reaction threshold is close to values of the order of τ_η^{-1} in a very narrow range. The fact that the range is narrow is ultimately linked to the intermittent distribution of the turbulence dissipation rate [67]. We have shown that clustering approaches its maximum when the threshold rate value $\dot{\gamma}_T$ roughly divide the shear-rate ($\dot{\gamma}$) spatial field in equal-volume regions. Since this mechanism mainly depends on the average value of small-turbulence scales rather than on their fluctuations, we expect it to have a weak dependence on the Reynolds number of the turbulent flow. A second implication of the model is that for any given shear-rate reaction value $\dot{\gamma}_T$ there is a maximal intensity jump velocity beyond which clustering cannot be further increased. Finally, the analysis of the correlation dimension suggests the formation of local quasibidimensional clusters enclosing the nonpermitted flow regions. From a physical point of view, we remark that the clustering mechanism at work in turbulence for the LC model is different from the one shown in other model systems of particulate active matter. For instance, the clustering observed for motile algal cells in turbulence is given by the gyrotactic effect, which is a nonisotropic effect induced by the presence of the the external gravity field [22]. On the opposite, the LC model discussed here is isotropic but it is nonhomogeneous in space (it depends on the local value of the shear rate). We have tested the fact that clustering also appears when LC particles are made sensitive to other flow quantities such as enstrophy or fluid acceleration. The minimal fractal dimension we observed is always above the value of 2, confirming the fact that particles in this case aggregate in order to cover the surface of the forbidden regions. Based on these observations we do not expect that such clustering processes could lead to filamentary like clusters, $D_2 \simeq 1$, as the ones observed for microbubbles in turbulent flows. Another notable result is the negligible impact of the particle orientational dynamics on the clustering. This is likely to be linked to the limited duration of jumps (note that here $\tau_J \ll \tau_\eta$), but might become important for longer jumps, particularly in the modeling of larger motile plankton. The negligible impact of orientation for the case examined here suggests the possibility to formulate accurate eulerian mean-field particle models based on the introduction of a space-dependent effective diffusivity (κ) whose amplitude may be linked directly to jump shape parameters, via a dimensional relation of the type $\kappa \propto u_J^2 \tau_J$.

From a more biological perspective, although behavioral mechanisms leading to clustering had been already suggested in the past, such as the formation of patches through swimming against the flow [68], the possibility of cluster formation by escape jumps in a no-mean flow situation was never reported before. As discussed in Ref. [38], clustering of copepods has an ecological importance: an effect may be to strongly increase the contact rate with mates, and hence improve the reproduction. Indeed, several models have been proposed to express copepod contact rates in turbulence [69–71], reviewed in Ref. [72]. In case of clustering, the contact rate is strongly increased [38,73–75]. The clustering that would result from a behavior of predator avoidance (a reaction to turbulent shears similar to predators' signals) would have as side effect a positive consequence with a strong enhancement of the mating contact rate. Of course, such copepod concentration could also attract predators. Due to different tradeoffs, each copepod species may have an optimal jump behavior in response to turbulence. For example, the copepod *E. affinis* used in our experimental section is an estuarine species adapted to maintain the bulk of its population in a salinity gradient in highly turbulent conditions [76,77]. By using high-frequency sampling data of all life stages of *E. affinis*, Schmitt *et al.* [77] confirmed that the late developmental stages (mainly adults) exhibited active vertical migration during the flood. Consequently, the population was not homogeneously distributed in the water column, as dense patches are observed during short time window and near the bottom [76].

Our model can be improved in the future to test such situations with tidally induced turbulence in shallow estuaries where copepods can use their jump abilities to simply avoid to be flushed out of their optimal habitat. This could lead to the identification of some optimal clustering strategy that may be in relation with the dome-shapes proposed earlier, on purely speculative intuitions [78,79]. The presented LC model can also be improved by refining the jumping protocol in order to take into account the fact that the temporal sequence of jumps in copepods occurs in fast sequences (bursts) interposed to inactive moments. Another possible direction of research concerns the investigation of the impact of a spatial radius of perception for copepods to react to turbulent shear. This may produce a smoothing or a delay in the perceived turbulent signal.

ACKNOWLEDGMENTS

The authors acknowledge support from European COST Action MP1305 "Flowing Matter" and the "GIP Seine-Aval ZOOGLOBAL project". Dominique Menu is acknowledged for technical help concerning the copepod experiment devices, and Regis Sion for advices and help on the use of the fast camera. Marion Roussin and Guénolé Alizard are thanked for help with copepod sorting. We acknowledge discussion with Massimo Cencini and Guido Boffetta. H.A. is supported by the Ph.D. grant for interdisciplinary research "Allocation President 2013" of the Université de Lille 1.

[1] H. C. Berg and L. Turner, Movement of microorganisms in viscous environments, Nature **278**, 349 (1979).

[2] R. Di Leonardo, L. Angelani, D. Dell'Arciprete, G. Ruocco, V. Iebba, S. Schippa, M. P. Conte, F. Mecarini, F. De Angelis, and E. Di Fabrizio, Bacterial ratchet motors, Proc. Natl. Acad. Sci. USA **107**, 9541 (2010).

[3] A. W. Visser and T. Kiørboe, Plankton motility patterns and encounter rates, Oecologia **148**, 538 (2006).

[4] E. Lauga, Bacterial hydrodynamics, Annu. Rev. Fluid Mech. **48**, 105 (2016).

[5] J. Teran, L. Fauci, and M. Shelley, Viscoelastic Fluid Response can Increase the Speed and Efficiency of a Free Swimmer, Phys. Rev. Lett. **104**, 038101 (2010).

[6] J. P. Hernandez-Ortiz, C. G. Stoltz, and M. D. Graham, Transport and Collective Dynamics in Suspensions of Confined Swimming Particles, Phys. Rev. Lett. **95**, 204501 (2005).

[7] A. Baskaran and M. C. Marchetti, Statistical mechanics and hydrodynamics of bacterial suspensions, Proc. Natl. Acad. Sci. USA **106**, 15567 (2009).

[8] R. A. Lambert, F. Picano, W. P. Breugem, and L. Brandt, Active suspensions in thin films: Nutrient uptake and swimmer motion, J. Fluid Mech. **733**, 528 (2013).

[9] E. Lushi, H. Wioland, and R. E. Goldstein, Fluid flows created by swimming bacteria drive self-organization in confined suspensions, Proc. Natl. Acad. Sci. USA **111**, 9733 (2014).

[10] K. Drescher, J. Dunkel, L. H. Cisneros, S. Ganguly, and R. E. Goldstein, Fluid dynamics and noise in bacterial cell-cell and cell-surface scattering, Proc. Natl. Acad. Sci. USA **108**, 10940 (2011).

[11] C. Hohenegger and M. J. Shelley, Stability of active suspensions, Phys. Rev. E **81**, 046311 (2010).

[12] J. Dunkel, S. Heidenreich, K. Drescher, H. H. Wensink, M. Bär, and R. E. Goldstein, Fluid Dynamics of Bacterial Turbulence, Phys. Rev. Lett. **110**, 228102 (2013).

[13] A. Kaiser, A. Peshkov, A. Sokolov, B. ten Hagen, H. Löwen, and I. S. Aranson, Transport Powered by Bacterial Turbulence, Phys. Rev. Lett. **112**, 158101 (2014).

[14] O. A. Croze, G. Sardina, M. Ahmed, M. A. Bees, and L. Brandt, Dispersion of swimming algae in laminar and turbulent channel flows: consequences for photobioreactors, J. R. Soc. Interface **10**, 20121041 (2013).

[15] W. M. Durham, E. Climent, M. Barry, F. De Lillo, G. Boffetta, M. Cencini, and R. Stocker, Turbulence drives microscale patches of motile phytoplankton, Nat. Commun. **4**, 1 (2013).

[16] T. J. Pedley and J. O. Kessler, Hydrodynamic phenomena in suspensions of swimming microorganisms, Annu. Rev. Fluid Mech. **24**, 313 (1992).

[17] T. A. Warnaas and M. Hondzo, Small-scale fluid motion mediates growth and nutrient uptake of selenastrum capricornutum, Freshwater Biol. **51**, 999 (2006).

[18] J. S. Guasto, R. Rusconi, and R. Stocker, Fluid mechanics of planktonic microorganisms, Annu. Rev. Fluid Mech. **44**, 373 (2012).

[19] M. S. Bergstedt, M. M. Hondzo, and Cotner J. B, Effects of small scale fluid motion on bacterial growth and respiration, Freshwater Biol. **49**, 28 (2004).

[20] R. Stocker, Marine microbes see a sea of gradients, Science **338**, 628 (2012).

[21] K. Gustavsson, F. Berglund, P. R. Jonsson, and B. Mehlig, Preferential Sampling and Small-Scale Clustering of Gyrotactic Microswimmers in Turbulence, Phys. Rev. Lett. **116**, 108104 (2016).

[22] F. De Lillo, M. Cencini, W. M. Durham, M. Barry, R. Stocker, E. Climent, and G. Boffetta, Turbulent Fluid Acceleration Generates Clusters of Gyrotactic Microorganisms, Phys. Rev. Lett. **112**, 044502 (2014).

[23] C. Frangoulis, E. D. Christou, and J. H. Hecq, Comparison of marine copepod outfluxes: Nature, rate, fate and role in the carbon and nitrogen cycles, Adv. Marine Biol. **47**, 253 (2005).

[24] S. Satapoomin, Carbon content of some common tropical andaman sea copepods, J. Plankton Res. **21**, 2117 (1999).

[25] S. H. Jonasdottir, A. W. Visser, K. Richardson, and M. R. Heath, Seasonal copepod lipid pump promotes carbon sequestration in the deep north atlantic, Proc. Natl. Acad. Sci. U.S.A. **112**, 12122 (2015).

[26] T. C. Walter and G. Boxshall, "World of copepods database", http://www.marinespecies.org/copepoda (2015).

[27] G. H. Theilacker and A. M. Kimball, Rotifers and copepods as larval fish foods, CalCOFI Rep. **25**, 80 (1984).

[28] A. Souissi, S. Souissi, and B. W. Hansen, Physiological improvement in the copepod eurytemora affinis through thermal and multi-generational selection, Aquaculture Res. (2014).

[29] J. Yen, Life in transition: balancing inertial and viscous forces by planktonic copepods, Biol. Bull. **198**, 213 (2000).

[30] T. Kiørboe, E. Saiz, and A. Visser, Hydrodynamic signal perception in the copepod acartia tonsa, Marine Ecol. Progr. Ser. **179**, 97 (1999).

[31] T. Kiørboe and A. Visser, Predator and prey perception in copepods due to hydromechanical signals, Marine Ecol. Progr. Ser. **179**, 81 (1999).

[32] T. Kiørboe, *A Mechanistic Approach to Plankton Ecology* (Princeton University Press, Princeton, NJ, 2008).

[33] E. J. Buskey, P. H. Lenz, and D. K. Hartline, Escape behavior of planktonic copepods in response to hydrodynamic disturbances: high speed video analysis, Marine Ecol. Progr. Ser. **235**, 135 (2002).

[34] E. J. Buskey and D. K. Hartline, High-speed video analysis of the escape responses of the copepod acartia tonsa to shadows, Biol. Bull. **204**, 28 (2003).

[35] P. H. Lenz and D. K. Hartline, Reaction times and force production during escape behavior of a calanoid copepod, undinula vulgaris, Marine Biol. **133**, 249 (1999).

[36] C. H. Lee, H. U. Dahms, S. H. Cheng, S. Souissi, F. G. Schmitt, R. Kumar, and J. S. Hwang, Mating behavior of pseudodiaptomus annandalei (copepoda, calanoida) at calm and hydrodynamically disturbed waters, Marine Biol. **158**, 1085 (2011).

[37] S. Souissi, F. G. Michalec, G. Dur, S. Mahjoub, F. G. Schmitt, and J. S. Hwang, How does salinity influence the swimming speed of the estuarine calanoid copepodeurytemora affinis?:Reply, J. Plankton Res. **32**, 1227 (2010).

[38] F. G. Schmitt and L. Seuront, Intermittent turbulence and copepod dynamics: Increase in encounter rates through preferential concentration, Marine Syst. **70**, 263 (2008).

[39] D. A. Fields, S. D. Shema, H. I. Browman, T. Q. Browne, and A. B. Skiftesvik, Light primes the escape response of the calanoid copepod, calanus finmarchicus, PLoS ONE **7**, e39594 (2012).

[40] M. Moison, F. G. Schmitt, S. Souissi, L. Seuront, and J. S. Hwang, Symbolic dynamics and entropies of copepod behavior under non-turbulent and turbulent conditions, Marine Syst. **77**, 388 (2009).

[41] R. J. Waggett and E. J. Buskey, Copepod escape behavior in non-turbulent and turbulent hydrodynamic regimes, Marine Ecol. Progr. Ser. **334**, 193 (2007).

[42] J. Yen, K. D. Rasberry, and D. R. Webster, Quantifying copepod kinematics in a laboratory turbulence apparatus, Marine Syst. **69**, 283 (2008).

[43] F. G. Michalec, S. Souissi, and M. Holzner, Turbulence triggers vigorous swimming but hinders motion strategy in planktonic copepods, J. R. Soc. Interface **12**, 20150158 (2015).

[44] F. G. Michalec, F. G. Schmitt, S. Souissi, and M. Holzner, Characterization of intermittency in zooplankton behavior in turbulence, Eur. Phys. J. E **38**, 108 (2015).

[45] H. Jiang and T. R. Osborn, Hydrodynamics of copepods: A review, Surveys Geophys. **25**, 339 (2004).

[46] H. Jiang and G. A. Paffenhofer, Hydrodynamic signal perception by the copepod oithona plumifera, Marine Ecol. Progr. Ser. **373**, 37 (2008).

[47] H. Jiang and T. Kiørboe, The fluid dynamics of swimming by jumping in copepods, J. R. Soc. Interface **8**, 1090 (2011).

[48] T. Kiørboe, A. Anderson, V. J. Langlois, and H. H. Jakobsen, Unsteady motion: Escape jumps in planktonic copepods, their kinematics and energetics, J. R. Soc. Interface **7**, 1591 (2010).

[49] J. Yen and D. M. Fields, Escape response of acartia hudsonica (copepoda) nauplii from the flow field of temora longicornis (copepoda), Ergebnisse der Limnologie/ Advances in Limnology. Stuttgart **36**, 123 (1992).

[50] P. H. Lenz, A. E. Hower, and D. K. Hartline, Force production during pereiopod power strokes in calanus finmarchicus, Marine Syst. **49**, 133 (2004).

[51] L. A. Duren and J. J. Videler, Escape from viscosity: The kinematics and hydrodynamics of copepod foraging and escape swimming, J. Exp. Biol. **206**, 269 (2003).

[52] F. Toschi and E. Bodenschatz, Lagrangian properties of particles in turbulence, Annu. Rev. Fluid Mech. **41**, 375 (2009).

[53] G. A. Voth, A La Porta, A. M. Crawford, J. Alexander, and E. Bodenschatz, Measurement of particle accelerations in fully developed turbulence, J. Fluid Mech. **469**, 121 (2002).

[54] S. Parsa, E. Calzavarini, F. Toschi, and G. A. Voth, Rotation Rate of Rods in Turbulent Fluid Flow, Phys. Rev. Lett. **109**, 134501 (2012).

[55] L. Chevillard and C. Meneveau, Orientation dynamics of small, triaxial-ellipsoidal particles in isotropic turbulence, J. Fluid Mech. **737**, 571 (2013).

[56] C. Zhan, G. Sardina, E. Lushi, and L. Brandt, Accumulation of motile elongated micro-organisms in turbulence, J. Fluid Mech. **739**, 22 (2014).

[57] R. Stocker and W. M. Durham, Tumbling for stealth? Science **325**, 400 (2009).

[58] J. O. Kessler, Hydrodynamic focusing of motile algal cells, Nature **313**, 218 (1985).

[59] G. B. Jeffery, The motion of ellipsoidal particles immersed in a viscous fluid, Proc. Roy. Soc. A **102**, 161 (1992).

[60] B. R. MacKenzie and W. C. Leggett, Wind-based models for estimating the dissipation rates of turbulent energy in aquatic environments: Empirical comparisons, Marine Ecol. Progr. Ser. **94**, 207 (1993).

[61] J. Jiménez, Oceanic turbulence at millimeter scales, Sci. Mar. **61**, 47 (1997).

[62] K. D. Squires and J. K. Eaton, Particle response and turbulence modification in isotropic turbulence, Phys. Fluids A **2**, 1191 (1990).

[63] S. Elghobashi and G.C. Truesdell, On the twoway interaction between homogeneous turbulence and dispersed solid particles. i: Turbulence modification, Phys. Fluids A **5**, 1790 (1993).

[64] See Supplemental Material at http://link.aps.org/supplemental/10.1103/PhysRevE.93.043117 for 2D visualization of copepod's motion in turbulent flow.

[65] P. Grassberger and I. Procaccia, Measuring the strangeness of strange attractors, Physica D: Nonlin. Phenom. **9**, 189 (1983).

[66] G. Falkovich, K. Gawedzki, and M. Vergassola, Particles and fields in fluid turbulence, Rev. Mod. Phys. **73**, 913 (2001).

[67] U. Frisch, *Turbulence: The Legacy of A. N. Kolmogorov* (Cambridge University Press, Cambridge, 1995).

[68] A. Genin, J. S. Jaffe, R. Reef, C. Richter, and P. J. Franks, Swimming against the flow: A mechanism of zooplankton aggregation, Science **308**, 860 (2005).

[69] B. J. Rothschild and T. R. Osborn, Small-scale turbulence and plankton contact rates, J. Plankton Res. **10**, 465 (1998).

[70] G. T. Evans, The encounter speed of moving predator and prey, J. Plankton Res. **11**, 415 (1989).

[71] A. W. Visser and B. R. MacKenzie, Turbulence-induced contact rates of plankton: The question of scale, Marine Ecol. Progr. Ser. **166**, 307 (1998).

[72] D. M. Lewis and T. J. Pedley, Planktonic contact rates in homogeneous isotropic turbulence: Theoretical predictions and kinematic simulations, J. Theor. Biol. **205**, 377 (2000).

[73] L. P. Wang, A. S. Wexler, and Y. Zhou, Statistical mechanical descriptions of turbulent coagulation, Phys. Fluids **10**, 2647 (1998).

[74] W. C. Reade and L. R. Collins, Effect of preferential concentration on turbulent collision rates, Phys. Fluids **12**, 2530 (2000).

[75] L. R. Collins and A. Keswani, Reynolds number scaling of particle clustering in turbulent aerosols, New J. Phys. **6**, 119 (2004).

[76] D. Devreker, S. Souissi, J. C. Molinero, and F. Nkubito, Tradeoffs of the copepod eurytemora affinis in mega-tidal estuaries: Insights from high-frequency sampling in the seine estuary, J. Plankton Res. **30**, 1329 (2008).

[77] F. G. Schmitt, D. Devreker, G. Dur, and S. Souissi, Direct evidence of tidally-oriented behavior of the copepod eurytemora affinis in the seine estuary, Ecol. Res. **26**, 773 (2011).

[78] P. Cury and C. Roy, Optimal environmental window and pelagic fish recruitment success in upwelling areas, Can. J. Fish. Aquatic Sci. **46**, 670 (1989).

[79] B. R. MacKenzie, Turbulence, larval fish ecology and fisheries recruitment: A review of field studies, Oceanol. Acta **23**, 357 (2000).

Appendix B

Copepods encounter rates from a model of escape jump behaviour in turbulence

The manuscript is in preparation and will be submitted to an ecological journal (*e.g.,* Journal of Plankton Research or Journal of Marine Systems).

Copepods encounter rates from a model of escape jump behaviour in turbulence

H. Ardeshiri[1,2], F. G. Schmitt[2], S. Souissi[2], F. Toschi[3,4], and E. Calzavarini[1]

[1] *Univ. Lille, CNRS, FRE 3723, LML, Laboratoire de Mécanique de Lille, F 59000 Lille, France*
[2] *Univ. Lille, CNRS, Univ. Littoral Cote d'Opale, UMR 8187, LOG,Laboratoire d'Océanologie et de Géoscience, F 62930 Wimereux, France*
[3] *Department of Applied Physics and Department of Mathematics and Computer Science, Eindhoven University of Technology, 5600 MB, Eindhoven, The Netherlands*
[4] *Istituto per le Applicazioni del Calcolo CNR, Via dei Taurini 19, 00185 Rome, Italy*

Abstract

A crucial parameter for planktonic copepods is their interspecies contact rate which is driven by their behavior and it is also strongly influenced by turbulence. The most important feature of copepods is their ability to exhibit a powerful jump in order to escape from flow disturbances due to the predators or other external causes. In the present study, the encounter rate of copepods in homogeneous isotropic turbulent flows is assessed, by means of copepods' statistics in turbulence, which are obtained through a Lagrangian copepod (LC) model that mimics the behavior of the most abundant form of plankton in turbulent flows. Using LC model which leads to preferential concentration of copepods as low as a fractal dimension of $\sim$ 2.3, our analysis shows that the encounter rate can be increased by a factor of the order of $\mathcal{O}(10^3)$ at dissipative scales.

1 Introduction

Many biological processes are determined by individual-interaction or contacts between organisms. An essential aspect in marine biology is the encounters between individual organisms which is vital for males and females in order to mate or for predators to locate their prey to capture and consume them [1, 2, 3]. Finding a suitable habitat (colonization) for organisms is also encounter-dependent [4]. Organism speed, size, motility and abundance can affect the biological encounter rates, the rates at which individuals meet other organisms of the same or different species. It is thus fundamentally important to understand the phenomenon that affect the encounter rates and the biological processes in oceanic flows.

The encounter rate of plankton species has been studied by many authors in the past [5, 6, 7, 8, 9, 10]. Gerritsen et al. [5] were the pioneers who introduced the theory of contact rate in laminar flow. However living habitats of the plankton species are rarely laminar. It is now widely known that turbulence has a strong influence on dispersal, feeding and reproduction of plankton [11]. Not only the small-scale but also other scales within the turbulence spectrum are important contributors to encounter process [9]. Some authors regarded the small-scale turbulent processes as homogenizing factors, so that the encounter-rate model, assumed the distribution of plankton to be random in space and time [10, 12, 13, 14, 15], whilst turbulence increases inhomogeneity at small scales

[16, 17, 18].
The encounter rate in oceanic turbulence is governed by two biologically- and physically-driven processes [10, 19, 20]. First, it is likely due to the behavior of organisms (biologically-driven process) and secondly it is affected by the turbulent motion of the carrier fluid (physically-driven process). However notice that turbulence has a great impact on microorganisms and can induce some behavioral responses in swimmers [21, 22]. Hence, it is more reasonable not to sum up the contribution of these processes linearly as it is the case for [19, 10, 20]. The encounter rate formulation developed by Sundaram and Collins [23], Wang et al. [24], Reade et al. [25] and Collins and Keswani [26] can be used in turbulence in case of preferential concentration of species. This is to be discussed in details in the next section.
Despite many studies which have been performed on the effect of the preferential concentration on the coagulation of colloidal particles [27, 28, 29, 30], and of the inertial particles [31, 32], only few studies [33, 34] are available in the context of copepods ecology whilst the study of Squires and Yamazaki [33] was published before including the precise effect of the preferential concentration in the theory of contact rate. Rather than swimming behavior, other mechanisms can also play a role in encounter rate for copepods, i.e. chemoreception and mechanoreception [35, 36], prey movement detection [37, 38] and feeding currents [39], which are outside the scope of the present study.
The goal of the present study is to estimate the mutual encounter rate of copepods (encounter rate of the same species) based on the previously proposed behavioral model in turbulent flows [40]. The Lagrangian copepod model was introduced based on the experimental data analysis to quantify copepods' dynamics in homogeneous isotropic turbulence. To the best of our knowledge, this is the first numerical simulation of copepods behavior in turbulent flows, which result in preferential concentration in some condition.
The paper is organized as follows: in section 2 we briefly introduce our Lagrangian copepod model and the parameters and assumption we made. Furthermore, the encounter rate formulation where there is a preferential concentration of particles in the flow, is discussed in this section. We then present our analysis in details on the pair correlation function, and the encounter rate in Sec. 3 and end the paper by results and discussion in Sec. 4.

2 Methods and Tools

In this section we introduce the Lagrangian copepod model in turbulence which has been used to quantify copepods' behavior. The model was implemented via an Eulerian-Lagrangian approach where the fluid flow was obtained by solving the incompressible Navier- Stokes equations, in turbulent conditions by means of Direct Numerical Simulation (DNS). The Lagrangian part will be described in section 2.1. Moreover the encounter rate formulation will be given in this section in the case of preferential concentration which is the direct result of our LC model [40].

2.1 Lagrangian copepod model

Recorded velocity track of copepods showed that their jump intensity decays almost exponentially, from which the equation of motion is chosen as follows:

$$\dot{\mathbf{x}}(t) = \mathbf{u}(\mathbf{x}(t), t) + \boldsymbol{J}(t, t_i, t_e, \dot{\gamma}, \mathbf{p}) \tag{1}$$

where $\mathbf{u}(\mathbf{x}(t), t)$ is the velocity of the carrying fluid and $\boldsymbol{J}$ is an added velocity term that describes the active behaviour (jump) of the copepod. $\boldsymbol{J}(t, t_i, t_e, \dot{\gamma}, \mathbf{p})$ is a function of time t, it depends also on an initial and a final time t_i and t_e, on flow shear rate value $\dot{\gamma}$ and on orientation vector $\mathbf{p}$, which

in its most simplified form is given by:

$$\dot{\mathbf{p}}(t) = \mathbf{\Omega} \cdot \mathbf{p}(t) \tag{2}$$

where $\mathbf{\Omega}$ is the fluid rotation rate antisymmetric tensor, defined as $\Omega_{ij} = 1/2(\partial_i u_j - \partial_j u_i)$. Copepods react to the shear rate which is obtained by $\dot{\gamma} = \sqrt{2\mathcal{S} : \mathcal{S}}$ in which $\mathcal{S}$ is the fluid deformation rate symmetric tensor, defined as $\mathcal{S}_{ij} = 1/2(\partial_i u_j + \partial_j u_i)$. Therefore copepods drift with the carrier fluid, when they find themselves in the alert regions (regions with shear rate larger than the threshold value $\dot{\gamma} > \dot{\gamma}_T$), they start to jump with exponentially decaying intensity over the time. Notice that a jump will finish when it's amplitude reach to very low value and a new jump cannot happen if the previous one is not finished. This jumping process can thus read mathematically as:

$$\boldsymbol{J}(t, t_i, t_e, \dot{\gamma}, \mathbf{p}) = H[\dot{\gamma}(t_i) - \dot{\gamma}_T]\, H[t_e - t] u_J\, e^{\frac{t_i - t}{\tau_J}}\, \mathbf{p}(t_i) \tag{3}$$

where $H[x]$ denotes the Heaviside step function meaning that it is unity if $x \geq 0$, $\dot{\gamma}_T$ is a threshold value of the shear rate, u_J and τ_J are two characteristic parameters characterising the jump shape, its velocity amplitude (u_J) and duration τ_J respectively. This implies that a jump can start if a copepod is in an alert region ($\dot{\gamma}(t_i) \geq \dot{\gamma}_T$) and its previous jump has finished ($t \leq t_e$). More information of development and implementation of the LC model can be found in [40].

2.2 Encounter rate in case of preferential concentration

The encounter rate, *i.e.,* the number of encounters per unit time under the condition of statistically homogeneous and isotropic movement can be written in the following form:

$$E(r) = n\pi r^2\, g(r)\, \langle \delta v_{rad}(r) \rangle \tag{4}$$

where n is the organisms number density (*i.e.,* number of copepods per unit volume), r is the encounter, or perceptive, radius of organisms and $\langle \delta v_{rad}(r) \rangle$ is the mean radial velocity between two particles separated by a distance r [23, 24, 26, 25]. In the latter expression $\langle \ldots \rangle$ indicate ensemble average and $\delta v_{rad}(r)$ is the amplitude of the relative radial velocity:

$$\delta v_{rad}(r) = |(\boldsymbol{v}(\boldsymbol{x} + \boldsymbol{r}) - \boldsymbol{v}(\boldsymbol{x})) \cdot \hat{\boldsymbol{r}}| \tag{5}$$

A detailed explanation on the appropriate choice of the mean radial velocity to be used in expression 4, can be found in [41, 24]. $g(r)$ represents the radial distribution function, which describes the variation of the particles' density from a reference particle. This is linked to the fractal dimension [42], for very small values of r. It has thus the following form:

$$g(r) = \frac{1}{4\pi r^2} \frac{1}{N\rho} \sum_{i=1}^{N} \sum_{k \neq i}^{N} \delta\left(r - |r_k - r_i|\right) \tag{6}$$

r in this equation represents the given distance from a particle, N is the total number of particles, $\rho = N/V$ is an average number density of N particles in a volume V and $|r_k - r_i|$ is the distance between pair of particles.

Non-homogeneous distribution of particles has been studied comprehensively, where heavy particles (particles denser than then fluid) concentrate in low vorticity and high strain rate regions [17, 43, 31, 44, 45, 46] whereas light particles are trapped by vortices in the flow [17, 31, 46, 47, 48], however zero inertia particles (passive tracers) are purely passively advected by the flow. This preferential

concentration is due to the particles' Stokes number ($St = \tau_p/\tau_\eta$, ratio of the aerodynamic response time of a particle τ_p to the turbulent characteristic time scale τ_η) and the ratio of the particle density to the fluid density $\beta = \rho_p/\rho_f$.
For swimming microorganisms, a preferential concentration effect has been found resulting from the gyrotactic motility [49, 50], a competition between the spatial gradients in fluid velocity that contributes to vorticity and the stablizing torque due to the displacement of the center of gravity from the center of geomtry.
Compared to the other microorganisms, copepods show a different type of complexity due to their jumping behavior. Contrary to the previously observed clustering, patchiness of copepods in our simulations, is tightly linked to the behavioral model in turbulent flows.
In the following section, the radial distribution function $g(r)$ and its link to the fractal dimension, the radial velocity $\langle \delta v_{rad}(r) \rangle$ and their contribution in encounter rate between copepods will be addressed and discussed in detail.

3 Analysis

The pair correlation function of LC model is shown in figure 1 where the slope of $g(r)$ at small r is linked to the correlation dimension of copepods' distribution in turbulence, as can be found in the inset of this figure. This slope increases by increasing the shear rate threshold value up to $\tau_\eta \dot{\gamma}_T = 0.5$, then further growth of the shear rate threshold value, decreases the steepness of $g(r)$. The inset of the Fig. 1 confirms these descriptions.

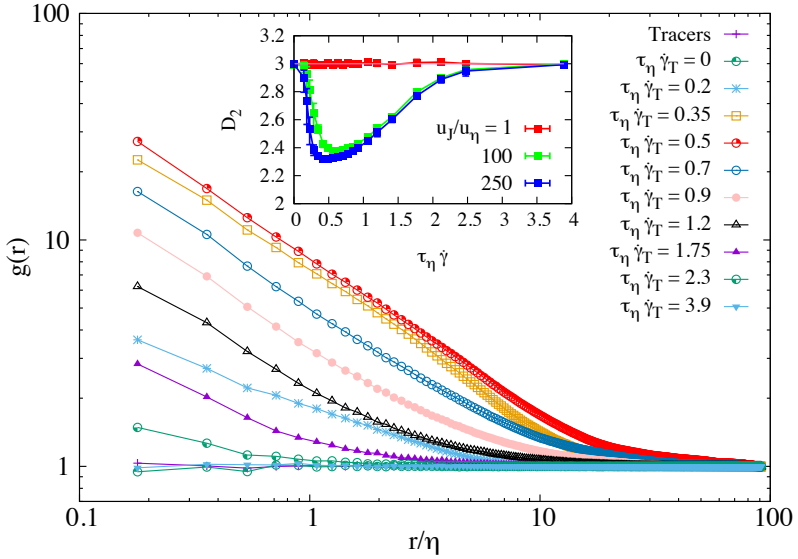

Figure 1: Pair-radial-distribution function $g(r)$ for different Lagrangian copepod families with different threshold values of the deformation-rate $\tau_\eta \dot{\gamma}_T$. Inset represents the correlation dimension of copepod distribution with different jump intensity.

The mean radial velocity between two copepods is shown in Fig. 2. Our findings for tracers are in good agreement with the Eulerian longitudinal velocity structure function of the fluid, given by the

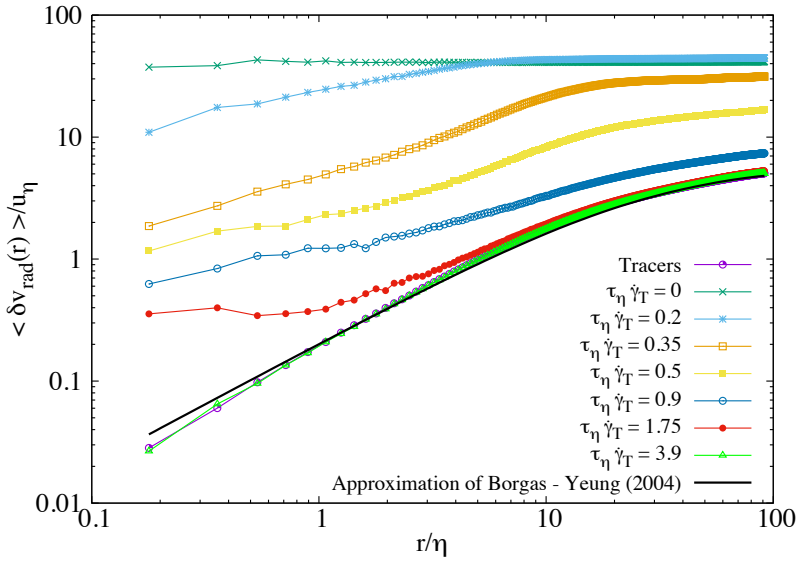

Figure 2: Radial velocity $\langle \delta v_{rad}(r) \rangle$ between two particles separated by a distance r.

empirical approximation of Borgas and Yeung [51]:

$$\bar{S}_{II} = \frac{2Re_\lambda}{15^{1/2}} \left[1 - exp\left(-\frac{r}{(15C)^{3/4}} \right) \right]^{4/3} \left(\frac{15^3 r^4}{15^3 r^4 + (2Re_\lambda/C)^6} \right)^{1/6} \tag{7}$$

with $C = 2$ and $\langle \delta v_{rad}(r) \rangle = \left(2\bar{S}_{II}/\pi\right)^{1/2}$. The Eulerian structure function grows linearly as r^{ζ_d} with $\zeta_d = 1$ for dissipative scales (small r) and at inertial-range it is proportional to r^{ζ_i} with $\zeta_i = 1/3$. Copepods with the shear rate threshold value of $\tau_\eta \dot{\gamma}_T = 3.9$ have less frequent jump behavior, so that they behave almost like a tracers and they are advected by the flow. For this reason they go very close to the prediction given by expression 7. In a case where all the copepods are in alert regions ($\tau_\eta \dot{\gamma}_T = 0$), one can expect the Brownian like motion of copepods according to the LC model. The diffusivity of the copepods would be dimensionally proportional to a relation of the type $u_J^2 \tau_J$. For this case, the copepod's relative velocity tends to be constant and its amplitude would be proportional to the jump intensity (u_J). For other cases (different shear rate threshold values $\tau_\eta \dot{\gamma}$), such an estimation is not applicable since the exponential term does not exist for copepods in safe regions.

Therefore for copepods, estimation of such a relation (Borgas and Yeung [51]) is not straightforward. It might be due to the fact that copepods at distance r may have different behavior. This is shown in Fig. 3 where two copepods at an immediate vicinity may have very large velocity difference. Establishing the Eulerian structure function, thus is linked to the local threshold value of the shear rate.

Scaling exponents ζ_d, ζ_i for copepod families through power law fits, is shown in Fig. 4. The change of the power law scaling exponent in inertial-range is smooth, but in dissipative scale it shows non monotonic behavior as observed in Fig. 1 for the fractal dimension as a function of the shear rate threshold values.

Having the pair correlation function $g(r)$ and mean radial velocity $\delta v_{rad}(r)$ one can estimate the encounter rate kernel $E(r)$. In reality there is no contact between tracers, since they are passive particles advected by the flow where the fluid streamlines does not cross each other. However to

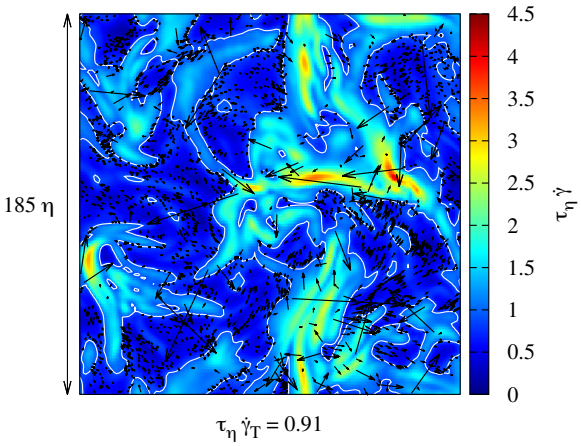

Figure 3: Spatial distribution of copepods in turbulent flow along with their velocity vectors. Shading represents the instantaneous field of the absolute value of the shear rate of the Eulerian field. Contour lines are traced at threshold value of $\tau_\eta \dot{\gamma}_T = 0.91$.

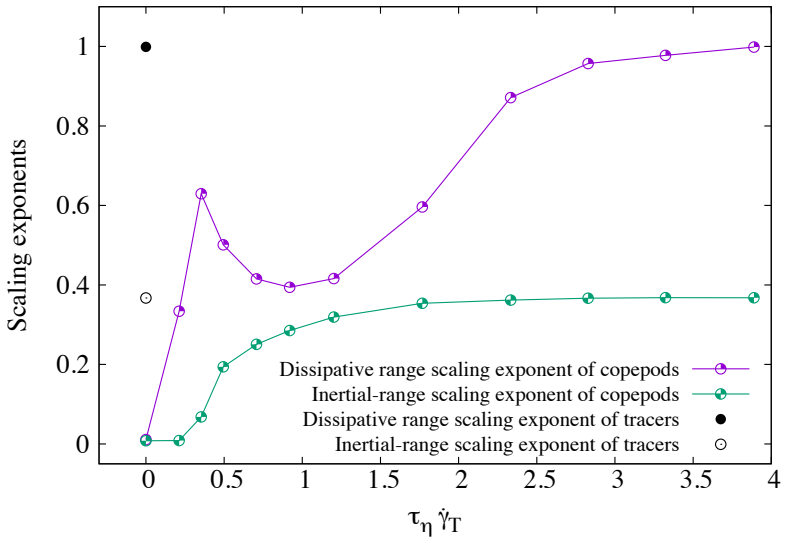

Figure 4: Scaling exponents of $\langle \delta v_{rad}(r) \rangle$ vs. r from power law fits in the dissipative r^{ζ_d} and inertial-range limit r^{ζ_i}.

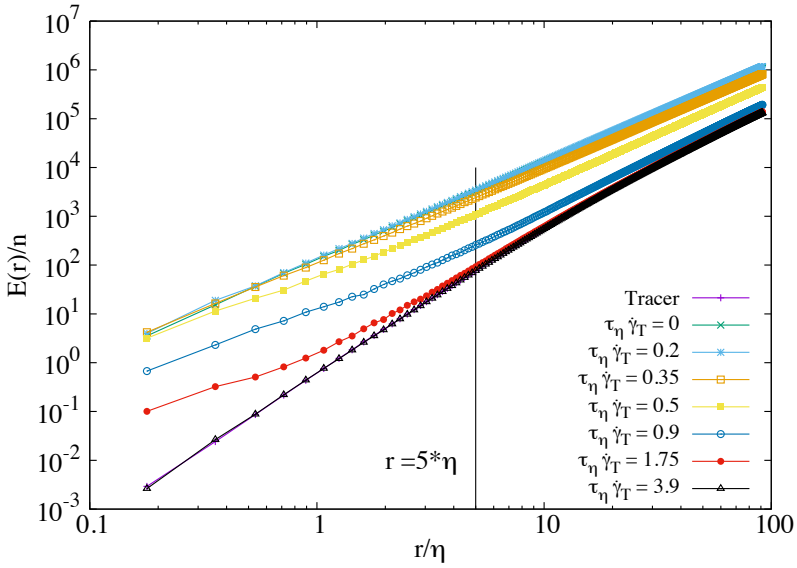

Figure 5: Encounter rate per unit particle density for different Lagrangian copepod families with different values of deformation-rate thresholds $\dot{\gamma}_T$.

have an effective contact rate, it is not necessary for copepods to have physical contacts. Copepods thus can grab their prey or an incoming mate before the contact happens [34]. This is why r in eq. 4 represents the radius of perception of particles rather than their their characteristic radius of geometry.

Fig. 5 represents the encounter kernel as a function of r for different copepod families. Here the encounter rate of copepods are introduced as a reference case for other copepod families. Notice that copepod-copepod interaction has been neglected from the beginning as an assumption to introduce LC model. It is evident that by increasing the shear rate threshold value ($\tau_\eta \dot{\gamma}_T$), the encounter rate of copepods decreases monotonically, although the growth of the shear rate $\tau_\eta \dot{\gamma}_T$ had non-uniform impact on the pair correlation dimension (see Fig. 1).

The vertical line shows the radius of perception for Lagrangian copepod particles, here 5 times greater than the Kolmogorov length scale of the carrier fluid. The ratio of the radius of perception to the copepods' body size is reported to be in the range of $1-3$ [52, 53, 54]. In terms of η unit, this means that the radius of perception of copepods is of the order of $\mathcal{O}(1)$. In order to see how effective the shear rate threshold value is on the encounter rate of Lagrangian copepods at different perception radius, one can estimate the ratio between the encounter rates experienced by copepod families and tracers. This is shown in Fig. 6 where it is realistic to have larger encounter rate at small distances, nevertheless this figure suggests that at optimum clustering corresponding to the shear rate threshold value of $\tau_\eta \dot{\gamma}_T = 0.5$, the encounter rate can be of the order of $\mathcal{O}(10)$ with respect to the tracers at $r = 5\eta$. The LC model shows no contact rate enhancement at shear rate values larger than 2.75.

4 Conclusion

The paper reports the encounter rate of copepods in turbulent flows. Numerical results of a previously applied LC model in turbulence were used in which copepods were simulated in turbulence

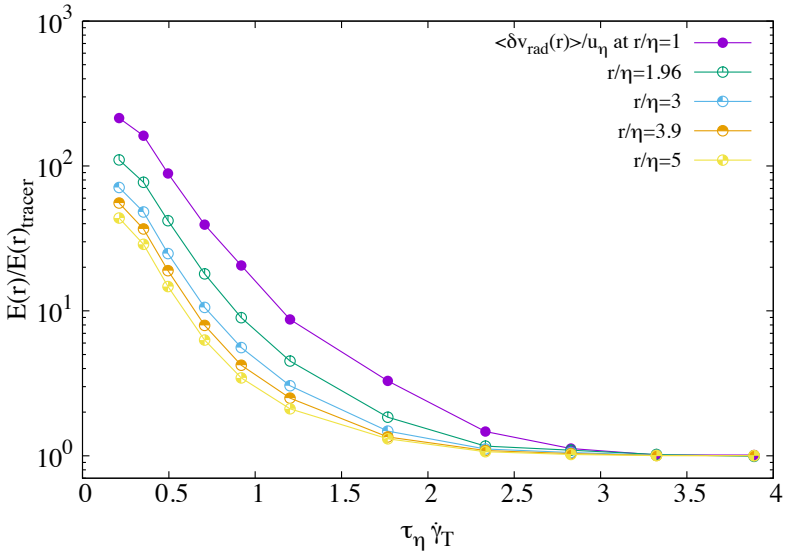

Figure 6: Ratio between encounter rates experienced by Lagrangian copepod particles and the one experienced by fluid tracer particles with the same perception radius.

with a possibility to perform jump in response to a variation of the local shear rate of the fluid-flow. The main feature of the LC model was the preferential concentration of copepods in narrow range of the shear rate.

The LC model shows an enhanced contact rate with respect to the case where copepods are considered as passive particles. This enhancement comes from two terms in the contact rate expression; one is the variation of the $g(r)$ which accounts for the preferential concentration and the other one is the variation of the $\langle \delta v_{rad}(r) \rangle$, which comes from the fact that copepods are swimming. Both contributions are important in the encounter rate enhancement in zooplankton which is a key parameter for sexual reproduction and feeding of plankton species.

Here we have shown that the small scale clustering of copepods which is linked to behavioral model in turbulence, can increase largely the encounter rate. Our studies shows that, this increase depends on copepods' perception radius and can be of the order of $\mathcal{O}(10^2)$ at dissipative scales.

The enhancement of the contact rate is relevant for mating behavior of copepods but it is less relevant for the nutrient uptake. As a perspective it would be interesting to see the consequence of our LC model for the nutrient uptake by using the Lagrangian model of copepods in one side and larger particles drifting in the flow which represent modeling predators.

References

[1] A. M. Hein, S. A. McKinley, Sensory information and encounter rates of interacting species, PLOS Computational Biolog 9 (2013) e1003178.

[2] S. Menden-Deuer, An integrated model simulation and empirical laboratory on biological encounter rates, Ocheanography 19 (2006) 185–189.

[3] T. Kiørboe, A Mechanistic Approach to Plankton Ecology, Princeton University Press, 2008.

[4] M. E. Wosniack, M. C. Santos, M. R. Pie, M. C. M. Marques, E. P. Raposo, G. M. Viswanathan, M. G. E. da Luz, Unveiling a mechanism for species decline in fragmented habitats: fragmentation induced reduction in encounter rates, Journal of The Royal Society Interface 11 (2014) 20130887.

[5] J. Gerritsen, J. R. Strikler, Encounter probabilities and community structure in zooplankton: a mathematical model, Journal of the Fisheries Research Board of Canada 34 (1977) 73–82.

[6] B. J. Rothschild, T. R. Osborn, Small-scale turbulence and plankton contact rates, Journal of Plankton Research 10 (1988) 465–474.

[7] G. T. Evans, The encounter speed of moving predator and prey, Journal of Plankton Research 11 (1989) 415–417.

[8] B. R. MacKenzie, T. J. Miller, S. Cyr, W. C. Leggett, Evidence for a dome shaped relationship between turbulence and larval fish ingestion rates, Limnology and Oceanography 39 (1994) 1790–1799.

[9] A. W. Visser, B. R. MacKenzie, Turbulence-induced contact rates of plankton: the question of scale, Journal of Plankton Research 166 (1998) 307–310.

[10] T. Kiørboe, E. Saiz, Planktivorous feeding in calm and turbulent environments, with emphasis on copepods, Marine Ecology Progress Series 122 (1995) 135–145.

[11] H. L. Pécseli, J. Trulsen, Ø. Fiksen, Predator-prey encounter and capture rates for plankton in turbulent environments, Progress in Oceanography 101 (2012) 14–32.

[12] S. Sundby, P. Fossum, Feeding conditions of arcto-norwegian cod larvae compared with the rothschild-osborn theory on small-scale turbulence and plankton contact rates, Journal of Plankton Research 12 (1990) 1153–1162.

[13] C. S. Davis, G. R. FLierl, P. H. Wiebe, P. J. S. Franks, Micropatchiness, turbulence and recruitment in plankton, Journal of Marine Research 49 (1991) 109–151.

[14] B. R. MacKenzie, W. C. Leggett, Quantifying the contribution of small-scale turbulence to the encounter rates between larval fish and their zooplankton prey: effects of wind and tide, Marine Ecology Progress Series 73 (1991) 149–160.

[15] P. Caparroy, F. Carlotti, A model for acartia tonsa: effect of turbulence and consequences for the related physiological processes, Journal of Plankton Research 18 (1996) 2139–2177.

[16] U. Frisch, Turbulence: The Legacy of A. N. Kolmogorov., Cambridge University Press, 1995.

[17] F. Toschi, E. Bodenschatz, Lagrangian properties of particles in turbulence, Annual Review of Fluid Mechanics 41 (2009) 375–404.

[18] F. G. Schmitt, Y. Huang, Stochastic Analysis of Scaling Time Series: From Turbulence Theory to Applications, Cambridge University Press, 2016.

[19] L. Seuront, F. G. Schmitt, Y. Lagadeuc, Turbulence intermittency, small-scale phytoplankton patchiness and encounter rates in plankton: where do we go from here?, Deep-Sea Research Part I 48 (2001) 1199–1215.

[20] L. Dzierzbicka-Glowacka, Encounter rates in zooplankton, Polish Journal of Environmental Studies 15 (2006) 243–257.

[21] C. P. Jennifer, R. S. Kelly, J. N. Kerry, M. K. Amanda, Biophysical interactions in the plankton: A cross-scale review, Limnology and Oceanography 2 (2012) 121–145.

[22] W. M. Durham, R. Stocker, Thin phytoplankton layers: Characteristics, mechanisms, and consequences, Annual Review of Marine Science 4 (2012) 177–207.

[23] S. Sundaram, L. R. Collins, Collision statistics in an isotropic particle-laden turbulent suspension. part 1. direct numerical simulations, Journal of Fluid Mechanics 335 (1977) 75–109.

[24] L. P. Wang, A. S. Wexler, Y. Zhou, Statistical mechanical descriptions of turbulent coagulation, Physics of Fluids 10 (1998) 2647.

[25] W. C. Reade, L. R. Collins, Effect of preferential concentration on turbulent collision rates, Physics of Fluids 12 (2000) 2530–2540.

[26] L. R. Collins, A. Keswani, Reynolds number scaling of particle clustering in turbulent aerosols, New Journal of Physics 6 (2004) 119.

[27] L. P. Wang, A. S. Wexler, Y. Zhou, Statistical mechanical description and modelling of turbulent collision of inertial particles, Journal of Fluid Mechanics 415 (2000) 117–153.

[28] H. Lian, G. Charalampous, Y. Hardalupas, Preferential concentration of poly-dispersed droplets in stationary isotropic turbulence, Experiments in Fluids 54 (2013) 1525.

[29] G. Falkovich, A. Fouxon, M. G. Stepanov, Acceleration of rain initiation by cloud turbulence, Nature 419 (2002) 151–154.

[30] B. K. Brunk, D. L. Koch, L. W. Lion, Turbulent coagulation of colloidal particles, Journal of Fluid Mechanics 364 (1998) 81–113.

[31] K. D. Squires, J. K. Eaton, Preferential concentration of particles by turbulence, Physics of Fluids 3 (1991) 1169–1178.

[32] R. Monchaux, M. Bourgoin, A. Cartellier., Preferential concentration of heavy particles: A voronoi analysis, Physics of Fluids 22 (2010) 103304.

[33] K. D. Squires, H. Yamazaki, Preferential concentration of marine particles in isotropic turbulence, Deep Sea Research Part I: Oceanographic Research Papers 42 (1995) 1989–2004.

[34] F. G. Schmitt, L. Seuront, Intermittent turbulence and copepod dynamics: Increase in encounter rates through preferential concentration, Marine Systems 70 (2008) 263–272.

[35] E. J. Buskey, Swimming pattern as an indicator of the roles of copepod sensory systems in the recognition of food, Marine Biology 79 (1984) 165–175.

[36] M. J. Weissburg, M. H. Doall, J. Yen, Following the invisible trail: kinematic analysis of mate-tracking in the copepod temora longicornis, Philosophical transactions of the Royal Society of London 353 (1998) 701–712.

[37] A. W. Visser, Hydromechanical signals in the plankton, Marine Ecology Progress Series 222 (2001) 1–24.

[38] H. Jiang, T. R. Osborn, C. Meneveau, Hydrodynamic interaction between two copepods: a numerical study, Journal of Plankton Research 24 (2002) 235–253.

[39] C. Marrasé, J. H. Costello, T. Granata, J. R. Strickler, Grazing in a turbulent environment: energy dissipation, encounter rates, and efficacy of feeding currents in centropages hamatus, PNAS, Proceedings of the National Academy of Sciences 87 (1990) 1653–1657.

[40] H. Ardeshiri, I. Benkeddad, F. G. Schmitt, S. Souissi, F. Toschi, E. Calzavarini, Lagrangian model of copepod dynamics: Clustering by escape jumps in turbulence, Physical Review E 93 (2016) 043117.

[41] P. G. Saffman, J. S. Turner, On the collision of drops in turbulent clouds, Journal of Fluid Mechanics 1 (1956) 16–30.

[42] P. Grassberger, I. Procaccia, Measuring the strangeness of strange attractors, Physica D: Nonlinear Phenomena 9 (1983) 189–208.

[43] M. R. Maxey, The gravitational settling of aerosol particles in homogeneous turbulence and random flow fields, Journal of Fluid Mechanics 174 (1987) 441–465.

[44] L. P. Wang, M. R. Maxey, Settling velocity and concentration distribution of heavy particles in homogeneous isotropic turbulence, Journal of Fluid Mechanics 256 (1993) 27–68.

[45] J. R. Fessler, J. D. Kullick, J. K. Eaton, Preferential concentration of heavy particles in a turbulent channel flow, Physics of Fluids 6 (1994) 3742–3749.

[46] L. Zaichik, V. Alipchenkov, A. Avetissian, Modelling turbulent collision rates of inertial particles, International Journal of Heat and Fluid Flow 27 (2006) 937–944.

[47] E. Calzavarini, M. Kerscher, D. Lohse, F. Toschi, Minkowski functionals: characterizing particle and bubble clusters in turbulent flow, Journal of Fluid Mechanics 607 (2008) 13–24.

[48] E. Calzavarini, T. H. van den Berg, F. Toschi, D. Lohse, Quantifying microbubble clustering in turbulent flow from single-point measurements, Physics of Fluids 20 (2008) 040702.

[49] W. M. Durham, E. Climent, M. Barry, F. D. Lillo, G. Boffetta, M. Cencini, R. Stocker, Turbulence drives microscale patches of motile phytoplankton, Nature Communication 4 (2013) 1–7.

[50] F. D. Lillo, M. Cencini, W. M. Durham, M. Barry, R. Stocker, E. Climent, G. Boffetta, Turbulent fluid acceleration generates clusters of gyrotactic microorganisms, Physical Review Letters 112 (2014) 044502.

[51] M. S. Borgas, P. K. Yeung, Relative dispersion in isotropic turbulence. part 2. a new stochastic model with reynolds-number dependence, Journal of Fluid Mechanics 503 (2004) 125–160.

[52] P. H. Lenz, J. Yen, Distal setal mechanoreceptors of the first antennae of marine copepods, Bulletin of Marine Science 53 (1993) 170–179.

[53] E. Bagoien, T. Kiørboe, Blind dating-mate finding in planktonic copepods. i. tracking the pheromone trail of centropages typicus, Marine Ecology Progress Series 300 (2005) 105–115.

[54] M. H. Doall, S. P. Colin, J. R. Strickler, J. Yen, Locating a mate in 3d: the case of temora longicornis, Philosophical transactions of the Royal Society of London, Series B 353 (1998) 681–689.

Appendix C

Curriculum Vitae

Hamidreza Ardeshiri

Personal Details

Address: Mechanic Laboratory of Lille (LML), Avenue Paul Langevin, France
Email: hamidreza.ardeshiri@polytech-lille.fr, ardeshirih@gmail.com
Web page: https://fr.linkedin.com/in/hamidrezaardeshiri

Education

October 2013 to October 2016 — Ph.D in Mechanical Engineering, **Lille 1 University**, France
Major: Active matters in turbulent flows
Thesis: "Dynamics of copepods in turbulent flows"
Advisors: Prof. François G. Schmitt, Dr. Enrico Calzavarini
Collaborators: Prof. Federico Toschi, Prof. Sami Souissi
Visiting student, **Eindhoven University of Technology**, COST short term mission, COST Action MP1305 "Flowing Matter", The Netherlands, Oct. 2014

September 2011 — M.Sc in Mechanical Engineering, **University of Tehran**, Iran
Major: Energy conversion
Thesis: "LES/FMDF of Trapped Vortex Combustor"
Advisor: Prof. Asghar Afshari
GPA: 18.25/20

July 2009 — B.Sc in Mechanical Engineering , **University of Tehran**, Iran
Thesis: "Hydraulic Analysis of Butterfly valves"
Advisor: Prof. Ahmad Nourbakhsh
GPA: 17.72/20

July 2005 — Diploma in Physics and Mathematics, **NODET**, Larestan
National Organization for Development of Exceptional Talents
GPA: 19.74/20

Research Interests

LES/DNS of turbulent (reacting) flows, Active matters in turbulence, Conventional and renewable energy systems, Simulation of single and multiphase flows, High-order numerical schemes for complex geometries

Publications

- H. Ardeshiri, I. Benkeddad, F. G. Schmitt, S. Souissi, F. Toschi, E. Calzavarini, "A Lagrangian model of copepod dynamics: clustering by escape jumps in turbulence", Phys. Rev. E 93, 043117, 2016.
- H. Ardeshiri, F. G. Schmitt, S. Souissi, F. Toschi, E. Calzavarini, "Copepods encounter rates from a model of escape jump behaviour in turbulence", under preparation, 2016.
- H. Ardeshiri, A. Afshari, "LES/FMDF of Trapped Vortex Combustors", 7h international symposium on Turbulence, Heat and Mass Transfer, Italy, September 2012.

Oral Contributions

- H. Ardeshiri, I. Benkeddad, F. G. Schmitt, S. Souissi, F. Toschi, E. Calzavarini, "A Lagrangian model of copepod dynamics in turbulent flows", 11^{th} European Fluid Mechanic Conference, Spain, 2016.
- H. Ardeshiri, I. Benkeddad, F. G. Schmitt, S. Souissi, F. Toschi, E. Calzavarini, "A Lagrangian model of copepod dynamics in turbulent flows", European Geosciences Union, Austria, 2016.
- H. Ardeshiri, I. Benkeddad, F. G. Schmitt, S. Souissi, F. Toschi, E. Calzavarini, "A Lagrangian model of copepod dynamics: clustering by escape jumps in turbulence", COST Action MP1305 Flowing matter meeting, Portugal, 2016.
- H. Ardeshiri, F. G. Schmitt, F. Toschi, E. Calzavarini, "Numerical modeling of copepod's behaviour in turbulent flows", Doctoral Day (JDD), North of France, 2015

Invited Seminars

- Norwegian Institute for Air Research - NILU, Kjeller, Norway, September, 2016.
- Università degli Studi di Roma "Tor Vergata", Rome, Italy, September, 2016.

Honors and Awards

- Awarded scholarship of the Ministry of Higher Education and Research of France: PhD program (2013-2016)
- Awarded 3rd prize for best poster presentation in doctoral day (JDD), north of France (2014)
- Ranked 2nd among 33 graduates studying in the school of mechanical engineering (2011)
- Awarded scholarship of the University of Tehran and AmirKabir University (graduate program): accepted without participating in the national entrance examination as an exceptional student (2009)
- FOE (Faculty of Engineering) award: ranked 3rd among 115 undergraduates studying in the School of Mechanical Engineering (2005 to 2009)
- FOE (Faculty of Engineering) award: ranked 3rd among 115 undergraduates studying in the School of Mechanical Engineering (2006 and 2009 academic years)
- Ranked 74th (top 0.1%) in university entrance exam among more than 400,000 participants, Tehran, Iran, summer 2005

Professional Experience

- **Teaching Assistant**, UFR Mathematics, Lille 1 University, Science & Technology
  - **Mechanic: research and industrial application**, 48h (Fall 2014 & 2015)
  - **Applied fluid mechanics**, 7h (Winter 2015)
  - **Mechanics of structures**, 16h (Fall 2015)
  - **Experimental methods and projects**, 39h (Winter 2015 & 2016)

- **Teaching Assistant**, School of Mechanical Engineering, University of Tehran
  - **Thermodynamics I, Thermodynamics II**, (Spring 2010 & 2011)
  - **Calculus I, Calculus II**, (Fall 2009 & 2011)
  - **Optimization of thermal systems**, (Spring 2010)
  - **Differential equations**, (Fall 2009)

- **Research Assistant**, Lille 1 University, Science & Technology (2013 - 2016):
  - Performing particle dispersion simulation in turbulent flows (Direct Numerical Simulation (DNS) via spectral method to solve the Navier-Stokes equation).
  - Data analysis & statistics and mathematical modeling of fluid flow problems.

  - Lagrangian simulation, programming in python and handling HDF5 data formatting.
  - Basic knowledge of parallel computing (open-MPI).
  - Basic knowledge of Smoothed-Particle Hydrodynamics (SPH) and Lattice-Boltzmann methods (LBM).

- **Research Assistant**, School of Mechanical Engineering, University of Tehran (2009 - 2012):
  - Modification and application of a high-order multi-block finite difference scheme to turbulent reacting flows in complex geometries.
  - Modification on boundary condition implementation to gain a better consistency between Eulerian and Lagrangian component of a hybrid schemes.
  - Modification of particle search and locate algorithms in a multi-block grid system.
  - Application and evaluation of different inlet and outlet boundary condition.
  - Research and study of the internal combustion engines, gas turbines and compressors.
  - Performing flame simulation inside a combustion chamber using Gambit & FLUENT.
  - Developing UDF's (User Defined Functions) and setting up Dynamic Mesh Problems in ANSYS-FLUENT.

Work Experience

Summer & Fall 2012	Head of Engineering group at MORECO, Tehran *Renewable Energy Field* Design, modeling and optimization of anaerobic digestion systems and wind turbines. Consulting engineering services in combined heat and power (CHP) plant, cogeneration, solar and wind. Basic knowledge of project management.
Fall 2011	Senior researcher at Niroo Research Institute (NRI), Tehran *Energy and Environment group* Conducting comprehensive study of the gasification systems and biomass energy. Designing 1st Downdraft Gasifier in Iran
Spring 2011	Senior researcher at Niroo Research Institute (NRI), Tehran *Mechanical Engineering group* Conducting research and providing the Gas turbine combustion dynamics monitoring system (CDMS) to satisfy the standards in gas turbine safety.
Summer 2008	Internship job at Sazeh Consultants Engineering and Construction Co., Tehran Extensive knowledge of engineering rotating instruments (Turbine, Pump, etc.). Modelling the turbine rotor using SolidWorks/CATIA. Performing hydraulique analysis of Francis turbine using ANSYS-CFX.
Summer 2007	Internship job at Hadid profile Co., Larestan Production Engineer
Summer 2006	Internship job at Potk Co., Shiraz Production Engineer

Languages

- English (Fluent)
- French (Fluent)
- German (Basic)
- Persian (Native)

Bibliography

Alcaraz, M. and J. R. Strickler (1988). "Locomotion in copepods: pattern of movement and energetics of Cyclops". *Hydrobiologia* 409, pp. 167–168.

Ardekani, A. M. and E. Gore (2012). "Emergence of a limit cycle for swimming microorganisms in a vortical flow of a viscoelastic fluid". *Physical Review E* 85, p. 056309.

Ardeshiri, H. et al. (2016). "Lagrangian model of copepod dynamics: Clustering by escape jumps in turbulence". *Physical Review E* 93, p. 043117.

Arin, L. et al. (2002). "Combined effects of nutrients and small-scale turbulence in a microcosm experiment. I. Dynamics and size distribution of osmotrophic plankton". *Aquatic Microbial Ecology* 29, pp. 51–61.

Auton, T. R. (1987). "The lift force on a spherical body in a rotational flow". *Journal of Fluid Mechanics* 183, pp. 199–218.

Auton, T. R., J. C. R. Hunt, and M.Prud'Homme (1988). "The force exerted on a body in inviscid unsteady non-uniform rotational flow". *Journal of Fluid Mechanics* 197.1, pp. 241–257.

Ayyalasomayajula, S., Z. Warhaft, and L. Collins (2008). "Modeling inertial particle acceleration statistics in isotropic turbulence". *Physics of Fluid* 20, p. 095104.

Ayyalasomayajula, S. et al. (2006). "Lagrangian measurements of inertial particle accelerations in grid generated wind tunnel turbulence". *Physical Review Letter* 97, p. 144507.

Bagoien, E. and T. Kiørboe (2005). "Blind dating-mate finding in planktonic copepods. I. Tracking the pheromone trail of Centropages typicus". *Marine Ecology Progress Series* 300, pp. 105–115.

Balkovsky, E., G. Falkovich, and A. Fouxon (2001). "Intermittent distribution of inertial particles in turbulent flows". *Physical Review Letters* 86, pp. 2790–2793.

Barnes, R. S. K. and R. N. Hughes (1999). *An Introduction to Marine Ecology*. Blackwell Publishing.

Baskaran, A. and M. C. Marchetti (2009). "Statistical mechanics and hydrodynamics of bacterial suspensions". *Proceeding of the National Academy of Science* 106, pp. 15567–15572.

Batchelor, G. K. (1967). *An Introduction to Fluid Dynamics*. Cambridge University press.

Bec, J. et al. (2006). "Acceleration statistics of heavy particles in turbulence". *Journal of Fluid Mechanics* 550, pp. 349–358.

Benkeddad, I. (2015). "Accélération des Copépodes Calanoides: Utilisation de Caméra Rapide". *Master 1 thesis, Lille 1 University - Science and Technology*, pp. 1–29.

Benoit-Bird, K. J., T. J. Cowles, and C. E. Wingard (2009). "Edge gradients provide evidence of ecological interactions in planktonic thin layers". *Limnology and Oceanography* 54, pp. 1382–1392.

Berg, H. C. and L. Turner (1979). "Movement of microorganisms in viscous environments". *Nature* 278, pp. 349–351.

Bergstedt, M. S., M. M. Hondzo, and Cotner J. B (2004). "Effects of small scale fluid motion on bacterial growth and respiration". *Freshwater Biology* 49, pp. 28–40.

Bernard, D. et al. (2006). "Conformal invariance in two-dimensional turbulence". *Nature Physics* 2, pp. 124–128.

Borazjani, I. et al. (2010). "On the role of copepod antennae in the production of hydrodynamic force during hopping". *Journal of Experimental Biology* 213, pp. 3019–3035.

Borgas, M. S. and P. K. Yeung (2004). "Relative dispersion in isotropic turbulence. Part 2. A new stochastic model with Reynolds-number dependence". *Journal of Fluid Mechanics* 503, pp. 125–160.

Bowman, J. C. and M. Roberts (2011). "Efficient Dealiased Convolutions without Padding". *Journal of Scientific Computing* 33, pp. 386–406.

Boxshall, G. A. (1985). "The Comparative Anatomy of Two Copepods, a Predatory Calanoid and a Particle-Feeding Mormonilloid". *Philosophical Transactions of The Royal Society B Biological Sciences* 311, pp. 303–377.

Boxshall, G. A. (2004). *An Introduction to Copepod Diversity*. Ray Society.

Boyd, J. P. (2001). *Chebyshev and Fourier Spectral Methods*. Dover Publications, Inc.

Brandl, Z. (2005). "Freshwater copepods and rotifers: predators and their prey". *Hydrobiologia* 546, pp. 475–489.

Bron, J. et al. (2011). "Observing Copepods through a Genomic Lens". *Frontiers in Zoology* 8, p. 22.

Brunk, B. K., D. L. Koch, and L. W. Lion (1998). "Turbulent coagulation of colloidal particles". *Journal of Fluid Mechanics* 364, pp. 81–113.

Buskey, E. J. (1984). "Swimming pattern as an indicator of the roles of copepod sensory systems in the recognition of food". *Marine Biology* 79, pp. 165–175.

Buskey, E. J. and D. K. Hartline (2003). "High-Speed Video Analysis of the Escape Responses of the Copepod Acartia tonsa to Shadows". *The Biological Bulletin* 204, pp. 28–37.

Buskey, E. J., P. H. Lenz, and D. K. Hartline (2002). "Escape behavior of planktonic copepods in response to hydrodynamic disturbances: high speed video analysis". *Marine Ecology Progress Series* 235, pp. 135–146.

Calzavarini, E. et al. (2008a). "Minkowski functionals: characterizing particle and bubble clusters in turbulent flow". *Journal of Fluid Mechanics* 607, pp. 13–24.

Calzavarini, E. et al. (2008b). "Quantifying microbubble clustering in turbulent flow from single-point measurements". *Physics of Fluids* 20, p. 040702.

Canuto, C. et al. (2007). *Spectral Methods, Evolution to Complex Geometries and Applications to Fluid Dynamics*. Springer.

Caparroy, P. and F. Carlotti (1996). "A model for Acartia tonsa: effect of turbulence and consequences for the related physiological processes". *Journal of Plankton Research* 18, pp. 2139–2177.

Cencini, M., F. Cencini, and A. Vulpiani (2009). *Chaos from simple models to complex systems*. World Scientific.

Cencini, M. et al. (2006). "Dynamics and statistics of heavy particles in turbulent flows". *Journal of Turbulence* 7, pp. 1–16.

Chen, S. et al. (1993). "On statistical correlations between velocity increments and locally averaged dissipation in homogeneous turbulence". *Physics of Fluids A* 5, pp. 458–463.

Choi, J., J. J. Dongarra, and D. W. Walker (1995). "Parallel matrix transpose algorithms on distributed memory concurrent computers". *Parallel Computing* 21, pp. 1387–1405.

Clift, R., J. R. Grace, and M. E. Weber (1978). *Bubbles, Drops and Particles*. Academic Press New York.

Collins, L. R. and A. Keswani (2004). "Reynolds number scaling of particle clustering in turbulent aerosols." *New Journal of Physics* 6, p. 119.

Cooley, J. W. and J. W. Tukey (1965). "An algorithm for the machine calculation of complex Fourier series". *Mathematics of Computation* 19, pp. 297–301.

Croze, O. A. et al. (2013). "Dispersion of swimming algae in laminar and turbulent channel flows: consequences for photobioreactors". *Journal of The Royal Society Interface* 10, p. 20121041.

Cury, P. and C. Roy (1989). "Optimal environmental window and pelagic fish recruitment success in upwelling areas." *Canadian Journal of Fisheries and Aquatic Sciences* 46, pp. 670–680.

Damkaer, D. M. (2002). *The copepodologist's cabinet, The biographical and bibliographical history*. American Physiological Society.

Davidson, P. A. (2004). *Turbulence, an introduction for scientists and engineers*. Oxfrod University Press.

Davis, C. S. et al. (1991). "Micropatchiness, turbulence and recruitment in plankton". *Journal of Marine Research* 49, pp. 109–151.

Dekshenieks, M. M. et al. (2001). "Temporal and spatial occurrence of thin phytoplankton layers in relation to physical processes". *Marine Ecology Progress Series* 223, pp. 61–71.

Devreker, D. et al. (2008). "Trade-offs of the copepod Eurytemora affinis in mega-tidal estuaries. Insights from high frequency sampling in the Seine Estuary". *Journal of Plankton Research* 30(12), pp. 1329–1342.

Doall, M. H. et al. (1998). "Locating a mate in 3D: the case of Temora longicornis". *Philosophical transactions of the Royal Society of London, Series B* 353, pp. 681–689.

Dolan, J. et al. (2003). "Effects of turbulence on the feeding and growth of a marine oligotrich ciliate". *Aquatic Microbial Ecology* 31, pp. 183–192.

Dower, J. F., T. J. Miller, and W. C. Leggett (1997). "The role of microscale turbulence in the feeding ecology of larval fish". *Advances in Marine Biology* 31, pp. 169–220.

Drescher, K. et al. (2011). "Fluid dynamics and noise in bacterial cell-cell and cell-surface scattering". *Proceeding of the National Academy of Science* 108, pp. 10940–10945.

Dunkel, J. et al. (2013). "Fluid Dynamics of Bacterial Turbulence". *Physical Review Letters* 110, p. 228102.

Duren, L. A. van, E. J. Stamhuis, and J. J. Videler (1998). "Reading the copepod personal ads: increasing encounter probability with hydromechanical signals". *Philosophical transactions of the Royal Society of London. Series B, Biological sciences* 353, pp. 691–700.

Duren, L. A. van and J. J. Videler (2003). "Escape from viscosity: the kinematics and hydrodynamics of copepod foraging and escape swimming". *Journal of Experimental Biology* 206, pp. 269–279.

Durham, W. M., E. Climent, and R. Stocker (2011). "Gyrotaxis in a Steady Vortical Flow". *Physical Review Letters* 106, p. 238102.

Durham, W. M. and R. Stocker (2012). "Thin phytoplankton layers: Characteristics, mechanisms, and consequences". *Annual Review of Marine Science* 4, pp. 177–207.

Durham, W. M. et al. (2013). "Turbulence drives microscale patches of motile phytoplankton". *Nature Communication* 4, pp. 1–7.

Dzierzbicka-Glowacka, L. (2006). "Encounter Rates in Zooplankton". *Polish Journal of Environmental Studies* 15, pp. 243–257.

Eaton, J. K. and J. R. Fessler (1994). "Preferential concentration of particles by turbulence". *International Journal of Multiphase Flow* 20, pp. 169–209.

Evans, G. T. (1989). "The encounter speed of moving predator and prey". *Journal of Plankton Research* 11, pp. 415–417.

Falkovich, G., A. Fouxon, and M. G. Stepanov (2002). "Acceleration of rain initiation by cloud turbulence". *Nature* 419, pp. 151–154.

Falkovich, G., K. Gawedzki, and M. Vergassola (2001). "Particles and fields in fluid turbulence". *Reviews of Modern Physics* 73, pp. 913–975.

Fields, D. A. and J. Yen (1997). "The escape behavior of marine copepods in response to a quantifiable fluid mechanical disturbance". *Journal of Plankton Research* 19, pp. 1289–1304.

Fields, D. A. et al. (2012). "Light Primes the Escape Response of the Calanoid Copepod, Calanus finmarchicus". *PLOS ONE* 7(6), e39594.

Fields, D. M. and J. Yen (1996). "The escape behaviour of Pleuromamma xiphias in response to a quantifiable fluid mechanical disturbance". *Zooplankton: sensory ecology and physiology*, pp. 323–339.

Fornberg, B. (1996). *A practical guide to pseudospectral methods*. Cambridge University Press.

Frangoulis, C., E. D. Christou, and J. H. Hecq (2005). "Comparison of Marine Copepod Outfluxes: Nature, Rate, Fate and Role in the Carbon and Nitrogen Cycles". *Advances in Marine Biology* 47, pp. 253–309.

Frisch, U. (1995). *Turbulence: The Legacy of A. N. Kolmogorov.* Cambridge University Press.

Gallager, S. M., H. Yamazaki, and C. S. Davis (2004). "Contribution of fine-scale vertical structure and swimming behavior to formation of plankton layers on Georges Bank". *Marine Ecology Progress Series* 267, pp. 27–43.

Gallager, S. M., H. Yamazaki, and C. S. Davis (2008). "The modulation of biological production by oceanic mesoscale turbulence". *Transport and Mixing in Geophysical Flows, ed. JB Weiss, A Provenzale, Lect. Notes Phys. 744. Berlin: Springer-Verlag*, pp. 219–261.

Gatignol, R. (1983). "The Faxen formulae for a rigid particle in an unsteady nonuniform stokes flow". *Journal of Theoretical and Applied Mechanics* 1, pp. 143–160.

Genin, A. et al. (2005). "Swimming against the flow: a mechanism of zooplankton aggregation". *Science* 308, pp. 860–862.

Gerritsen, J. and J. R. Strikler (1977). "Encounter probabilities and community structure in zooplankton: a mathematical model". *Journal of the Fisheries Research Board of Canada* 34, pp. 73–82.

Grassberger, P. and I. Procaccia (1983). "Measuring the Strangeness of Strange Attractors". *Physica D: Nonlinear Phenomena* 9, pp. 189–208.

Guasto, J. S., R. Rusconi, and R. Stocker (2012). "Fluid Mechanics of Planktonic Microorganisms". *Annual Review of Fluid Mechanics* 44, pp. 373–400.

Gustavsson, K. et al. (2016). "Preferential Sampling and Small-Scale Clustering of Gyrotactic Microswimmers in Turbulence". *Physical Review Letters* 116, p. 108104.

Haury, L. R., D. E. Kenyon, and J. R. Brooks (1980). "Experimental evaluation of the avoidance reaction of Calanus finmarchicus". *Journal of Plankton Research*, pp. 187–202.

Hausch, S., J. B. Shurin, and B. Matthews (2013). "Variation in Body Shape across Species and Populations in a Radiation of Diaptomid Copepods". *PLOS ONE* 8, e68272.

Hein, A. M. and S. A. McKinley (2013). "Sensory Information and Encounter Rates of Interacting Species". *PLOS Computational Biolog* 9, e1003178.

Hernandez-Ortiz, J. P., C. G. Stoltz, and M. D. Graham (2005). "Transport and Collective Dynamics in Suspensions of Confined Swimming Particles". *Physical Review Letters* 95, p. 204501.

Hohenegger, C. and M. J. Shelley (2010). "Stability of active suspensions". *Physical Review E* 81, p. 046311.

Hussaini, M. Y. and T. A. Zang (1987). "Spectral Methods in Fluid Dynamics". *Annual Review of Fluid Mechanics* 19, pp. 339–367.

Huys, R. and G. A. Boxshall (1991). *Copepod Evolution*. The Ray Society, London, England.

Jeffery, G. (1922). "The Motion of Ellipsoidal Particles Immersed in a Viscous Fluid". *Proceedings of the Royal Society of London. Series A* 102, pp. 161–179.

Jenkinson, I. R. and J. Sun (2010). "Rheological properties of natural waters with regard to plankton thin layers. A short review". *Journal of Marine System.* 83, pp. 287–297.

Jennifer, C. P. et al. (2012). "Biophysical interactions in the plankton: A cross-scale review". *Limnology and Oceanography* 2, pp. 121–145.

Jiang, H. and T. Kiørboe (2011). "The fluid dynamics of swimming by jumping in copepods". *Journal of The Royal Society Interface* 8, pp. 1090–1103.

Jiang, H. and T. R. Osborn (2004). "Hydrodynamics of copepods: a review". *Surveys in Geophysics, Kluwer Academic Publishers* 25, pp. 339–370.

Jiang, H., T. R. Osborn, and C. Meneveau (2002). "Hydrodynamic interaction between two copepods: a numerical study". *Journal of Plankton Research* 24, pp. 235–253.

Jiménez, J. (1997). "Oceanic turbulence at millimeter scales". *Scientia Marina* 61, pp. 47–56.

Jonasdottir, S. H. et al. (2015). "Seasonal copepod lipid pump promotes carbon sequestration in the deep North Atlantic". *Proceeding of the National Academy of Science* 112, pp. 12122–12126.

Jr, G. S. Patterson and S. A. Orszag (1971). "Spectral Calculations of Isotropic Turbulence: Efficient Removal of Aliasing Interactions". *Physics of Fluids* 14, pp. 2538–2541.

Kaiser, A. et al. (2014). "Transport Powered by Bacterial Turbulence". *Physical Review Letters* 112, p. 158101.

Kampen, N. G. Van (2007). *Stochastic processes in physics and chemistry*. Elsevier Science & Technology Books.

Karp-Boss, L., E. Boss, and P. A. Jumars (1996). "Nutrient fluxes to planktonic osmotrophs in the presence of fluid motion". *Oceanography and Marine Biology* 34, pp. 71–107.

Kessler, J. O. (1985). "Hydrodynamic focusing of motile algal cells". *Nature* 313, pp. 218–220.

Kiørboe, T. (2008). *A Mechanistic Approch to Plankon Ecology*. Princeton University Press.

Kiørboe, T., H. Jiang, and S. P. Colin (2010). "Danger of zooplankton feeding: the fluid signal generated by ambush-feeding copepods". *Proceedings of the Royal Society B: Biological Sciences* 277, pp. 3229–3237.

Kiørboe, T., H. Ploug, and U. H. Thygesen (2001). "Fluid motion and solute distribution around sinking aggregates. I. Small-scale fluxes and heterogeneity of nutrients in the pelagic environment". *Marine Ecology Progress Series* 211, pp. 1–13.

Kiørboe, T. and E. Saiz (1995). "Planktivorous feeding in calm and turbulent environments, with emphasis on copepods". *Marine Ecology Progress Series* 122, pp. 135–145.

Kiørboe, T., E. Saiz, and A. Visser (1999). "Hydrodynamic signal perception in the copepod Acartia tonsa". *Marine Ecology Progress Series* 179, pp. 97–111.

Kiørboe, T. and A. Visser (1999). "Predator and prey perception in copepods due to hydromechanical signals". *Marine Ecology Progress Series* 179, pp. 81–95.

Koehl, M. A. R. and J. R. Strickler (1981). "Copepod feeding currents: food capture at low reynolds number". *Limnology and Oceanography* 26, pp. 1062–1073.

Kolmogorov, A. N. (1991a). "Dissipation of Energy in the Locally Isotropic Turbulence". *Proceedings: Mathematical and Physical Sciences* 434, pp. 15–17.

Kolmogorov, A. N. (1991b). "The Local Structure of Turbulence in Incompressible Viscous Fluid for Very Large Reynolds Numbers". *Proceedings: Mathematical and Physical Sciences* 434, pp. 9–13.

Lambert, R. A. et al. (2013). "Active suspensions in thin films: nutrient uptake and swimmer motion". *Journal of Fluid Mechanics* 733, pp. 528–557.

Lamorgese, A. G., D. A. Caughey, and S. B. Pope (2005). "Direct numerical simulation of homogeneous turbulence with hyperviscosity". *Physics of Fluids* 17, p. 015106.

Landau, L. D. and L. M. Lifshitz (1959). *Fluid Mechanics*. Pergamon press, New York.

Landry, M. R. (1978). "Predatory feeding behaviour of a marine copepod, Labidocera trispinosa". *Limnology and Oceanography* 23, pp. 1103–1113.

Landry, M. R. and J. J. Gilbert (1988). "Escape behaviour of Polyathra in response to artificial flow stimuli". *Bulletin of Marine Science* 53, pp. 96–105.

Lauga, E. (2016). "Bacterial hydrodynamics". *Annual Review of Fluid Mechanics* 48, pp. 105–130.

Lee, C. H. et al. (2011). "Mating behaviour of Pseudodiaptomus annandalei (Copepoda, Calanoida) at calm and hydrodynamically disturbed waters". *Marine Biology* 158, pp. 1085–1094.

Lee, M. and R. D. Moser (2015). "Direct numerical simulation of turbulent channel flow up to Re=5200". *Journal of Fluid Mechanics* 774, pp. 395–415.

Lenz, P. H. and D. K. Hartline (1999). "Reaction times and force production during escape behavior of a calanoid copepod, Undinula vulgaris". *Marine Biology* 133, pp. 249–258.

Lenz, P. H., A.E. Hower, and D. K. Hartline (2004). "Force production during pereiopod power strokes in Calanus finmarchicus". *Journal of Marine Systems* 49, pp. 133–144.

Lenz, P. H. and J. Yen (1993). "Distal setal mechanoreceptors of the first antennae of marine copepods". *Bulletin of Marine Science* 53, pp. 170–179.

Leonardo, R. Di et al. (2010). "Bacterial ratchet motors". *Proceeding of the National Academy of Science* 107, pp. 9541–9545.

Lewis, D. M. and T. J. Pedley (2000). "Planktonic contact rates in homogeneous isotropic turbulence: theoretical predictions and kinematic simulations". *Journal of Theoretical Biology* 205, pp. 377–408.

Lian, H., G. Charalampous, and Y. Hardalupas (2013). "Preferential concentration of poly-dispersed droplets in stationary isotropic turbulence". *Experiments in Fluids* 54, p. 1525.

Lillo, F. De et al. (2014). "Turbulent Fluid Acceleration Generates Clusters of Gyrotactic Microorganisms". *Physical Review Letters* 112, p. 044502.

Lomax, H., T. H. Pulliam, and D. W. Zingg (1999). *Fundamentals of Computational Fluid Dynamics*. Springer.

Lushi, E., H. Wioland, and R. E. Goldstein (2014). "Fluid flows created by swimming bacteria drive self-organization in confined suspensions". *Proceeding of the National Academy of Science* 111, pp. 9733–9738.

MacKenzie, B. R. (2000). "Turbulence, larval fish ecology and fisheries recruitment: a review of field studies." *Oceanologica Acta* 23, pp. 357–375.

MacKenzie, B. R. and W. C. Leggett (1991). "Quantifying the contribution of small-scale turbulence to the encounter rates between larval fish and their zooplankton prey: effects of wind and tide". *Marine Ecology Progress Series* 73, pp. 149–160.

MacKenzie, B. R. and W. C. Leggett (1993). "Wind-based models for estimating the dissipation rates of turbulent energy in aquatic environments: empirical comparisons". *Marine Ecology Progress Series* 94, pp. 207–216.

MacKenzie, B. R. et al. (1994). "Evidence for a dome-shaped relationship between turbulence and larval fish ingestion rates". *Limnology and Oceanography* 39, pp. 1790–1799.

Marchioli, C., M. Fantoni, and A. Soldati (2007). "Influence of added mass on anomalous high rise velocity of light particles in cellular flow field: A note on the paper by Maxey (1987)". *Physics of Fluids* 19, p. 098101.

Margalef, R. (1997). "Turbulence and marine life". *Scientia marina* 61, pp. 109–123.

Marrasé, C. et al. (1990). "Grazing in a turbulent environment: energy dissipation, encounter rates, and efficacy of feeding currents in Centropages hamatus". *PNAS, Proceedings of the National Academy of Sciences* 87, pp. 1653–1657.

Maxey, M. R. and J. J. Riley (1983). "Equation of motion for a small rigid sphere in a nonuniform flow". *Physics of Fluids* 26, p. 883.

Mazzitelli, I.M., D. Lohse, and F. Toschi (2003a). "On the relevance of the lift force in bubbly turbulence". *Journal of Fluid Mechanics* 488, pp. 283–313.

Mazzitelli, I.M., D. Lohse, and F. Toschi (2003b). "The effect of microbubbles on developed turbulence". *Physics of Fluids* 15, pp. L5–8.

Menden-Deuer, S. (2006). "An Integrated Model Simulation and Empirical Laboratory on Biological Encounter Rates". *Ocheanography* 19, pp. 185–189.

Michalec, F. G., S. Souissi, and M. Holzner (2015). "Turbulence triggers vigorous swimming but hinders motion strategy in planktonic copepods". *Journal of The Royal Society Interface* 12, p. 20150158.

Michalec, F. G. et al. (2015). "Characterization of intermittency in zooplankton behaviour in turbulence". *The European Physical Journal E* 38, p. 108.

Moison, M. et al. (2009). "Symbolic dynamics and entropies of copepod behaviour under non-turbulent and turbulent conditions". *Journal of Marine Systems* 77, pp. 388–396.

Moore, P., D. M. Fields, and J. Yen (1999). "Physical constraints of chemoreception in foraging copepods". *Limnology and Oceanography* 44, pp. 166–177.

Morales, E. S. (2016). *World Association of Copepodologists*. http://www.monoculus.org/de/home.html.

Nishihara, G. N. and J. D. Ackerman (2009). "Diffusive boundary layers do not limit the photosynthesis of the aquatic macrophyte, Vallisneria americana, at moderate flows and saturating light levels". *Limnology and Oceanography* 54, pp. 1874–1882.

Oboukov, A. M. (1941). "On the distribution of energy in the spectrum of turbulent flow". *Doklady Akademii nauk SSSR* 32, pp. 22–24.

Orszag, S. A. (1971). "On the Elimination of Aliasing in Finite-Difference Schemes by Filtering High-Wavenumber Components". *Journal of The Atmospheric Sciences* 28, pp. 1074–1074.

Paladin, G. and A. Vulpiani (1987). "Anomalous scaling laws in multifractal objects". *Physics Reports* 156, pp. 147–225.

Parsa, S. et al. (2012). "Rotation Rate of Rods in Turbulent Fluid Flow". *Physical Review Letters* 109, p. 134501.

Pedley, T. J. and J. O. Kessler (1992). "Hydrodynamic Phenomena In Suspensions of Swimming Microorganisms". *Annual Review of Fluid Mechanics* 24, pp. 313–358.

Peters, F. et al. (2006). "Effects of small-scale turbulence on the growth of two diatoms of different size in a phosphorous-limited medium". *Journal of Marine System* 61, pp. 134–148.

Phillips, N. A. (1959). "An example of nonlinear computational instability". *The Atmosphere and the Sea in Motion*, pp. 501–504.

Pope, S. B. (2000). *Turbulent flows*. Cambridge University Press.

Qureshi, N. et al. (2008). "Acceleration statistics of inertial particles in turbulent flow". *The European Physical Journal B* 66, pp. 531–536.

Ray, G. C. and J. McCormick-Ray (2004). *Coastal-Marine Conservation: Science and Policy*. Blackwell Publishing, Oxford, UK.

Reade, W. C. and L. R. Collins (2000). "Effect of preferential concentration on turbulent collision rates." *Physics of Fluids* 12, pp. 2530–2540.

Reddy, J. (2005). *An Introduction to the Finite Element Method*. McGraw-Hill Education.

Richardson, L. F. (1922). *Weather prediction by numerical process*. Cambridge University Press.

Rines, J. E. B. et al. (2010). "Thin layers and species-specific characterization of the phytoplankton community in Monterey Bay, California, USA". *Continental Shelf Research* 30, pp. 66–80.

Rombouts, I et al. (2009). "Global latitudinal variations in marine copepod diversity and environmental factors". *Proceedings of the Royal Society of London B* 276, pp. 3053–3062.

Ross, O. N. (2006). "Particles in motion: How turbulence affects plankton sedimentation from an oceanic mixed layer". *Geophysical Research Letters* 33, p. L10609.

Rothschild, B. J. and T. R. Osborn (1988). "Small-scale turbulence and plankton contact rates". *Journal of Plankton Research* 10, pp. 465–474.

Ruiz, J., D. Maci as, and F. Peters (2004). "Turbulence increases the average settling velocity of phytoplankton cells". *Proceedings of the National Academy of Sciences* 101, pp. 17720–17724.

Saffman, P. G. and J. S. Turner (1956). "On the collision of drops in turbulent clouds". *Journal of Fluid Mechanics* 1, pp. 16–30.

Sagaut, P., S. Deck, and M. Terracol (2006). *Multiscale and multiresolution approaches in turbulence*. Imperial College Press.

Salazar, J. P. L. C. et al. (2008). "Experimental and numerical investigation of inertial particle clustering in isotropic turbulence". *Journal of Fluid Mechanics* 600, pp. 245–256.

Satapoomin, S. (1999). "Carbon content of some common tropical Andaman Sea copepods". *Journal of Plankton Research* 21, pp. 2117–2123.

Saw, E. W. et al. (2008). "Inertial clustering of particles in high-Reynolds-number turbulence". *Physical Review Letters* 100, p. 214501.

Schiller, L. and A. Neumann (1933). "Über die grundlegenden Berechnungen bei der Schwerkraft-aufbereitung". *Z. Ver. Dtsch. Ing.* 77, pp. 318–320.

Schmitt, F. G. (2007). "About Boussinesq's turbulent viscosity hypothesis: historical remarks and a direct evaluation of its validity". *Comptes Rendus Mécanique* 335, pp. 617–627.

Schmitt, F. G. and Y. Huang (2016). *Stochastic Analysis of Scaling Time Series: From Turbulence Theory to Applications*. Cambridge University Press.

Schmitt, F. G. and L. Seuront (2008). "Intermittent turbulence and copepod dynamics: Increase in encounter rates through preferential concentration". *Journal of Marine Systems* 70, pp. 263–272.

Schmitt, F. G. et al. (2011). "Direct evidence of tidally-oriented behaviour of the copepod Eurytemora affinis in the Seine estuary". *Ecological Research* 26(4), pp. 773–780.

Seuront, L., F. G. Schmitt, and Y. Lagadeuc (2001). "Turbulence intermittency, small-scale phytoplankton patchiness and encounter rates in plankton: where do we go from here?" *Deep Sea Research Part I: Oceanographic Research Papers* 48, pp. 1199–1215.

Seymour, J. R., Marcos, and R. Stocker (2009). "Resource patch formation and exploitation throughout the marine microbial food web". *The American Naturalist* 173, pp. 15–29.

Singarajah, K. V. (1969). "Escape reactions of zooplankton: the avoidance of a pursuing siphon tube". *Journal of Experimental Marine Biology and Ecology* 3, pp. 171–178.

Singarajah, K. V. (1975). "Escape reactions of zooplankton: effects of light and turbulence". *Journal of the Marine Biological Association of the United Kingdom* 55, pp. 627–639.

Smyth, W.D. and J.N. Moum (2001). "Efficient Dealiased Convolutions without Padding". *Encyclopedia of Ocean Sciences, Academic Press*.

Solomon, T. H. and J. P. Gollub (1988). "Chaotic particle transport in time-dependent Rayleigh-Benard convection". *Physical Review A* 38, p. 6280.

Souissi, A., S. Souissi, and B. W. Hansen (2014). "Physiological improvement in the copepod Eurytemora affinis through thermal and multigenerational selection". *Aquaculture Research*, pp. 1–16.

Souissi, S. et al. (2010). "How does salinity influence the swimming speed of the estuarine calanoid copepodEurytemora affinis?:Reply". *Journal of Plankton Research* 32, pp. 1227–1229.

Squires, K. D. and J. K. Eaton (1991). "Preferential concentration of particles by turbulence". *Physics of Fluids* 3, pp. 1169–1203.

Squires, K. D. and H. Yamazaki (1995). "Preferential concentration of marine particles in isotropic turbulence". *Deep Sea Research Part I: Oceanographic Research Papers* 42, pp. 1989–2004.

Stocker, R. (2012). "Marine microbes see a sea of gradients". *Science* 338, pp. 628–633.

Stokes, G. G. (1851). "On the Effect of the Internal Friction of Fluids on the Motion of Pendulums". *Transactions of the Cambridge Philosophical Society* 9, p. 8.

Strickland, J. D. H. (1968). "A comparison of profiles of nutrient and chlorophyll concentrations taken from discrete depths and by continuous recording". *Limnology and Oceanography* 13.2, pp. 388–391.

Strickler, J. R. (1975). "Swimming of planktonic Cyclops species (Copepoda, Crustacea): pattern, movements and their control". *Swimming and Flying in Nature edited by T. Y. T. Wu, C. J. Brokaw and C. Brennen* 2, pp. 599–613.

Sundaram, S. and L. R. Collins (1977). "Collision statistics in an isotropic particle-laden turbulent suspension. Part 1. Direct numerical simulations". *Journal of Fluid Mechanics* 335, pp. 75–109.

Sundby, S. and P. Fossum (1990). "Feeding conditions of Arcto-Norwegian cod larvae compared with the Rothschild-Osborn theory on small-scale turbulence and plankton contact rates". *Journal of Plankton Research* 12, pp. 1153–1162.

Taylor, G. I. (1928). "The Forces on a Body Placed in a Curved or Converging Stream of Fluid". *Proceedings of the Royal Society of London. Series A, Containing Papers of a Mathematical and Physical Character* 120, pp. 260–283.

Taylor, G. I. (1938). "The Spectrum of Turbulence". *Proceedings of the Royal Society of London A* 164, pp. 476–490.

Tennekes, H. and J. L. Lumley (1972). *A First Course in Turbulence*. MIT Press.

Teran, J., L. Fauci, and M. Shelley (2010). "Viscoelastic Fluid Response Can Increase the Speed and Efficiency of a Free Swimmer". *Physical Review Letters* 104, p. 038101.

Theilacker, G. H. and A. M. Kimball (1984). "Comparative quality of Rotifers and Copepods as foods for larval fishes". *CalCOFI Rep* 25, pp. 80–86.

Torney, C. and Z. Neufeld (2007). "Transport and Aggregation of Self-Propelled Particles in Fluid Flows". *Physical Review Letters* 99, p. 078101.

Toschi, F. and E. Bodenschatz (2009). "Lagrangian Properties of Particles in Turbulence". *Annual Review of Fluid Mechanics* 41, pp. 375–404.

Trager, G., Y. Achituv, and A. Genin (1994). "Effects of prey escape ability, flow speed, and predator feeding mode on zooplankton capture by barnacles". *Marine Biology* 120, pp. 251–259.

Visser, A. W. (2001). "Hydromechanical signals in the plankton". *Marine Ecology Progress Series* 222, pp. 1–24.

Visser, A. W. and T. Kiørboe (2006). "Plankton motility patterns and encounter rates". *Oecologia* 148, pp. 538–546.

Visser, A. W. and B. R. MacKenzie (1998). "Turbulence-induced contact rates of plankton: the question of scale". *Marine Ecology Progress Series* 166, pp. 307–310.

Visser, A. W., P. Mariani, and S. Pigolotti (2009). "Swimming in turbulence: Zooplankton fitness in terms of foraging efficiency and predation risk". *Journal of Plankton Research* 31, pp. 121–133.

Volk, R. et al. (2008). "Acceleration of heavy and light particles in turbulence: Comparison between experiments and direct numerical simulations". *Physica D: Nonlinear Phenomena* 237, pp. 2084–2089.

Voth, G. A. et al. (2001). "A silicon strip detector system for high resolution particle tracking in turbulence". *Review of Scientific Instruments* 72, pp. 4348–4353.

Waggett, R. J. and E. J. Buskey (2007). "Copepod escape behavior in non-turbulent and turbulent hydrodynamic regimes". *Marine Ecology Progress Series* 334, pp. 193–198.

Walter, T. C. and G. Boxshall (2016). *World of Copepods database*. http://www.marinespecies.org/copepoda.

Wang, L. P. and M. R. Maxey (1993). "Settling velocity and concentration distribution of heavy particles in homogeneous isotropic turbulence". *Journal of Fluid Mechanics* 256, pp. 27–68.

Wang, L. P., A. S. Wexler, and Y. Zhou (1998). "Statistical mechanical descriptions of turbulent coagulation." *Physics of Fluids* 10, pp. 2647–2651.

Wang, L. P., A. S. Wexler, and Y. Zhou (2000). "Statistical mechanical description and modelling of turbulent collision of inertial particles". *Journal of Fluid Mechanics* 415, pp. 117–153.

Warnaas, T. A. and M. Hondzo (2006). "Small-scale fluid motion mediates growth and nutrient uptake of Selenastrum capricornutum". *Freshwater Biology* 51, pp. 999–1015.

Waters, R. L., J. G. Mitchell, and J. Seymour (2003). "Geostatistical characterisation of centimetre-scale spatial structure of in vivo fluorescence". *Marine Ecology Progress Series* 251, pp. 49–58.

Webster, D. R., D. L. Young, and J. Yen (2015). "Copepods' Response to Burgers' Vortex: Deconstructing Interactions of Copepods with Turbulence". *Integrative and Comparative Biology* 55, pp. 706–718.

Weissburg, M. J., M. H. Doall, and J. Yen (1998). "Following the invisible trail: kinematic analysis of mate-tracking in the copepod Temora longicornis". *Philosophical transactions of the Royal Society of London* 353, pp. 701–712.

Woodson, C. B. et al. (2005). "Response of copepods to physical gradients associated with structure in the ocean". *Limnology and Oceanography* 50(5), pp. 1552–1564.

Woodson, C. B. et al. (2007). "Cue hierarchy and foraging in calanoid copepods: ecological implications of oceanographic structure". *Marine Ecology Progress Series* 330, pp. 163–177.

Wosniack, M. E. et al. (2014). "Unveiling a mechanism for species decline in fragmented habitats: fragmentation induced reduction in encounter rates". *Journal of The Royal Society Interface* 11, p. 20130887.

Yang, T. S. and S. S. Shy (2005). "Two-way interaction between solid particles and air turbulence: particle settling rate and turbulence modification measurements." *Journal of Fluid Mechanics* 526, pp. 171–216.

Yen, J. (2000). "Life in transition: balancing inertial and viscous forces by planktonic copepods". *The Biological Bulletin* 198, pp. 213–244.

Yen, J. and D. M. Fields (1992). "Escape response of Acartioa budsonica (Copepoda) nauplii from the flow field of Temora longicornis (Copepoda)". *Archiv für Hydrobiologie. Beiheft. Ergebnisse der Limnologie* 36, pp. 123–134.

Yen, J., K. D. Rasberry, and D. R. Webster (2008). "Quantifying copepod kinematics in a laboratory turbulence apparatus". *Journal of Marine systems* 69, pp. 283–294.

Yen, J. and J. R. Strickler (1996). "Advertisement and concealment in the plankton: what makes a copepod hydrodynamically conspicuous?" *Invertebrate Biology* 115, pp. 191–205.

Zamansky, R., I. Vinkovic, and M. Gorokhovski (2011). "Acceleration statistics of solid particles in turbulent channel flow". *Physics of Fluid* 23, p. 113304.

Zhan, C. et al. (2014). "Accumulation of motile elongated microorganisms in turbulence". *Journal of Fluid Mechanics* 739, pp. 22–36.

Zhu, Z. W., Z. L. Zhou, and B. G. Jia (2003). "On the Lower Bound of the Hausdorff Measure of the Koch Curve". *Acta Mathematica Sinica* 19, pp. 715–728.

Zollner, F. (2004). *Leonardo Da Vinci 1452-1519; Sketches and Drawings*. Taschen.